Analysis of the notional permeability of rubble mound breakwaters by means of a VOF model

E.M. van der Neut

Technische Universiteit Delft

TU Delft Delft University of Technology

Challenge the future

Analysis of the notional permeability of rubble mound breakwaters by means of a VOF model

by

Erwin Matthijs van der Neut

in partial fulfilment of the requirements for the degree of

Master of Science

in Hydraulic Engineering

at the Delft University of Technology,

to be defended publicly on Wednesday June 17, 2015 at 10:00 AM.

Student number:	1504703	
Thesis committee:	Prof. dr. ir. W.S.J. Uijttewaal,	TU Delft
	Ir. H.J. Verhagen,	TU Delft
	Ir. J.P. van den Bos	TU Delft

An electronic version of this thesis is available at `http://repository.tudelft.nl/`.
Numerical data is available at `http://datacentrum.3tu.nl/`.
DOI: 10.4121/uuid:deed39cd-7eee-4e10-a469-422ee57953cc

TU Delft Delft University of Technology

ABSTRACT

All over the world rubble mound breakwaters can be found. They are typically constructed out of loose rock, originating from quarries, and are used to protect harbours and coast lines from wave impact. When designing such a breakwater, one would like to predict the stability of the armour layer of the breakwater.

For this purpose several armour layer stability formula are developed. The most reliable is considered to be the stability formula of Van der Meer (1988). With this method, the armour layer stability is predicted based on several parameters. One of these parameters is the so-called notional permeability, P. This parameter makes this stability formula unique and gives the prediction a higher accuracy as compared to, for example, Hudson.

The stability formula was developed based on a large set of physical model tests. Three structures with an apparently different permeability were tested, they were designated as *impermeable*, *permeable* and *homogeneous*. All three structures showed a clear distinction in stability. This was the basis of the introduction of the notional permeability. Based on curve fitting the three structures were given P-values of 0.1, 0.5 and 0.6 respectively.

The definition of the word *notional* is important to keep in mind; *existing as or based on a suggestion, estimate, or theory; not existing in reality*. Or, in other words, the notional permeability is not a physical description of the real permeability of a breakwater. Furthermore, there are no methods to calculate the notional permeability. This makes it difficult to estimate a safe and reliable P-value for an arbitrary structure.

Furthermore, the definition of the notional permeability suggests that a single P-value can be attributed to an arbitrary structure. However, previous research has suggested that the notional permeability is not only dependent on structural parameters, but also on hydraulic parameters. This makes the assumption of a single P-value for a particular structure under arbitrary hydraulic conditions invalid. The notional permeability should therefore not be regarded as a structural property, but rather as a parameter for optimal stability prediction. The P-value should therefore vary under varying hydraulic conditions.

This thesis aims for a better understanding of the physical processes behind the notional permeability. Some of the original physical model tests of Van der Meer (1988) are selected for analysis to achieve this goal. Only tests with outer bounds of the notional permeability, namely the impermeable ($P \sim 0.1$) and homogeneous structures ($P \sim 0.6$), are considered since these would intuitively result in clear physical differences. As a tool the numerical model IH2VOF is used. This 2D vertical model is able to simulate flow interaction with porous media. And makes it possible to measure pressures and flow velocities at any point within a breakwater. In this way physical processes can be described as functions of pressures and flow velocities.

The model is able to simulate porous flows by Volume Averaging the Reynolds Averaged Navier Stokes equations. This Volume Averaging introduces a porosity into the equations. Furthermore, the extended Forchheimer equation is needed to close the equations. This additionally introduces the laminar and turbulent Forchheimer coefficients and added mass coefficients to the equations. These four variables describe the porous media and are required as input to the model.

The uncertain values of these four model inputs requires a validation of the model results. The validation is performed by using pressure difference measurements from physical models and comparing them to the numerical results. First, it is shown that the model simulates flow in porous media reasonable well and second the Forchheimer coefficients are calibrated for 'optimum' model results. This results in the conclusion that flow inside the breakwaters is fully turbulent, according to the classification of Troch (2000), and can be described by the extended Forchheimer equation without the laminar term.

Based on a literature study a hypothesis is made about the variables on which the notional permeability is dependent. The Buckingham Π theorem is applied to these variables, resulting in four dimensionless Π terms. The analysis of the model results is done based on these four Π terms. They describe a ratio of two physical processes and should show a correlation with the notional permeability.

Eventually it is concluded that the Π terms are best measured 0.5 times the significant wave height below the initial water level, inside the armour layer and in a normal direction to the front slope of the structure. With this approach, all four Π terms show a positive correlation with P, namely: the rate of acceleration, the pressure to inertial force ratio, the drag to inertial force ratio and the inertial to viscous force ratio. Furthermore, at the lowest bound of P drag forces are small to negligible and the flow is classified as fully turbulent for all values of P.

These correlations can be translated to functional relations for P. This is based on curve fitting of the data, were the P-value is allowed to vary under different hydraulic conditions. This results in four functional relations, one for each Π term. The Buckingham Π states that this can be expressed as a single functional relations. However, due to the limited number of data points and the assumptions made in the hypotheses, it is decided to keep the functional relations separate. With this method, four predictions of the P-value for an arbitrary structure under arbitrary hydraulic conditions can be made. Based on these predictions, it is up to the engineering judgement to choose a safe and reliable value.

Although not a subject of this work, the numerical results suggest a correlation between the measured damages from the physical model tests and pressures and flow velocities inside the armour layer of the breakwaters. It is highly recommended to conduct research on this topic. If a good correlation is found, armour layer stability could be predicted with a numerical model without the need for modelling of individual stones.

PREFACE

This thesis marks the end of my Hydraulic Engineering study at the Delft University of Technology. The work is completed for the Coastal Engineering section at the faculty of Civil Engineering and Geosciences and intends to create more insight in the permeability of breakwaters.

The topic of this work was proposed by Jeroen van den Bos. My special thanks go to Jeroen for giving me the opportunity to work on this interesting topic and for the inspiring talks we had. Many thanks go to Henk Jan Verhagen and Wim Uijttewaal as well. Their feedback and constructive comments are greatly appreciated. Without it, the achieved results of this work would not have been possible.

I also like to thank all my friends, with whom I have spent hours and hours working on our studies. You have made many study days enjoyable and inspiring. Special thanks go to Daan van Campen and Isabeau Dieleman for reviewing this report.

None of this would have been possible without the unconditional support from my parents. Thank you very much for giving me the opportunity to study in Delft and for supporting me throughout seven years of study. A special word of gratitude goes to my uncle and aunt for their enthusiasm and interest in my studies.

Erwin van der Neut
Delft, June 2015

CONTENTS

LIST OF FIGURES

LIST OF TABLES

LIST OF SYMBOLS

Symbol	Unit	Description
α	rad	1. Slope angle 2. Dimensionless laminar Forchheimer coefficient 3. Constant in JONSWAP spectrum
β		Dimensionless turbulent Forchheimer coefficient
β_c		Dimensionless turbulent Forchheimer coefficient in case of oscillatory flows, $\beta = \beta_c(1 + \frac{7.5}{KC})$
Δ		Relative mass density, $\Delta = \frac{\rho_s - \rho_w}{\rho_w}$
Δx	m	Horizontal size of numerical cell
Δy	m	Vertical size of numerical cell
$\frac{D_{85}}{D_{15}}$		Stone grading
γ		1. Added mass coefficient 2. JONSWAP peak enhancement factor
γ_{cr}		Correction factor for observed/calculated core run-up
γ_{Ru}		Correction factor for observed/calculated infiltration
$\hat{U}$	$\frac{m}{s}$	Peak flow velocity under a single wave
κ		Spectral shape parameter
μ	$\frac{kg}{ms}$	1. Dynamic viscosity 2. Friction coefficient in the Iribarren formula
ν	$\frac{m^2}{s}$	Kinematic viscosity
ρ_s	$\frac{kg}{m^3}$	Density of porous material
ρ_w	$\frac{kg}{m^3}$	Density of water
ξ_m		Iribarren number, based on the mean wave period ($\xi_m = \frac{\tan(\alpha)}{\sqrt{H/\left(\frac{g}{2\pi}T_m^2\right)}}$)
a	$\frac{s}{m}$	Dimensional laminar Forchheimer coefficient
Ac		Acceleration parameter, $\frac{\hat{u}}{ngT}$
B	N	Buoyancy of a single rock
b	$\frac{s^2}{m^2}$	Dimensional turbulent Forchheimer coefficient
c	$\frac{s^2}{m}$	Dimensional inertial Forchheimer coefficient
c_{pl}		Van der Meer curve-fitting factor for plunging waves
$c_{r\gamma}$		Run-up reduction coefficient
c_s		Van der Meer curve-fitting factor for surging waves
D_n	m	Nominal (rock) diameter
D_{n50}	m	Median nominal (rock) diameter
$E(f)$	$\frac{m^2}{Hz}$	Variance density
E_p	$\frac{m^2}{Hz}$	Spectral peak period
Eu		Euler number, $\frac{n^2\Delta p}{\rho u^2}$
F_{wave}	N	Force exerted by wave action on a structure
g	$\frac{m}{s^2}$	Gravitational acceleration
H	m	Wave height
H_0		Dimensionless wave height parameter, $H_0 = \frac{H_s}{\Delta D_{n50}}$
H_{m0}	m	Spectral wave height, $H_{m0} = 4\sqrt{(m0)}$
H_s	m	Significant wave height
I	$\frac{m}{m}$	Hydraulic pressure gradient
K		Permeability parameter

Continued on next page

Continued from previous page

Symbol	Unit	Description
K_D		Hudson curve-fitting factor
KC		Keulegan-Carpenter number, $\frac{\hat{u}T}{nD_{n50}}$
m_i	$\frac{m^2}{s^i}$	Spectral moment, $m_i = \int_{-\infty}^{\infty} f^i E(f) df$
N		1. Number of waves
		2. Iribarren curve-fitting coefficient
n		Porosity
P		Notional permeability
p	Pa	Pressure
R_c	m	Crest height
$R_{u,c}$	m	Run-up at the core
$R_{u,imp}$	m	Imposed run-up
Re		Reynolds number, $\frac{uD}{\nu(1-n)}$
S		Damage level
s_m		Wave steepness
T	s	Characteristic (wave) period
T_m	s	Mean wave period
$T_{m-1,0}$	s	Spectral period, $T_{m-1,0} = \frac{m_{-1}}{m_0}$
T_p	s	Peak period
u	$\frac{m}{s}$	Horizontal flow velocity
V_a		Volume of air/no-fluid
V_f		Volume of fluid
$V_{Ru,c}$	m^3	Run-up volume
W	N	Weight of a single rock
W_{50}	N	Mean weight of rock

GLOSSARY

Term	Definition
Fifth notional permeability structure	The structure tested by Kik (2011) for which a notional permeability value was determined of $P = 0.35$
Fourth structure of Van der Meer OR Fourth notional permeability structure	The Van der Meer structure with an interpolated notional permeability value of $P = 0.4$. This structure was actually not tested during the original physical model tests. The value was validated by Kluwen (2012).
JONSWAP spectrum	Joint North Sea Wave Observation Project spectrum
Notional permeability structures	The four structures for which the notional permeability values were determined by Van der Meer (1988)
NS	Navier stokes
Optimum P-value	The P-value which, together with the other measured variables, gives an 'exact' prediction of the damage
PM spectrum	Pierson-Moskowitz spectrum
P-value	The value of the notional permeability, attributed to a certain structure (under certain hydraulic parameters)
RANS	Reynolds Averaged Navier Stokes
VARANS	Volume Averaged Navier Stokes
VdM PM spectrum	This name is used to refer to the PM spectrum as used by Van der Meer (1988), since this PM spectrum has a significantly higher peak than an ideal PM spectrum.
VOF	Volume Of Fluid

1

INTRODUCTION

1.1. BACKGROUND

The topic of this thesis is the notional permeability of rubble mound breakwaters. Breakwaters can be found all over the world and are constructed as coastal defence structures or to protect ships at anchorage inside harbours. By breaking incoming waves onto the breakwater, the structure absorbs a large part of the wave energy and thus prevents this energy from reaching the coast or ships. Figure 1.1 shows two typical breakwaters.

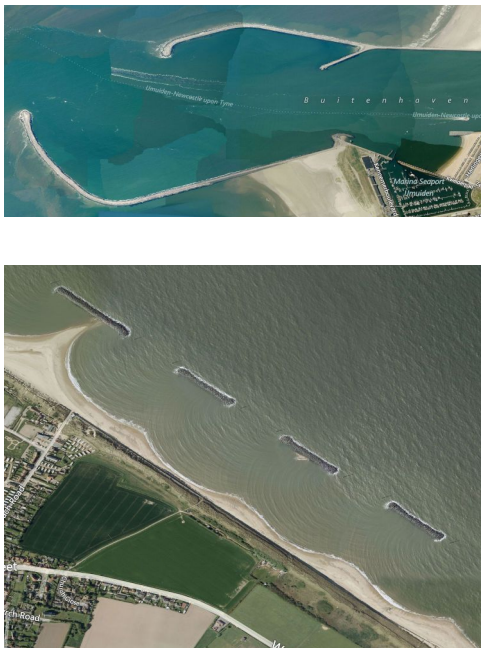

Figure 1.1: Above: breakwaters at the harbour entrance of IJmuiden, the Netherlands. Below: breakwaters at the coast near Sea Palling, United Kingdom. Source: Bing Maps

There are several types of breakwaters, this thesis concerns the rubble mound breakwaters. Or in other words; breakwaters constructed out of loose natural rock originating from quarries. Besides this type several other types of breakwaters exist, such as caissons or concrete armour structures, where the top layer consists of concrete armour units instead of loose rock. These are not a subject of this report. A typical cross-section of a rubble mound structure is shown in Figure 1.2.

The stability in general, and more specific the stability of the armour layer of such a rock mound is of great importance when designing a breakwater, but a theoretical expression to calculate the armour layer stability

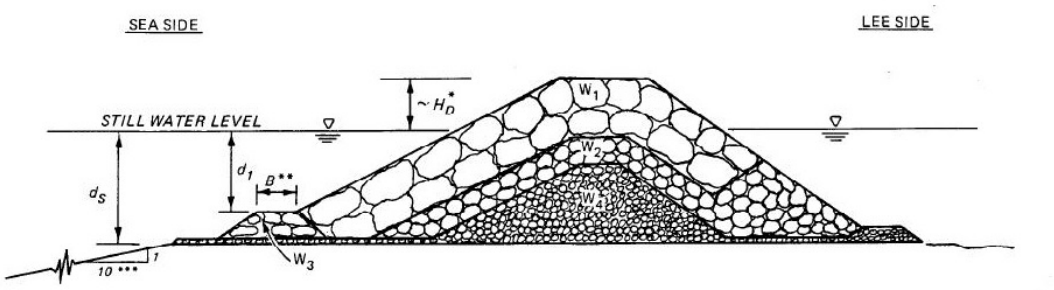

Figure 1.2: Typical cross-section of a rubble mound breakwater. Source: http://coastalengineering.tpub.com/cetn-iii-37/cetn-iii-370003im.jpg

does not exist. Since halfway of the previous century a lot of research has been carried out, which has resulted in two important empirical formulas; the Hudson formula and the Van der Meer formula.

The Hudson formula was one of the first empirical relations to calculate breakwater stability. Van der Meer (1988) came up with an improved formula by taking more variables into account during the physical model tests, see equation 1.1. One of these variables was the permeability of the structure, described with the notional permeability parameter. This thesis focuses on the notional permeability, as introduced by Van der Meer (1988).

$$\begin{aligned} \frac{H_s}{\Delta D_{n50}} &= 6.2P^{0.18}\left(\frac{S}{\sqrt{N}}\right)^{0.2}\xi_m^{-0.5} && \text{for plunging waves} \\ \frac{H_s}{\Delta D_{n50}} &= 1.0P^{-0.13}\left(\frac{S}{\sqrt{N}}\right)^{0.2}\xi_m^{P}\sqrt{\cot\alpha} && \text{for surging waves} \end{aligned} \tag{1.1}$$

In the following sections the problem formulation is described and the research questions are defined. Finally the methodology to answer the research questions is discussed. This chapter concludes with an overview of the research path that has been taken and an overview of the report structure.

1.2. PROBLEM ANALYSIS

When considering rubble mound structures, the permeability of the structure is one of the parameters that has an influence on the stability of the armour layer. This can be understood if one thinks of two different breakwaters; one with an impermeable sub layer and one with a permeable sub layer. In the first case pressure is build up under the armour layer under wave action and additional lift forces are created. In the second case wave energy is dissipated through the permeable sub layer, resulting in less pressure build up and in general a higher armour layer stability. This effect can also be explained by the movement of the internal water table. The water table inside a very permeable structure follows the movement of the water run-up on top of the structure. While the water table inside a structure with a less permeable sub layer lags behind the run-up. This is illustrated in Figure 2.5.

On of the advantages of the Van der Meer formula compared to the Hudson formula is the addition of the permeability. Van der Meer (1988) incorporated the permeability of the structure in his stability formulas by introducing the notional permeability parameter, expressed by the variable 'P'. Strictly speaking P is not defined as a permeability parameter, but it does indicate the composition of a structure. The value of P is the result of a curve fitting procedure based on three structures with obvious different permeabilities. These three structures were given the names 'impermeable' (armour layer on top of a fully impermeable core), 'homogeneous' (whole structure consists out of the same rock class) and 'permeable' (armour layer on top of a permeable core). The impermeable and homogeneous structures are considered to be the two outer bounds as far as permeability is concerned. The curve fitting resulted in a value of $P = 0.1$ for the impermeable, $P = 0.5$ for the permeable and $P = 0.6$ for the homogeneous structure, see Figure 1.3. See section 2.3 for the exact definition of P.

As a result, the value of P is only known for these three specific structures (and a fourth with an interpolated value). No proven methods exists to determine P for an arbitrary structure. This already indicates that the physical background of P is not yet fully understood. Instead value of P has to be determined with model tests in a laboratory setting. In recent years this has been done for some additional structures by Kik (2011) and Kluwen (2012). In practice however, a rock mound structure will rarely be exactly designed as one of these structures. Therefore the value of P has to be estimated, which creates a large uncertainty in the final stability parameter, or extensive scale model tests have to be carried out. In the latter case the determination of P becomes obsolete since the rock mound stability can then be directly determined from the scale model. This leads to the desire for a more fundamental understanding of the notional permeability.

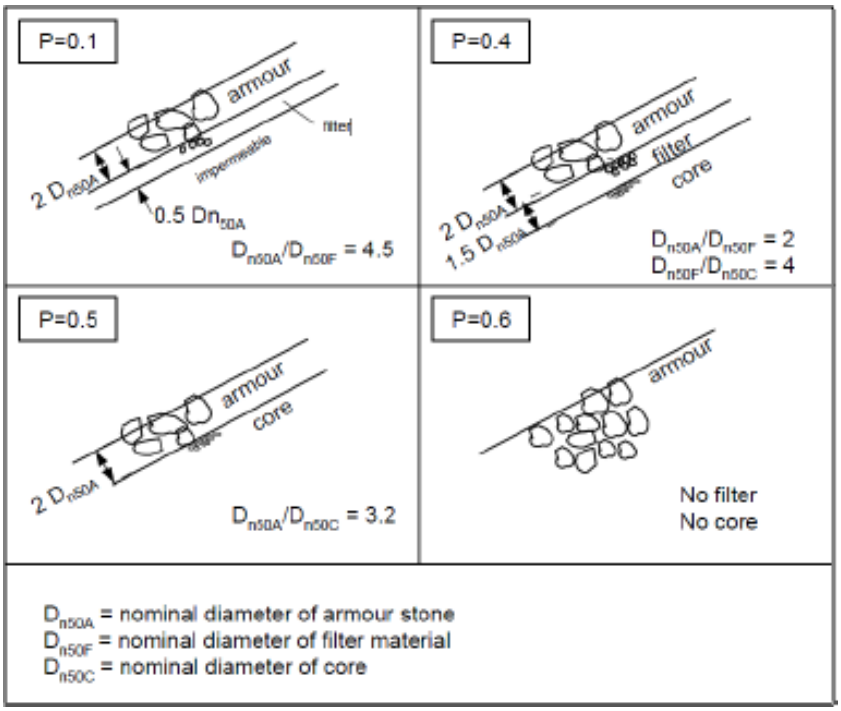

Figure 1.3: The four notional permeability structures of Van der Meer (1988)

1.3. RESEARCH QUESTION

Current situation From the standard 'notional permeability structures' of van der Meer it would seem that P is only dependent on structural parameters. However in recent studies of Jumelet (2010); Vilaplana Domingo (2010); Broekhoven (2011) it has been shown that P also depends on hydraulic parameters and P was expressed as a function of a run-up reduction coefficient. This coefficient is calculated with a volume-exchange-model, where the external process of wave run-up is linked to the internal process of flow through a porous medium. With this approach a first attempt was made to link P to a more physical basis.

Kik (2011) reproduced the P values of the impermeable and homogeneous structures of van der Meer in a laboratory setting and consequently determined the P value for a new structure. Kluwen (2012) validated the interpolated P value of the fourth structure of van der Meer ($P = 0.4$) and stated that P has a maximum value of 0.45 when applying two filter layers and increasing the thickness of the second filter layer to infinity.

Objective Following the previous studies the next step is to get a more fundamental understanding of the notional permeablity and possibly to express P directly as a function of one or more structural parameters and/or hydraulic conditions. In recent years it has been attempted to get an expression for P in an analytical way, but this has partially come to a dead end. Since the notional permeability influences the stability it is likely that there must be a measurable effect on pressure and flow patterns inside a rubble mound structure (see Section 2.11). Therefore and because of the desire to get a more fundamental understanding of the notional permeability, the following research questions are formulated:

Research questions

1 Can the notional permeability be correlated to pressure and flow patterns inside a rubble mound structure under wave attack?

2 Which physical processes, or combination of physical processes, inside a rubble mound structure can be used to describe the notional permeability.

1.4. METHODOLOGY

To answer the research questions, ideally one would like to measure pressures and flow velocities inside a rubble mound structure for a large range of boundary conditions (wave forcing) and a large range of structures. Some physical model tests have already been done recently, where the pressure at a few points inside the structure were measured (Kik (2011); Kluwen (2012)). However, it proves to be rather difficult to measure both pressures and velocities inside a structure.

Besides physical model tests one could also make use of numerical modelling. The advantages of numerical modelling are that in theory one could model any structure and measure pressure and flow velocities at every location inside that structure. The disadvantage is that a numerical model does not by definition give an exact description of reality. Therefore great care has to be taken to asses the reliability and accuracy of numerical results.

For this thesis, the numerical model IH-2VOF has been chosen as a tool to answer the research questions. Because this model gives flexibility regarding hydraulic conditions, type of structure and, most importantly, solves the 2DV Reynold Averaged Navier-Stokes equations both outside as well as inside porous media. With this model it is thus possible to measure pressures and flow velocities at 'any' point within a breakwater. Therefore this model will be used to conduct numerical simulations of breakwaters under wave attack.

Figure 1.4 shows an overview of the research approach. The methodology to answering the research questions is discussed in detail in Chapter 3.

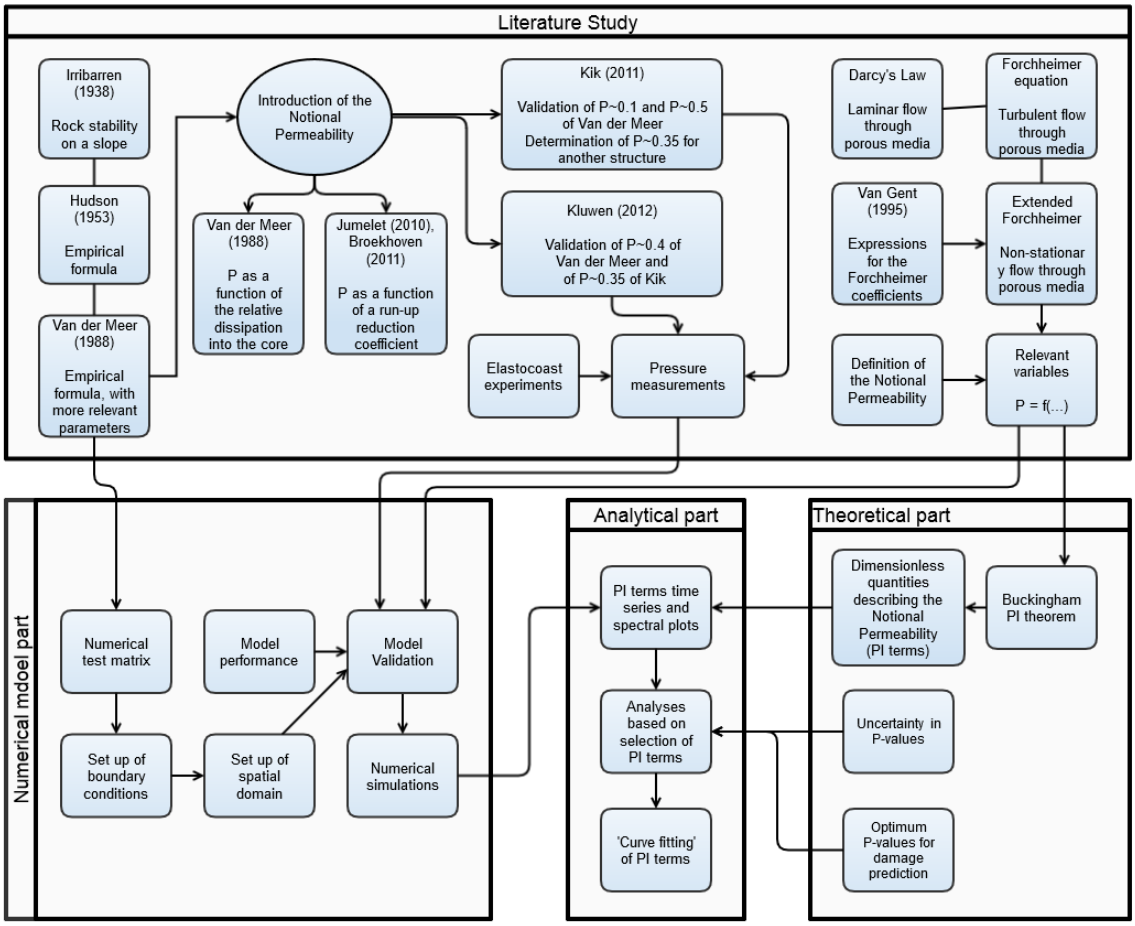

Figure 1.4: Overview of the research approach

1.5. GOALS OF THE RESEARCH

The primary goals of this research are to:

1 Arrive at a more fundamental understanding of the notional permeability

2 Find a correlation between the notional permeability and the pressure and flow patterns inside a rubble mound structure

A side goal of the research is to express P directly into one or more measurable quantities.

1.6. STRUCTURE OF THE REPORT

The structure of this report is as follows: first, a literature study is performed in Chapter 2. Next the methodology to answer the research questions is discussed in Chapter 3. The evaluation of the numerical model is presented in Chapter 4 and finally the results are discussed in Chapter 5. This report concludes with answers to the research question and a list of conclusions and recommendations.

2

LITERATURE STUDY

In this chapter the results of a literature study are presented. It provides more background information supporting the statements made in Chapter 1 and more relevant information for this study is elaborated. Further details of each topic can be found in the references.

Figure 2.1 shows an overview of the steps that led to the introduction of the notional permeability and the researches that followed. Parallel to this the historical steps in the theoretical expression of flow through porous media are presented. Finally, both are connected into a hypothesis about the notional permeability. This diagram is in no way intended to be a complete overview of all historical research on the topics, only a selection of relevant researches for this thesis are presented.

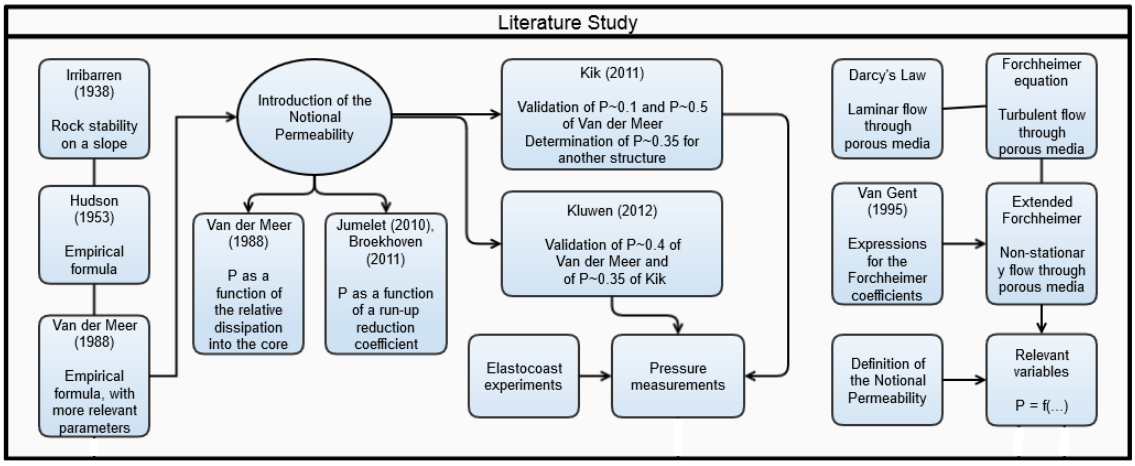

Figure 2.1: Overview of literature study

2.1. ROCK STABILITY ON A SLOPE (IRIBARREN)

Iribarren Cavanilles (1938) was probably one of the first who tried to mathematically describe the stability of rubble mound structures. The basis of the description was the consideration of forces acting on a single rock on a slope, see Figure 2.2. The forces are decomposed into vectors acting parallel and normal to the slope. In this case instability would occur if the friction is smaller than the sum of all other forces acting parallel to the slope.

The forces acting on the rock in Figure 2.2 are:

Weight of the rock

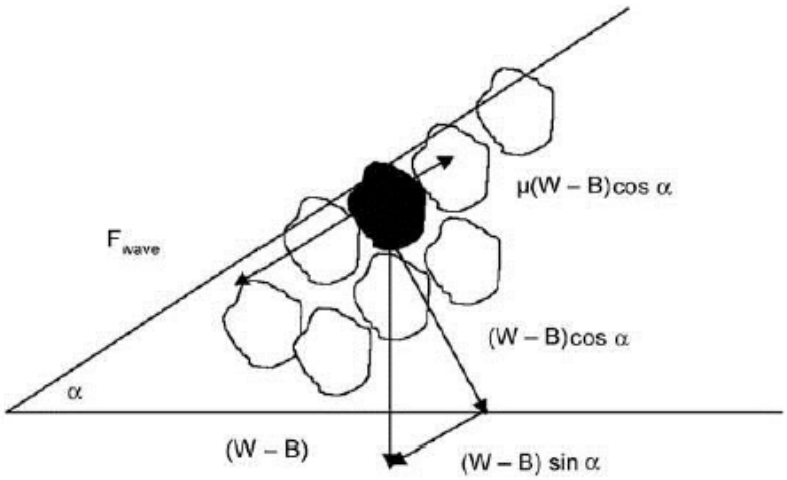

Figure 2.2: Forces acting on a single rock on a slope, according to Iribarren. From Schiereck and Verhagen (2012).

Buoyancy of the rock
Wave forcing, parallel to the slope
Frictional resistance, parallel to the slope

The wave forcing parallel to the slope is expressed in hydraulic and structural variables with the following formula:

$$F_{wave} = \rho_w g d_n^2 H \tag{2.1}$$

In case of a downward wave forcing parallel to the slope, the equilibrium of forces leads to the following stability requirement:

$$\begin{aligned} F_{wave} &< N[\mu(W-B)cos\alpha - (W-B)sin\alpha] \\ \rho_w g d_n^2 H &< N[(\rho_s - \rho_w) g d_n^3 (\mu cos\alpha - sin\alpha)] \\ \frac{H}{\Delta d_n} &< N(\mu cos\alpha - sin\alpha) \end{aligned} \tag{2.2}$$

In a similar way, the upward wave forcing stability requirement is:

$$\frac{H}{\Delta d_n} > N(\mu cos\alpha + sin\alpha) \tag{2.3}$$

In these formulas, N is a coefficient to account for forces that have not been taken into consideration in this analysis, or in other words, all unknown factors that play a role in stability. Thus, N must be determined experimentally. Iribarren gave some recommendations for the value of N, but the main observation in this report is that the stability is a function of the slope angle and that this has been shown on a theoretical basis.

2.2. EMPIRICAL FORMULA BY HUDSON

Starting in 1953, Hudson carried out research with a infinitely high slope and exposed it to regular wave series. The wave height was increased step by step until loss of stability occurred. In this way a large data set was obtained and Hudson developed a stability formula by means of a dimension analysis and curve fitting. With some adaptations throughout the years, the most recent Hudson formula is:

$$W_{50} = \frac{\rho_s g H_{1/10}^3}{K_D \Delta^3 cot\alpha} \tag{2.4}$$

The empirical research of Hudson confirms the influence of the slope angle on stability and the expression of the wave forcing as proposed by Iribarren, see equation 2.1. When the formula of Iribarren is written in the same form as the Hudson formula (an expression for the rock weight) it is clear that both formulas consider the same variables and have the same form. The difference is in the factor which takes unknown influences into account.

2.3. EMPIRICAL FORMULA BY VAN DER MEER

Around 1985 another extensive research program was carried out by Van der Meer (1988). The result was an empirical formula taking into account more relevant variables compared to Iribarren and Hudson, such as the permeability, see equation 2.5.

$$\begin{aligned} \frac{H_s}{\Delta d_{n50}} &= c_{pl} P^{0.18} \left(\frac{S}{\sqrt{N}}\right)^{0.2} \xi_m^{-0.5} && \text{for plunging waves} \\ \frac{H_s}{\Delta d_{n50}} &= c_s P^{-0.13} \left(\frac{S}{\sqrt{N}}\right)^{0.2} \xi_m^{P} \sqrt{\cot\alpha} && \text{for surging waves} \end{aligned} \tag{2.5}$$

Van der Meer investigated the stability of slopes consisting of loose rocks. Both statically stable and dynamically stable slopes were considered. For this study only the statically stable part is relevant. First of all, Van der Meer made a list of variables which might play a role in stability. The final list of variables (made dimensionless) which would be considered in the research is shown in Table 2.1.

Table 2.1: Governing variables in the research of Van der Meer

Variable	Expression	Range
The wave height parameter	$\frac{H_s}{\Delta D_{n50}}$	1 - 4
Wave steepness	s_m	0.01 - 0.06
surf similarity parameter	ξ_m	0.7 - 7
The damage as a function of the number of waves	$\frac{S}{\sqrt{N}}$	<0.9
The slope angle	$cot\alpha$	1.5 - 6
The grading of the armour stones	$\frac{D_{85}}{D_{15}}$	1 - 2.5
The permeability of the structure	P	imperm. - hom.
The spectral shape parameter	κ	0.3 - 0.9
The crest height	$\frac{R_c}{H_s}$	-1 - 2

Based on these variables and their ranges a test program was made. A summary of this test program is shown in Table 2.2.

The permeability of the structure was taken into account by testing three different structures. The structures were given the description 'impermeable', 'permeable' and 'homogenous', according to the composition of the structures, see Figure 2.3.

The influence of the variables on the stability were all described with so-called $\frac{H_s}{\Delta D_{n50}} - \xi_m$ plots. This showed a clear distinction between plunging and surging waves and the necessity for two separate formulas. Furthermore, in the surging region the plots showed clear influence of the permeability on the armour layer stability, see Figure 2.4.

The next step was to take all the variables into account in a curve fitting procedure. This led to the Van der Meer formulas (Equation 2.5). The P variable in these formulas was also a direct result of the curve fitting

Table 2.2: Summary of the test program of Van der Meer

slope angle	grading	spectral shape	core permeability	relative mass density	number of tests	range	range
$cot(\alpha)$	$\frac{D_{85}}{D_{15}}$	-	-	-	-	$\frac{H_s}{\Delta D_{n50}}$	s_m
2	2.25	PM	none	1.63	19	0.8-1.6	0.005-0.016
3	2.25	PM	none	1.63	20	1.2-2.3	0.006-0.024
4	2.25	PM	none	1.63	21	1.2-3.3	0.005-0.059
5	2.25	PM	none	1.63	26	1.2-4.4	0.004-0.063
3	1.25	PM	none	1.62	21	1.4-2.9	0.006-0.038
4	1.25	PM	none	1.62	20	1.2-3.4	0.005-0.059
3	2.25	narrow	none	1.63	19	1.0-2.8	0.004-0.054
3	2.25	wide	none	1.63	20	1.0-2.4	0.004-0.043
3	1.25	PM	permeable	1.62	19	1.6-3.2	0.008-0.060
2	1.25	PM	permeable	1.62	20	1.5-2.8	0.007-0.056
1.5	1.25	PM	permeable	1.62	21	1.5-2.6	0.008-0.050
2	1.25	PM	homogeneous	1.62	16	1.8-3.2	0.008-0.059
2	1.25	PM	permeable	0.95	10	1.7-2.7	0.016-0.037
2	1.25	PM	permeable	2.05	10	1.6-2.5	0.014-0.032
2*	1.25	PM	permeable	1.62	16	1.6-2.5	0.014-0.031
2**	1.25	PM	permeable	1.62	31	1.4-5.9	0.010-0.046

PM = Pierson-Moskowitz spectrum
* = foreshore 1:30
** = low crested structure with foreshore 1:30

procedure, it directly comes from a power function describing the influence of the wave steepness in the surging region. This resulted in three different powers for the three tested structures:

$$\frac{H_s}{\Delta d_{n50}} = a_1 \xi_m^{0.1} \qquad \text{(impermeable)}$$
$$\frac{H_s}{\Delta d_{n50}} = a_2 \xi_m^{0.5} \qquad \text{(permeable)}$$
$$\frac{H_s}{\Delta d_{n50}} = a_3 \xi_m^{0.6} \qquad \text{(homogeneous)}$$

Thus, the three structures were given a P value of 0.1, 0.5 and 0.6. The main observation here should be, as stated before, that the notional permeability is actually not a physical permeability variable, but it does indicate the composition of a rubble mound structure and thus indirectly the permeability of the structure as a whole and its influence on the stability.

According to Van der Meer (1988), the test program almost completely covers the application range of the governing values. Meaning that the formulas must have a wide range of application and are supported by sufficient physical tests. The notional permeability variable introduced in this study, however, is not a value that can easily be measured or calculated for any arbitrary structure.

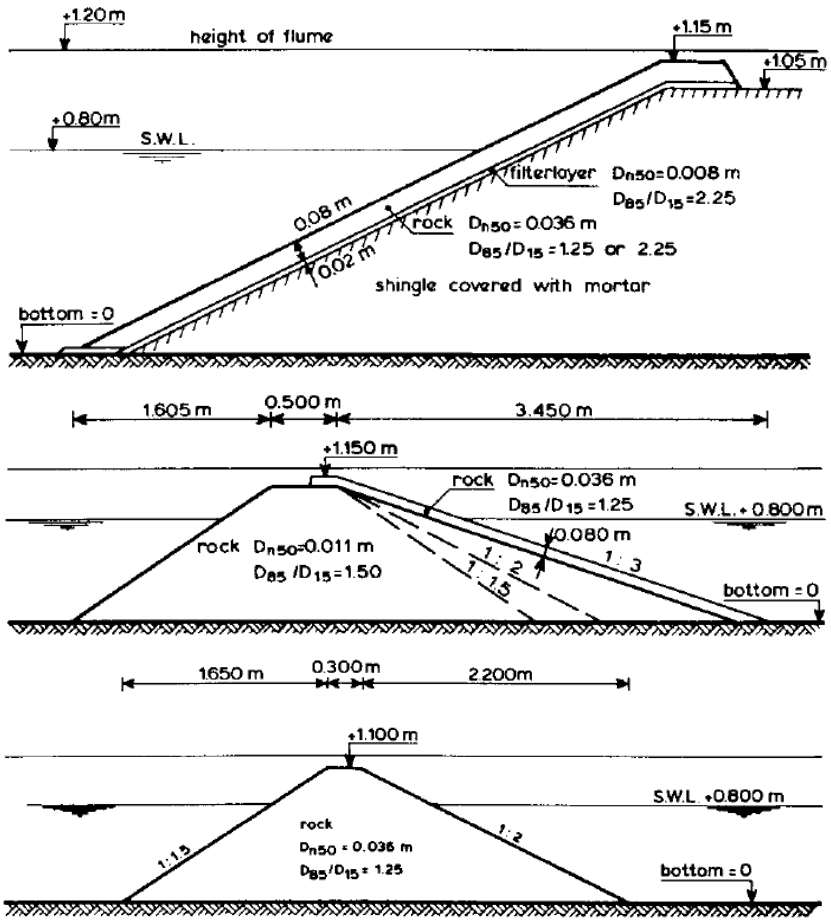

Figure 2.3: Tested structures during the research of Van der Meer (1988), impermeable (above), permeable (middle) and homogeneous (below)

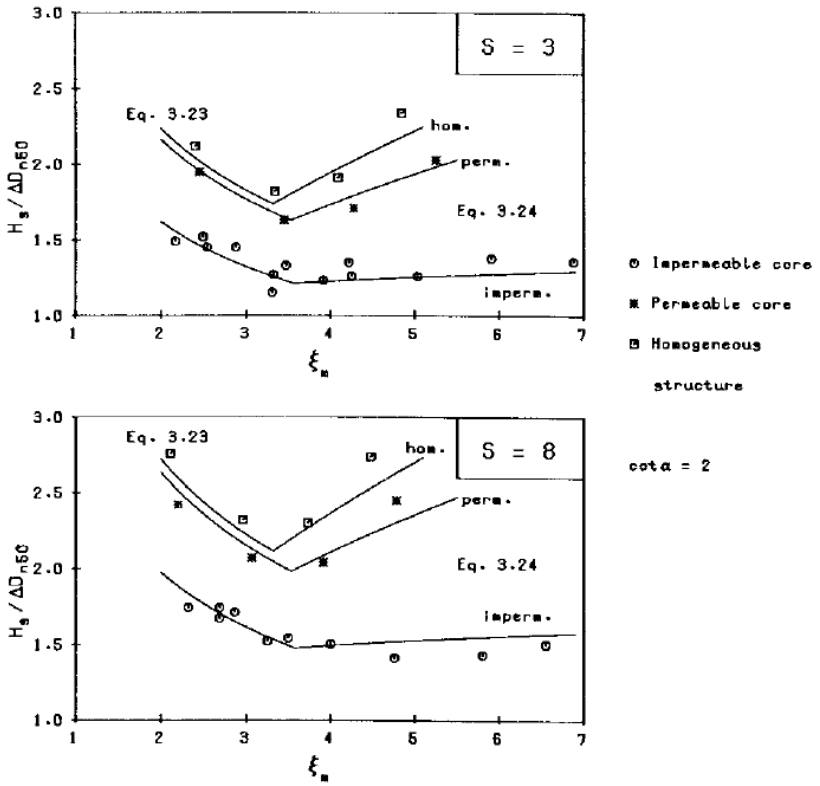

Figure 2.4: Influence of permeability on stability

2.4. INFLUENCE OF THE PERMEABILITY ON STABILITY

In this section the influence of the permeability of a rubble mound structure on armour layer stability is discussed. The influence of the permeability was discussed on a descriptive basis in the previous section.

The influence of the permeability on stability can be understood by considering the effect of wave forcing on various limit scenarios. The structures considered are:

Fully impermeable slope
Infinitely permeable slope
Permeable armour layer and a fully impermeable core
Permeable armour layer and a permeable core

Fully impermeable slope In case of a fully impermeable slope all wave energy acting on the structure is dissipated along the slope. The energy dissipation is governed by frictional resistance along the slope. The stability is well described by the analysis of the equilibrium of forces by Iribarren.

Infinitely permeable slope In case of an infinitely permeable slope, the wave energy partially penetrates into the structure and is dissipated by flow resistance (for rubble mound structures usually also turbulent dissipation) inside the porous media. Thus less wave energy acts along the slope when compared to the fully impermeable structure and from the analysis by Iribarren it follows that the stability is, in general, higher. It can also be expected that the run-up will be lower, since a volume of water is dissipated into the structure.

Permeable armour layer and a fully impermeable core In this case the wave energy can only penetrate through the armour layer. Along the impermeable core the same process happens as along the slope. Wave energy acts along the impermeable core along with a core run-up. From this scenario it can be understood that pressure can be build up along the impermeable core, resulting in a pressure gradient normal to the slope. This is visualized by a gradient in the internal water table, see figure 2.5. Besides the stability requirement as described by Iribarren, this effect also plays a role. A higher gradient results in a lower stability. And a higher gradient can be expected for less permeable cores.

Permeable armour layer and a permeable core The same processes will occur as with the impermeable core, only in this case the core is also able to dissipate a portion of the wave energy, resulting in less pressure build up and run-up along the core. The difference in permeability between the armour layer and the core determines the extent of the pressure build up. In general, for higher overall permeabilities, the internal water table gradient will be lower.

Figure 2.5 shows an illustration of flow patterns on an impermeable and permeable slope, along with the influence on the internal water table.

In general it can be concluded that an overall higher permeability leads to a higher armour layer stability. This is only the case for surging waves, since plunging waves have a different interaction with a rubble mound structure. In fact, according to the stability formula the permeability has little influence in case of plunging waves.

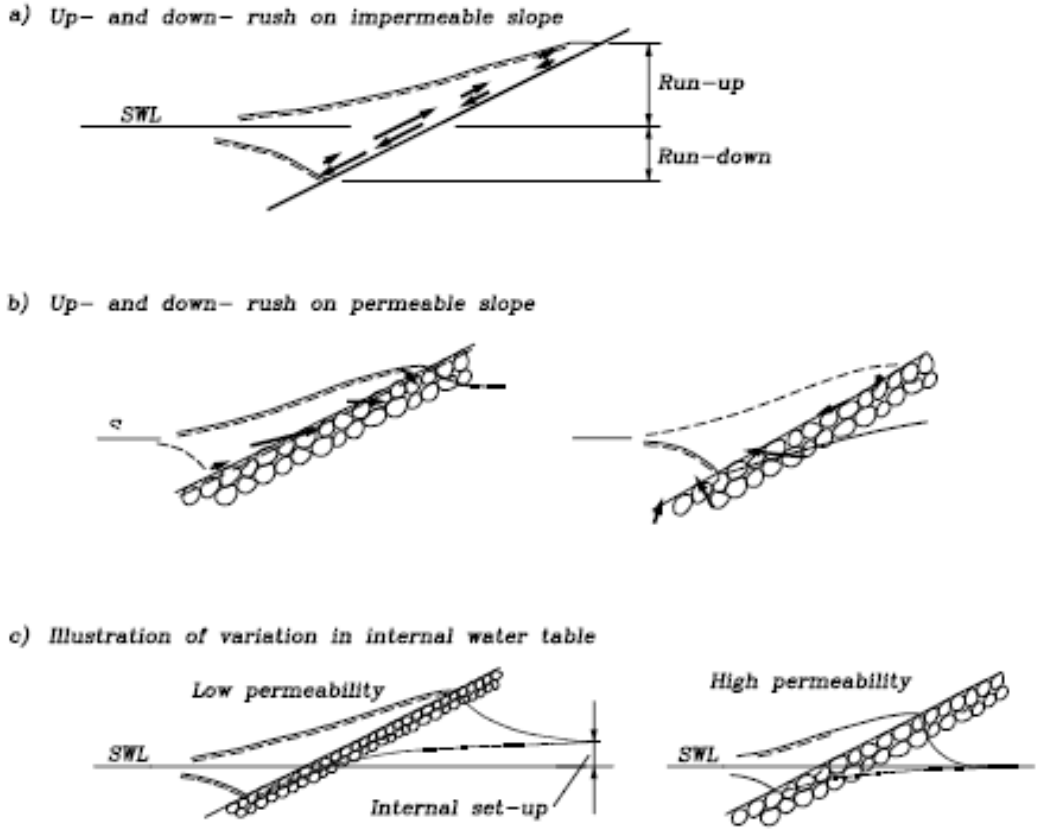

Figure 2.5: Illustration of wave run-up and run-down on an impermeable and permeable slope, from Lykke Andersen (2006)

2.5. DEFINITION OF THE NOTIONAL PERMEABILITY

In the previous sections the notional permeability as introduced by Van der Meer (1988) was discussed. Here again the empirical/non-physical basis of the notional permeability is stressed. The following definition of the word 'notional' must be kept in mind:

NOTIONAL
Existing as or based on a suggestion, estimate, or theory; not existing in reality:

Furthermore, the definition of the permeability, as used in this report, is:

PERMEABILITY
The capability of a porous material to permit the flow of fluids through its pore spaces.

With this definition of the permeability, the intrinsic permeability is described. That is, the permeability is only dependent on material properties. It should not be confused with the hydraulic conductivity:

HYDRAULIC CONDUCTIVITY
The ease with which a fluid can move through pore spaces of a material. This depends on the permeability of the material and on the fluid properties.

Although the notional permeability was introduced to describe the permeability of a rubble mound structure, it is not by definition solely dependent on structural properties. It may well be the case that it is dependent on other parameters as well. In any case, it is evident from the definitions that the (notional) permeability is related to the flow of fluids through the pores of a porous media. Therefore, an analytical description of flow through porous media is necessary for a more physical based understanding of the notional permeability. This is described in Section 2.10. First, previous attempts to describe P will be discussed in the next sections.

2.6. P AS FUNCTION OF THE RELATIVE DISSIPATION INTO THE CORE

Van der Meer (1988) also recognized the limitation to calculate the notional permeability due to the limited physical background and a first attempt was made to correlate the notional permeability to the relative dissipation of water into the core during wave attack, see Figure 2.7.

Based on the numerical model HADEER by Barends (1985) and calibrations by Hölscher and Barends (1986) based on run-down and run-up measurements along the slope, the homogeneous and impermeable Van der Meer structures were modelled. The structures were modelled with three different core stone diameters and subjected to three regular wave conditions. Based on the resulting flow velocities, the dissipation into the core was calculated. These results are shown in Figure 2.6.

This figure shows that a longer wave period and a higher permeability of the structure result in a higher dissipation into the core. A maximum dissipation was assumed to occur for the homogeneous structure and a dissipation of zero for the impermeable structure. In this way a relative dissipation compared to the homogeneous structure was determined for a fourth structure. The result was a plot of the relative dissipation as function of the notional permeability. The different wave periods gave slightly different curves. The P-value was approximately 0.44-0.45, which was rounded to $P = 0.4$.

With this method a rough estimation of the notional permeability can be obtained (under regular wave conditions). Simulations have to be made for the structure of interest, a similar structure with a impermeable core, a similar structure with a homogeneous core and all under various wave periods. The main observation here is that apparently the notional permeability is indeed dependent on the flow characteristics inside the rubble mound structure. See Van der Meer (1988) for further details.

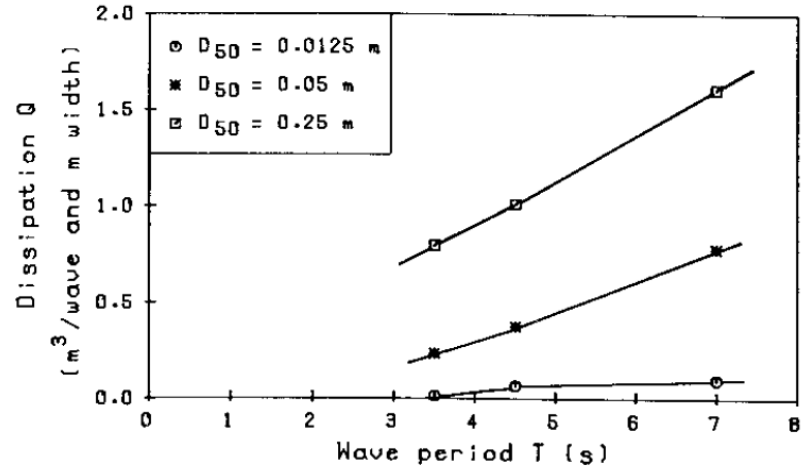

Figure 2.6: Dissipation into the core, calculated with HADEER

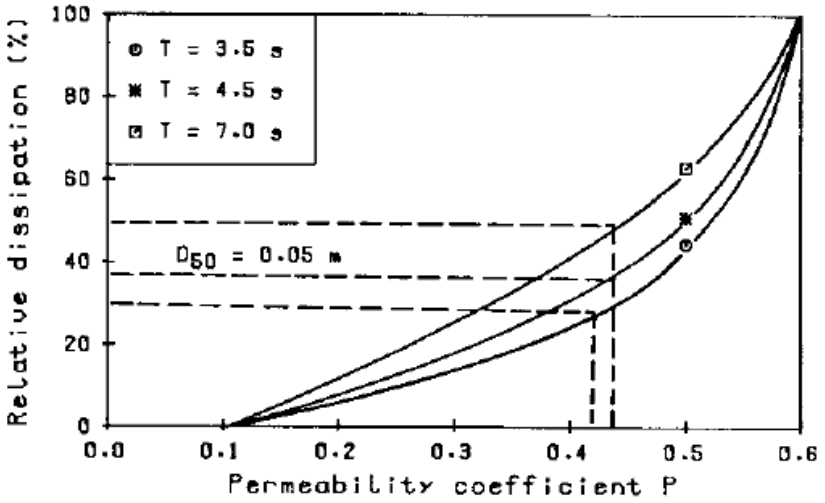

Figure 2.7: Relative dissipation into the core as a function of P

2.7. P AS FUNCTION OF A RUN-UP REDUCTION COEFFICIENT

In recent years, new studies started by Jumelet (2010) have been carried out to arrive at an expression for the notional permeability via a volume-exchange-model. The main idea behind this approach was to be able to quantify the notional permeability without the need of physical model tests. A volume-exchange-model was introduced to couple the external process of wave run-up with the internal process of flow through a porous medium. From this model follows a so-called run-up reduction coefficient. The reduction coefficient is defined as the reduction in run-up for a particular structure compared with a similar structure with an impermeable core. A clear correlation between this coefficient and the notional permeability was visible.

Vilaplana Domingo (2010); Broekhoven (2011) improved the volume-exchange-model based on additional physical model tests. The main conclusion was that the run-up at the core should be used instead of the run-up at the armour layer slope. The studies resulted in the following formulas:

$$R_{u,c} = (\gamma_{cr} \frac{V_{Ru,c} - V_b}{V_{Ru,c}}) R_{u,imp}$$
$$R_{u,imp} = \gamma_{Ru} R_{u,f}$$

$$c_{r\gamma} = \frac{R_{u,c}}{R_{u,imp}} = \gamma_{cr} \frac{V_{Ru,c} - V_b}{V_{Ru,c}}$$

Elaboration on the results for the physical model tests of Van der Meer (1988) resulted in:

$$P = 0.5 \xi^{-1} c_{r\gamma}^{-3.4} \tag{2.6}$$

The main observation here is that apparently the notional permeability is also dependent on the Iribarren number, and thus not solely on structural parameters. See Jumelet (2010); Vilaplana Domingo (2010); Broekhoven (2011) for further details.

2.8. PHYSICAL MODEL TESTS BY KIK

In the thesis by Kik (2011), the demand for more notional permeability values for other structures besides the four Van der Meer structures was fulfilled by performing physical model tests on a fifth structure. First of all Kik tested two reference structures, namely the impermeable and permeable Van der Meer structures. Similar P-values ($P = 0.08$ and $P = 0.55$) were found and thus it was concluded that the method to determine P gave similar results as the original physical tests.

The method to determine P was based on the existing stability formula. This formula was assumed as given and all parameters, for a range of Iribarren numbers, were measured. This resulted in only one unknown, namely P. With the least squares method the value of P which gave the best fit with the stability formula was determined.

The fifth structure consists of an impermeable core, followed by a thick filter layer with a relatively small stone size and a second thin and coarse filter layer, covered by an armour layer. The value of the notional permeability was determined at $P = 0.35$. See Figure 2.8

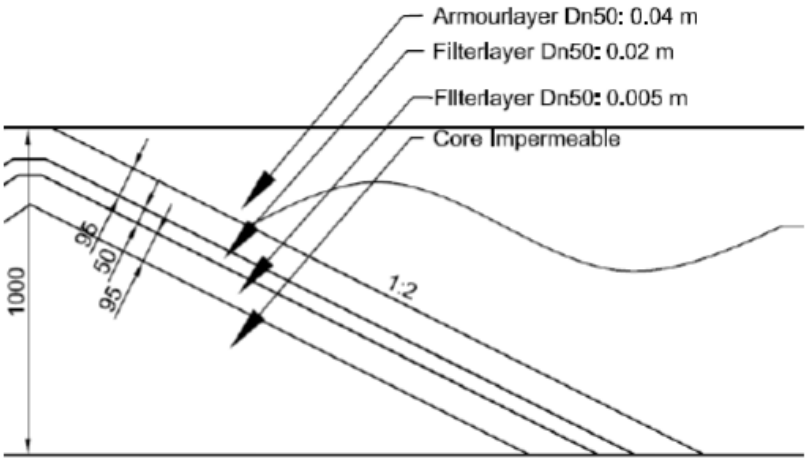

Figure 2.8: Fifth notional permeability structure by Kik (2011)

2.9. PHYSICAL MODEL TESTS BY KLUWEN

After the research by Kik (2011), Kluwen (2012) performed additional physical model tests. First of all the fifth notional permeability structure with a value of P = 0.35 was verified with the same method as used by Kik, namely assuming the Van der Meer formula as given and determining P with the least squares method. The experiments gave similar results. Furthermore, the fourth structure of Van der Meer with a notional permeability value of P = 0.4 was tested. This structure was actually never tested by Van der Meer, the P-value was determined via interpolation with the numerical model HADEER and the 'P as function of the relative dissipation into the core'-method. The P value for this structure was verified for the first time and showed similar results.

2.10. FLOW THROUGH POROUS MEDIA

In this section the flow through porous media will be described in an analytical way. It will become clear that the present state of knowledge does not yet allow for a full analytical description of the flow. Therefore, some variables in the equations still have to be determined empirically.

Darcy Flow through porous material with very small particle sizes, is described by Darcy's Law:

$$u = -\frac{K}{\rho g}(\nabla p + \rho g) \tag{2.7}$$

Although Darcy originally derived the equation based on empirical research, the equation has later been derived analytically and was thus given the name Darcy's Law. Darcy's law is applicable for laminar stationary flows through a homogeneous porous medium and incompressible fluids. In this equation, K is a permeability parameter which depends on the porous media properties.

Forchheimer Due to the large rock sizes in rubble mound structures, turbulence starts to play a role in flows through these porous media. Therefore Darcy's Law is not valid since it describes purely laminar flows only. Forchheimer proposed an additional term to Darcy's Law to account for the turbulent contribution to the flow. First, equation 2.7 is rewritten in an expression for the pressure gradient in one-dimensional form:

$$u = -\frac{K}{\rho g}\frac{\partial p}{\partial x}$$
$$-\frac{1}{\rho g}\frac{\partial p}{\partial x} = \frac{1}{K}u$$

Substituting $I = -\frac{1}{\rho g}\frac{\partial p}{\partial x}$ and $a = \frac{1}{K}$ in the above equation, results in:

$$I = au$$

With the additional term as proposed by Forchheimer, the equation becomes:

$$I = au + bu|u| \tag{2.8}$$

This equation is known as the Forchheimer equation. It is valid for stationary flow through porous media.

Extended Forchheimer Rubble mound structures under wave attack often do not show a stationary flow in the pores. Therefore, an additional term is needed to account for the time dependency:

$$I = au + bu|u| + c\frac{\partial u}{\partial t} \tag{2.9}$$

This equation is known as the extended Forchheimer equation. Although the Forchheimer equations have not been derived here, but merely explained by adding relevant terms for turbulence and non-stationary flow to Darcy's Law, they can be derived analytically from the Navier-Stokes equations. Thus, the extended Forchheimer equation can be assumed to be an analytical expression of the flow through a porous media. See Van Gent (1992) for a detailed description of this derivation.

Forchheimer coefficients The coefficients a, b and c in the Forchheimer equation are dimensional and can be seen as the laminar, turbulent and non-stationary contributions to the pressure gradient. Various expressions for these coefficients have been proposed in literature. The following expressions are commonly used, since these can be derived analytically (see Van Gent (1992)):

$$\begin{aligned} a &= \alpha\frac{(1-n)^2}{n^3}\frac{\nu}{gD_{n50}^2} \\ b &= \beta\frac{1-n}{n^3}\frac{1}{gD_{n50}} \\ c &= \frac{1+\gamma\frac{1-n}{n}}{ng} \end{aligned} \tag{2.10}$$

α and β are dimensionless coefficients that have to be determined empirically. This indicates that the expressions for a and b are over-simplified and do not take all relevant processes into account.

To accelerate a volume of fluid momentum is needed. Relatively more momentum is needed when the same volume of fluid has to be accelerated inside a porous media. This is accounted for by the so-called added mass coefficient γ.

Physical tests by Van Gent (1995) show the contribution of each coefficient to the total hydraulic gradient for a non-stationary turbulent flow, see Figure 2.9

From the figure it is clear that by far the largest contribution to the total hydraulic gradient is from the turbulent coefficient and that the contribution of the non-stationary coefficient is very small. On the basis of these tests results, Van Gent proposed the following expressions:

$$\begin{aligned} a &= \alpha\frac{(1-n)^2}{n^3}\frac{\nu}{gD_{n50}^2} \\ b &= \beta_c(1+\frac{7.5}{KC})\frac{1-n}{n^3}\frac{1}{gD_{n50}} \qquad \text{In which: } KC = \frac{\hat{U}T}{nD_{n50}} \\ c &= \frac{1+\gamma\frac{1-n}{n}}{ng} \qquad \text{In which: } \gamma = 0.85 - \frac{0.015}{Ac} \text{ and } Ac = \frac{\hat{U}}{ngT} \end{aligned} \tag{2.11}$$

Where KC is the Keulegan-Carpenter number and Ac is the Acceleration parameter. The numerical model does not use dynamic updating γ through the Acceleration parameter. Therefore this parameter is assumed to be constant henceforth. The parameter β is dynamically updated in the model through the KC number. Part of the contribution of an oscillatory behaviour of a flow to the total hydraulic gradient is therefore incorporated in the turbulent Forchheimer coefficient through the KC number.

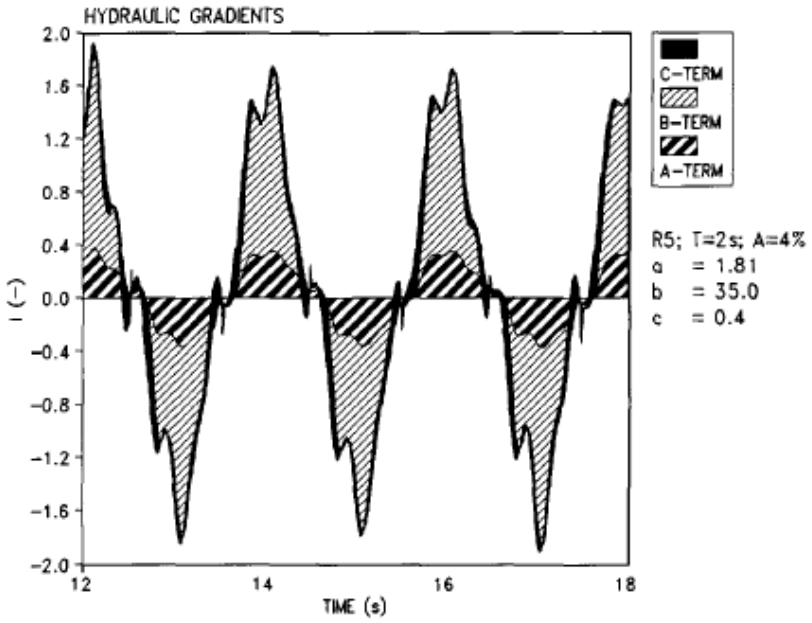

Figure 2.9: Contribution of each Forchheimer coefficient to the total hydraulic gradient

2.11. RELEVANT VARIABLES

In the previous section an analytical description of flow through porous media was presented. Based on this description, the capability of a porous material to permit the flow of fluids through its pore spaces of which the definition was given in section 2.5), can be quantified by:

> The hydraulic gradient in a porous medium, where a high hydraulic gradient indicates a low permeability.
>
> AND
>
> The flow velocity in a porous medium, where a high flow velocity indicates a high permeability.

This is supported by Darcy's Law (equation 2.7) for one dimensional laminar stationary flow in homogeneous porous media with small particle sizes, where the permeability coefficient K is calculated by:

$$K = \frac{u}{-\frac{1}{\rho g}\frac{\partial p}{\partial x}} \tag{2.12}$$

$$K = \frac{u}{I} \tag{2.13}$$

Thus it can be stated that the permeability is a function of u and I:

$$K = f(u, I) \tag{2.14}$$

As discussed previously, the flow inside a rubble mound structure under wave attack is governed by the extended Forchheimer equation. In this equation the hydraulic gradient is expressed by additional terms as compared to Darcy flows. Therefore, the following hypothesis about the notional permeability, following from the equations 2.9 and 2.11, is made:

$$
\begin{array}{ll}
P = f(u, I) & I = f(u, a, b, c) \\
 & I = f(u, \alpha, \beta, \gamma, n, D_{n50}, g, \nu) \\
 & I = f(u, \alpha, \beta_c, \gamma, n, D_{n50}, g, \nu, KC) \\
 & I = f(u, \alpha, \beta_c, \gamma, n, D_{n50}, g, \nu, T) \\
P = f(u, \alpha, \beta_c, \gamma, n, D_{n50}, g, \nu, T) &
\end{array}
\tag{2.15}
$$

3

METHODOLOGY

In this chapter the approach to answer the research question will be elaborated. First, the influence of hydraulic parameters on the notional permeability will be discussed and a test program will be made and explained. Second, the method to evaluate the results will be discussed. Finally, the uncertainty in the P-values and the practical application of P are discussed in more detail.

3.1. INFLUENCE OF HYDRAULIC PARAMETERS

To show that the influence of hydraulic parameters on the notional permeability is small to negligible on the two outer bounds of the notional permeability structures, the two previous methods to determine P are used. Namely the 'P as function of the relative dissipation into the core'-method by Van der Meer (1988) and the 'P as function of a run-up reduction coefficient'-method by Jumelet (2010); Vilaplana Domingo (2010); Broekhoven (2011).

P as function of the relative dissipation into the core As discussed in Chapter 2 Van der Meer used the numerical program HADEER to correlate P to the relative dissipation into the core. In this way the P-value (P = 0.4) for the fourth Van der Meer structure was defined. The results of this method applied to this fourth structure is again shown in Figure 3.1. From the figure it is clear the P-value varies with the wave period. However, for an impermeable structure the relative dissipation is always zero regardless of the wave period and for a homogeneous structure it is always 100% because of the definition of the relative dissipation. Therefore, it can be carefully stated that the influence of the hydraulic parameters on the notional permeability is small to negligible for the outer bounds of the notional permeability structures. Figure 3.1 shows that the influence of the wave period increases for intermediate values of P.

P as function of a relative run-up coefficient As discussed in Chapter 2 Jumelet (2010); Vilaplana Domingo (2010); Broekhoven (2011) developed a method to determine P based on a relative run-up coefficient. P was found to not only be dependent on this relative run-up, but also on the Iribarren number:

$$P = 0.5\xi^{-1}c_{r\gamma}^{-3.4} \tag{3.1}$$

The relative run-up value has a maximum of 1 and is typically larger than 0.6. Furthermore, the Iribarren number can vary between approximately 1 and 7. With this information, P can be calculated for various combinations of c_r and ξ, see Figure 3.2. The figure shows that the influence of the Iribarren number in the surging region ($\xi > 3-4$) is very small for lower bound of P (~ 0.1). This confirms the conclusion made above based on the work by Van der Meer. For the upper bound of P (~ 0.6) the influence of the Iribarren number is not negligible according to this figure.

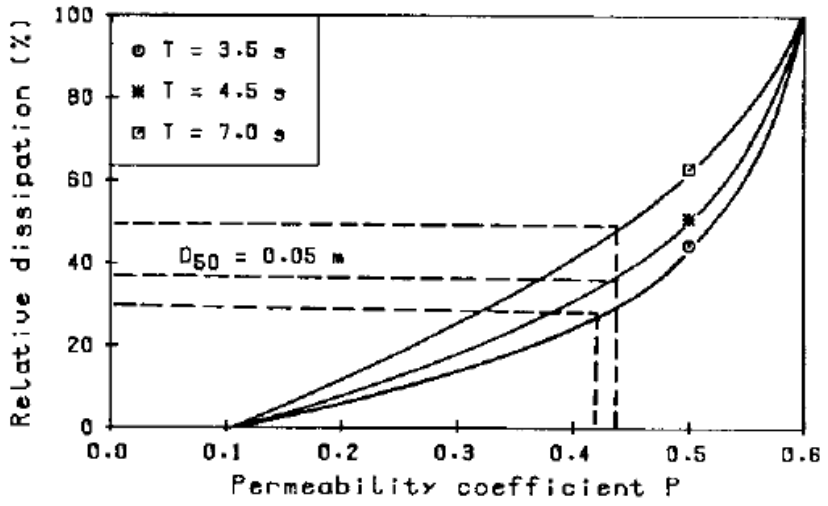

Figure 3.1: Relative dissipation into the core as a function of P

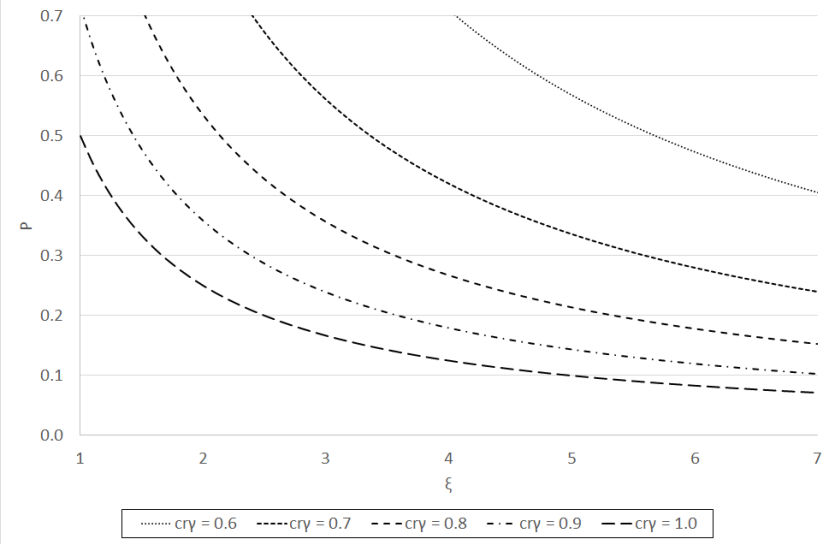

Figure 3.2: P as function of a relative run-up coefficient

standard deviation of P The standard deviation of P, calculated above, shows approximately the same value for the outer bounds of P. The P-value of the permeable structure has a larger standard deviation. Together with the conclusions from the work of Van der Meer (1988) and Jumelet (2010); Vilaplana Domingo (2010); Broekhoven (2011) it is concluded that the influence of hydraulic parameters is indeed higher for intermediate P-values and lower for the upper and lower bounds.

3.2. TEST PROGRAM

The goals of this research are to arrive at an expression for P and to get more insight into the physical basis of the notional permeability. From which it follows that structures for which the P-value is 'known' (taking into account the discussion in the previous section) should be investigated. The 'notional permeability Structures', see Figure 1.3, are tested extensively and damage levels for each physical model test are known. Therefore these physical model test will be reproduced in the numerical model.

Variables A lot of hydraulic and structural variables influence the stability of breakwaters (and possibly the notional permeability). A relevant list of variables for this study is given below. See Van der Meer (1988) for a

complete list of governing variables. Not all these variables are given below, because they can not be used as an input to the numerical model (such as the stone grading).

Wave height and period
Wave steepness
Slope angle
Iribarren number
Spectral shape
Permeability

Wave height and period
Obviously, the physical model test were performed under scaled conditions. With a numerical model this is not necessary and tests can be performed without scaling. However, it is the intention to reproduce the physical model test as accurately as possible because the notional permeability values were based on these tests. Therefore, the choice is made to reproduce the wave height and period from the physical model tests as accurately as possible.

Wave steepness
Wave steepness can typically vary between 1% and 6% and should not be modelled outside of this range.

Slope angle
The slope angle has an influence on the stability of the armour layer and the type of wave breaking (see below). For breakwaters it typically varies between $\cot\alpha = 1$ and $\cot\alpha = 6$. In the original physical tests slope angles of 1.5, 2, 3, 4 and 6 were used.

Iribarren number
The Iribarren number indicates the type of wave breaking in front of a structure and has a large influence on stability. It typically varies between 0.5 (plunging waves) and 7 (surging waves). Van der Meer (1988) found a significant difference of the armour layer stability under plunging and surging waves. Hence the two separate formulas.

Spectral shape
In case of irregular waves, the spectral shape determines the energy distribution over the wave frequency. Two common spectral shape functions are available; the Pierson-Moskowitz shape for fully developed sea states and the JONSWAP spectrum for young sea states. The model is able to create both these spectra based on the significant wave height and peak period.

Permeability
The permeability influences the stability, as stated before, and is the main focus of this study. The available 'notional permeability structures' are shown in Figure 1.3. A description of the influence of the permeability on armour layer stability is given in Chapter 2.

Other variables Other common variables in breakwater stability studies, which will not be used in this study due to the choice of a numerical test program, are:

Number of waves
Damage
Structural variables

Number of waves and Damage
The number of waves is usually taken into account because the more waves (in a single storm) impact a structure, the more damage occurs. Damage is no longer dependent on the number of waves in a range of about 5000-7000 waves. Single rocks are not defined in the model. Instead the Volume Averaging method is used to calculate flow through the porous media. This method is described in Section 4.1. In any case, nothing in the model will 'move', it is therefore impossible to measure damage from the model. From this it also follows

that varying the number of waves in the model is not necessary. Thus one value for this variable will suffice. However, the number of waves must at least be large enough to represent all waves that occur in a spectrum.

Structural variables
Since the aim of this research is to investigate the notional permeability, modelling should start with the structures for which the notional permeability is already known. The five available structures are the ones from Van der Meer (1988); Kik (2011). Only the slope angle can be varied. The ratio of nominal diameter of the armour layer over filter/core and the layer thickness are given fixed values for these structures.

Test program Van der Meer (1988) carried out more than 300 physical model tests relevant to this research. It is not possible to reproduce all these tests in the scope of this research, therefore some choices on which model tests to perform are made below. These choices will be made on basis of some of the variables and the their ranges as used in the physical model tests.

Notional permeability structures
Because of the conclusion made in Section 3.5 the choice is made to investigate only two structures with upper and lower boundaries of P, namely the impermeable ($P = 0.1$) and homogeneous ($P = 0.6$) structures, see Figure 1.3. Also the choice for these two structures is based on the expectations that a correlation between the flow and pressure patterns inside the breakwaters is most easily measurable and detectable when the difference in notional permeability is largest. Furthermore, it was stated in Chapter 2 that the notional permeability is not solely dependable on structural parameters but on hydraulic parameters as well, such as the Iribarren number. However, for these structures the influence of hydraulic parameters on the notional permeability, which are basically unknown, can assumed to be small to negligible. This is discussed in Section 3.5.

Relative mass density
Second, a selection is made based on the relative mass density. Van der Meer (1988) stated that the relative mass density has a negligible effect on the armour layer stability. Which would mean that it has a negligible effect on the notional permeability as well, since the notional permeability does have a large effect on the armour layer stability. However, since this parameter can not be used as an input to the numerical model and is not used in solving the RANS equations, it is impossible to demonstrate that this parameter is indeed negligible afterwards. Therefore only physical model tests with the same value for the relative mass density are selected. This value is chosen at 1.615, since this is the only relative mass density at which the homogeneous structure was tested. See Table 2.2

Stone grading
Third, the same reasoning as for the relative mass density is used for the stone grading. Only physical model tests with a stone grading of 1.25 are chosen, since this is the only value at which the homogeneous structure was tested.

Spectral shape
Van der Meer (1988) mainly used one PM spectrum for his tests, with some variation in the width of the spectrum. The homogeneous structure was only tested with a PM spectrum, therefore in this study the PM spectrum will be used as well. The 'narrow' and 'wide' PM spectra will not be used.

Plunging and surging waves
Van der Meer (1988) found a clear distinction between 'plunging' and 'surging' waves (see Equation 2.5) and based his definition of P on curve fitting of the results of the surging wave tests. This was done because an increasing influence of the notional permeability on the armour layer stability for an increasing Iribarren number in the surging region was found. However, P has a large influence on the armour layer stability under plunging waves as well, as can be seen in Figure 2.4. Therefore, both surging as well as plunging waves are used.

Note that the transition between the two formulas is given by an expression for the Iribarren number:

$$\xi_m = (6.2P^{0.31}\sqrt{(\tan\alpha)})^{\frac{1}{P+0.5}} \tag{3.2}$$

And is thus dependent on the notional permeability and slope angle. Therefore it strictly indicates the transition between the two formulas rather than the wave type. For some cases, depending on P and the slope angle, the surging formula must also be applied for waves with a more plunging character.

Taking all of the above into account, a test program is made from the physical model tests consisting of, in total, 24 numerical model tests, see Table 3.1. 16 tests for the impermeable structure and 16 for the homogeneous structure. See Van der Meer (1988) for a complete list of physical model tests carried out in the research.

Table 3.1: Numerical test program

Test nr.	Remark	d_{n50}	Δ	$\cot\alpha$	d_{85}/d_{15}		H_s	T_m	T_p	H_0	ξ_m	ξ_p	$S_{N=1000}$	$S_{N=3000}$
36	Rock imperm	0.036	1.615	3	1.25	PM	0.1002	2.20	2.50	1.72	2.91	3.29	4.93	9.11
37	Rock imperm	0.036	1.615	3	1.25	PM	0.0860	2.20	2.50	1.48	3.12	3.55	1.71	3.66
38	Rock imperm	0.036	1.615	3	1.25	PM	0.0742	2.19	2.50	1.28	3.35	3.82	0.89	1.48
51	Rock imperm	0.036	1.615	3	1.25	PM	0.1145	2.97	3.57	1.97	3.66	4.39	9.90	18.41
52	Rock imperm	0.036	1.615	3	1.25	PM	0.1049	2.99	3.45	1.80	3.85	4.44	3.76	6.40
53	Rock imperm	0.036	1.615	3	1.25	PM	0.0975	3.00	3.51	1.68	4.00	4.68	3.49	5.26
54	Rock imperm	0.036	1.615	3	1.25	PM	0.0799	3.02	3.45	1.37	4.45	5.08	0.83	1.50
55	Rock imperm	0.036	1.615	3	1.25	PM	0.1120	2.98	3.45	1.93	3.71	4.29	7.02	9.14
85	Rock imperm	0.036	1.615	4	1.25	PM	0.0991	2.20	2.50	1.70	2.18	2.48	3.16	5.56
86	Rock imperm	0.036	1.615	4	1.25	PM	0.0695	2.20	2.53	1.20	2.61	3.00	1.50	1.91
88	Rock imperm	0.036	1.615	4	1.25	PM	0.1190	2.98	3.51	2.05	2.70	3.18	7.42	13.36
89	Rock imperm	0.036	1.615	4	1.25	PM	0.0830	3.00	3.51	1.43	3.25	3.81	1.53	1.74
90	Rock imperm	0.036	1.615	4	1.25	PM	0.1084	3.02	3.51	1.86	2.87	3.33	6.01	9.41
91	Rock imperm	0.036	1.615	4	1.25	PM	0.0965	3.02	3.51	1.66	3.04	3.53	3.55	5.56
92	Rock imperm	0.036	1.615	4	1.25	PM	0.1396	2.95	3.51	2.40	2.47	2.93	15.34	28.75
104	Rock imperm	0.036	1.615	4	1.25	PM	0.1806	1.77	2.00	3.11	1.30	1.47	3.60	6.02
258	Rock hom	0.036	1.615	2	1.25	PM	0.1049	2.15	2.60	1.80	4.15	5.02	1.57	1.86
259	Rock hom	0.036	1.615	2	1.25	PM	0.1384	2.14	2.60	2.38	3.59	4.37	4.83	8.77
260	Rock hom	0.036	1.615	2	1.25	PM	0.1715	2.14	2.63	2.95	3.23	3.97	17.68	30.80
261	Rock hom	0.036	1.615	2	1.25	PM	0.1532	2.14	2.60	2.64	3.42	4.15	10.02	15.33
262	Rock hom	0.036	1.615	2	1.25	PM	0.1346	1.70	2.00	2.32	2.89	3.41	4.84	7.99
263	Rock hom	0.036	1.615	2	1.25	PM	0.1805	1.71	1.98	3.10	2.51	2.91	16.48	27.30
264	Rock hom	0.036	1.615	2	1.25	PM	0.1583	1.71	2.00	2.72	2.69	3.14	11.45	17.68
265	Rock hom	0.036	1.615	2	1.25	PM	0.1053	1.69	2.00	1.81	3.25	3.85	2.60	2.47
266	Rock hom	0.036	1.615	2	1.25	PM	0.1420	1.33	1.40	2.44	2.21	2.32	3.00	4.79
267	Rock hom	0.036	1.615	2	1.25	PM	0.1679	1.37	1.47	2.89	2.09	2.24	5.96	12.04
268	Rock hom	0.036	1.615	2	1.25	PM	0.1009	1.31	1.45	1.74	2.58	2.85	1.13	1.30
269	Rock hom	0.036	1.615	2	1.25	PM	0.1882	1.40	1.47	3.24	2.02	2.12	10.64	18.76
270	Rock hom	0.036	1.615	2	1.25	PM	0.1385	2.90	3.64	2.38	4.87	6.11	2.07	3.77
271	Rock hom	0.036	1.615	2	1.25	PM	0.1613	2.82	3.70	2.77	4.39	5.76	6.07	10.30
272	Rock hom	0.036	1.615	2	1.25	PM	0.1762	2.76	3.64	3.03	4.11	5.42	10.80	34.00
273	Rock hom	0.036	1.615	2	1.25	PM	0.1111	2.97	3.57	1.91	5.57	6.69	1.09	1.29

3.3. MODEL OUTPUTS

The model is able to generate the following outputs:

Pressure field around impermeable media, inside predefined areas.
Horizontal and vertical velocities at predefined sensor locations.
Free surface time series at predefined sensor locations.
Upper and lower envelopes and the mean water level.

Alternatively the model can also store the turbulent intensity, pressure, horizontal velocity, vertical velocity and VOF (Volume Of Fluid) function for each cell or for a selection of cells at each time step.

As stated in Chapter 2, the notional permeability will likely have an influence on pressures and flow patterns inside a rubble mound structure. A distinction between the two tested structures in these outputs should be searched for and preferably linked to one or more of the imposed hydraulic/structural parameters. The model tests for each of the two notional permeability structures should all result in more or less the same P value (0.1 and 0.6), thus it is probable that P is dependent on one or more dimensionless numbers. This also allows for a physical analysis of the model results.

In Chapter 2 relevant variables for this research were determined. Based on these variables some measurable quantities have to be determined on which a comparison between the two Van der Meer structures can be made. These quantities need to be dimensionless to be able to make a proper comparison, otherwise a comparison will not make any sense. For example, a high wave will automatically lead to higher pressure change inside a breakwater when compared to a low wave. A comparison of the pressure changes will therefore not give any information that was not already known. A dimensionless number however, can always be used in such an analysis, regardless of the forcing. Additionally, dimensionless numbers always represent a ratio of two forces and thus indicates which one dominates over the other. For example the ratio of inertial forces over viscous forces is given by the Reynolds number.

3.4. BUCKINGHAM Π THEOREM

In case a physical process can be described by an equation, but this equation is not known, the dimensionless quantities describing the process are also not known. In these cases the Buckingham Π theorem must be applied. This theorem states that if there exists a physically meaningful equation describing a certain process, where n relevant variables are involved, the process can be described by an equation in terms of $p = n - k$ dimensionless numbers. k is the number of dimensions involved. The dimensionless numbers are called Π terms. This theorem can be applied even if the equation describing the process is not known.

The basis and most important part of applying the theorem is determining the relevant variables. If a variable is missed in this stage, the analysis might not be complete. The hypothesis from Chapter 2 states that:

$$P = f(u, \alpha, \beta_c, \gamma, n, D_{n50}, g, \nu, T) \tag{3.3}$$

α, β_c and γ are deterministic properties of the flow, which are used in the Forchheimer equations to calculate the flow velocity and pressure. Therefore these variables are dependent on flow velocity and pressure and vice versa. Additionally the variables are required as input values for the model. Thus they must be left out of the Buckingham Π theorem application. To compensate for this loss of information the hydraulic gradient I is used instead of α, β_c, γ, which is by definition influenced by the Forchheimer coefficients. The hydraulic gradient is for convenience expressed as a function of the difference in pressure Δp (which does follow from the model), density ρ and gravity g ($I = -\frac{1}{\rho g}\frac{\partial p}{\partial x}$). This results in nine relevant variables.

The relevant variables along with their dimension are listed below.

P	[-]
u	$[\frac{L}{T}]$
Δp	$[\frac{M}{LT^2}]$
n	[-]
D_{n50}	$[L]$
T	$[T]$
ρ	$[\frac{M}{L^3}]$
ν	$[\frac{L^2}{T}]$
g	$[\frac{L}{T^2}]$

Three dimensions are involved, thus the number of Π terms is $9-3=6$. Subsequently, three repeating variables need to be selected, equal to the number of dimensions. There is no specific guideline to do this, but the general rule is to selected variables with basic dimensions. Restrictions are that variables without a dimension cannot be chosen since these already form a Π term by themselves and each of the three dimensions must appear in at least one of the repeating variables, otherwise the procedure will not work.

The three repeating variables that are chosen are the flow velocity u, pressure difference Δp and the characteristic time scale T. The Π terms are now given by:

$$\Pi_1 = P$$
$$\Pi_2 = n$$
$$\Pi_3 = Du^a \Delta p^b T^c$$
$$\Pi_4 = \rho u^a \Delta p^b T^c$$
$$\Pi_5 = \nu u^a \Delta p^b T^c$$
$$\Pi_6 = g u^a \Delta p^b T^c$$

The values of the exponents a, b and c are determined by the fact that the Π terms are dimensionless. Once the exponents are known, commonly used dimensionless numbers can be recognized in the Π terms. They are rewritten and given their respective names:

$$\Pi_1 = P$$
$$\Pi_2 = n$$
$$\Pi_3 = Du^{-1}T^{-1} = \frac{uT}{D} \quad \text{Keulegan-Carpenter number}$$
$$\Pi_4 = \rho u^2 \Delta p^{-1} = \frac{\Delta p}{\rho u^2} \quad \text{Euler number}$$
$$\Pi_5 = \nu u^{-2} T^{-1} = \frac{uD}{\nu}\frac{uT}{D} \quad \text{Reynolds number x Keulegan-Carpenter number}$$
$$\Pi_6 = g u^{-1} T^1 = \frac{u}{gT} \quad \text{Acceleration parameter}$$

Since the fifth Π term is a product of the Reynolds number and Keulegan-Carpenter (KC) number, and the KC number already forms another Π term by itself, the fifth Π term may be written as the Reynolds number only. Additionally the Π terms are modified for porous flows by including the porosity. Henceforth, if the KC number, Euler number, Acceleration parameter and Reynolds number are mentioned in this report, the modified versions for porous media are meant. The final list of Π terms becomes:

$$\Pi_1 = P$$
$$\Pi_2 = n$$
$$\Pi_3 = \frac{uT}{nD} \quad \text{KC number}$$
$$\Pi_4 = \frac{n^2 \Delta p}{\rho u^2} \quad \text{Euler number}$$
$$\Pi_5 = \frac{uD}{\nu(1-n)} \quad \text{Reynolds number}$$
$$\Pi_6 = \frac{u}{ngT} \quad \text{Acceleration parameter}$$

According to the Buckingham Π theorem any Π term may be expressed in terms of the others. The second Π term (porosity) is henceforth not used since it is already incorporated in the other terms and kept constant during the numerical simulations. The hypothesis now becomes:

$$\begin{aligned} \Pi_1 &= f(\Pi_3, \Pi_4, \Pi_5, \Pi_6) \\ P &= f(KC, Eu, Re, Ac) \end{aligned} \tag{3.4}$$

The Π terms have a specific physical meaning and all describe a ratio of forces, they are briefly discussed below.

Keulegan-Carpenter number
The Keulegan-Carpenter (KC) number describes the ratio of drag forces over inertial forces in an oscillatory flow. It can be applied for flows around objects as well as flows through porous media. The flow inside a breakwater under wave attack is an oscillatory flow. In the numerical model the KC number is used in the Forchheimer equation to increase the turbulent Forchheimer coefficient β to account for oscillatory flow. See Figure 2.11.

Euler number
The Euler number is a dimensionless number which is used to analyse the pressure difference between two points. It describes the ratio of the pressure forces over the inertial forces.

Reynolds number
The Reynolds number describes the ratio of inertial forces over viscous forces.

Acceleration parameter
The Acceleration parameter is proposed by Van Gent (1992) and used to estimate the non-stationary Forchheimer coefficient. It is a dimensionless quantity that indicates the rate of acceleration for a particular (wave) period.

3.5. UNCERTAINTY IN THE P-VALUES

As stated in Chapter 2 the notional permeability does not solely depend on structural properties, but on the external forcing as well. Therefore, the assumption that all structures have a fixed P-value is fundamentally wrong. However, taking into account that the impermeable and homogeneous structures represent the two outer limit cases of the notional permeability, an analysis can still be performed. To find an actual relationship between the notional permeability and the flow and pressure patterns inside the structure, the results from the numerical simulations (selected in the next chapter) should not be 'forced' to a fixed P-value (such as 0.1, 0.4, 0.5 or 0.6). Instead, P should be forced to its actual value for a particular structure under a particular hydraulic condition. But the actual values are not known, hence this research. To be able to make a proper analysis, part of the derivation of the Van der Meer formula is redone in this report to give more insight in the uncertainty in the P value for a particular structure under arbitrary wave conditions.

Below, the derivation process of the stability formula is described. From the literature study the exact definition of the notional permeability became clear. To summarise, Van der Meer tested three different structures,

which all had an apparently different permeability. After a whole series of tests, damage levels as function of the wave height parameter ($\frac{H_s}{\Delta D_{n50}}$) were defined for each combination of wave period and structural parameters. With this method the wave height parameter and corresponding Iribarren numbers are known for fixed damage levels. Figure 3.3 shows a typical example of a damage curve.

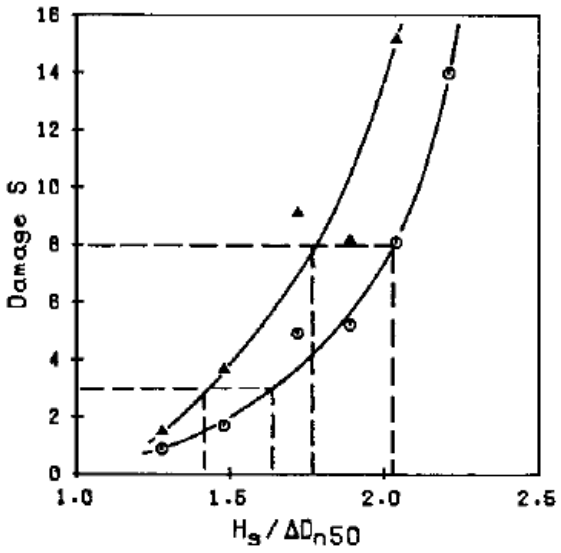

Figure 3.3: Typical damage curve

Van der Meer consequently fitted the experimental data to the following power function:

$$\frac{H_s}{\Delta D_{n50}} = a\xi_m^b \qquad \text{with} \qquad a = f(S, N, P, \cot\alpha) \tag{3.5}$$

To make this curve fitting, all other relevant variables, namely the damage level S, number of waves N, slope angle α and permeability of the structure P, have to be kept constant. For various groups of S, N and P the exponent b is determined. If these b values all have approximately the same value, the relation can be described by a single equation with an average b. If not, then multiple equations describe the relation. Which was the case for the surging wave region. Resulting in a formula for each structure:

$$\begin{aligned} \frac{H_s}{\Delta D_{n50}} &= a\xi_m^{0.1} && \text{impermeable} \\ \frac{H_s}{\Delta D_{n50}} &= a\xi_m^{0.5} && \text{permeable} \\ \frac{H_s}{\Delta D_{n50}} &= a\xi_m^{0.6} && \text{homogeneous} \end{aligned} \tag{3.6}$$

To write these equations as a single equation, the notional permeability P was defined as the b-values of the power function. The Van der Meer formula was thus made under the assumption that each structure has a constant P value under all circumstances.

After this step the equation was fitted to the other variables with the same curve fitting procedure. This eventually resulted in the known stability formula. Since all data points used in the curve fitting procedure are documented, the analysis can be redone. In this way, the actual spread in the three P-values of 0.1, 0.5 and 0.6 under different circumstances can be determined. The relevant data points can be found in Appendix B.

As stated before, all other variables have to be kept constant to perform the same curve fitting procedure. See Table 3.2 for the b-values for all possible combinations of variables. Note that this is only done for the data

points inside the surging wave region. The transition between plunging and surging waves is defined by the function:

$$\xi_m = (6.2P^{0.31}\sqrt{(\tan\alpha)})^{\frac{1}{P+0.5}} \tag{3.7}$$

This transition was determined after the curve fitting procedure as the intersection between the two stability formulas. Since this transition was not known in advance by Van der Meer, the found b-values may deviate slightly from the values found by Van der Meer. However, Van der Meer used a transition of approximately $xi_m = 3-4$. The exact value is not known and could well have been varied slightly depending on the amount of data points available.

Table 3.2: Curve fitting for each combination of S, N and $\cot\alpha$

	Impermeable		Permeable		Homogeneous	
S	$N=1000$	$N=3000$	$N=1000$	$N=3000$	$N=1000$	$N=3000$
			$\cot\alpha = 1.5$			
2	-	-	0.51	0.61	-	-
3	-	-	0.55	0.64	-	-
5	-	-	0.60	0.68	-	-
8	-	-	0.57	0.62	-	-
12	-	-	-	-	-	-
			$\cot\alpha = 2$			
2	0.07	0.27	0.56	0.46	0.82	0.54
3	-0.03	0.09	0.27	0.41	0.55	0.66
5	-0.05	0.05	0.21	0.57	0.67	0.42
8	0.38	-0.06	0.71	0.21	0.61	0.96
12	-	-	0.90	0.70	0.45	0.76
			$\cot\alpha = 3$			
2	0.06	0.20	-	-	-	-
3	0.01	0.18	-	-	-	-
5	-0.07	0.12	-	-	-	-
8	-0.09	0.10	-	-	-	-
12	-0.12	0.03	-	-	-	-
			$\cot\alpha = 4$			
2	-0.23	0.09	-	-	-	-
3	-0.29	0.01	-	-	-	-
5	0.01	-0.03	-	-	-	-
8	-0.09	-0.28	-	-	-	-
12	-0.32	-0.04	-	-	-	-
			$\cot\alpha = 6$			
2	-0.84	-1.07	-	-	-	-
3	-0.67	-0.93	-	-	-	-
5	-0.73	-0.78	-	-	-	-
8	-	-0.66	-	-	-	-
12	-	-	-	-	-	-

As can be seen in Table 3.2 not all combinations of variables result in a b-value. This is either because only

one data point is available or none at all. Furthermore, the only slope angle for which all three structures are tested is $\cot\alpha = 2$. This also seems to be the slope angle from which Van der Meer originally determined the b-values, since the b-values for the other slope angles deviate too much. The choice to neglect the other slope angles is acceptable since they do not supply information for all three structures.

In this way, the average b-values are found to be 0.09, 0.50 and 0.64 for the impermeable, permeable and homogeneous structures respectively. These values are very close to the values found by Van der Meer, especially because these were rounded to one decimal. The standard deviations in the b-values for each structure was found to be 0.15, 0.22 and 0.16 respectively. With this additional information, more is known about the spread or uncertainty of the notional permeability. This is visualized in Figure 3.4.

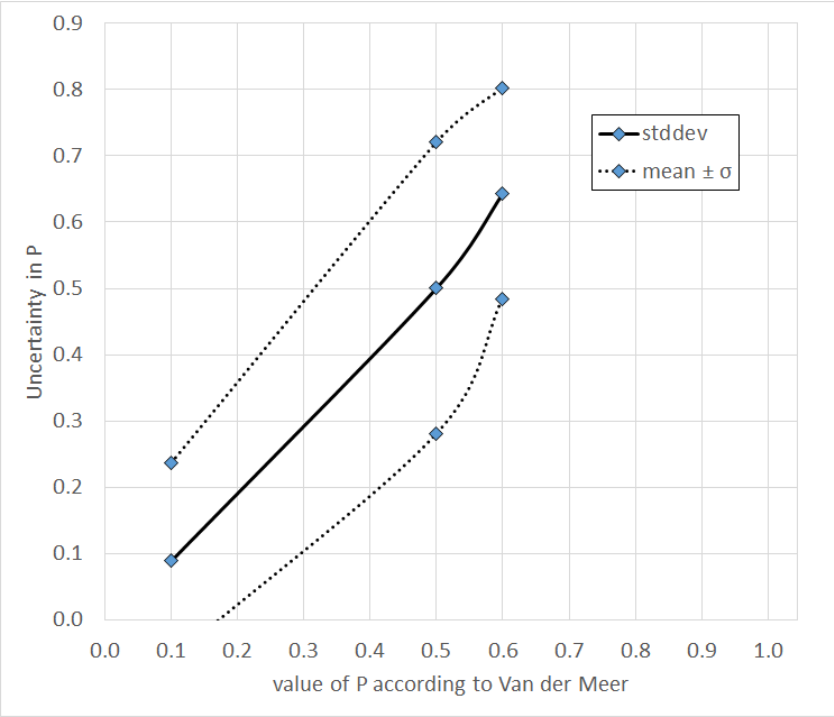

Figure 3.4: Uncertainty in the notional permeability (for the surging region)

3.6. OPTIMUM P-VALUE FOR DAMAGE PREDICTION

The four standard P-values are a result of an average best fit for several combinations of relevant parameters. It can therefore be seen as an average P-value for a particular structure under various conditions. In the first section of this chapter the uncertainty was determined, which gives insight in the spread in P-values for each structure based on the original physical model tests.

Taking the stability formula as given, the real P-values can be regarded as the values which give the best prediction for the damage. Since all other variables in the Van der Meer formula are known for all original model tests, the 'optimum' P-value for each physical test can be calculated. In this way all other unknowns and measurement errors are incorporated in the P-value as well, but it is assumed that these are small compared to the spread in P. The P-values are shown in Table 3.6.

Table 3.3: Optimum P-values for each test of the numerical test matrix

Test nr.	Remark	D_{n50}	Δ	$\cot\alpha$	H_s	ξ_m	$S_{N=1000}$	$S_{N=3000}$	$P_{N=1000}$	$P_{N=3000}$
36	Rock imperm	0.036	1.615	3	0.1002	2.91	4.93	9.11	0.09	0.07
37	Rock imperm	0.036	1.615	3	0.0860	3.12	1.71	3.66	0.07	0.09
38	Rock imperm	0.036	1.615	3	0.0742	3.35	0.89	1.48	0.10	0.11

Continued on next page

Table 3.3 – *Continued from previous page*

Test nr.	Remark	D_{n50}	Δ	$\cot\alpha$	H_s	ξ_m	$S_{N=1000}$	$S_{N=3000}$	$P_{N=1000}$	$P_{N=3000}$
51	Rock imperm	0.036	1.615	3	0.1145	3.66	9.90	18.41	0.05	0.04
52	Rock imperm	0.036	1.615	3	0.1049	3.85	3.76	6.40	0.04	0.04
53	Rock imperm	0.036	1.615	3	0.0975	4.00	3.49	5.26	0.07	0.09
54	Rock imperm	0.036	1.615	3	0.0799	4.45	0.83	1.50	0.03	0.04
55	Rock imperm	0.036	1.615	3	0.1120	3.71	7.02	9.14	0.08	0.19
85	Rock imperm	0.036	1.615	4	0.0991	2.18	3.16	5.56	0.09	0.08
86	Rock imperm	0.036	1.615	4	0.0695	2.61	1.50	1.91	0.01	0.01
88	Rock imperm	0.036	1.615	4	0.1190	2.70	7.42	13.36	0.05	0.04
89	Rock imperm	0.036	1.615	4	0.0830	3.25	1.53	1.74	0.01	0.06
90	Rock imperm	0.036	1.615	4	0.1084	2.87	6.01	9.41	0.01	0.01
91	Rock imperm	0.036	1.615	4	0.0965	3.04	3.55	5.56	0.01	0.01
92	Rock imperm	0.036	1.615	4	0.1396	2.47	15.34	28.75	0.08	0.07
104	Rock imperm	0.036	1.615	4	0.1806	1.30	3.60	6.02	0.01	0.01
258	Rock hom	0.036	1.615	2	0.1049	4.15	1.57	1.86	0.54	0.60
259	Rock hom	0.036	1.615	2	0.1384	3.59	4.83	8.77	0.66	0.65
260	Rock hom	0.036	1.615	2	0.1715	3.23	17.68	30.80	0.68	0.68
261	Rock hom	0.036	1.615	2	0.1532	3.42	10.02	15.33	0.65	0.67
262	Rock hom	0.036	1.615	2	0.1346	2.89	4.84	7.99	0.65	0.68
263	Rock hom	0.036	1.615	2	0.1805	2.51	16.48	27.30	0.57	0.60
264	Rock hom	0.036	1.615	2	0.1583	2.69	11.45	17.68	0.50	0.56
265	Rock hom	0.036	1.615	2	0.1053	3.25	2.60	2.47	0.46	0.69
266	Rock hom	0.036	1.615	2	0.1420	2.21	3.00	4.79	0.70	0.76
267	Rock hom	0.036	1.615	2	0.1679	2.09	5.96	12.04	0.71	0.60
268	Rock hom	0.036	1.615	2	0.1009	2.58	1.13	1.30	0.48	0.75
269	Rock hom	0.036	1.615	2	0.1882	2.02	10.64	18.76	0.64	0.62
270	Rock hom	0.036	1.615	2	0.1385	4.87	2.07	3.77	0.64	0.63
271	Rock hom	0.036	1.615	2	0.1613	4.39	6.07	10.30	0.64	0.64
272	Rock hom	0.036	1.615	2	0.1762	4.11	10.80	34.00	0.65	0.55
273	Rock hom	0.036	1.615	2	0.1111	5.57	1.09	1.29	0.52	0.57

The uncertainty in P and the optimum P-values as discussed above will eventually be used in the analysis of the numerical results.

4

EVALUATION OF THE NUMERICAL MODEL

In this chapter the numerical model is evaluated. The evaluation steps are shown in Figure 4.1. First the model performance is discussed, this mainly focuses on some problems encountered during the use of the model. Next, the validation steps from the figure are elaborated one-by-one. Finally, the numerical models for the final simulations are presented.

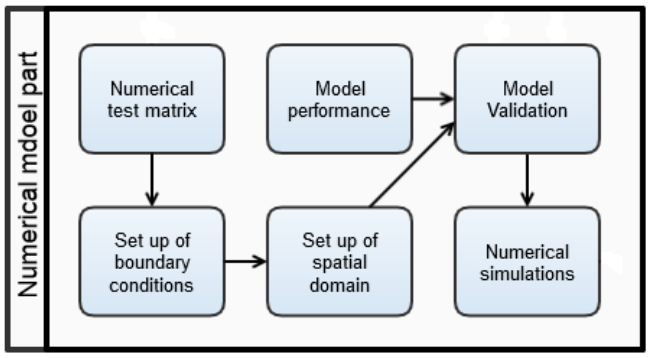

Figure 4.1: Overview of the numerical part

4.1. OVERVIEW

The numerical model used in this thesis is the IH2VOF model developed by Environmental Hydraulics Institute 'IH Cantabria', Spain. It is a 2D vertical numerical model which can simulate wave interaction with rubble mound breakwaters or revetments.

VARANS The model solves the Volume Averaged Reynolds Averaged Navier Stoke equations (VARANS). The RANS equations are solved with the k-ϵ turbulence closure model. The 'Volume Averaging' part is the method which enables the simulation of flow through porous media. The basic idea behind this adaption of the RANS equations is illustrated in Figure 4.2.

As illustrated in the figure the RANS equations are not solved at each point inside the pores, but the equations are solved for a specific volume (in this case 2D) of the porous media. For which a certain quantity is averaged over the volume as follows:

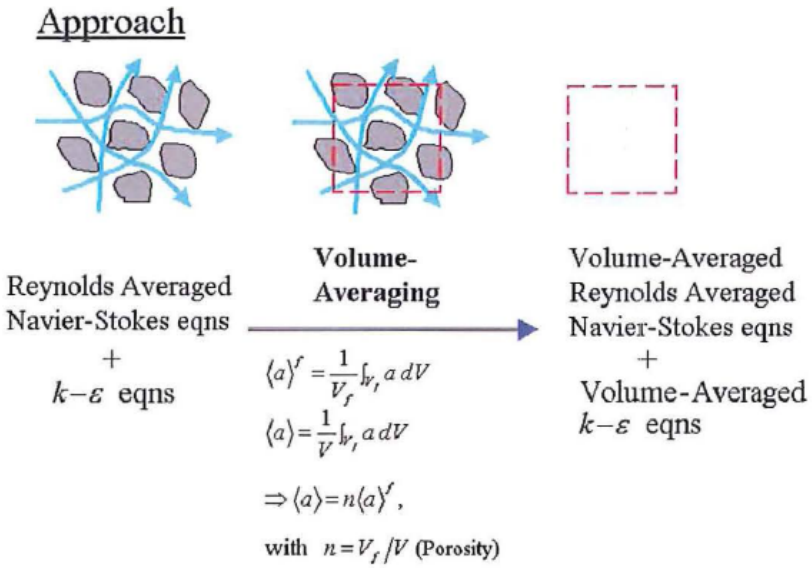

Figure 4.2: Illustration of the Volume Averaging method, from Cantabria (2012)

$$\langle a \rangle = \frac{1}{V_f} \int a dV \tag{4.1}$$

Where '<>' denotes the intrinsic volume averaging. If the quantity a is the flow velocity, the equation returns an average filtration velocity since the integral is divided by the fluid V_f (and not the total volume), rather than the seepage velocity.

After applying this volume averaging method to the RANS equations two additional terms arise; a residual stress (which arise in the same way as the Reynolds stresses after Reynolds averaging) and a term representing the momentum transfer between the fluid phase and solid material. The VARANS equations can now be used to describe flows in porous media, while only supplying the porosity of this media. However, analogous to the requirement of a turbulence closure model to solve the Navier Stokes equations after Reynolds Averaging, a closure model is needed to close the equations after Volume Averaging. This closing is done using the extended Forchheimer equations.

With the introduction of the Forchheimer equations four additional variables are introduced into the equations, namely the laminar and turbulent Forchheimer coefficients, added mass coefficient and the nominal diameter. These variables must be given as input and describe the corresponding porous media.

Volume Of Fluid The Volume Of Fluid (VOF) method used by the model allows tracking of the free surface. The location of free surface is found by analysing the density change in each cell. In this way the model can identify three cell types: empty (no fluid / air), interior (fully occupied by fluid) and surface (partially occupied by fluid). The VOF function is defined as follows:

$$\begin{aligned} F &= \frac{\rho}{\rho_f} \\ \rho &= \frac{\rho_f V_f}{V_f + V_a} \end{aligned} \tag{4.2}$$

F is introduced in the equation of mass conservation, which leads to the transport equation for F:

$$\rho(x,y,t) = F(x,y,t)\rho_f$$
$$\frac{\partial F}{\partial t} + \frac{\partial}{\partial x}(\bar{u}F) + \frac{\partial}{\partial y}(\bar{v}F) = 0 \tag{4.3}$$

With this equation F can be solved. A value of 1, 0 and >0 indicate an interior, empty and surface cell respectively.

Computational domain The VARANS equations are discretised with an orthogonal grid structure. The cell spacing can vary over the computational domain, allowing for a finer grid at certain locations. See Figure 4.3.

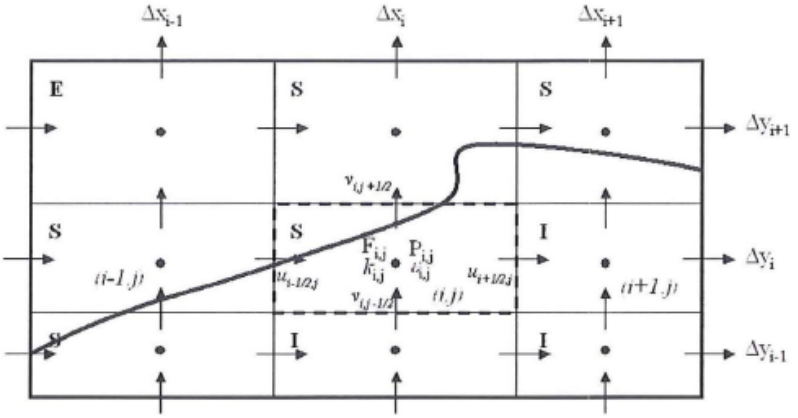

Figure 4.3: Computational domain

All scalar quantities are defined in the centre of the cells. The scalar quantities are: pressure, turbulent kinetic energy, dissipation rate, VOF function and an openness function. The vector quantities of horizontal and vertical flow velocity and two additional openness functions are defined at the faces of the cells.

Because of the orthogonal grid choice, sawtooth-shaped surfaces arise when defining solid boundaries under a slope. Since the surfaces will be defined at the cell faces. This often leads to non-physical reflections at these boundaries. Therefore, the model uses a different method of partial cell treatment. The method consists of modelling solid objects as fluids with an infinite density. This introduces the openness functions θ. This function is a ratio of space not occupied by an solid object over the total space. At the cell centre θ_c equals the ratio of 'open space' over the cell area. At the cell top and right faces, θ_t and θ_r are defined as the ratio of length of 'open space' to the total length of the cell face. With this function, the model can thus identify if a cell corresponds to a solid object, fluid domain or a solid-fluid domain. The openness function is is similar to the VOF function, with the only difference that the openness function does not change with time (solid boundaries do not move). In case a cell is identified as a fluid domain, the VARANS equations are solved with the density of water. In case a cell is identified as a solid domain, the VARANS equations are skipped. In case a cell is identified as a solid-fluid domain, the equations are solved with a special porosity value which is linked to the openness function.

4.2. MODEL ISSUES

During the first few tests with the numerical model several model settings were tested, such as the wave series generation, static and dynamic paddles, boundary absorption and turbulence model. Some problems were found, which are briefly discussed below.

Wave generation The Matlab GUI of the numerical model offers three options to generate the wave series for the boundary condition. The first option is to supply the type of wave to be generated (solitary, regular, irregular) and a number of relevant variables such as significant wave height, (peak) period and series length. The second option is to load a previously generated wave series, which allows one to use exactly the same boundary condition in several different simulations. The third is to 'reconstruct' a wave series from a user supplied file which contains a water level elevation time series. With this option an observed wave series in the field can be used as a boundary condition in the model, for example. The model reads the user input and calculates the corresponding variance density spectra. For some reason however, the tail of the spectra 'disappears' somewhere in the calculation. This does not happen in all cases and the frequency where the tail 'disappears' also seems to vary. This was discovered by calculating the variance density spectra of the input wave series and the wave series file which is written by the model. Figure 4.4 shows an example.

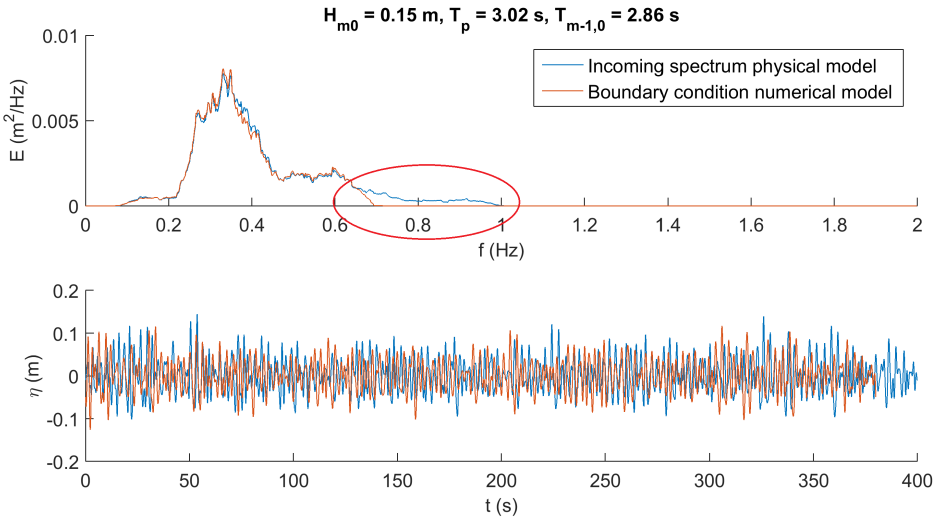

Figure 4.4: Wave series reconstruction error

Figure 4.4 shows the largest deviation between the two spectra tails of all cases where a wave series was reconstructed in this report. The effect on the final results is considered negligible since the variance density is small relative to the other frequencies.

Paddle The numerical model offers two options to impose the boundary condition. The first is a static paddle, which, simply said, raises the water level at the boundary to generate waves. The second is a dynamic paddle. The dynamic paddle simulates a paddle which would be used in a physical flume, by oscillating a paddle in horizontal direction. In the model this is achieved by changing the openness function of the boundary cells in time, which effectively creates a moving solid object at the boundary (see the previous section). With suggested initial and maximum positions from the manual (Cantabria, 2012), large deviations in the water level elevation time series halfway along the flume were observed. Several other settings were tested without better results. Since the static paddle did produce good results, the static paddle was chosen to be used in this report. The reason why the dynamic paddle did not work was not further investigated.

Turbulence closure model Turbulence is by default switched off in the model. This means that the Reynolds stresses in the (VA)RANS equation are not solved and are equal to zero for the whole simulation. Therefore turbulence is not modelled. If turbulence is switched on, the Reynolds stresses are solved with the $k-\epsilon$ closure model. In flows where turbulence is important, this is necessary for a proper modelling of the flow. However, during the first tests some of the simulations encountered an error when the turbulence was switched on. It appeared that if a simulation was run long enough the turbulence closure model would eventually lead to an error. Therefore, turbulence had to be switched off for all models. It is assumed that turbulence in front of the structure does not play a major role, and that the effect of turbulence inside the structure is fully incorporated in the equations through the turbulent Forchheimer coefficient.

Turbulent Forchheimer coefficient The turbulent Forchheimer coefficient β is calculated in the model as follows:

$$\begin{aligned} \beta &= \beta_c \frac{1+7.5}{KC} \\ KC &= \frac{UT}{nD_{50}} \end{aligned} \tag{4.4}$$

KC is the Keulegan-Carpenter number. β is in this way dynamically updated each time step based on the maximum velocity inside the porous media and the mean wave period. Changing the variable *xxt* in the input file allows the user to use another representative period value for this calculation. However, several model tests with varying values for T showed exactly the same results. Investigation of the source code showed that this is because the model first reads the *xxt* value from the input file and consequently overwrites this values with the mean period. The source code was adjusted to fix this issue and an additional output line for the command prompt was added to show the value of *xxt* for each iteration. See Figure 4.5.

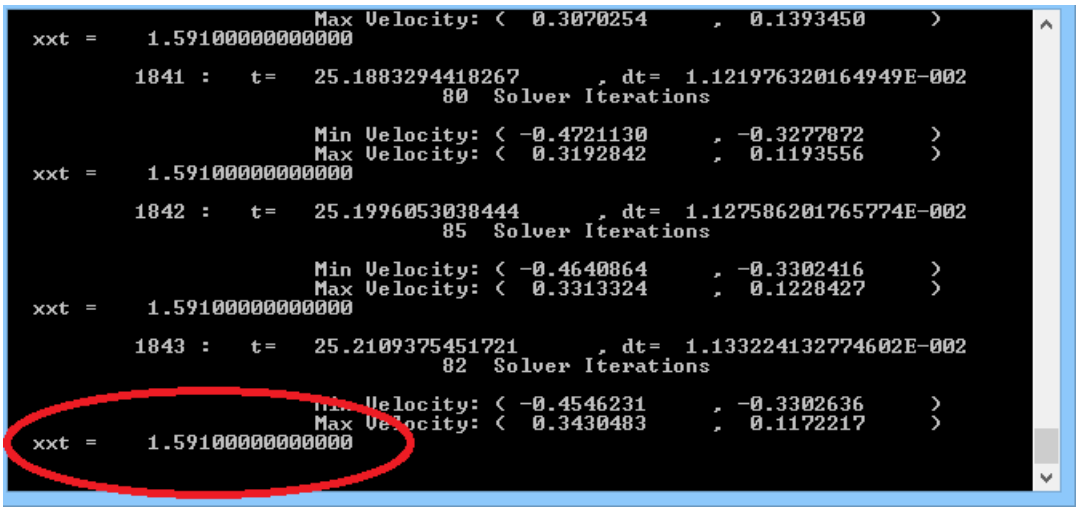

Figure 4.5: Command prompt showing an adjusted source code

Inconsistencies between the manual and source code Some inconsistencies between the description of the volume averaging closure model (Forchheimer equation) in the manual and the actual equation used in the source code were found. The equation in the manual is as follows:

$$\ldots = \frac{\alpha\nu(1-n)^2}{n^2 D_{50}^2}\langle\overline{u_i}\rangle + \frac{\beta(1-n)}{nD_{50}}\sqrt{\langle\overline{u_1}\rangle^2 + \langle\overline{u_2}\rangle^2}\langle\overline{u_i}\rangle + c_A\frac{\partial\langle\overline{u_i}\rangle}{\partial t} \tag{4.5}$$

(the gravitational acceleration is incorporated as a separate vector in the equations)

With suggested values of: $c_A = 0.34\frac{1-n}{n}$, $\alpha = 200$ and $\beta = 1.1$. From this equation the coefficient of the extended Forchheimer equation can be read. They are listed along with the coefficients used in the source code and in Equation 2.10, see Table 4.1.

Fortunately, the equation in the source code corresponds with literature. Unfortunately, it was only later in this research discovered that there was a slight error in the manual. The manual suggest a value of $c_A = 0.34\frac{1-n}{n}$, which is called the added mass coefficient in the manual. However, in the source code γ is used as the added mass coefficient and should therefore not be multiplied by $\frac{1-n}{n}$ this coefficient was overestimated for all numerical simulations. However, the effect on the results is considered small because of the small influence of c in the first place, see Figure 2.9

Table 4.1: Forchheimer equation in manual vs. source code

	Manual	Source code	Literature
a	$\frac{\alpha\nu(1-n)^2}{n^2 D_{n50}^2}$	$\alpha\frac{(1-n)^2}{n^3}\frac{\nu}{D_{n50}^2}$	$\alpha\frac{(1-n)^2}{n^3}\frac{\nu}{gD_{n50}^2}$
b	$\frac{\beta(1-n)}{nD_{n50}}$	$\beta\frac{1-n}{n^3}\frac{1}{D_{n50}}$	$\beta\frac{1-n}{n^3}\frac{1}{gD_{n50}}$
c	c_A	$\frac{1+\gamma\frac{1-n}{n}}{n}$	$\frac{1+\gamma\frac{1-n}{n}}{ng}$

4.3. BOUNDARY CONDITIONS

In this section it is investigated if the imposed wave conditions in the numerical model resemble the wave conditions of the physical model tests. Van der Meer (1988) gave the three variance density spectra (PM, wide and narrow) for one specific set of significant wave height and average wave period, which were used as a boundary condition in the research. See Figure 4.6.

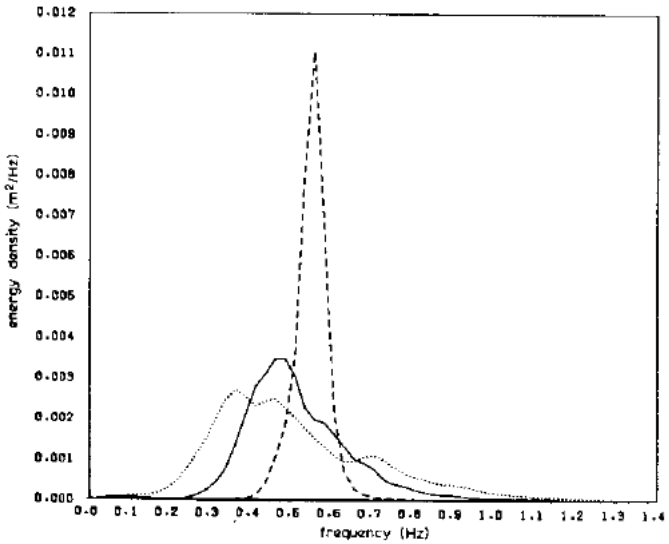

Spectrum	H_s (m)	T_m (s)	T_p (s)	κ_f	$\kappa_{HH,t}$
..... wide	0.122	1.81	2.67	0.25	0.48
——— PM	0.116	1.84	2.17	0.47	0.62
- - - - - narrow	0.119	1.79	1.79	0.90	0.92

Figure 4.6: Three spectra used in the original physical model tests

The numerical program calculates an energy density spectrum from a significant wave height, peak period, and a peak enhancement factor. The peak enhancement factor actually determines the type of spectrum. A value of 3.3 produces a JONSWAP spectrum and a value of 1.0 a Pierson-Moskowitz spectrum, see equation 4.6. From this spectrum a wave series is calculated. In the numerical test matrix only a PM spectrum is used, so the peak enhancement factor should be set to 1.0.

$$E(f) = \underbrace{\alpha g^2 (2\pi)^{-4} f^{-5} \exp\left[-\frac{5}{4}\left(\frac{f}{f_{peak}}\right)^{-4}\right]}_{\text{Pierson-Moskowitz}} \underbrace{\gamma^{\exp\left[-\frac{1}{2}\left(\frac{f/f_{peak}-1}{\sigma}\right)^2\right]}}_{\text{JONSWAP}} \tag{4.6}$$

An ideal PM spectrum with values from Figure 4.6 has been calculated with the Matlab GUI. Based on this spectrum, the model returns a wave series by means of the random-phase amplitude model. From this wave series the actual energy density spectrum has been calculated with a Fast Fourier Transform algorithm, see Appendix A for the matlab script. This spectrum was compared to PM spectrum of Van der Meer, henceforth called the 'vdM PM spectrum'. It appeared that the vdM PM spectrum had a significantly higher peak. Comparison between the vdM PM spectrum and an ideal PM spectrum , calculated from Equation 4.6, showed the same result. Apparently, the vdM PM spectrum is not an ideal PM spectrum, but is better resembled with a JONSWAP spectrum with a peak enhancement factor of $\gamma = 1.5$, see Figure 4.7. The figure shows that for $\gamma = 1.5$ the spectral peaks have approximately the same value. The energy in the lower frequencies is higher for the vdM PM spectrum than for the ideal spectrum. However, this is not the case for the spectrum calculated from the wave series. The tail of the spectrum is higher than the tail of the vdM PM spectrum, but the difference is small. It should be noted that the spectra have been calculated with a Fast Fourier Transform algorithm, and is an (moving) average of the raw spectrum. Especially the height of the spectral peak is influenced by the frequency range over which the energy density is averaged. A smaller frequency range results in a more erratic spectrum.

Since a JONSWAP spectrum with a peak enhancement factor of $\gamma = 1.5$ gave the best fit to the Van der Meer PM spectrum, the same factor will be used to calculate the other spectra in the test matrix. All boundary conditions can be found in Appendix C.

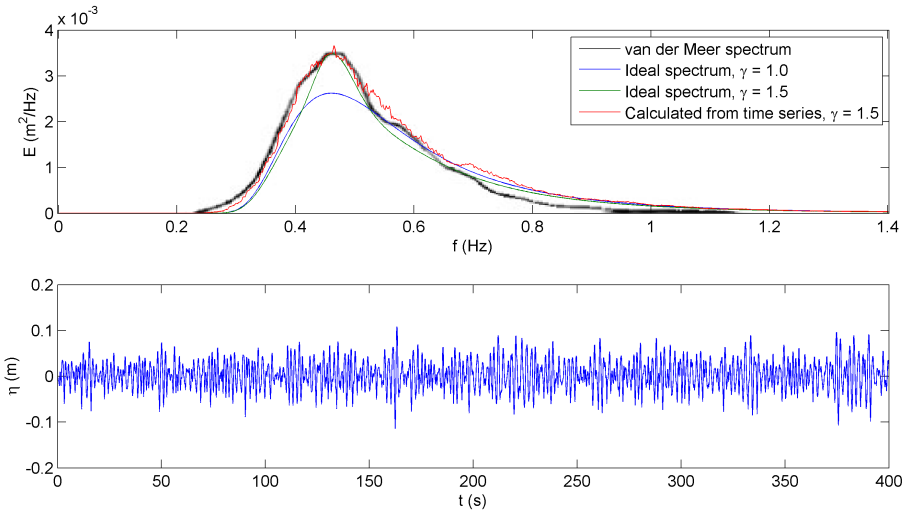

Figure 4.7: Above: comparison of the van der Meer PM spectrum and a spectrum from the numerical model. Below: corresponding water level time series

4.4. MODEL SET-UP

A whole range of numerical model tests will be carried out in this study, but first the numerical model has to be tested and choices have to be made for the spatial resolution and simulation time. First of all the structures to be tested are drawn with CORAL, which produces the mesh files for the IH-2VOF software. The structures from the physical model tests are shown in Figure 4.8.

Domain size In the physical model tests a wave flume with a length of 50 m was used. For a numerical calculation this seems to be unnecessary large. The manual of the software states that two times the wavelength in front of the structure should be sufficient to allow for the dissipation of (numerical) errors from the boundary. The largest peak period from the test matrix is 3.7 s, see Table 3.1. This results, together with a water depth of 0.8 m, in a wavelength of 10 m. Allowing 5 m space for the structures, the total domain length becomes 25 m.

The three models that will be used are shown in Figure 4.9.

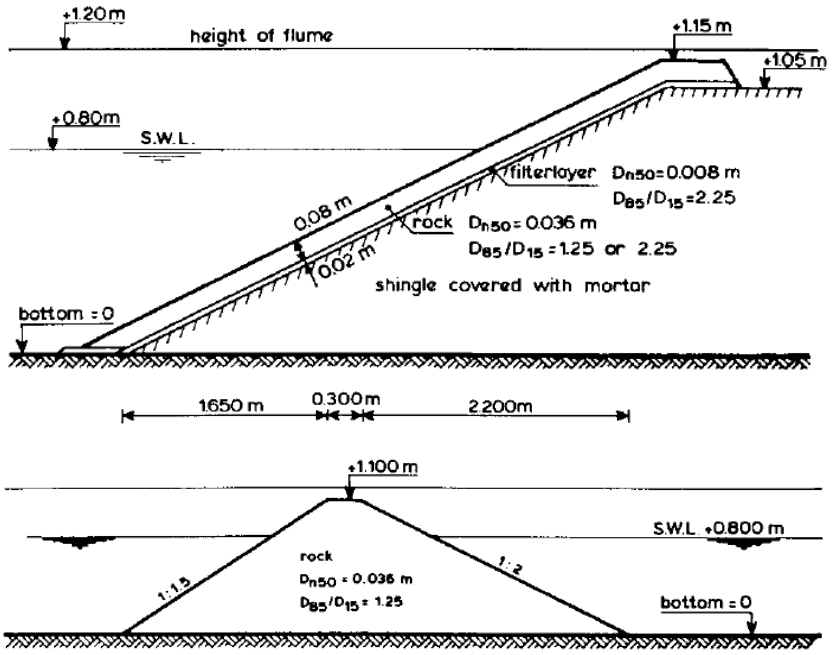

Figure 4.8: Physical model test set-up, impermeable structure $P = 0.1$ (above) and homogeneous structure $P = 0.6$ (below), the impermeable structure has a variable slope

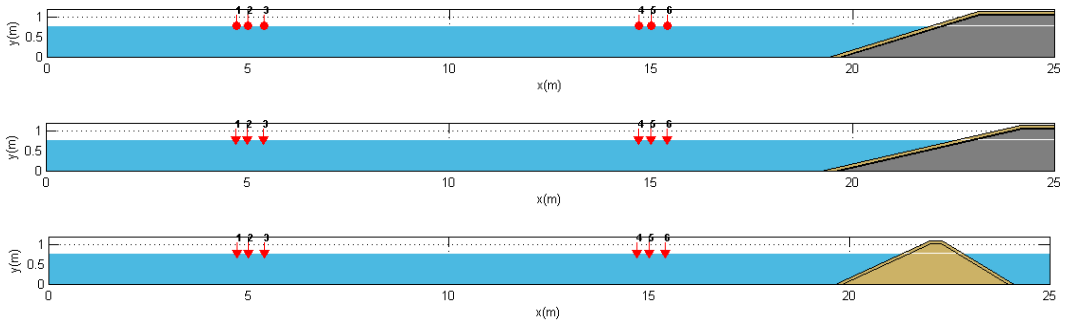

Figure 4.9: Domains used in the numerical model

Grid size Next, the grid size has to be chosen. In this paragraph the spatial resolution which is sufficient for accurate results is determined. A very small grid size, namely $\Delta y = 0.005$ m and $\Delta x = 0.010$ is chosen as a benchmark. This is practically the smallest grid size possible with respect to an acceptable computational time. The values for Δy and Δx are dependent on each other via $\Delta x < 2.5\Delta y$, which follows from the requirement to prevent the false breaking effect (Cantabria, 2012).

With the choice for a grid size, the layer thicknesses of the breakwaters have to be taken into account. After all, this is the main area of interest for this study. The smallest layer thickness is 0.02 m. Since only rectangular grids can be used in the model, it has to be understood when the model 'choses' to assign a grid cell as a certain layer. See Figure 4.10 for an illustration. This figure shows that the rectangular form of the grid cells is far from ideal to represent layers on a slope. One could make the grid cells much smaller for a smoother representation of the layers, but this would amount to huge computational times and would not be feasible. Therefore, a choice is made that the thinnest layer (0.02 m, see Figure 4.8) should always be represented by at least two cells in the horizontal, see Figure 4.10. In this way the layer is basically split up in at least two 'sub-layers', so results can be obtained near each boundary of the filter layer. From this it follows that the maximum grid size is $\Delta y = 0.015$ m and $\Delta x = 0.030$ (for the steepest slope of 1:3).

From this basic idea, 5 models are investigated, each with different grid sizes, ranging from a vertical grid size of 0.015 m until 0.010 m. The limit is set at 0.010 m for practical reasons with respect to computational time.

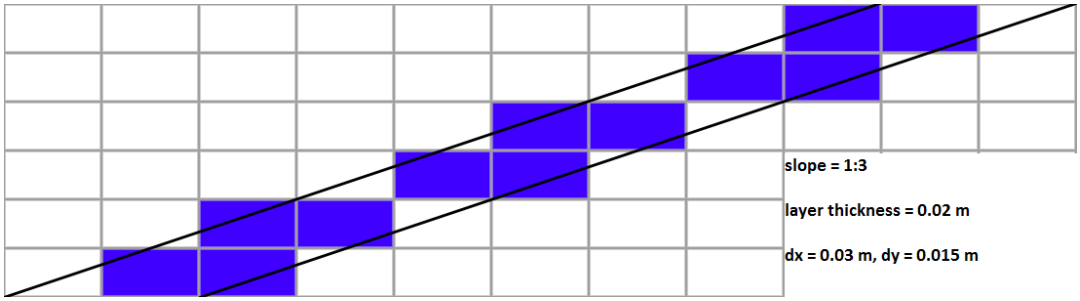

Figure 4.10: Grid cells inside the thinnest layer, blue cells represent actual filter layers cells

The wave conditions from test number 269 (see Table 3.1) are imposed on the 5 models since these waves have the largest steepness of all the tests. It is thus expected that this wave series requires the smallest vertical grid size to produce accurate results. For practical reasons each model is only simulated for 100 seconds. 5 meter in front of the structure the free surface elevation time records are obtained for each model and the root mean square error compared to the free surface elevation of the benchmark model is calculated. The result is shown in Figure 4.11.

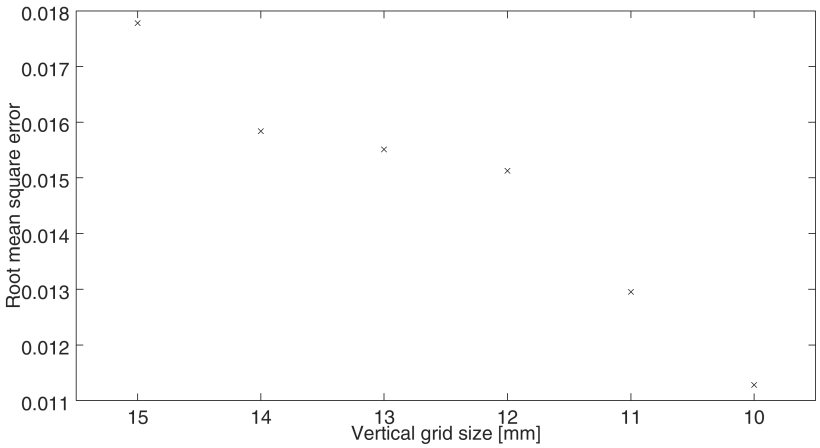

Figure 4.11: Root mean square error against mesh size

The root mean square error converges towards zero, which indicates that the model results also converges for smaller grid sizes. To determine the required spatial resolution an estimate of H_{m0} is used, which is intuitively an important parameter for armour layer stability. See Figure 4.12. The value for H_{m0} slowly converges towards the benchmark value. In Table 4.2 the difference in percentage from the exact value is shown. Hereby it is assumed that the calculated value of H_{m0} from the benchmark model is the exact solution. As can be seen from the table, the difference in percentage is more or less the same from a vertical grid size of 0.012 m. Chosing a finer grid than this, does not result in a more accurate representation of H_{m0}. Therefore a grid size of $\Delta y = 0.012$ m and $\Delta x = 0.024$ is used henceforth.

Simulation period In this paragraph the required simulation period is determined. Since the model does not measure damage levels, the number of waves to this respect is unimportant. I.e. in laboratory tests, one would measure damage levels a couple of times after some number of waves until it reaches an equilibrium. The thought behind these numerical tests is that the simulation period should be long enough (i.e. enough waves should be generated) to capture the whole variance density spectrum. Therefore the model is simulated several times with different simulation periods. Afterwards the variance density spectra 5 meter in front of the structure are analyzed and compared to the imposed spectra.

For these tests the wave condition from test number 271 is used, since these waves have the largest peak period and should thus require the longest simulation period. The variance density spectrum for test number

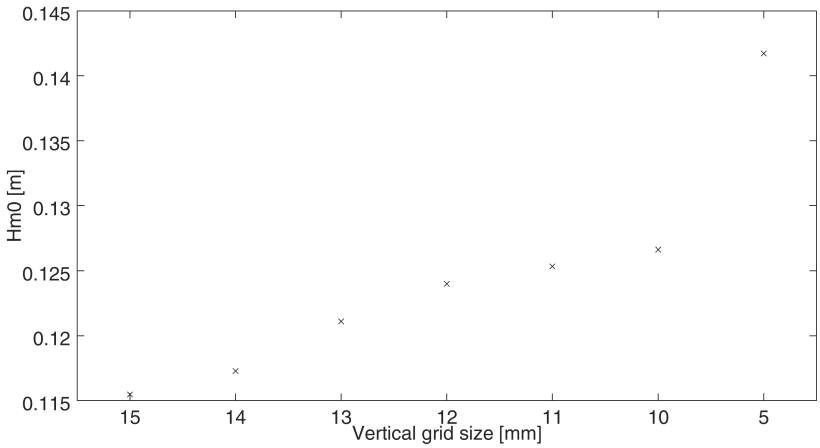

Figure 4.12: Zero-order wave height against mesh size

Table 4.2: Difference in zero-order wave height between model tests and benchmark

Vertical cell size [mm]	H_{m0} [m]	Difference from benchmark [%]
15	0.116	19
14	0.117	17
13	0.121	15
12	0.124	12
11	0.125	12
10	0.127	11
5	0.142	-

271 is shown in Figure 4.13

Seven models have been tested, with wave series periods ranging from 100 until 700 seconds. The free surface elevation time records 5 meter in front of the structure are stored. With a Fast Fourier Transform algorithm these free surface time records can be transformed back into variance density functions. See Figure 4.14 for the results.

From Figure 4.14 it can be seen that the spectra all have a 'gap' where the peak should be and an additional peak at the tail. This is probably due to reflection from the structure. If one looks closely, it can also be seen that the spectra for simulation periods ranging from 300 until 700 seconds are quite similar, while the spectra for simulation periods of 100 and 200 seconds show a larger deviation from the imposed spectrum. Therefore it can be concluded that a simulation period of at least 300 seconds is required. This is also illustrated by the root mean square error between the spectra and the imposed spectrum, see Figure 4.15. A conservative simulation period of 400 seconds is chosen for the final simulations.

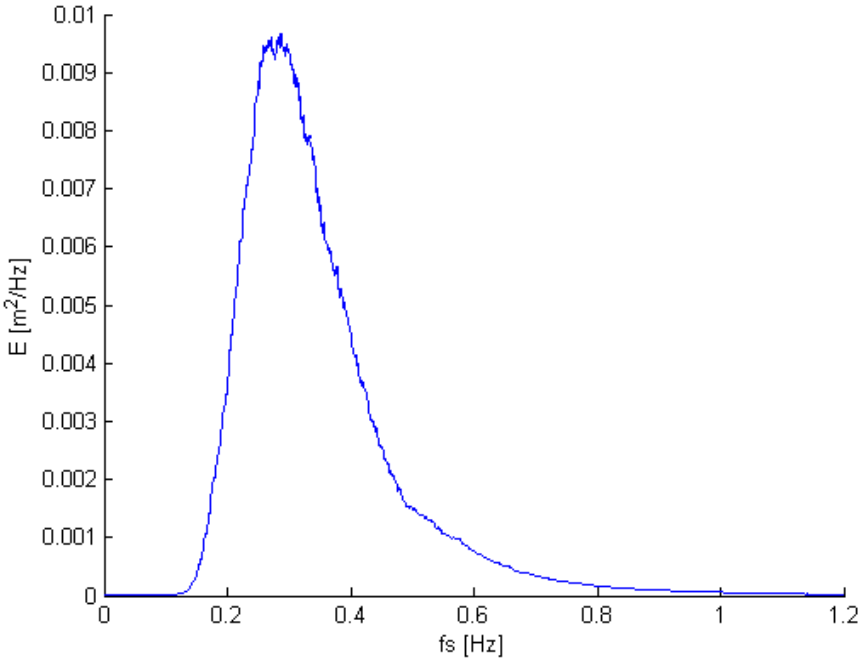

Figure 4.13: Imposed spectrum for test number 271

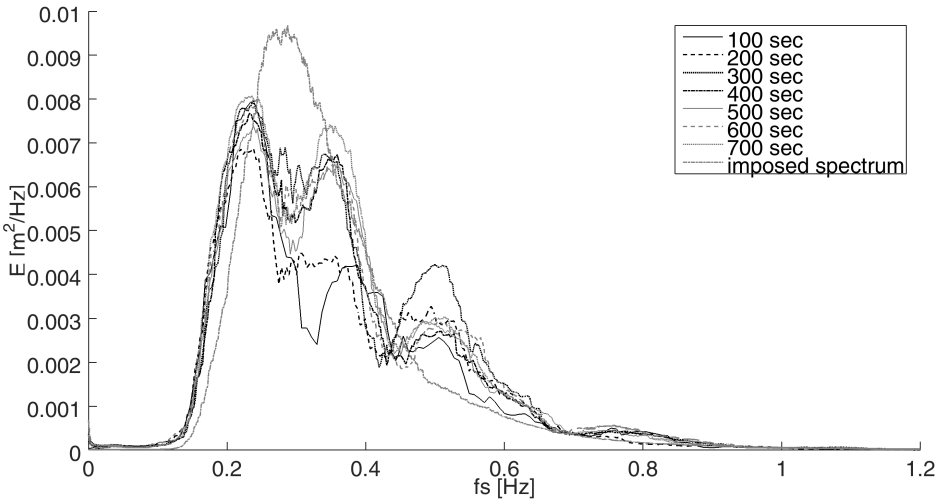

Figure 4.14: Spectra 5 meters in front of the structure, for different simulation lengths

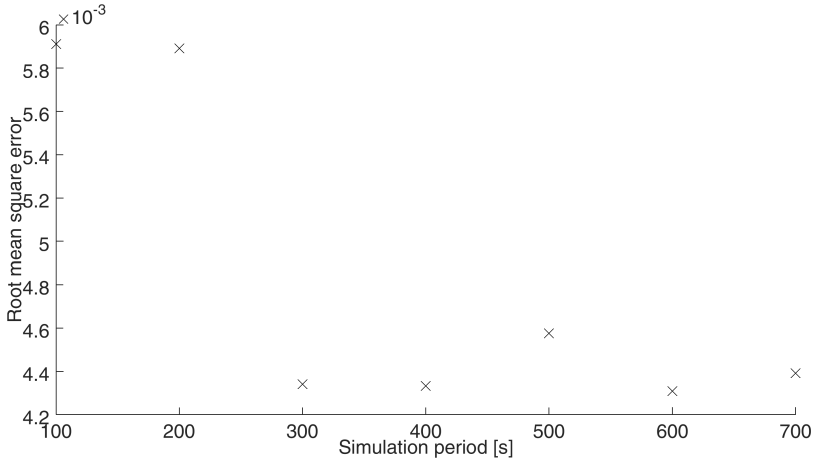

Figure 4.15: Root mean square error against simulation period

Final model The final model thus consist of a grid size of $\Delta y = 0.012$ m and $\Delta x = 0.024$ and a simulation period of 400 seconds. The time scale of the calculation is automatically chosen by the program and varies during the calculations. With the current settings one model tests takes around 12 hours to complete. However, the source code is written single-threaded so multiple models can be calculated simultaneously on computers with a multi-core processor. It is unfortunately not possible to calculate one model parallel on multiple cores.

4.5. MODEL VALIDATION

In this chapter the validation of the numerical model based on relevant variables is discussed. To validate the numerical model a number of comparisons have te be made with physical model tests to assess the overall performance of the numerical model and the influence of the different settings. The model has to be validated with respect to relevant variables for this research. These were obtained from literature research in Chapter 2 and applied to the Buckingham Π theorem in Chapter 3. The variables are repeated below.

u	flow velocity
Δp	pressure difference
α	laminar Forchheimer coefficient
β_c	turbulent Forchheimer coefficient
γ	added mass coefficient
n	porosity
D_{n50}	nominal stone diameter
g	gravitational acceleration
ν	kinematic viscosity
T	characteristic period

Six of these variables are required as input, these are $\alpha, \beta_c, \gamma, D_{n50}, T$ (because the numerical program solves the Forchheimer equations) and n (because of the volume averaging). This leaves the flow velocity and pressure difference as variables on which the model can be validated. Since this research focuses on the notional permeability, only measurements from inside a breakwater structure are of interest.

Kik (2011) and Kluwen (2012) both measured pressure differences at specific points inside the breakwater during their physical model tests. Although it is stated in both reports that these measurements are sensitive to errors due to the delicate measurement method, they will be used to validate the model.

Selection of physical model tests Initial numerical model tests with standard input values showed a better resemblance with the physical model tests by Kik (2011) compared to the tests by Kluwen (2012). Therefore results from Kik (2011) will be used to calibrate the model. After a satisfactory calibration the same settings will be applied to the results from Kluwen (2012).

Table 4.3 shows the testmatrix for structure 1 of Kik. After analysis of the water elevation and pressure difference time signals, test 1, 3, 4 and 6 are chosen for calibration. Other tests contained too much disturbances in the time signals. For each test a period of 400 seconds (equal to the numerical simulation period) is chosen during which no disturbances in the time signals are observed. This period ensures a minimum of 100 waves per simulation.

Table 4.3: Test matrix for structure 1 of Kik (2011)

Test nr.	H_s [m]	T_m [s]	T_p [s]	ξ_m
1	0.15	1.39	1.82	2.24
2	0.15	1.80	2.35	2.90
3	0.15	2.22	2.90	3.58
4	0.15	2.80	3.66	4.52
5	0.15	3.30	4.31	5.32
6	0.15	3.60	4.71	5.81

The four tests were all performed on the same structure, see Figure 4.16. During these tests several pressure difference gauges were placed inside the structure at 0.46 meter from the bottom. These measured the pressure difference over one layer and between the atmosphere and the armour layer surface.

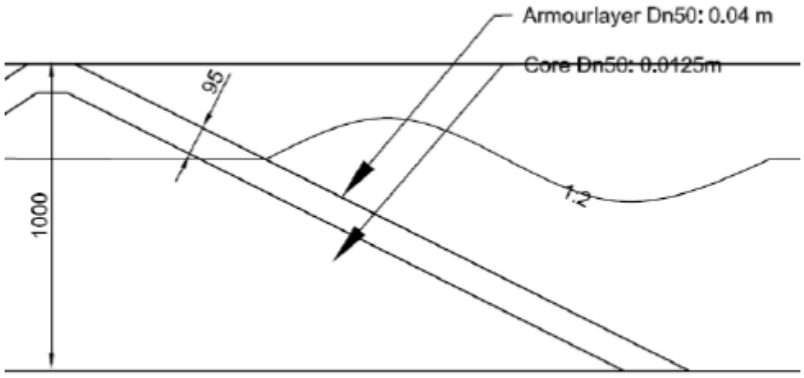

Figure 4.16: Structure 1 of Kik (2011)

Boundary conditions To accurately reproduce the wave conditions from the physical model tests in the numerical model, the surface elevation time series is decomposed into an incoming signal and a reflected signal. This is done by first transforming the wave series to a variance density spectrum. This spectrum is decomposed in an incoming and reflected spectrum, by means of matrix decomposition (Zelt and Skjelbreia, 1992). Consequently the incoming wave series is calculated from the incoming spectrum by means of the random-phase amplitude model. This incoming signal is directly used as a boundary condition in the numerical model. An example of spectrum decomposition is show in Figure 4.17.

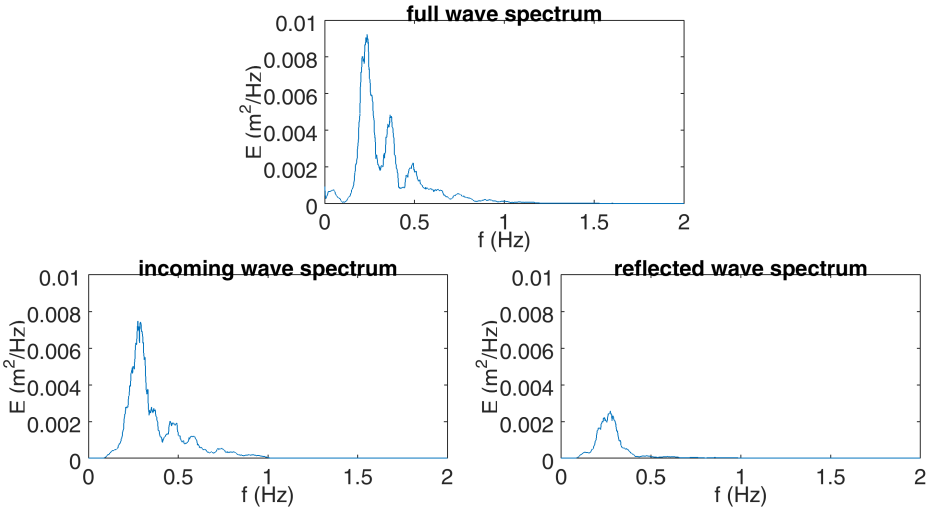

Figure 4.17: Variance density spectrum decomposition

Validation procedure To run the model the Forchheimer coefficients, added mass coefficient and porosity and nominal stone diameter have to be given as input values. Especially the physical inputs contain a large uncertainty. The porosity is unknown as well. For all layers the porosity is estimated at a value of 0.4. The nominal stone diameter can be read from Figure 4.16.

From several physical model test summarised by Troch (2000) it is clear that the laminar Forchheimer coefficient varies approximately between 0 and 10,000. The turbulent coefficient between 0 and 10. And the non-stationary coefficient between 0 and 1.

As stated in Chapter 2, the Forchheimer coefficients cannot be exactly calculated and thus have to be estimated. The model validation will largely consist of acquiring the right Forchheimer coefficient values to accurately simulate the flow inside a breakwater under wave attack.

Based on research of Lara *et al.* (2011), the software manual proposes the following α and β values:

$$\alpha = 4409.22 D_{50}^{0.43}$$
$$\beta = 12.27 \frac{n^3}{(1-n)^{1.5}} D_{50}^{-0.1075}$$
$$c = 0.34 \frac{1-n}{n}$$

The representative period is usually chosen equal to the mean wave period.

A first model run is made with these standard values and will be used as a benchmark henceforth, see Table 4.4.

Table 4.4: Model validation, test 1

Test nr.	Layer	α	β	c	n	T
1	armour	1100	2.4	0.51	0.4	T_m
	core	700	2.7	0.51	0.4	T_m

Wave conditions The model validation primarily concerns the pressures inside the breakwater, but the wave conditions in front of the structure must off course also resemble reality. This is visualised first in Figures 4.18-4.20. The figures of the surface elevation time series and the full and decomposed spectra all show a good comparison between the physical and numerical models. Thus, it is concluded that the wave conditions in front of the structure are simulated correctly.

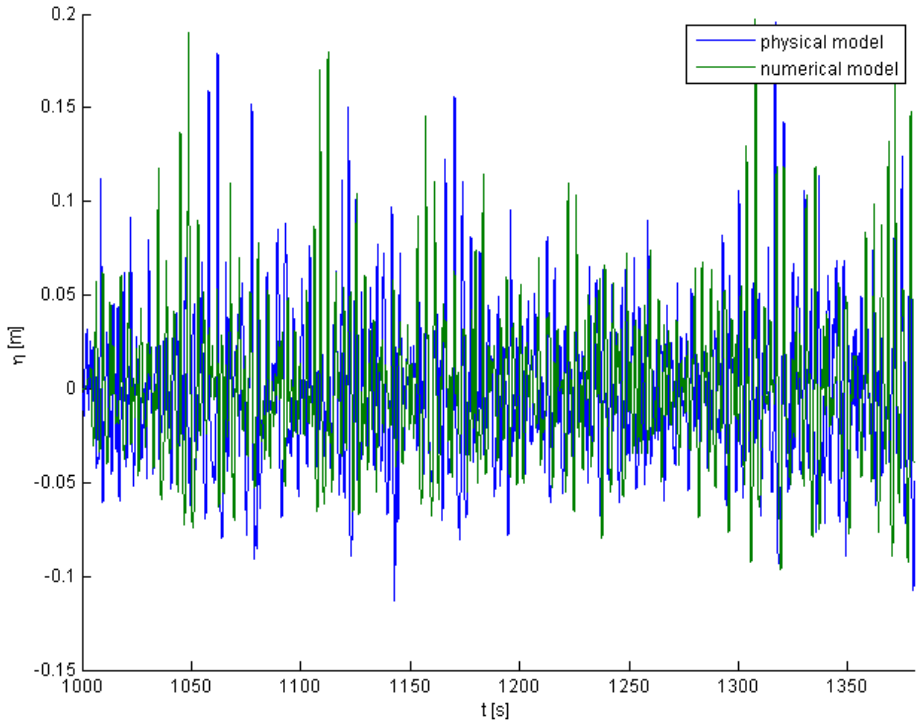

Figure 4.18: Surface elevation time series of validation test 1 of test 4 by Kik (2011)

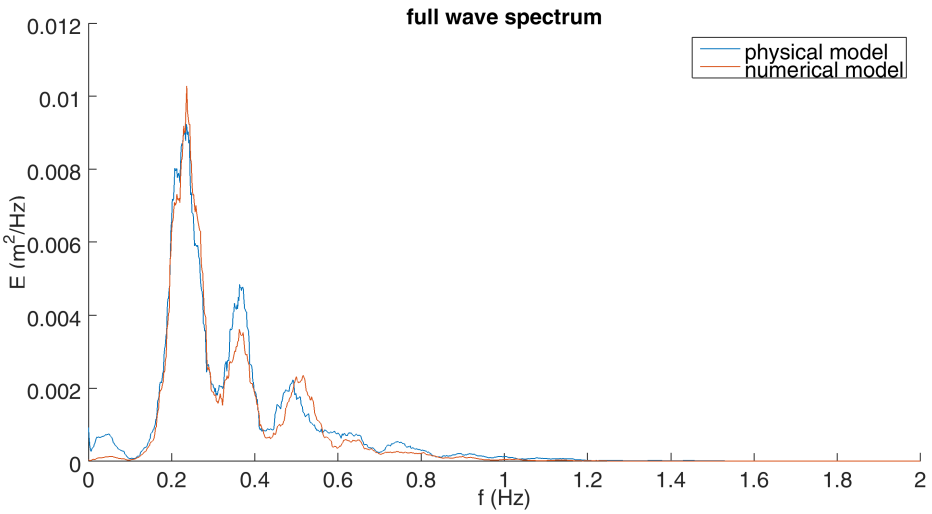

Figure 4.19: Full spectrum of validation test 1 of test 4 by Kik (2011)

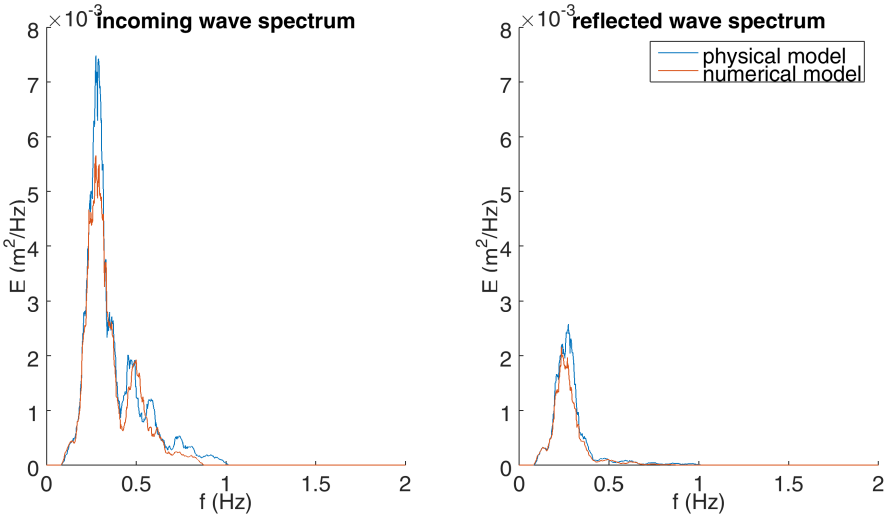

Figure 4.20: Decomposed spectrum of validation test 1 of test 4 by Kik (2011)

Validation The pressures inside the breakwater are analysed with a plot of the maximum hydraulic gradient, the maximum and minimum horizontal pressure deviation from the mean and an energy density spectrum of the pressure time signal, see Figures 4.21-4.23. Pressures are expressed as hydraulic heads in meters and are measured 0.46 m from the bottom of the flume.

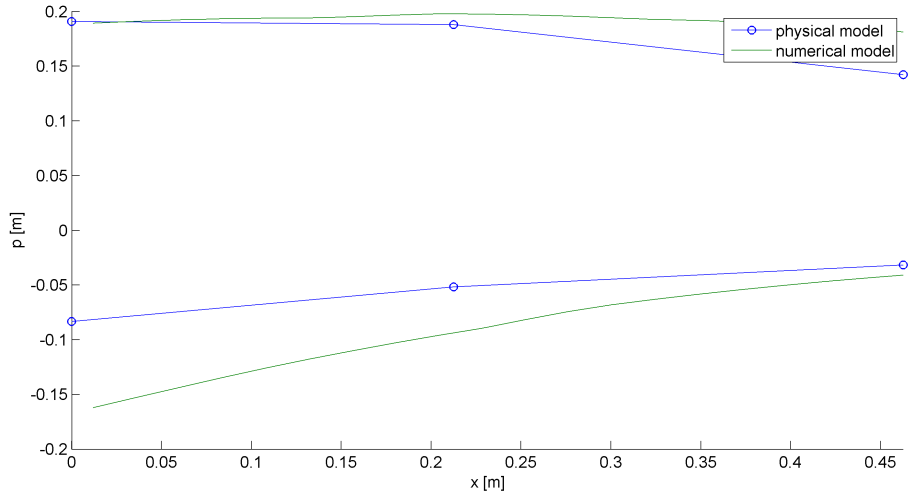

Figure 4.21: Maximum and minimum horizontal pressure distribution inside the structure (0.46 m from the bottom) of validation test 1 of test 4 by Kik (2011). The blue circles indicate the measurement points during the physical model tests.

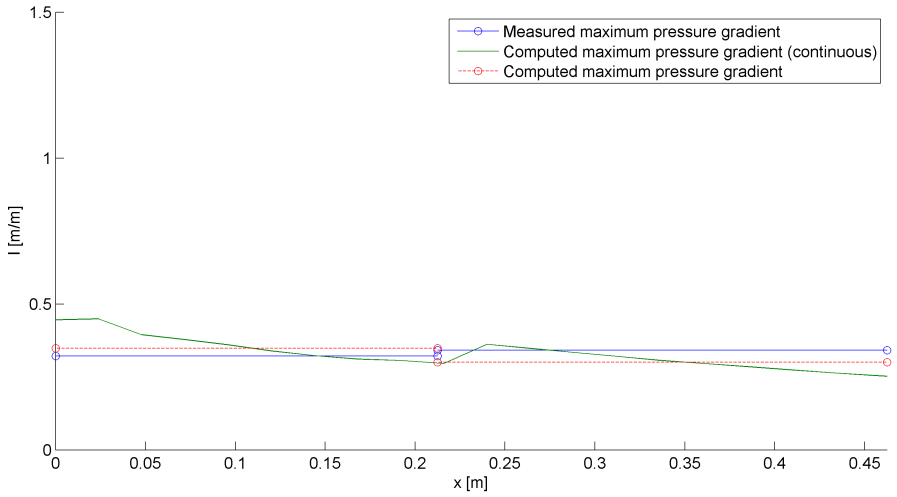

Figure 4.22: Maximum pressure gradient inside the structure (0.46 m from the bottom) of validation test 1 of test 4 by Kik (2011). The blue circles indicate the measurement points during the physical model tests.

From Figure 4.21 it can be seen that the horizontal pressure distribution is reasonably well simulated. Although the absolute minimum values are significantly overestimated, the pattern of decrease in pressure for both models is the same.

Figure 4.22 shows the observed maximum pressure gradient. For the physical model test this is the maximum pressure gradient between the measurement points. For the numerical model test a continuous pressure gradient is also given. A good comparison is observed for both the armour layer and the core.

Figure 4.23 shows the energy density spectra of the pressure time signals at three different locations inside the structure, namely at the armour layer surface (x = 0 m), at the interface between the armour layer and core (x = 0.2124 m) and inside the core (x = 0.4624 m). All three locations already show a good comparison between the measured and calculated results. From these spectra four important values are calculated, namely the

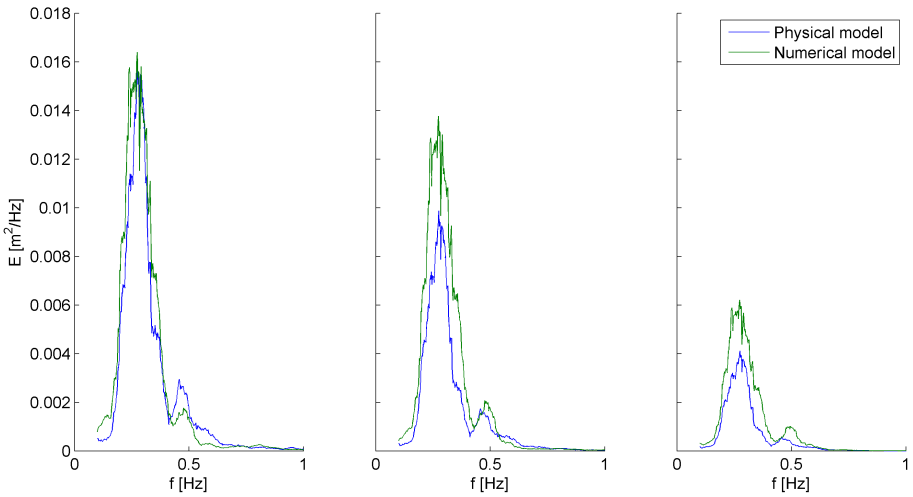

Figure 4.23: Energy spectra of pressure time signals at three different locations of validation test 1 of test 4 by Kik (2011). Left: Armour layer surface, middle: interface between armour layer and core, right: inside the core

spectral peak, zero-order moment (total energy of a spectrum), peak period and $T_{m-1,0}$ as can bee seen in Table 4.5. From this table it becomes more clear that the frequencies are simulated correctly, although large differences are observed for the spectral peak and total energy inside the breakwater. The spectral values at the surface of the armour layer are very reasonable. It must be kept in mind that these spectra are actually calculated from the raw spectra with a moving average method. Therefore, the frequency span over which the averages are calculated can have a large effect on the absolute value of the spectral peak. This is not the case for the zero-order moment, since this is calculated directly from the raw spectrum.

Table 4.5: Model validation results, test 1

	E_p $[10^{-2}m^2/Hz]$			m_0 $[10^{-3}m^2]$			$T_{m-1,0}$ $[s]$			T_p $[s]$		
Physical	1.61	0.99	0.41	2.25	1.37	0.54	3.4	3.45	3.62	3.64	3.64	3.64
Numerical	1.64	1.38	0.62	2.54	2.12	0.94	3.66	3.57	3.58	3.66	3.66	3.66
Diference	2%	39%	51%	13%	55%	74%	7%	3%	1%	0%	0%	0%

Influence of the input values Table 4.6 shows the test matrix that was made to assess the influence of the various input values.

Table 4.6: Model validation, test matrix

	Armour layer				Core				
Test nr.	α	β	c	n	α	β	c	n	T
1	1100	2.4	0.51	0.4	700	2.7	0.51	0.4	T_m
2	1100	2.4	0.51	0.4	700	2.7	0.51	0.4	$0.5T_m$
3	11000	2.4	0.51	0.4	700	2.7	0.51	0.4	T_m
4	1100	5.0	0.51	0.4	700	2.7	0.51	0.4	T_m
5	1100	2.4	0.51	0.6	700	2.7	0.51	0.4	T_m
6	1100	2.4	0.51	0.4	7000	2.7	0.51	0.4	T_m
7	1100	2.4	0.51	0.4	700	5.0	0.51	0.4	T_m
8	1100	2.4	0.51	0.4	700	2.7	0.51	0.6	T_m
9	11000	2.4	0.51	0.4	7000	2.7	0.51	0.4	T_m
10	1100	5.0	0.51	0.4	700	5.0	0.51	0.4	T_m
11	1100	2.4	0.51	0.6	700	2.7	0.51	0.6	T_m
12	1100	2.4	0.51	0.4	700	2.7	0.51	0.4	$2T_m$
13	0	2.4	0.51	0.4	1100	2.7	0.51	0.4	T_m
14	700	2.4	0.51	0.4	0	2.7	0.51	0.4	T_m
15	0	2.4	0.51	0.4	0	2.7	0.51	0.4	T_m

The added mass coefficient was not varied in this test matrix, because the literature review already showed a very small contribution of the parameter and because the contribution to the total hydraulic gradient due to the oscillatory flow behaviour is incorporated in the turbulent Forchheimer coefficient as well. This is done by dynamic updating of the trubulent Forchheimer coefficient via KC number. The turbulent coefficient was initially varied up to a value of 10, but this resulted in very unrealistic water levels inside the structure in a few cases. The visual results for these tests are shown in Appendix D. Table 4.7 shows the spectral values in the same way as was done for test 1. In Table 4.8 the difference with respect to the benchmark values (test 1) is given in percentages.

Table 4.7: Model validation, spectral values

Test nr.	$E_p[10^{-2}m^2/Hz]$			$m_0[10^{-3}m^2]$			$T_{m-1,0}[s]$			$T_p[s]$		
Physical	1.61	0.99	0.41	2.25	1.37	0.54	3.40	3.45	3.62	3.64	3.64	3.64
1	1.64	1.38	0.62	2.54	2.12	0.94	3.66	3.57	3.58	3.66	3.66	3.66
2	1.70	1.35	0.56	2.63	2.07	0.84	3.65	3.57	3.58	3.66	3.66	3.66
3	1.67	1.27	0.52	2.59	1.94	0.79	3.65	3.57	3.59	3.66	3.66	3.66
4	1.68	1.23	0.48	2.60	1.88	0.73	3.65	3.58	3.60	3.66	3.66	3.66
5	1.47	1.44	0.76	2.29	2.22	1.16	3.69	3.60	3.59	3.66	3.66	3.66
6	1.79	1.66	0.73	2.76	2.60	1.13	3.65	3.53	3.51	3.66	3.66	3.66
7	1.69	1.48	0.63	2.62	2.28	0.96	3.66	3.56	3.56	3.66	3.66	3.66
8	1.39	0.92	0.48	2.18	1.40	0.72	3.67	3.64	3.68	3.66	3.66	3.66
9	1.83	1.64	0.67	2.82	2.55	1.03	3.65	3.52	3.51	3.66	3.66	3.66
10	1.74	1.36	0.51	2.68	2.09	0.78	3.65	3.56	3.58	3.66	3.66	3.66
11	1.25	1.13	0.68	1.98	1.75	1.02	3.69	3.63	3.65	3.66	3.66	4.18
12	1.60	1.39	0.66	2.48	2.14	1.01	3.66	3.57	3.57	3.66	3.66	3.66
13	1.63	1.39	0.63	2.53	2.14	0.96	3.66	3.57	3.58	3.66	3.66	3.66
14	1.60	1.30	0.59	2.48	1.99	0.90	3.66	3.58	3.59	3.66	3.66	3.66
15	1.59	1.31	0.61	2.47	2.02	0.92	3.66	3.58	3.59	3.66	3.66	3.66

Influence of the laminar Forchheimer coefficient, α With the results from test 3, 6, 9, 13, 14 and 15 the influence of the laminar Forchheimer coefficient was analysed. For all these tests no significant change in

Table 4.8: Model validation, spectral values compared to benchmark values (test 1)

Test nr.	E_p[%]			m_0[%]			$T_{m-1,0}$[%]			T_p[%]		
2	4	-2	-15	4	-3	-19	0	0	0	0	0	0
3	2	-11	-24	2	-13	-28	0	0	0	0	0	0
4	3	-15	-33	3	-17	-39	0	0	-1	0	0	0
5	7	6	34	-11	8	40	1	1	0	0	0	0
6	9	29	26	10	35	36	0	-1	2	0	0	0
7	3	10	2	3	12	4	0	0	1	0	0	0
8	12	-33	-33	-10	-52	-41	0	2	0	0	0	0
9	12	27	11	12	31	16	0	-1	2	0	0	0
10	6	-1	-26	6	-2	-30	0	0	0	0	0	0
11	21	-25	15	-1	-27	15	1	2	-1	0	0	14
12	-1	1	10	-3	2	12	0	0	0	0	0	0
13	0	1	3	0	1	4	0	0	0	0	0	0
14	-1	-8	-6	-3	-9	-8	0	0	0	0	0	0
15	0	-7	-3	-3	-7	-4	0	0	0	0	0	0

pressure gradients and horizontal pressure distribution was observed. Concerning the pressure spectra, increasing the laminar coefficient with a factor 10 inside the armour layer decreases the spectral peak and zero-order moment values inside the structure. While increasing the laminar coefficient with a factor 10 inside the core or inside the entire structure increases the spectral peak and zero-order moment values inside the structure. No significant change in these values was observed when laminar coefficients were set to zero.

Influence of the turbulent Forchheimer coefficient, β With the results from test 4, 7, and 10 the influence of the turbulent Forchheimer coefficient was analysed. Increasing the turbulent coefficient by a factor 2 inside the armour layer or for the whole structure increases the pressure gradient just below the surface of the armour layer. However, further inside the structure no significant change is observed. The influence on the pressure distribution is also negligible. Concerning the pressure spectra, increasing the turbulent coefficient with a factor 2 inside the armour layer decreases the spectral peak and zero-order moment values inside the structure. While, increasing the turbulent coefficient with a factor 2 for the entire structure decreases these values in the core only. Increasing the turbulent coefficient in the core only has a small effect on the spectra at the layer interface. Overall, the difference in the turbulent coefficient between the layers seems to be important.

Influence of the porosity With the results from test 5, 8, and 11 the influence of the porosity was analysed. Increasing the porosity from 0.4 to 0.6 inside the armour layer gives an overall lower pressure gradient inside the armour layer, while it does not have a noticeable effect on the maximum pressure, the absolute minimum value is slightly higher. Increasing the porosity in the core also leads to a lower pressure gradient inside the core, and it also leads to a slightly higher pressure gradient throughout the armour layer. The maximum and minimum pressures are slightly lower. Increasing the porosity of the entire structure leads to an overall lower pressure gradient, lower maximum pressure and a slightly higher minimum pressure inside the core.

Changing the porosity has mixed influences on the spectral values. Increasing the porosity of the armour layer only significantly changes the spectral peak and zero-order moment inside the core (both increase) and increasing the porosity of the core decreases these values at the layer interface and inside the core. While increasing the porosity of the entire structure decreases the spectral peak and zero order moment at the layer interface and increases inside the core. Also the spectral peak at the armour layer surface increases.

Influence of the characteristic period The characteristic period is used to calculate the Keulegan-Carpenter number, which is used to adjust the turbulent Forchheimer coefficient during the calculation to account for the non-stationary effects in the flow. Test 2 and 12 are used to analyse the influence of the characteristic period by halving and doubling its value respectively. In the numerical model this could only be done for the entire structure and not for individual layers.

Changing the characteristic period did not have any noticeable effect on the pressure gradients or pressures. For the spectral values only a slight change was observed inside the core. Where a shorter period $0.5T_{m-1,0}$ decreased the spectral peak and zero-order moment slightly and a longer period $2T_{m-1,0}$ increased these values slightly.

Calibration to physical tests The above analysis of the influence of the input parameters were all made compared to validation test 1. Based on these results, several input value combinations are chosen which should accurately reproduce the physical test results.

The results from the benchmark test already showed good results for the pressure gradient. Although it was slightly lower in the armour layer and slightly higher in the core during the physical model test. Tests 5 and 6 had a positive effect on the pressure gradient, but the effects were very small.

The initial maximum and minimum horizontal pressure in the benchmark test were less accurate compared to the physical model test, especially the minimum pressure in the armour layer. During the validation tests these pressures did not change significantly.

Due to the small changes of these values during the validation tests it is difficult to quantify the results to determine the optimal input values. The pressure spectra and its spectral values, however, did change significantly during the validation tests. Therefore, these are used to determine the input values. The peak period and $T_{m-1,0}$ period were both very accurate for all tests. Thus, only the spectral peak and the zero-order moment will be used. Based on the analysis above, the following changes in the input values have a positive effect on these results:

Increasing the laminar Forchheimer coefficient inside the armour layer (by a factor 10)
Increasing the turbulent Forchheimer coefficient inside the armour layer (by a factor 2)
Increasing the porosity of the core (to 0.6)
Taking a shorter characteristic period.

Based on this a new validation test matrix was made. Setting the laminar Forchheimer coefficient to zero had no significant effect on the spectral peak and zero-order moment results. But is nevertheless taken into account because it can have a positive effect in combination with changes in other input values. Increasing the porosity of the core was not taken into account because it would be somewhat unrealistic if the core had a larger porosity than the armour layer for rubble mound structures. Although shortening the characteristic period had a positive effect, this is not taken into account because the influence was very small. From the analysis above it seemed that the difference in the turbulent Forchheimer coefficient was also important and from the literature review it followed that this coefficient gives the largest contribution to the total hydraulic gradient. Therefore this is the main focus of the following test matrix, see Table 4.9.

Table 4.9: Model validation part 2, test matrix

	Armour layer				Core				
Test nr.	α	β	c	n	α	β	c	n	T
16	11000	5.0	0.51	0.4	700	2.7	0.51	0.4	T_m
17	11000	5.0	0.51	0.4	700	5.0	0.51	0.4	T_m
18	11000	5.0	0.51	0.4	700	1.1	0.51	0.4	T_m
19	1100	5.0	0.51	0.4	700	1.1	0.51	0.4	T_m
20	0	5.0	0.51	0.4	700	2.7	0.51	0.4	T_m
21	0	5.0	0.51	0.4	700	5.0	0.51	0.4	T_m
22	0	5.0	0.51	0.4	700	1.1	0.51	0.4	T_m
23	0	5.0	0.51	0.4	0	2.7	0.51	0.4	T_m
24	0	5.0	0.51	0.4	0	5.0	0.51	0.4	T_m
25	0	5.0	0.51	0.4	0	1.1	0.51	0.4	T_m

The results from this test matrix are shown in Table 4.10. Test 18, 19 and 25 show the best comparison to the physical model test, which also indicates that the laminar Forchheimer coefficient is of lesser importance

in fully turbulent flows. This is also stated by Troch (2000). Test 18 and 19 show better results for the spectral peak and test 25 shows better results for the zero order moment. As stated before, the exact spectral peak value is more sensitive to the frequency bin over which the raw spectrum is averaged. The zero-order moment does not have this disadvantage. Therefore test 25 is chosen as the best fit for the physical results. This also corresponds to the thesis by Troch (2000), where a fully turbulent flow is modelled with a reduced Forchheimer equation, i.e. the laminar coefficient is set to zero:

$$I = bu|u| + c\frac{\partial u}{\partial t} \tag{4.7}$$

Table 4.10: Model validation part 2, spectral values and spectral values compared to the physical model test

Test nr.	$E_p[10^{-2}m^2/Hz]$			$m_0[10^{-3}m^2]$			E_p[%]			m_0[%]		
16	1.70	1.14	0.43	2.62	1.74	0.64	5	16	3	17	27	19
17	1.75	1.29	0.46	2.70	1.97	0.70	9	31	12	20	44	30
18	1.62	0.95	0.38	2.51	1.43	0.57	0	4	8	12	5	5
19	1.61	1.05	0.44	2.49	1.59	0.67	0	6	7	11	16	24
20	1.68	1.25	0.49	2.60	1.90	0.74	4	26	20	16	39	38
21	1.73	1.37	0.52	2.68	2.11	0.79	7	39	27	19	54	47
22	1.60	1.06	0.45	2.49	1.61	0.68	1	7	10	11	17	26
23	1.64	1.14	0.46	2.54	1.73	0.69	1	15	11	13	27	27
24	1.71	1.31	0.50	2.64	2.01	0.75	6	33	21	17	47	39
25	1.51	0.87	0.41	2.36	1.32	0.61	6	12	1	5	3	13

Validation based on more physical model tests The model settings of test 25 were also used to simulate the physical model tests 1, 3 and 6 by Kik (2011) (see Table 4.3) and test 56, 60, 64 and 68 by Kluwen (2012). See Table 4.11 and Figure 4.24 for the structure and test matrix for the tests by Kluwen. The results are shown in Appendix E.

Table 4.11: Test matrix for structure 5 of Kluwen (2012)

Test nr.	H_s [m]	T_m [s]	ξ_m
56	0.10	1.30	2.57
60	0.09	1.70	3.54
64	0.09	2.15	4.48
68	0.08	3.00	6.63

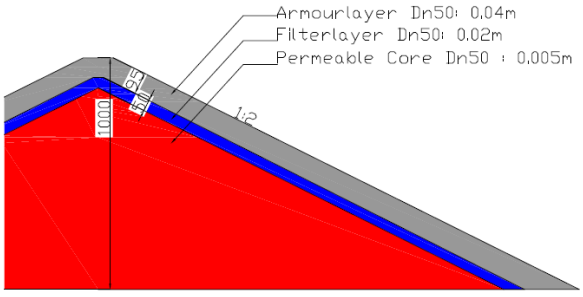

Figure 4.24: Structure 5 of Kluwen (2012)

Discussion of the results Pressure gauge 3 gave no signal during Kik test 1. Thus, unfortunately no comparison can be made between the physical and numerical results in the core. Similar to Kik test 4, the three

other Kik tests show a reasonable simulation of the maximum and minimum pressure distribution. Although especially in the armour layer the absolute values show a quite significant difference between the physical and numerical results. The maximum pressure gradients and the energy density spectra of the pressure signals show a good comparison. In he same way as previously done, the spectral values are shown Table 4.12. The results for test 1 and 3 are very good, test 6 deviates slightly more from the physical results but is still reasonable.

Table 4.12: Model validation of Kik test 1, 3 and 6, spectral values and spectral values compared to the physical model test

Test nr.	$E_p[10^{-2}m^2/Hz]$			$m_0[10^{-3}m^2]$			E_p[%]			m_0[%]		
1	3.07	1.99	1.15	3.22	2.05	1.14	12	14	-	15	15	-
3	2.00	1.28	0.75	2.91	1.82	0.97	1	7	4	8	12	7
6	1.79	0.93	0.36	2.66	1.36	0.56	13	19	29	3	26	28

The validation based on the physical model tests by Kluwen (2012) are far from ideal. The figures in Appendix E show that this is mainly due to minimum pressure inside the armour layer; the drop in pressure from the mean is much larger in the numerical model than observed in the physical model. This is the case for all four tests. Further inside the core the difference is much smaller. The maximum pressure, on the other hand, is simulated quite well. Despite the large difference in pressure in the armour layer, the pressure gradients are reasonable simulated. But, as can be expected, the energy density spectra of the pressure series are not. Although the shapes of the spectra are very similar and the peak periods are about the same, the total energy is much larger in the numerical model than in the physical model, see Figure 4.25 for an example.

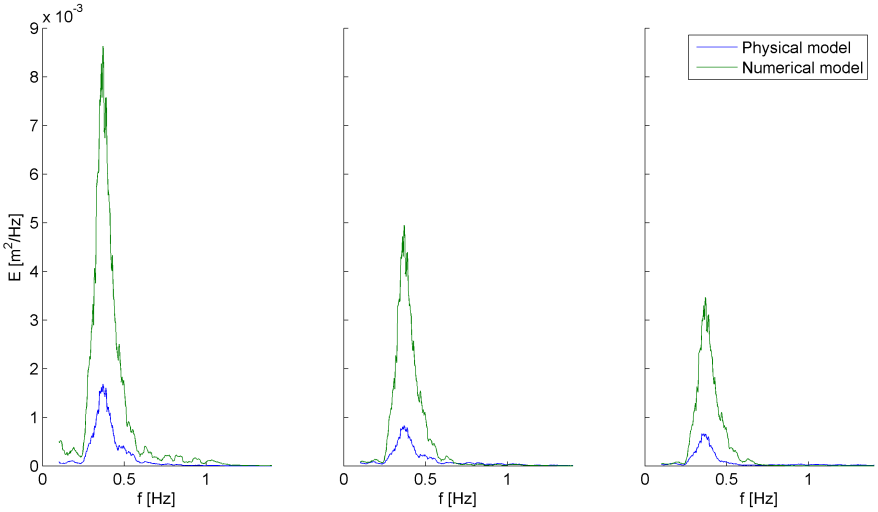

Figure 4.25: Energy spectra of pressure time signals at three different locations of test 64 by Kluwen (2012). Left: Armour layer surface, middle: interface between armour layer and core, right: inside the core

This validation is however, not completely useless because both the spectral shapes and peak periods show a very good comparison between the physical and numerical models. This indicates that the frequencies of the pressure signal are simulated correctly. The only 'problem' lies with the pressure amplitudes. To illustrate this further, the pressure time signals are shown in Figures 4.26-4.29.

The turbulent Forchheimer coefficient was varied for both the armour layer as well as the core, but this did not give results that showed more correspondence with the physical model tests. Because of this and because the difference between the physical and numerical models can be attributed to the difference in pressure drop from the mean inside the armour layer and because validation based on Kik did not show this difference it is cautiously assumed that the delicate test equipment was, for some reason, unable to measure large drops in pressure. Air bubbles inside the flow could for instance effect the pressure measurements.

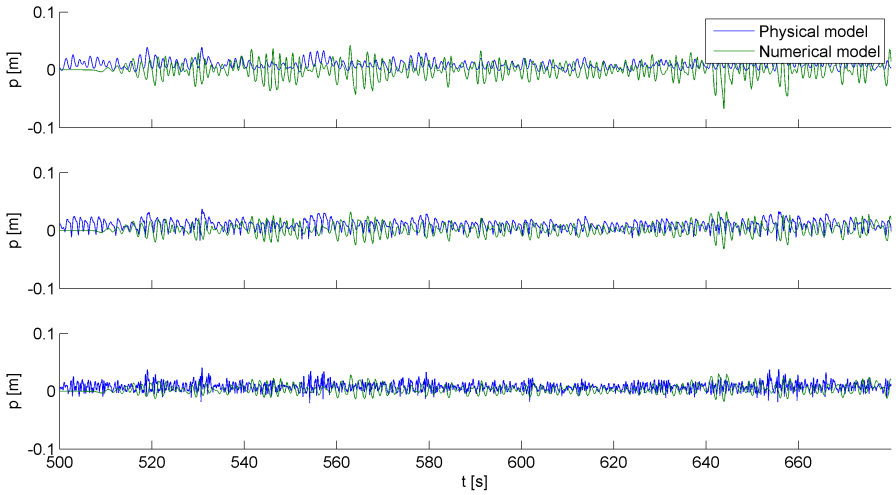

Figure 4.26: Kluwen test 56: pressure time signals at three different locations. Above: Armour layer surface, middle: interface between armour layer and core, below: inside the core.

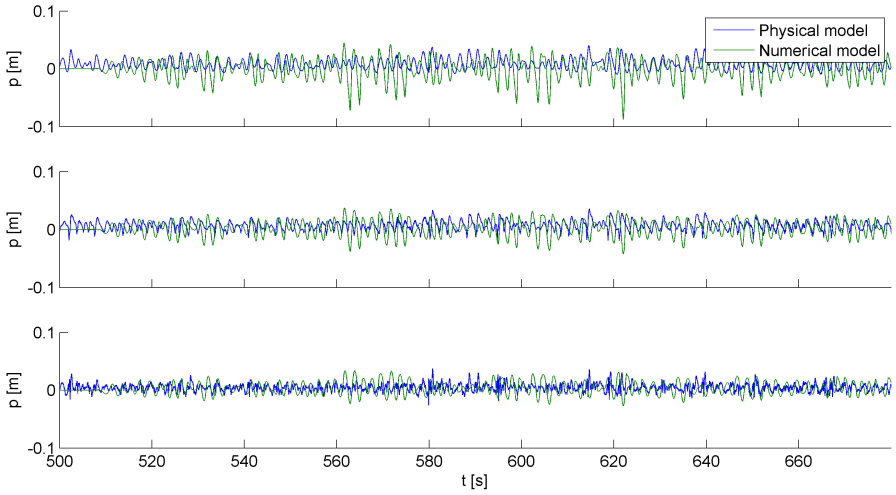

Figure 4.27: Kluwen test 60: pressure time signals at three different locations. Above: Armour layer surface, middle: interface between armour layer and core, below: inside the core.

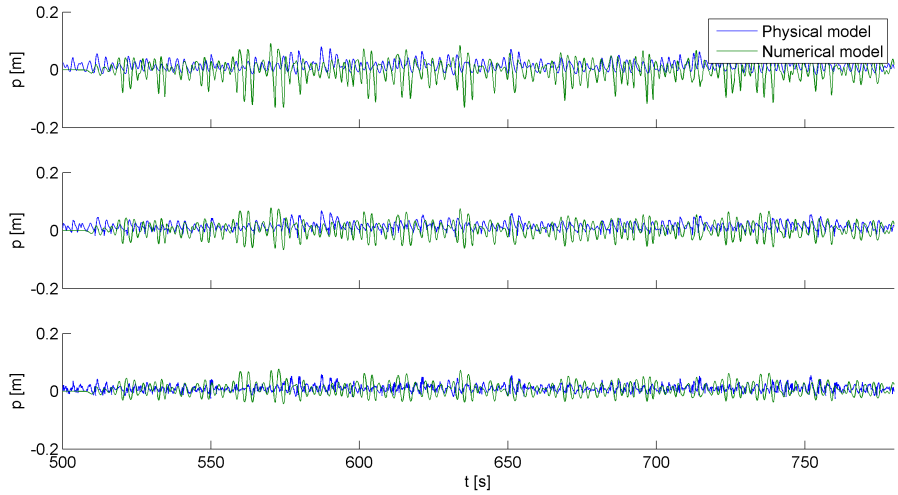

Figure 4.28: Kluwen test 64: pressure time signals at three different locations. Above: Armour layer surface, middle: interface between armour layer and core, below: inside the core.

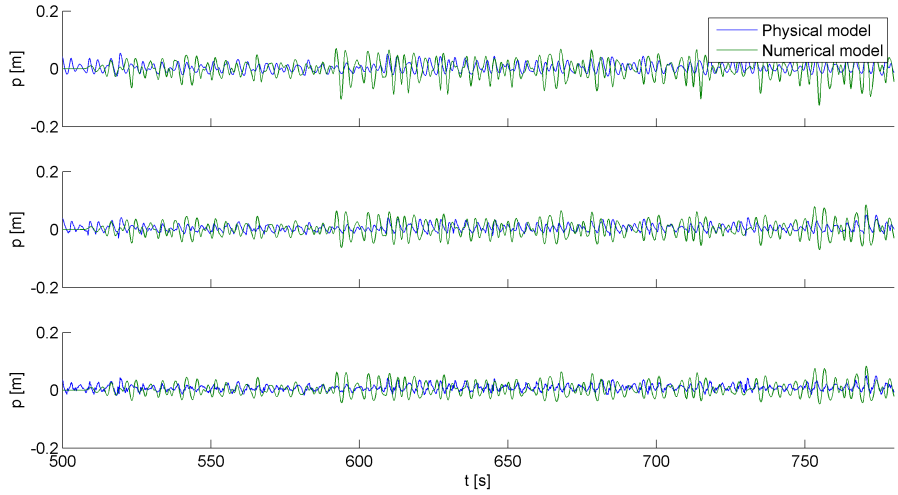

Figure 4.29: Kluwen test 68: pressure time signals at three different locations. Above: Armour layer surface, middle: interface between armour layer and core, below: inside the core.

4.6. WAVE DISSIPATION INSIDE THE ARMOUR LAYER

The VOF method of the model allows tracking of the free surface outside as well as inside the porous media. This makes it possible to visually observe the wave dissipation inside the breakwaters, or in other words the damping of the free surface elevation. It appeared that in general wave dissipation is very rapid and occurs mainly in the armour layer. Further, the 'wave steepness inside the armour layer', if one could give this description to the porous water level, becomes very high. The numerical observations were visually compared to a physical observation (see `http://youtu.be/YYMAbtBJ7jU`) and appear to reasonable simulations of reality.

4.7. FINAL MODELS

Based on the results from the previous sections, the numerical simulations will be made with the settings from test 25 and with a grid size of $\Delta y = 0.012$ m and $\Delta x = 0.024$. The porous media settings are repeated below:

Table 4.13: Final model settings

Armour layer				Core				
α	β	c	n	α	β	c	n	T
0	5.0	0.51	0.4	0	1.1	0.51	0.4	T_m

The homogeneous structure does not have an armour layer. However, to still account for the higher turbulence generation inside the front of the structure due to wave impact, an extra layer is made in the numerical model which is henceforth also called the armour layer. But, other than the turbulent Forchheimer coefficient, the properties of this layer are the same as the rest of the structure. The thickness of this 'armour layer' is chosen equal to the thickness of the armour layers of the impermeable structures, which is 0.08 m.

The numerical structures are visualized below:

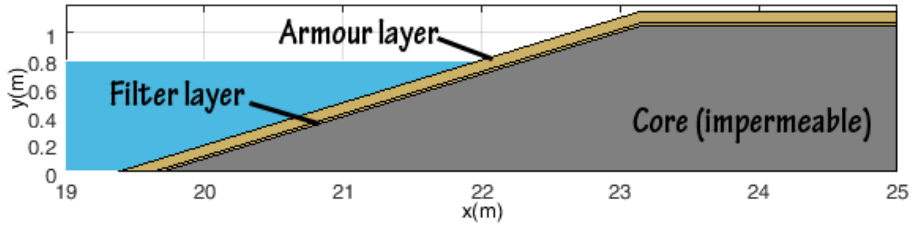

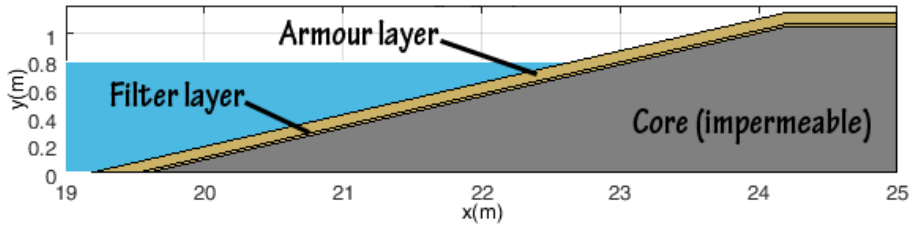

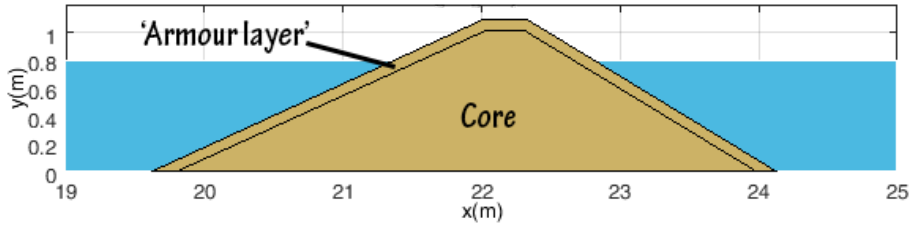

Figure 4.30: Numerical structures, impermeable $cot(\alpha) = 3$ (above), impermeable $cot(\alpha) = 4$ (middle), homogeneous $cot(\alpha) = 2$ (below)

5

RESULTS

In this chapter the results from the data analysis are discussed. First, the approach to the analysis is described. The results are eventually analysed with $P-\Pi$ plots and power curve fittings through these plots. Second, the results from the regular waves are analysed. Based on this a selection of Π terms is made for the analysis of the irregular waves. After analysis of the irregular wave simulations the chapter is concluded with a description of functional relations for P, arising from the analysis of the simulations.

5.1. APPROACH TO THE ANALYSIS

The numerical simulations from the test program have been run for both regular as well as irregular waves. The choice to also include regular waves is based on the idea that the first analysis of the Π terms would be easier for regular waves compared to irregular. Furthermore, the amount of (computational) time and effort would be negligible compared to the irregular simulations.

The goal of this research is to get a more physical understanding of the notional permeability and therefore, in understanding *why exactly* a difference in notional permeability exists between different structures. Numerically simulating the extremes in notional permeability, namely the two selected Van der Meer structures with a impermeable and homogeneous core, and analysing differences in physical processes between the two extremes would be the approach for finding answers to this question.

It was stated that these physical processes could be expressed in four Π terms (KC, Euler, Reynolds, Ac). These are calculated for each numerical cell for each time step inside the breakwaters, see Appendix A for a detailed description of the data processing. Since the Π terms are expressions of the flow velocity and pressure difference, calculations are made for four main directions, namely the horizontal (x) and vertical (y) and normal and parallel to structure slope. See Figure 5.1 for a definitions of these coordinate systems. In this way directional information is also taken into account during the analysis. This is important since, for example, intuitively the direction of the flow velocity might be important regarding armour layer stability. This results in time series of the Π terms for each numerical cell for four directions. See for example a time series of the KC number for an arbitrary simulation location and direction in Figure 5.2. A spectral analysis for these time series is made to analyse the variance density distribution over the frequencies. See for an example of a spectrum Figure 5.3.

Additionally, 2D-plots of the maxima and minima of the Π terms for each computational cell are made to visualize the distribution of these terms inside the breakwaters and to aid in the analysis. See for example Figure 5.4.

First analysis of the Π terms by means of the above $\Pi - t$ and spectrum plots for various points inside the breakwaters, 2D plots of the maximum Π values did not produce satisfactory results. It was difficult to indicate clear and consistent differences between the two Van der Meer structures, although it was apparent from $P-\Pi$ that differences indeed existed. The enormous amount of data resulting from this procedure, even for a relative small test program, also made the analysis more tedious.

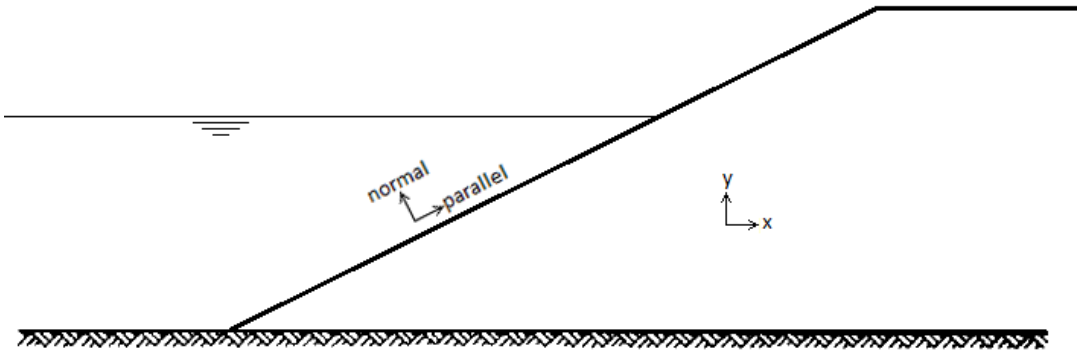

Figure 5.1: Coordinate systems

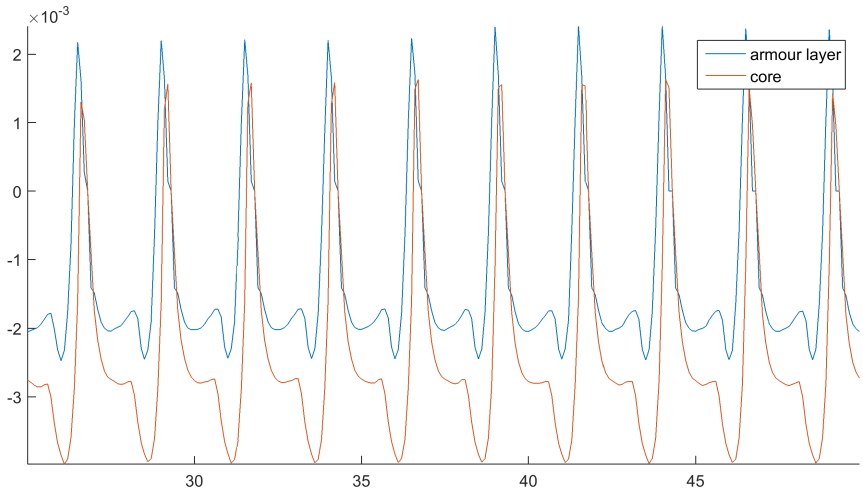

Figure 5.2: KC number time series

Therefore, it was decided to go more into statistical detail of the $\Pi - t$ and spectral plots by quantifying these results. First, the amount of measuring points in the computational domain is limited to three horizontal lines; 0.5, 1.5 and 2.5 times the significant wave height below the initial water level. The reasoning behind this choice is the same as in a laboratory setting where pressure gauges are used; when measuring at the mean/initial water level, the measuring points will be dry about half of the simulation time. Which means that half of the time no information is stored. This can also lead to statistical errors when calculating certain quantities. Second of all, a mean value of the Π terms over this horizontal line is calculated for a) armour layer and b) core, for each time step. See Figure 5.5 for a visualisation of the measuring points. Lastly, only the horizontal direction and the direction normal to the slope are considered. Since the velocity and pressure variations in vertical direction and parallel to the slope are considered to be of less influence on the armour layer stability.

The $\Pi - t$ series and spectral plots are quantified by calculating the maximum, mean and minimum of the Π time series and the zero order moment m_0 (representing the total energy of all frequencies), the $T_{m-1,0}$ (chosen as the characteristic period of the fluctuating time series) and the peak energy E_p and peak period T_p of the spectra. This results in 14 quantities describing each Π term (7 calculated inside the armour layer and 7 inside the core.) For better readability of the discussion of the results later in this chapter, the meaning of these 7 quantities are described below.

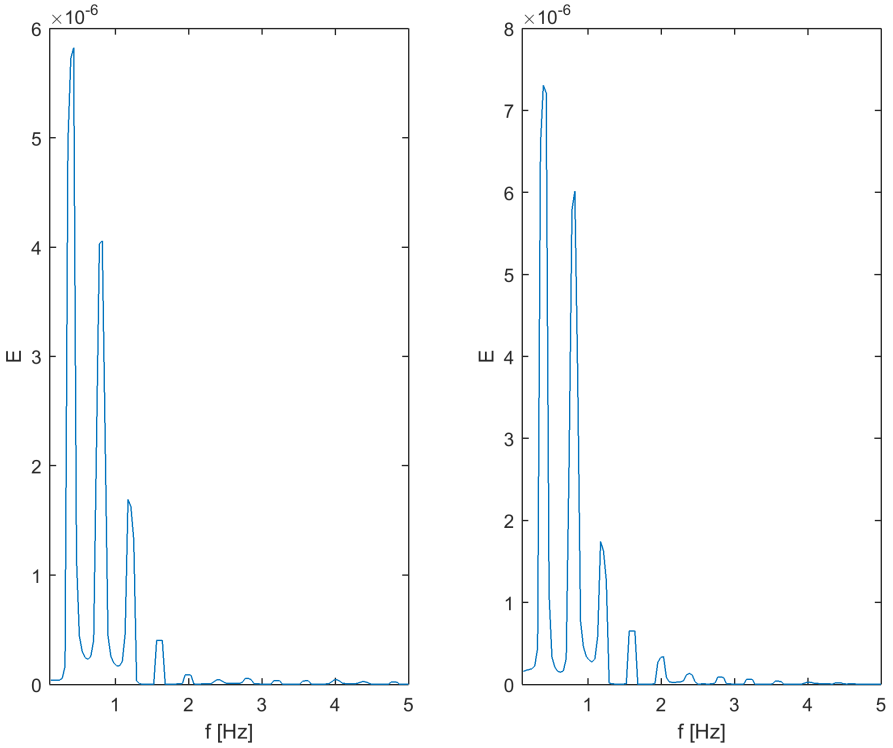

Figure 5.3: KC number spectrum

Zero order moment, m_0 The variance density spectrum of a time series of a certain quantity shows the distribution of the variance of this quantity over the frequencies. In this case of an oscillating flow pattern inside a breakwater, the variance can be regarded as a measure of the amplitude of the oscillating signal. The variance density therefore, describes the contribution of a certain frequency to the total oscillation amplitude of the signal. The zero order moment is defined as the sum of the variance density of each frequency:

$$m_0 = \int_{-\inf}^{\inf} E(f)\,df \tag{5.1}$$

It is therefore a quantitative description of the overall magnitude of the amplitude of an oscillating signal. And can indicate whether the oscillating character of a Π term is of influence on the armour layer stability.

Characteristic period, $T_{m-1,0}$ $T_{m-1,0}$ is defined as follows:

$$T_{m-1,0} = \frac{m_{-1}}{m_0} \tag{5.2}$$

Elaboration of this definition shows that $T_{m-1,0}$ has a unit time and can therefore be regarded as a characteristic wave period of the time signal. It is a better representation of the period of the time signal than the mean period because it adds more weight to the frequencies with a larger variance density, while still taking into account the other frequencies. The peak period does not have this advantage. $T_{m-1,0}$ is actually considered as the characteristic period of a time signal in most parts of this report. This value can indicate whether the period of a Π term is of influence on the armour layer stability.

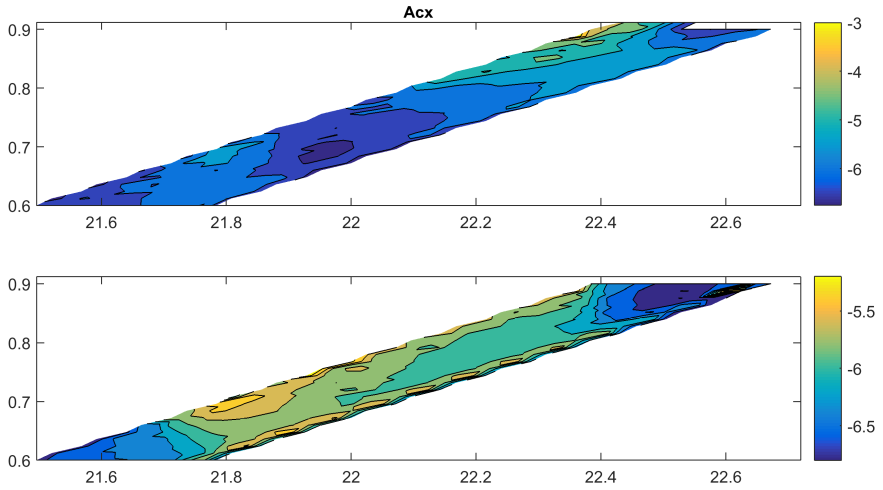

Figure 5.4: KC number 2D plot of the maxima (above) and minima (below)

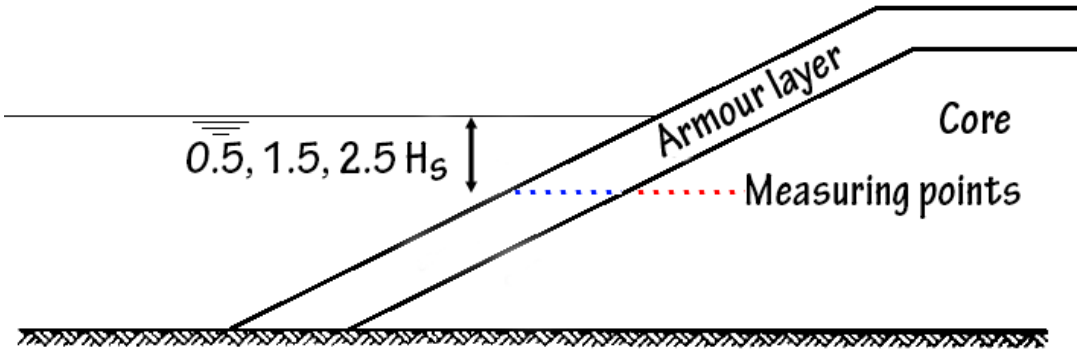

Figure 5.5: Measuring points in the numerical model

Spectral peak value, E_p The spectral peak value is the largest value of the variance density observed in the spectrum. It is a measure of the largest contribution of a single frequency to the total variance. This value can therefore indicate if there exists a 'single' frequency with corresponding amplitude which has a dominant effect on armour layer stability compared to the rest of the contributions to the oscillation.

Peak period, T_p The peak is the frequency corresponding to the largest value of the variance density observed in the spectrum. This value can indicate if there exists a single period which has a dominant effect on armour layer stability compared to the rest of the frequency domain.

Mean, maxima and minima The descriptive function of the mean value of a Π term is straightforward. The influence of the peak values of Π series is additionally described by the maximum and minimum values. The maximum values are associated with either a flow velocity or pressure gradient in positive direction and minimum values in negative direction. The coordinate systems are shown in Figure 5.1.

Analysis of the Π terms These quantities are visualized with $P-\Pi$ plots. See for an example Figure 5.6. The P-values in these plots are calculated in Section 3.6. The $P-\Pi$ plots indicate whether or not a difference

is observed in the Π terms between the two Van der Meer structures. If a large difference is observed, the physical meaning of the Π terms will give insight in the question why the two Van der Meer structures have a different notional permeability. However, it is not straightforward to draw conclusions from just the $P-\Pi$ plots. For example, if one subtracts the mean of the data points of $P = 0.6$ structure from the mean of the $P = 0.1$ structure, a large spread in the data points might wrongly indicate a difference in the Π term between the two structures. See for an example Figure 5.7. Although a difference is observed, the spreads are large and overlap each other. Furthermore, these plots do not show whether the difference in a Π term between the armour layer and core is of any significant importance. Therefore one cannot immediately include or exclude Π terms from the analysis based on just the figure or by means of the data points.

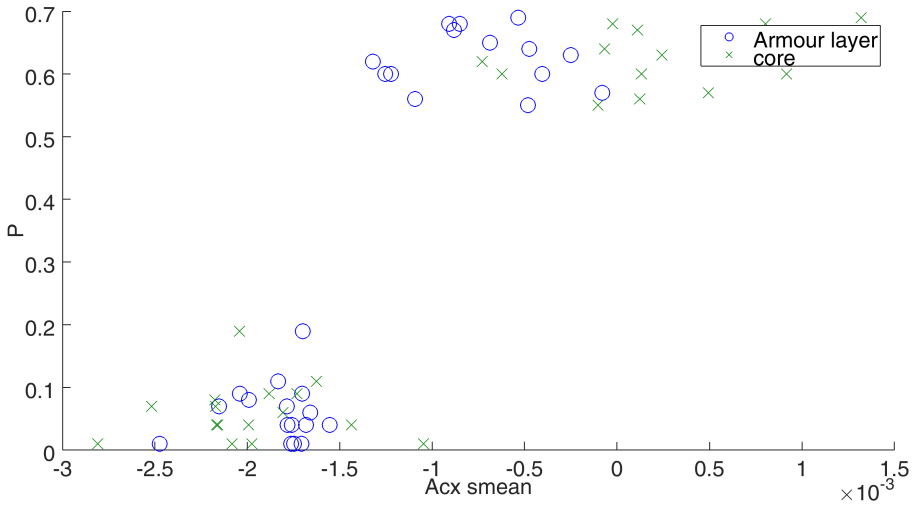

Figure 5.6: P-Π plot of the mean AC number in x-direction

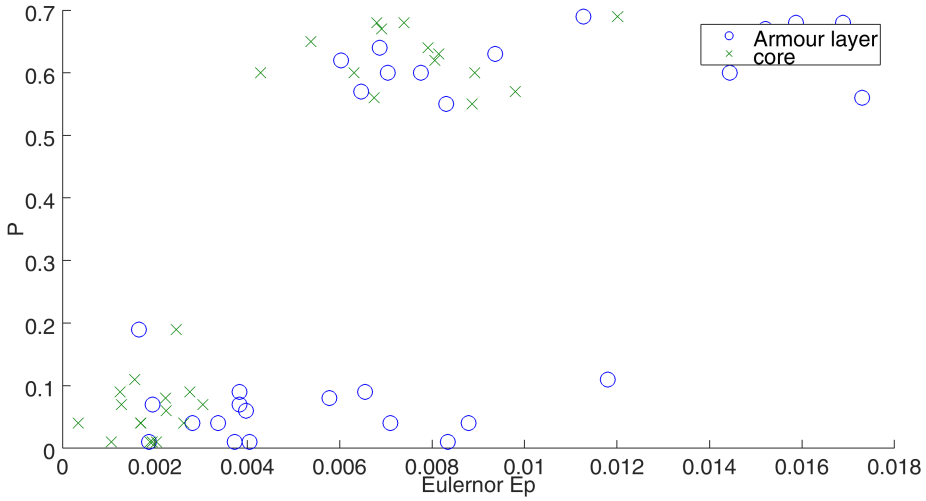

Figure 5.7: P-Π plot of the spectral peak of the Euler number in normal direction to the slope

Therefore the ability of each Π term to describe the notional permeability is determined by means of a curve fitting procedure for each individual term. It is assumed that the curve can be described by a power function of the Π term. The term for both the armour layer and the core will appear in the function. In this way the curve fitting will also indicate if the difference in the Π terms between the armour layer and core plays any role. The function on which the curve fitting is based is thus:

$$P_{calc} = a_1 \Pi_{armour}^{b_1} + a_2 \Pi_{core}^{b_2} + c \tag{5.3}$$

The curve fitting algorithm will vary the variables a_1, a_2, b_1, b_2 and c until a local minimum in the Root Mean Square Error (RMSE) is found. Since the power function can lead to complex numbers for negative Π terms, the equation is changed to:

$$P_{calc} = a_1 |\Pi_{armour}|^{b_1} \operatorname{sgn}(\Pi_{armour}) + a_2 |\Pi_{core}|^{b_2} \operatorname{sgn}(\Pi_{core}) + c \tag{5.4}$$

The sign function ensures that the directional information is retained. For example, a negative KC number (in x-direction) is associated with an outgoing flow. Taking the absolute value would result in a loss of this information. The RMSE is calculated next:

$$RMSE = \sqrt{\frac{\sum_{i=1}^{n} (P_{i,calc} - P_{i,target})^2}{n}} \tag{5.5}$$

The result is a curve fitting through the points of the $P-\Pi$ plots. The curve itself is not of very much importance since only two targets are used ($P = 0.1$ and $P = 0.6$). But the RMSE value is, since this indicates which Π terms can a give physical description of the notional permeability. For a perfect curve fit, the calculated difference of P between the two Van der Meer structures will be 0.5:

$$\begin{aligned} \Delta P &= P_{imp,calc} - P_{hom,calc} \\ &= a_1 |\Pi_{imp,armour}|^{b_1} \operatorname{sgn}(\Pi_{imp,armour}) + a_2 |\Pi_{imp,core}|^{b_2} \operatorname{sgn}(\Pi_{imp,core}) \\ &- (a_1 |\Pi_{hom,armour}|^{b_1} \operatorname{sgn}(\Pi_{hom,armour}) + a_2 |\Pi_{hom,core}|^{b_2} \operatorname{sgn}(\Pi_{hom,core})) \end{aligned} \tag{5.6}$$

This formula also indicates the contributions of the armour layer and core to ΔP. If the curve fitting finds more or less equal contributions and a_1 and a_2 have the same sign, it is ambiguous which data points are of more importance. In this case the data points inside the armour layer are preferred, because ultimately it is all about the armour layer stability. However, opposite signs indicate that the difference in Π terms between the armour layer and core are of importance. If additionally the powers b_1 and b_2 have the same value, the core is not neglected. In the all other cases the core is neglected.

$$\begin{aligned} \Delta P &= \Delta P_{armour} + \Delta P_{core} \\ \Delta P_{armour} &= a_1 |\Pi_{imp,armour}|^{b_1} \operatorname{sgn}(\Pi_{imp,armour}) - a_1 |\Pi_{hom,armour}|^{b_1} \operatorname{sgn}(\Pi_{hom,armour}) \\ \Delta P_{core} &= a_2 |\Pi_{imp,core}|^{b_2} \operatorname{sgn}(\Pi_{imp,core}) - a_2 |\Pi_{hom,core}|^{b_2} \operatorname{sgn}(\Pi_{hom,core}) \end{aligned} \tag{5.7}$$

5.2. REGULAR WAVES, 2.5 H_s BELOW INITIAL WATER LEVEL

The results of the procedure discussed in the previous section are summarised in Table 5.1. A RMSE of 0.1 or lower indicates a good fit with the data points. Everything above this value indicates a lower correlation between the Π term and the notional permeability. They are left out of the further analysis. The best results are studied further based on the $P-\Pi$ plots and the physical relations the terms describe, with or without the results from the core as indicated by Table 5.1. The best results are highlighted in blue in the table. First, it can be noticed that the results normal to the slope have a better ability to describe the notional permeability and that the Π terms in the core only seem to play a role for a few of the Π terms. The best Π terms from Table 5.1 are discussed one by one. For readability the $P-\Pi$ plots are not included in the text below. Instead they are presented in Appendix F in the order in which they are discussed below.

Table 5.1: Overview of the RMSE for regular waves, 2.5 H_s below initial water level

	normal to slope				x-direction			
	RMSE	ΔP_{armour}	ΔP_{core}	neglect core?	RMSE	ΔP_{armour}	ΔP_{core}	neglect core?
Ac								
E_p	0.04	0.1	0.3	yes	0.12	0.1	0.3	no
$T_{m-1,0}$	0.11	0.0	0.4	yes	0.20	0.2	0.0	yes
T_p	0.22	0.0	0.1	yes	0.19	0.3	-0.1	no
m_0	0.08	0.5	0.0	yes	0.15	0.0	0.3	yes
minimum	0.09	0.1	0.3	yes	0.23	0.0	0.1	yes
mean	0.13	0.0	0.4	yes	0.20	0.2	0.0	yes
minimum	0.13	0.4	0.0	yes	0.11	0.1	0.3	yes
Euler								
E_p	0.18	0.0	0.2	yes	0.22	0.0	0.1	yes
$T_{m-1,0}$	0.14	0.4	0.0	yes	0.19	0.2	0.0	yes
T_p	0.17	0.3	0.0	yes	0.17	0.1	0.1	yes
m_0	0.18	0.0	0.2	yes	0.19	0.0	0.2	yes
maximum	0.23	0.0	0.0	yes	0.13	0.3	0.1	yes
mean	0.13	0.2	0.1	yes	0.17	0.2	0.1	yes
minimum	0.07	0.0	0.5	yes	0.17	0.0	0.3	yes
KC								
E_p	0.10	0.0	0.4	yes	0.09	0.4	0.0	yes
$T_{m-1,0}$	0.23	0.0	0.1	yes	0.20	0.2	0.0	yes
T_p	0.23	0.1	0.0	yes	0.19	0.3	-0.1	no
m_0	0.07	0.0	0.5	yes	0.10	0.4	0.0	yes
maximum	0.11	-0.1	0.5	yes	0.11	0.4	0.0	yes
mean	0.15	0.0	0.3	yes	0.23	0.1	0.0	yes
minimum	0.12	0.1	0.3	yes	0.12	0.3	0.1	no
Re								
E_p	0.12	0.4	0.0	yes	0.16	0.3	0.0	yes
$T_{m-1,0}$	0.19	0.0	0.2	yes	0.13	0.7	-0.4	no
T_p	0.24	0.0	0.0	yes	0.19	0.3	-0.1	no
m_0	0.06	0.0	0.5	yes	0.12	0.3	0.1	yes
maximum	0.15	0.3	0.0	yes	0.19	0.2	0.0	yes
mean	0.14	0.0	0.3	yes	0.22	0.1	0.0	yes
minimum	0.07	0.0	0.4	yes	0.16	0.0	0.3	yes

ACCELERATION PARAMETER, NORMAL TO SLOPE

$$Ac_{\perp} = \frac{u_{\perp}}{ngT_{m-1,0}(u_{\perp})} \tag{5.8}$$

The Acceleration parameter indicates the rate of acceleration for a particular characteristic period. The characteristic period is chosen as the $T_{m-1,0}$ value of the flow velocity at the points where the parameter is calculated. In this way, the parameter is calculated independently of the forcing (incoming wave period) and directly related to the frequency of the flow velocity.

Spectral peak The spectral peak is the value of the variance density at the peak frequency. It quantifies the value of the acceleration parameter at the frequency which contains the most energy. A clear difference can be seen between the two Van der Meer structures; the homogeneous structure has a noticeable higher peak value than the impermeable structure. Closer inspection of the spectral plots show that this is because the homogeneous structure has its variance density concentrated at mainly one frequency (related to the period of the regular wave), while the variance density of the impermeable structure is distributed over a range of frequencies. Apparently, inside the impermeable structure reflection occurs normal to the slope that leads to these additional frequencies inside the armour layer.

zero order moment The zero order moment is the sum of the variance densities of each frequency and quantifies the total energy of the corresponding parameter. Apparently, not only the spectral peak value is higher for the homogeneous structure, but also the m_0 value. Thus, besides reflection inside the impermeable structure, another mechanism also plays a role. The time series show that the Acceleration parameter oscillates around zero for all simulations, thus a lower m_0 value indicates an overall lower acceleration parameter for the impermeable structure. The impermeability of the structure must prevent high accelerations to occur inside the armour layer; the flow inside the structure is restricted more than compared to the homogeneous structure.

maximum The maximum value means that it concerns the acceleration parameter associated with the velocity normal to slope, directed outward of the structure. As can be expected from the results of m_0, the maximum values show the same relations; the acceleration parameter is lower for the impermeable structure.

EULER NUMBER, NORMAL TO SLOPE

$$Eu_{\perp} = \frac{n^2 \Delta p_{\perp}}{\rho u_{\perp}^2} \tag{5.9}$$

The Euler numbers allows one to make a dimensionless analysis of the pressure difference between two points. It describes the ratio of pressure forces over inertial forces. It should be noted that, since the pressure difference normal to the slope is calculated, it also includes the difference in hydrostatic pressure. Therefore the values of the Euler number are different from what one would expect from the classical application of the Euler number.

minimum Although some overall difference between the two Van der Meer structures can be seen for the minimum value of the Euler number (or the absolute value associated with an outward directed pressure difference), there is too much overlap between the data points to make any proper conclusions.

KEULEGAN-CARPENTER NUMBER, NORMAL TO SLOPE

$$KC_{\perp} = \frac{u_{\perp} T_{m-1,0}(u_{\perp})}{nD} \tag{5.10}$$

The Keulegan-Carpenter (KC) number describes the ratio of drag forces divided by inertial forces in an oscillatory flow. The characteristic period in this formula is also chosen equal to the $T_{m-1,0}$ value of the flow velocity at the points where the KC number is calculated.

Spectral peak The spectral peak plots of the KC number in normal direction to the slope clearly shows that the peak values are larger for the homogeneous structure. This is explained in the same way as for the acceleration parameter; due to reflection inside the impermeable structure, other frequencies appear in the spectrum where part of the energy is transferred to. Besides this, the plot gives no additional information.

Zero order moment The zero order moment of the KC plot shows that, besides the spectral peak value, the total variance density summed over all frequencies is also higher for the homogeneous structure. The time series plots show that the KC number oscillates around zero for all simulations. The absolute value of the KC number is therefore larger for the homogeneous structure. Indicating that the drag force (relative to the inertial force) is of more importance for the homogeneous structure compared to the impermeable structure, i.e. drag forces play a larger role in the homogeneous structure.

KEULEGAN-CARPENTER NUMBER, X-DIRECTION

$$KC_x = \frac{u_x T_{m-1,0}(u_x)}{nD} \tag{5.11}$$

Spectral peak The spread in the spectral peak data points of the homogeneous structure is quit large and they overlap the data points of the impermeable structure. So no proper conclusions can be drawn from this figure.

Zero order moment and maximum Unfortunately, quite some overlap is again seen between the two structures, so no conclusions are drawn from this figure.

REYNOLDS NUMBER, NORMAL TO THE SLOPE

$$Re_{\perp} = \frac{u_{\perp} D}{\nu(1-n)} \tag{5.12}$$

The Reynolds number describes the ratio of inertial forces divided by viscous forces and indicates the degree of turbulence of a flow.

zero order moment The values of the zero order moment of the Reynolds number in the direction normal to the slope are also larger for the homogeneous structure. The time series show that the Reynolds number oscillates around zero for all simulations. Therefore a higher zero order moment for the homogeneous structures indicates a higher absolute value of the Reynolds number. And thus a more turbulent flow regime, compared to the impermeable structure.

minimum The minimum value of the Reynolds number (or the absolute value in negative normal direction to the slope (inward directed)) inside the armour layer and inside the core, in the direction normal to the slope shows larger values for the homogeneous structure are significantly larger, indicating a more turbulent flow. According to the classification by Troch (2000), most flows inside the impermeable structure are laminar, while all flows of the homogeneous simulations are fully turbulent.

5.2.1. SUMMARY

The results from the regular wave tests are summarised below.

1 Normal to the slope reflection occurs with higher frequencies than the incoming signal for the impermeable structure, which can be concluded from the spectral plots of the flow velocity.
2 The 'overall' acceleration parameter normal to the slope is lower for the impermeable structure.
3 No correlation between the Euler number and the notional permeability is found.
4 In normal direction to the slope, the flow directed inward of the structure is mostly laminar in the impermeable structure and fully turbulent for the homogeneous structure.

5.3. REGULAR WAVES, 1.5 H_s BELOW INITIAL WATER LEVEL

The same as in the previous section is done for the results 1.5 times the significant wave height below the initial water level. The table below shows in general comparable results with analysis in the previous section. However, for the KC number, the core also seems to play a role for these results.

Table 5.2: Overview of the RMSE for regular waves, 1.5 H_s below initial water level

	normal to slope				x-direction			
	RMSE	ΔP_{armour}	ΔP_{core}	neglect core?	RMSE	ΔP_{armour}	ΔP_{core}	neglect core?
Ac								
E_p	0.05	0.5	0.0	yes	0.12	0.0	0.4	yes
$T_{m-1,0}$	0.15	0.0	0.3	yes	0.22	0.1	0.1	yes
T_p	0.21	0.1	0.1	yes	0.22	0.0	0.1	yes
m_0	0.06	0.0	0.5	yes	0.14	0.0	0.3	yes
maximum	0.11	0.0	0.4	yes	0.20	0.0	0.2	yes
mean	0.22	0.0	0.1	yes	0.23	0.1	0.0	yes
minimum	0.06	0.5	0.0	yes	0.15	0.0	0.3	yes
Euler								
E_p	0.22	0.1	0.0	yes	0.10	0.4	0.0	yes
$T_{m-1,0}$	0.13	0.4	0.0	yes	0.19	0.2	0.0	yes
T_p	0.16	0.3	0.0	yes	0.19	0.2	0.0	yes
m_0	0.20	0.0	0.2	yes	0.11	0.4	0.0	yes
maximum	0.17	0.0	0.2	yes	0.09	0.5	0.0	yes
mean	0.19	0.0	0.2	yes	0.16	0.0	0.3	yes
minimum	0.15	0.0	0.3	yes	0.18	0.3	0.0	yes
KC								
E_p	0.08	0.1	0.4	no	0.10	0.1	0.3	yes
$T_{m-1,0}$	0.17	0.0	0.2	yes	0.22	0.1	0.0	yes
T_p	0.20	0.1	0.0	yes	0.22	-0.1	0.2	yes
m_0	0.08	-0.2	0.7	no	0.08	0.2	0.2	yes
maximum	0.09	-0.1	0.5	yes	0.16	-0.1	0.4	yes
mean	0.17	0.3	0.0	yes	0.20	0.1	0.0	yes
minimum	0.10	0.1	0.3	no	0.12	0.2	0.2	yes
Re								
E_p	0.06	0.0	0.5	yes	0.25	0.0	0.0	yes
$T_{m-1,0}$	0.17	0.0	0.3	yes	0.23	0.1	0.0	yes
T_p	0.20	0.1	0.0	yes	0.22	-0.1	0.2	yes
m_0	0.06	0.5	0.0	yes	0.23	0.1	0.0	yes
maximum	0.05	0.0	0.5	yes	0.21	0.0	0.2	yes
mean	0.20	0.1	0.1	yes	0.18	0.2	0.1	yes
minimum	0.05	0.0	0.5	yes	0.21	0.0	0.1	yes

ACCELERATION PARAMETER, NORMAL TO SLOPE

The Acceleration parameter in direction normal to the slope shows the same results for the spectral peak and zero order moment as in the previous section. Additionally the minimum value (absolute value directed inward of the structure), also shows a correlation with the notional permeability. As can be expected from the results of m_0, the minimum values also show the same relations; the acceleration parameter is lower for the impermeable structure.

EULER NUMBER, X-DIRECTION

$$Eu_x = \frac{n^2 \Delta p_x}{\rho u_x^2} \tag{5.13}$$

At this height inside the structures, the spectral peak and maximum values of the Euler number in x-direction show a correlation with the notional permeability. The spectral plots show no significant difference in variance density distribution over the frequencies and the time series show that the Euler number oscillates around zero for all simulations. Therefore, the amplitude of the Euler number is larger for the homogeneous structure compared to the impermeable structure. This is not only the case for the peak frequency, but for all frequencies, as indicated by the RMSE of 0.1 for the m_0 value. Practically this result is quantified by the maximum Euler number. The positive value indicates an outward directed pressure gradient.

KC NUMBER, NORMAL TO SLOPE

The KC number show the same results as in the previous section. Additionally a correlation between the notional permeability and the difference in KC number between the armour and core is found. It is clear that the oscillation of the KC number hardly dampens inside the core for the impermeable structure, while for most simulations of the homogeneous structure the oscillation does dampen. For a few simulations the difference is negative. It is unclear why some simulations give this result.

maximum At this height also a correlation with the maxima and minima values is found. These quantify the results from the spectral plots. The maximum value for the impermeable structure is much smaller compared to the homogeneous structure. Together with the low m_0 value and the results for the minimum values (see below), it can be concluded that inertia dominates over drag forces. For the homogeneous structure the drag forces play a larger role.

minimum The results for the minimum value of the KC number in normal direction to the slope supports the conclusions made above. Also the difference in minimum values between the armour layer and core is plotted, but this figure does not indicate a correlation with the notional permeability.

KC NUMBER, X-DIRECTION

The KC number in x-direction shows the same results as in the previous section.

REYNOLDS NUMBER, NORMAL TO SLOPE

The Reynolds number in direction normal to the slope shows the same results as in the previous section. Additionally the spectral peak and maximum values show a correlation with the notional permeability.

spectral peak The spectral peak value of the Reynolds number in the direction normal to the slope.are larger for the homogeneous structure than for the impermeable structure. Again, the spectral plots show additional frequencies besides the main frequency for the impermeable structure, while for the homogeneous structure one frequency is observed. For the impermeable structure, the variance density is distributed over a frequency band due to reflection.

maximum The maximum value of the Reynolds number inside the armour layer, in the direction normal to the slope (or the absolute value outward directed of the structure) confirms a fully turbulent flow in this direction for all simulation, while the flow was laminar at a depth of 2.5 H_s below the initial water level for the homogeneous structure. The fully turbulent flow at this height confirms the assumption made during the model validation of fully turbulent flows for each simulation.

5.3.1. SUMMARY

No contradicting results where found as compared to the results from 2.5 time the significant wave height below the initial water level. Additionally, some other correlations with the notional permeability where found. These are:

1 The Euler number in x-direction, associated with an outward directed pressure gradient, is smaller for the impermeable structure.
2 The KC number in direction normal to the slope, does not dampen inside the core for the impermeable structure.
3 In normal direction to the slope, inertial forces dominate over drag forces for the impermeable structure. For the homogeneous structure drag forces can not be neglected.
4 In x-direction, the pressure over inertial forces ratio is lower for the impermeable structure for pressures directed inward of the structure.

5.4. REGULAR WAVES, 0.5 H_s BELOW INITIAL WATER LEVEL

The same procedure as above was followed for the results 0.5 times the significant wave height below the initial water level. At this height, again more correlations between the notional permeability and the Π terms are found. The best results are highlighted in the table below.

Table 5.3: Overview of the RMSE for regular waves, 0.5 H_s below initial water level

	normal to slope				x-direction			
	RMSE	ΔP_{armour}	ΔP_{core}	neglect core?	RMSE	ΔP_{armour}	ΔP_{core}	neglect core?
Ac								
E_p	0.07	0.5	0.0	yes	0.08	0.5	0.0	yes
$T_{m-1,0}$	0.18	0.1	0.2	no	0.23	0.0	0.1	yes
T_p	0.21	0.1	0.1	no	0.22	0.0	0.1	yes
m_0	0.05	0.2	0.2	no	0.16	0.0	0.3	yes
maximum	0.24	0.0	0.0	yes	0.09	0.0	0.4	yes
mean	0.05	0.1	0.4	yes	0.10	0.0	0.4	yes
minimum	0.05	0.5	0.0	yes	0.23	0.0	0.0	yes
Euler								
E_p	0.11	0.1	0.3	no	0.04	0.5	0.0	yes
$T_{m-1,0}$	0.24	0.0	0.0	yes	0.18	0.0	0.3	yes
T_p	0.25	0.0	0.0	yes	0.20	0.0	0.2	yes
m_0	0.16	0.0	0.3	yes	0.05	0.5	0.0	yes
maximum	0.15	0.3	0.0	yes	0.12	0.4	0.0	yes
mean	0.08	0.4	0.1	yes	0.11	0.1	0.3	yes
minimum	0.15	0.0	0.3	yes	0.10	0.4	0.0	yes
KC								
E_p	0.06	0.4	0.1	no	0.22	-0.1	0.2	no
$T_{m-1,0}$	0.20	0.1	0.1	no	0.20	0.1	0.1	yes
T_p	0.22	0.1	0.1	no	0.21	0.0	0.1	yes
m_0	0.07	0.4	0.1	yes	0.19	-0.1	0.3	yes
maximum	0.11	0.4	0.0	yes	0.20	0.2	0.0	yes
mean	0.06	0.1	0.4	yes	0.09	0.0	0.5	yes
minimum	0.06	0.0	0.5	yes	0.23	0.0	0.1	yes
Re								
E_p	0.05	0.5	0.0	yes	0.18	0.3	0.0	yes
$T_{m-1,0}$	0.19	0.1	0.1	no	0.24	0.0	0.1	yes
T_p	0.21	0.1	0.1	no	0.21	0.0	0.1	yes
m_0	0.05	0.5	0.0	yes	0.20	0.2	0.0	yes
maximum	0.24	0.0	0.0	yes	0.14	-0.1	0.4	yes
mean	0.05	0.1	0.4	yes	0.08	0.0	0.4	yes
minimum	0.04	0.0	0.5	yes	0.24	0.0	0.0	yes

ACCELERATION PARAMETER, NORMAL TO THE SLOPE

The spectral peak, zero order moment and minima values show the same results as at the other heights. Additionally the difference in zero order moment between the armour layer and core seems to be off importance as well as the mean value.

zero order moment The difference in zero order moment between the armour layer and core shows that the acceleration hardly dampens inside the core of the impermeable structure for all frequencies. While for

the homogeneous structure the acceleration does dampen. For some simulations the zero order moment also increases inside the core, it is unclear what causes this.

mean The mean value of the Acceleration parameter in normal direction to the slope lies around zero for all simulations of the impermeable structure, while the for the homogeneous structure the mean acceleration is mostly negative. Which means in the direction outward of the structure. The time series plots show that this is mainly caused by the high peak values that are directed outward of the structure. This is again explained by the high permeability of the structure and the relative ease at which the water level inside the structure lowers with the run-down on top of the structure.

ACCELERATION PARAMETER, X-DIRECTION

In addition to the previous two sections, a correlation between the acceleration parameter in x-direction and the notional permeability is observed at this height.

Spectral peak The spectral peak is the value of the variance density at the peak frequency. It quantifies the value of the acceleration parameter at the frequency which contains the most 'energy'. A clear difference can be seen between the two Van der Meer structures; the homogeneous structure has a noticeable higher peak value than the impermeable structure. Closer inspection of the spectral plots show that this is because the homogeneous structure has its variance density concentrated at mainly one frequency (related to the period of the regular wave), while the variance density of the impermeable structure is distributed over a range of frequencies. Apparently, inside the impermeable structure reflection occurs in x-direction that leads to these additional frequencies inside the armour layer.

maximum A positive maximum value means that it concerns the acceleration parameter associated with the velocity directed outward of the structure. As can be expected from the results of the spectral peak, the maximum values show the same relations; the acceleration parameter is lower for the impermeable structure. For some simulations the maximum is even negative, indicating a continuous flow directed outward of the structure at this height.

mean The mean acceleration is outward directed for both structures, but other than that no further conclusions from this plot can be made.

EULER NUMBER, NORMAL TO SLOPE

mean Since is the Euler number is always negative, the figure indicates that the 'overall' Euler number is larger for the homogeneous structure. Or, that the pressure forces play a larger role as compared to the inertial forces.

EULER NUMBER, X-DIRECTION

The spectral peak shows the same results as at the previous height. Additionally the zero order moment and minimum value show a correlation with the notional permeability.

zero order moment The time series show that the Euler number oscillates around zero for all simulations. The figure thus indicates a larger amplitude of the Euler number for the homogeneous structure.

minimum As can be expected from the results of the zero order moment, the absolute minimum value should be higher for the homogeneous structure. The $P-\Pi$ plot also supports this.

KC NUMBER, NORMAL TO SLOPE

The KC number normal to the slope shows the same results as in the previous sections. Additionally the mean value seemd to be correlated to the notional permeability, but the overlap between the data points of the two structures is too large and does not provide any additional information.

KC NUMBER, X-DIRECTION

The in general lower mean KC number for the impermeable structure is explained with the time series plots. For the homogeneous it shows that the KC number oscillates approximately around zero, while for the impermeable structure the value is negative most of the time. Further conclusion cannot be made based solely on this figure.

REYNOLDS NUMBER, NORMAL TO SLOPE

The Reynolds number normal to the slope show the same results as at the previous heights. Additionally the mean value seemed to have a correlation with the notional permeability, but the plot showed that the overlap in data points between the two structures is still quite significant.

REYNOLDS NUMBER, X-DIRECTION

The previous heights did not show a correlation between the Reynolds number in x-direction and the notional permeability, but here a correlation with the mean value is found. In this particular direction the Reynolds number is higher for the impermeable structure. The flows are also fully turbulent for both structures. However, based solely on this mean value no further conclusions can be made.

5.4.1. SUMMARY

No contradicting results where found as compared to the previous results. Additionally, some other correlations with the notional permeability where found. These are:

1 In x-direction reflection occurs with higher frequencies than the incoming signal for the impermeable structure, which can be concluded from the spectral plots of the flow velocity.
2 The Acceleration parameter in direction normal to the slope, does not dampen inside the core for the impermeable structure.
3 Normal to the slope, lower Acceleration parameters outward of the structure are observed for the impermeable structure.
4 In x-direction, lower Acceleration parameters inward of the structure are observed for the impermeable structure.
5 In normal direction to the slope, the mean pressure over inertial forces ratio is lower for the impermeable structure.
6 In x-direction, the pressure over inertial forces ratio is lower for the impermeable structure for pressures directed outward of the structure.

5.5. CONCLUSIONS BASED ON THE REGULAR WAVES RESULTS

In the previous sections the Π terms were measured at three different heights for the regular wave simulations. These three heights were partly chosen to investigate any difference in the Π terms between these locations. First of all it can be concluded that at 2.5 H_s below the initial water level the same correlations between the notional permeability and the Ac parameter, KC number and Reynolds number, all in normal direction to the slope, can be found as at the other two heights. However, at the other two heights additional correlations are found. At 1.5 H_s below the initial water level, additional correlations with the Euler number in x-direction and with the KC number in normal direction to the slope are found. And at 0.5 H_s below the initial water level even more correlations with the Acceleration parameter in directions both normal to the slope and x-direction are found.

Since the correlations that are found at the lower height are in general also found higher in the structure, and because no contradicting correlations are found, it is concluded that evaluation of the Π terms at 0.5 H_s below the initial water level is sufficient for this analysis. Therefore, the other two heights are henceforth not used.

The results from the above analysis are again repeated below:

In direction normal to the slope

1 Reflection occurs with higher frequencies than the incoming signal inside the impermeable structure, which can be concluded from the spectral plots of the flow velocity.
2 The 'overall' acceleration parameter is lower for the impermeable structure.
3 In normal direction to the slope, the flow in the impermeable structure is less turbulent compared to the homogeneous structure, but still 'fully turbulent' according to the classification by Troch (2000).
4 The KC number in direction, does not dampen inside the core for the impermeable structure.
5 In normal direction to the slope, inertial forces dominate over drag forces for the impermeable structure. For the homogeneous structure drag forces can not be neglected.
6 The Acceleration parameter does not dampen inside the core for the impermeable structure.
7 Lower Acceleration parameters outward of the structure are observed for the impermeable structure.
8 In normal direction to the slope, the mean pressure over inertial forces ratio is lower for the impermeable structure.

In x-direction

9 The Euler number associated with an outward directed pressure gradient, is smaller for the impermeable structure.
10 The pressure over inertial forces ratio is lower for the impermeable structure for pressures directed inward of the structure.
11 Reflection occurs with higher frequencies than the incoming signal for the impermeable structure, which can be concluded from the spectral plots of the flow velocity.
12 Lower Acceleration parameters inward of the structure are observed for the impermeable structure.
13 The pressure over inertial forces ratio is lower for the impermeable structure for pressures directed outward of the structure.

For a clear overview, the results are also summarised in Table 5.4.

Table 5.4: Summary of analysis of regular waves simulations

	normal to slope			x-direction	
	impermeable	homogeneous		impermeable	homogeneous
Reflection	yes	no	Reflection	yes	no
Acc. par. dampens inside core?	no	yes	Acc. par. (inw. dir.)	-	+
Acceleration parameter	-	+	Euler number (outw. dir. pres.)	-	+
Euler number	-	+	Euler number (inw. dir. pres.)	-	+
KC nr. dampens inside core?	no	yes			
Neglect drag forces?	yes	no			
Turbulent flow	-	+			

- = relatively lower
+ = relatively higher

In most cases, when a correlation was found it was highes in the direction inward of the structure, or at least, the correlation was higher or more correlations at the various heights were found in this direction. Therefore, this direction is used henceforth in the analysis. The only exception is the Euler number in x-direction, were

there does not seem to be a more important direction. Since at the height that will be used henceforth (0.5 H_s below the initial water level) a correlation associated with the pressure directed outward of the structure was found, this direction will be used in the further analysis. Pressure directed outward of the structure are intuitively also the pressures which influence the armour layer stability most. Additionally, the $T_{m-1,0}$ of the Reynolds number are selected for further analysis to investigate the reflection that has been observed. The reason why reflection was observed, but no correlation with this wave period was found is probably due to the regular wave forcing with a single frequency. The irregular waves consist of the whole spectra, and thus the $T_{m-1,0}$ gives more information on the characteristic periods.

Based on the above and on Table 5.4, the following Π terms are selected for the analysis with the irregular waves, see Table 5.5.

Table 5.5: Π terms for further analysis

	normal to slope	x-direction
	Π term	Π term
Ac		
	$m_{0,armour} - m_{0,core}$	$\max_{armour}$
	$\min_{armour}$	
Euler		
	$\min_{armour}$	$\min_{armour}$
KC		
	$m_{0,armour} - m_{0,core}$	
	$\min_{armour}$	
Re		
	$T_{m-1,0,armour}$	$T_{m-1,0,armour}$
	$\min_{armour}$	

5.6. IRREGULAR WAVES, 0.5 H_s BELOW INITIAL WATER LEVEL

In this section the results of the irregular wave simulations are analysed. All relevant plots are presented on the following pages. The legend for all figures is shown Figure 5.8.

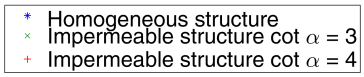

Figure 5.8: Legend for the $P-\Pi$ plots

ACCELERATION PARAMETER, NORMAL TO THE SLOPE

Figure 5.9 shows the difference in zero order moment of the acceleration parameter between the armour layer and core. It shows that the oscillation of the acceleration parameter dampens less inside the core for the impermeable structure as compared to the homogeneous structure. Although the damping is less as compared to the regular wave simulations, still a clear distinction between the two structures is found.

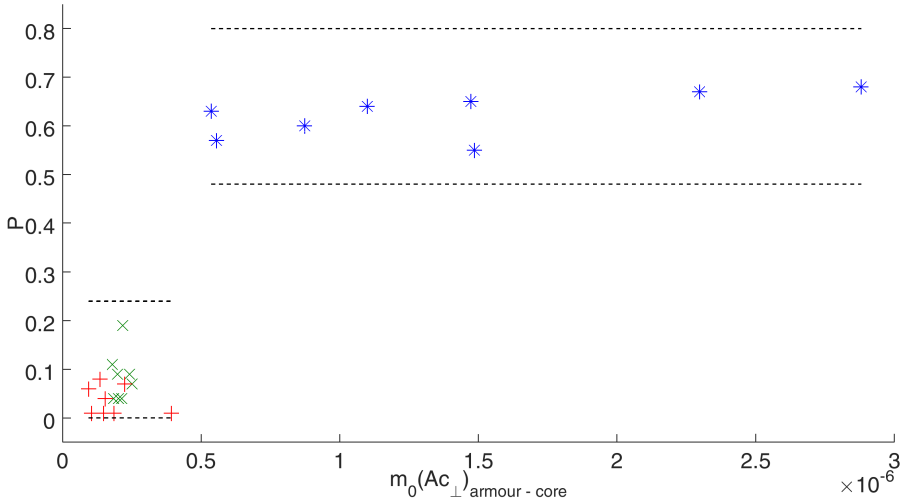

Figure 5.9: P-Π plot of the difference in zero order moment of the Acceleration parameter between the armour layer and core in normal direction to the slope

The minimum value of the acceleration parameter also shows a correlation with the notional permeability for irregular waves. The results are also far less binary than what has been observed so far, meaning that is more likely to also describe values of the notional permeability between the two outer limits.

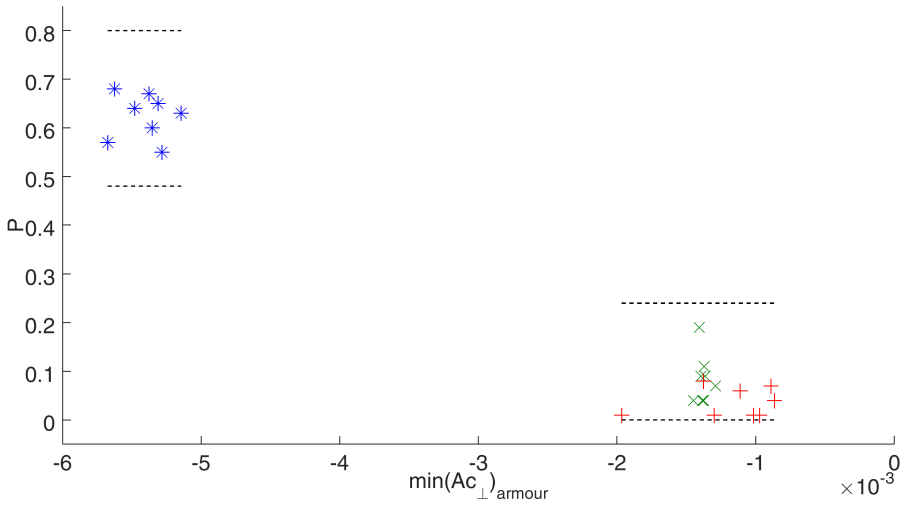

Figure 5.10: P-Π plot of the minima of the Acceleration parameter inside the armour layer in normal direction to the slope

ACCELERATION PARAMETER, X-DIRECTION

Figure 5.11 shows the maxima of the acceleration parameter inside the armour layer in x-direction. Unfortunately, due to a large spread in the data points, this figure does not indicate any correlation with the notional permeability.

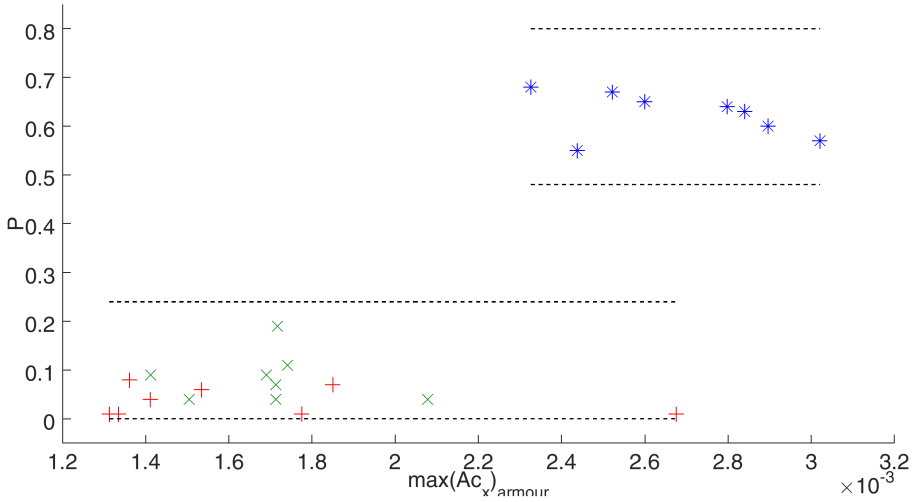

Figure 5.11: P-Π plot of the maxima of the Acceleration parameter inside the armour layer in x-direction

EULER NUMBER, NORMAL TO THE SLOPE

Figure 5.12 shows the minima of the Euler number inside the armour layer in normal direction to the slope. This figure also shows a correlation with the notional permeability.

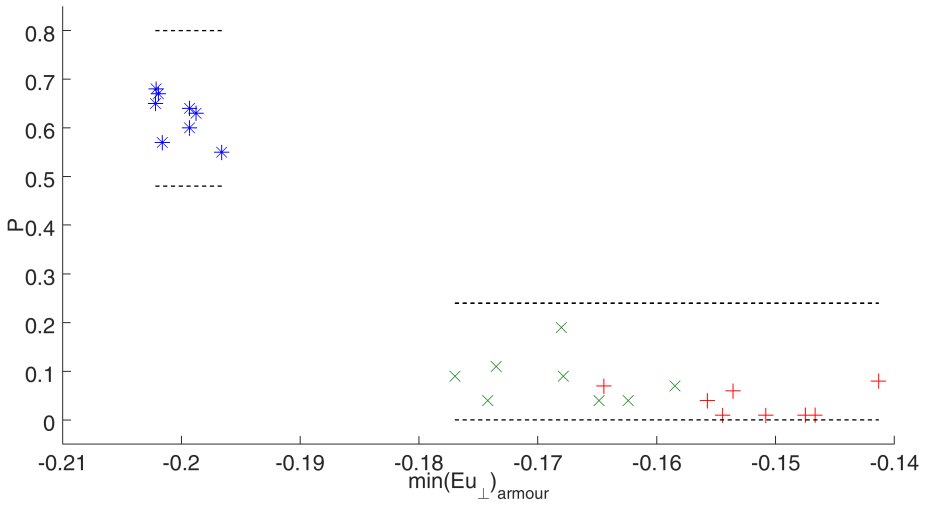

Figure 5.12: P-Π plot of the minima of the Euler number inside the armour layer in direction normal to the slope

EULER NUMBER, X-DIRECTION

Figure 5.13 shows the minima of the Euler number inside the armour layer in normal direction to the slope. Due to a large deviation of one of the data points no correlation seems to exist. However, it is common practice to ignore a single data point if it deviates significantly from the others. In this case a correlation is visible.

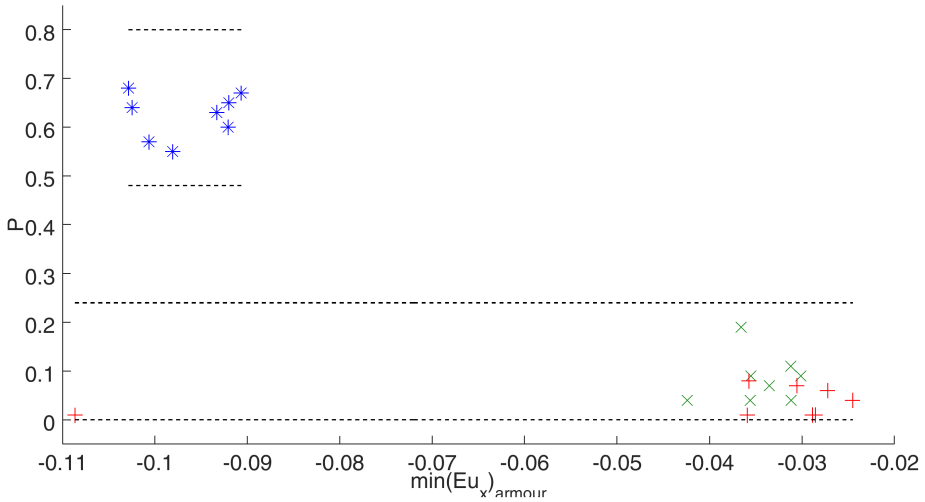

Figure 5.13: P-Π plot of the minima of the Euler number inside the armour layer in x-direction

KC NUMBER, NORMAL TO SLOPE

Figure 5.14 shows the difference in zero order moment of the KC number between the armour layer and core in normal direction to the slope. It clearly shows the same results as for the regular wave simulations. The KC number hardly dampens inside the core of the impermeable structure. While for the homogeneous structure the zero order moment either increases or decreases. Also in this case it is not clear why this value would increase.

Figure 5.15 shows the minima of the KC number inside the armour layer in direction normal to the slope. It clearly shows a correlation with the notional permeability.

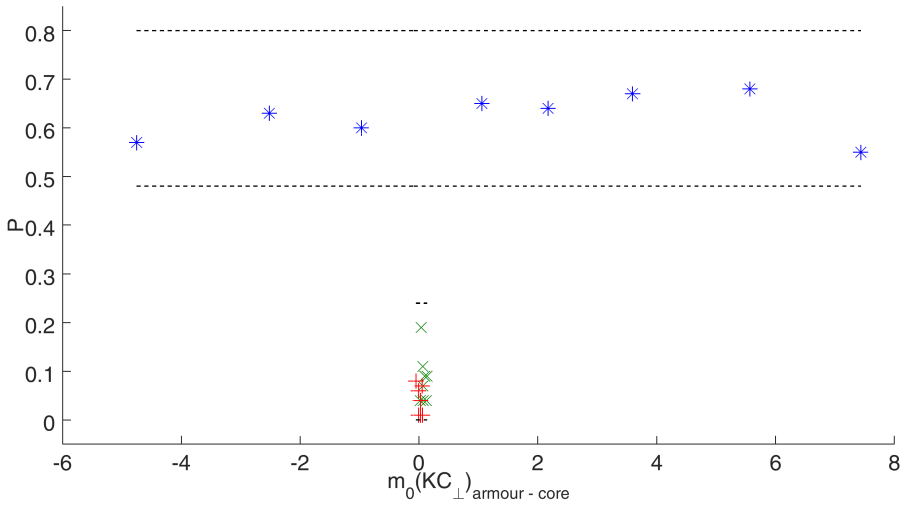

Figure 5.14: P-Π plot of the difference in zero order moment of the Euler number between the armour layer and core in normal direction to the slope

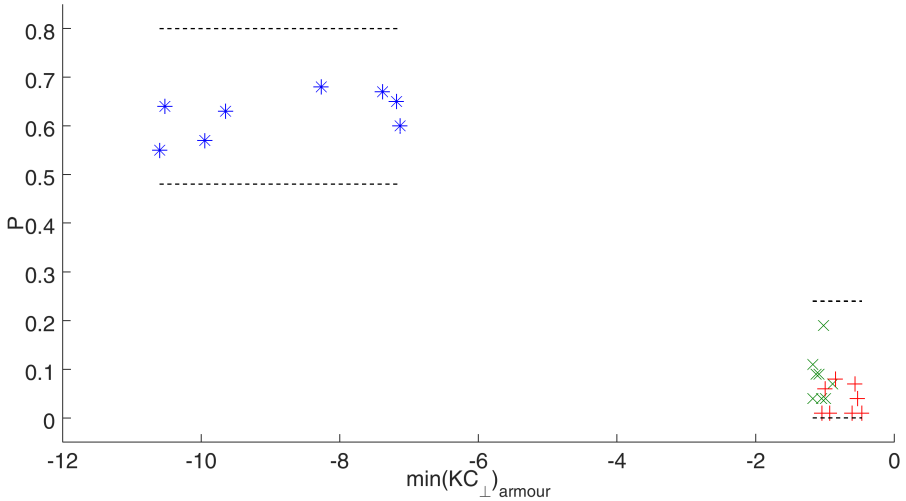

Figure 5.15: P-Π plot of the minima of the Euler number inside the armour layer in normal direction to the slope

REYNOLDS NUMBER, NORMAL TO SLOPE

Figure 5.16 shows the $T_{m-1,0}$ of the Reynolds number inside the armour layer in normal direction to the slope. It shows some correlation with the notional permeability, but the correlation is small and very binairy. Or in other words, it does not seem to be able the describe the P values between the two outer bounds.

Also, the minimum values are shown in Figure 5.17.It clearly shows a correlation with the notional permeability.

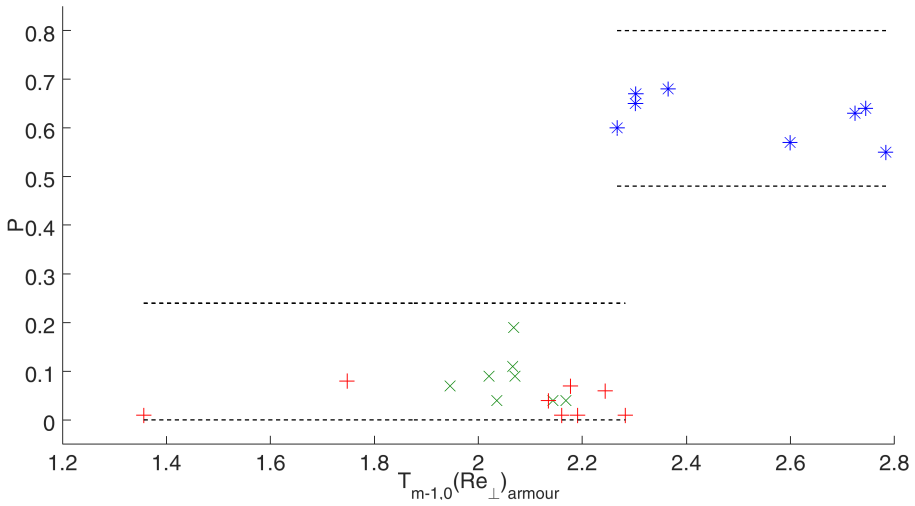

Figure 5.16: P-Π plot of the $T_{m-1,0}$ of the Reynolds number inside the armour layer in normal direction to the slope

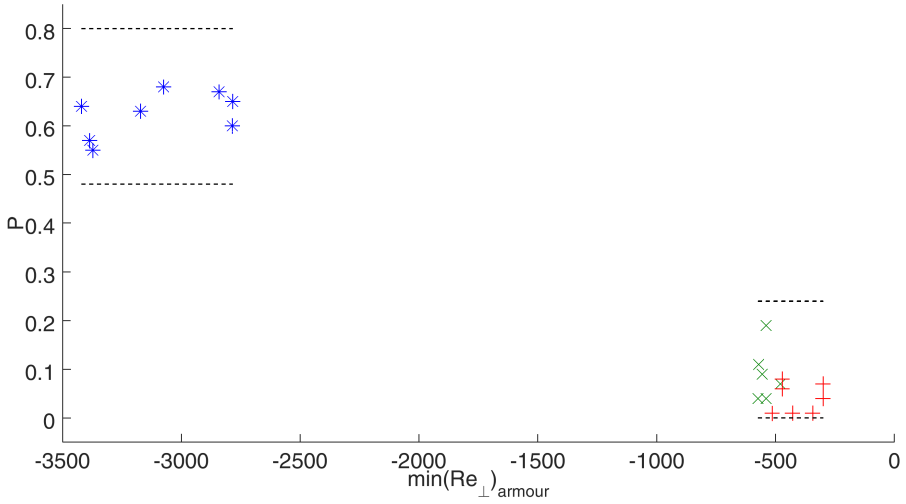

Figure 5.17: P-Π plot of the minima of the Reynolds number inside the armour layer in normal direction to the slope

REYNOLDS NUMBER, X-DIRECTION

Figure 5.16 shows the $T_{m-1,0}$ of the Reynolds number inside the armour layer in x-direction. It does not show any correlation with the notional permeability.

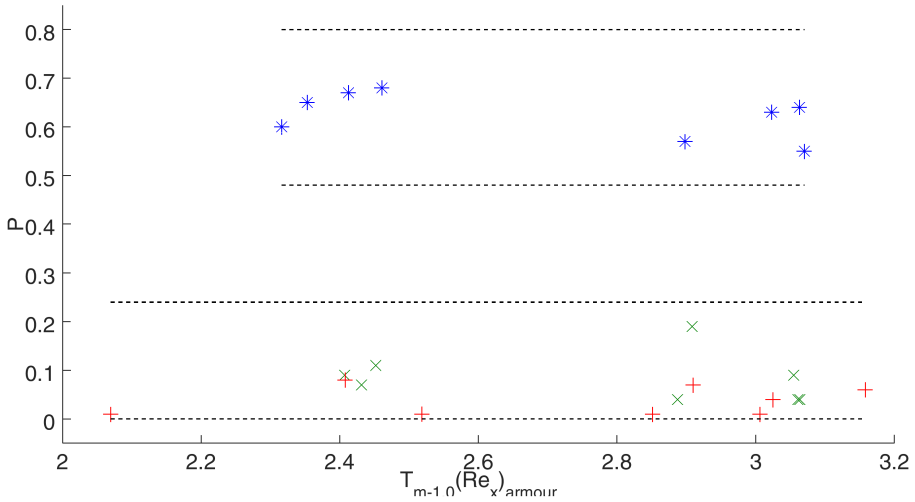

Figure 5.18: P-Π plot of the $T_{m-1,0}$ of the Reynolds number inside the armour layer in x-direction

5.7. CONCLUSIONS BASED ON THE IRREGULAR WAVES RESULTS

As has become clear from the figures presented in the previous sections, the Π terms seems to be able to describe the notional permeability of a structure. Particularly, the Π terms of interest are:

$$\Pi_1 = \frac{u_{\perp,\min}}{ngT_{u_\perp}} \qquad \text{Acceleration parameter}$$

$$\Pi_2 = \frac{n^2}{\rho}\left(\frac{\Delta p}{u^2}\right)_{\perp,\min} \qquad \text{Euler number}$$

$$\Pi_3 = \frac{u_{\perp,\min} T_{u_\perp}}{nD} \qquad \text{KC number}$$

$$\Pi_4 = \frac{u_{\perp,\min} D}{\nu(1-n)} \qquad \text{Reynolds number}$$

Or, in other words, the maximum values of the four Π terms in the direction normal to the slope, associated with an inward directed flow velocity or outward directed pressure gradient. All terms are measured on a line 0.5 times the significant wave height below the initial water level and are a spatial average of all numerical cells on this line and inside the armour layer. An additional benefit compared to the results of the regular waves is that the data points of the two structures seem to lie further away from each other. Therefore these terms have a better 'ability' to also describe intermediate P-values. Note that the subscripts 1,2,3 and 4 do not correspond to the previously defined Π terms, but these will be used henceforth to describe the relations with P.

These Π terms are now curve fitted to a function to arrive at a functional relationship with P. Common choices for curve fitting are power, logarithmic or exponential functions. Two of the Π terms show either a larger spread in lower bound of P (Π_2) or in the upper bound (Π_3), the other two show a similar spread for both bounds. This makes a power function the most logical choice for curve fitting:

$$P = a_i |\Pi_i|^{b_i} \operatorname{sgn}(\Pi_i)$$

Since all minimum values of the four Π terms are negative, the sign function can be left out for simplicity. This results in the following functional relations:

$$P = 421 \left| \frac{u_{\perp,\min}}{ngT_{u_\perp}} \right|^{1.3}$$

$$P = 7.44 \cdot 10^5 \left| \frac{n^2}{\rho}\left(\frac{\Delta p}{u^2}\right)_{\perp,\min} \right|^{8.7}$$

$$P = 0.12 \left| \frac{u_{\perp,\min} T_{u_\perp}}{nD} \right|^{0.7}$$

$$P = 3.43 \left| \frac{u_{\perp,\min} D}{\nu(1-n)} \right|^{0.9}$$

According to the Buckingham Π theorem P should be a function of all four Π terms, in the sense that $P = f(\Pi_1, \Pi_2, \Pi_3, \Pi_4)$. However, due to the limited information available (only the outer bounds are tested) and the uncertainty in the influence of hydraulic parameters on the notional permeability, there is not enough support to construct such a functional relationship. Or at least, it will not provide any additional information besides the four separate functional relations. It is advised to use all four predictors for P and use proper 'engineering judgement' to determine a safe and reliable P-value.

The uncertainty in P (under different hydraulic conditions) can be incorporated in the functional relationships through the previously calculated standard deviation of P. This is done by providing an indication of

the uncertainty in the calculated values of P for the above functional relationships. The average standard deviation was calculated at 0.18:

$$P = 3.1 \cdot 10^2 \left| \frac{u_{\perp,\min}}{n g T_{u_\perp}} \right|^{1.6} \pm 0.18$$

$$P = 4.1 \cdot 10^7 \left| \frac{n^2}{\rho} \left(\frac{\Delta p}{u^2} \right)_{\perp,\min} \right|^{11.2} \pm 0.18$$

$$P = 0.1 \left| \frac{u_{\perp,\min} T_{u_\perp}}{nD} \right|^{0.9} \pm 0.18$$

$$P = 7.2 \cdot 10^{-5} \left| \frac{u_{\perp,\min} D}{\nu(1-n)} \right|^{1.1} \pm 0.18$$

The four final functional relations are visualized in the following four figures:

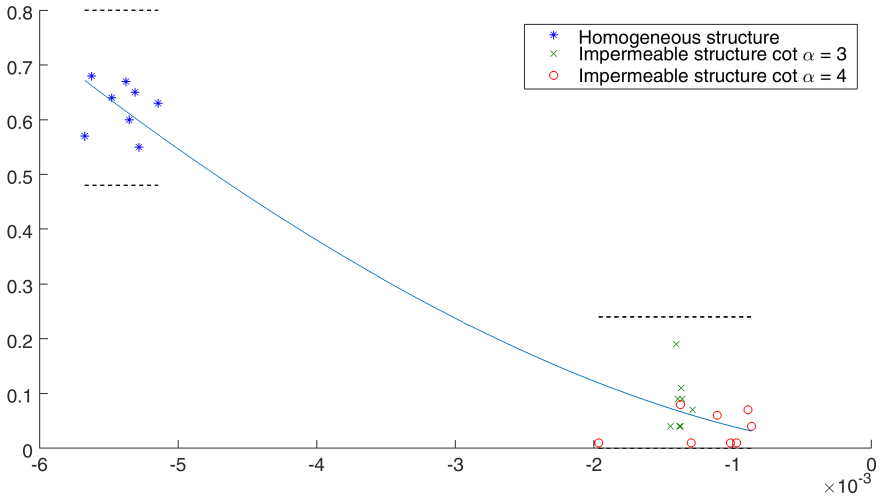

Figure 5.19: Functional relation $P = f(\Pi_1)$

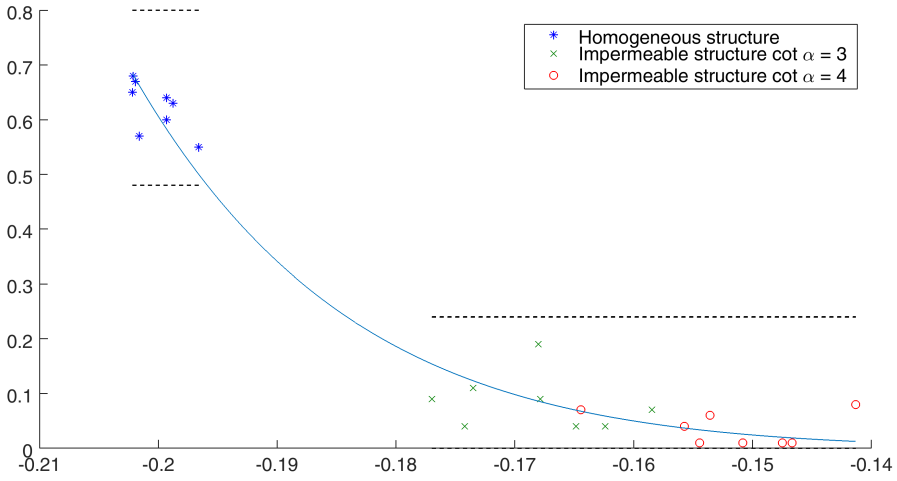

Figure 5.20: Functional relation $P = f(\Pi_2)$

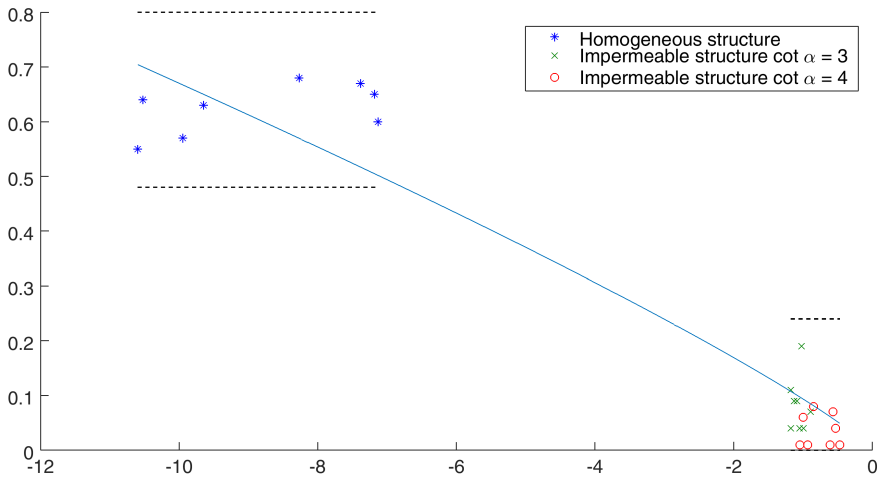

Figure 5.21: Functional relation $P = f(\Pi_3)$

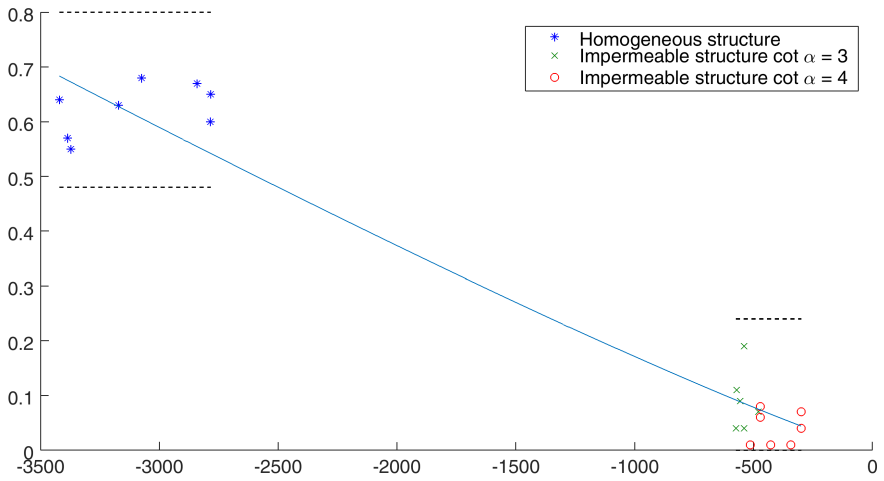

Figure 5.22: Functional relation $P = f(\Pi_4)$

5.8. APPLICATION OF THE FUNCTIONAL RELATIONS

In this section the four functional relations are tested on two structures of Kik (2011) and Kluwen (2012). Both structures are tested with four simulations with an Iribarren number ranging from 2.24 - 5.81 for the Kik structure and 2.57 - 6.63 for the Kluwen structure. Which are the same simulations from the evaluation tests, see Tables 4.3 and 4.11. The structure by Kik is actually the same as the permeable Van der Meer structure. Kik found a P-value of 0.55 while Van der Meer found a value of 0.5. The structure by Kluwen is similar to the fourth Van der Meer structure. Kluwen found a P-value of 0.45 and Van der Meer a value of 0.43-0.44 (which was rounded to 0.4).

The four functional relations are now applied to the results of these eight simulations. The results are plotted in the corresponding $P - \Pi$ plots. See Figures 5.23-5.26.

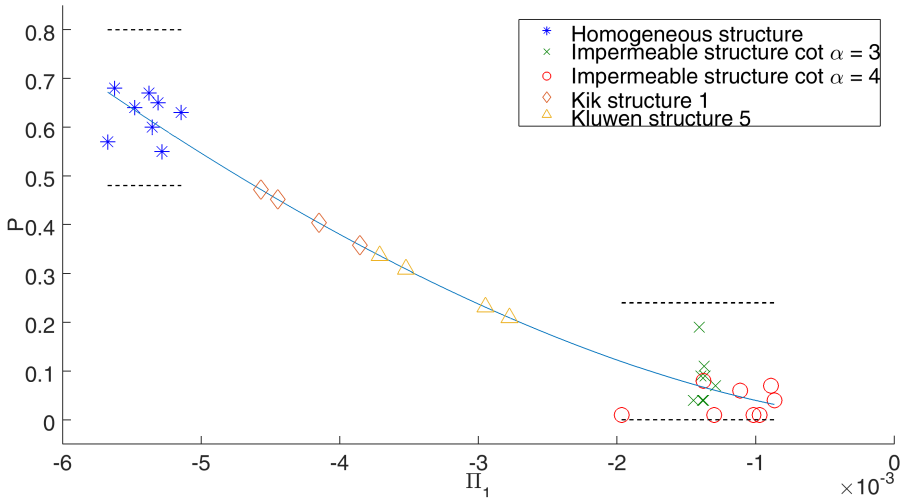

Figure 5.23: Application of $P = f(\Pi_1)$

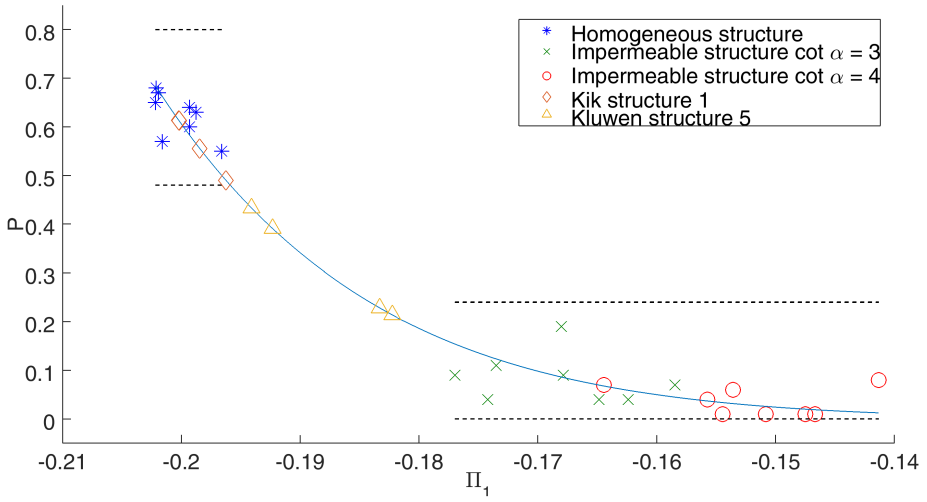

Figure 5.24: Application of $P = f(\Pi_2)$

The overall results are as expected; the data points of both structures all lie within the outer bounds of P. Some of the data points of the Kik structure partially overlap with the data points of the homogeneous, which not surprisingly since these P-values lie close to each other. Furthermore, all data points of the Kluwen structure (~ 0.45) results in a lower P-value than the Kik structure ($\sim 0.5 - 0.55$). The results are summarised in Table 5.6.

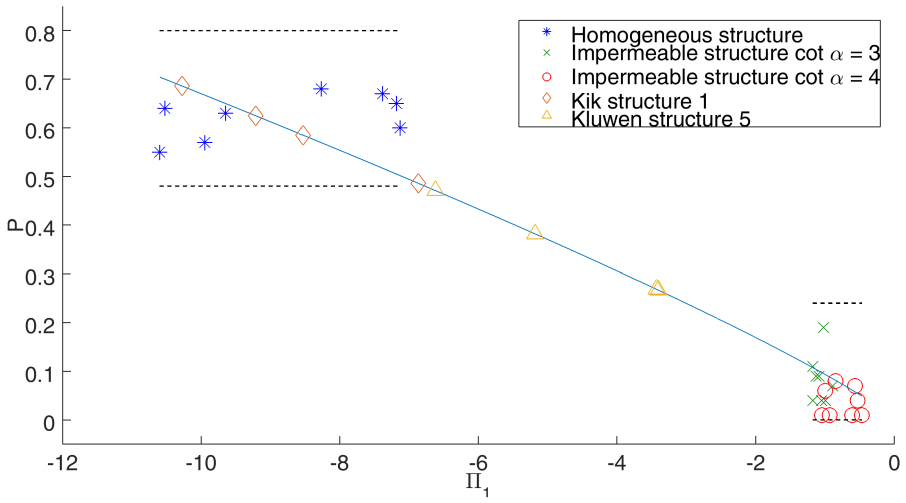

Figure 5.25: Application of $P = f(\Pi_3)$

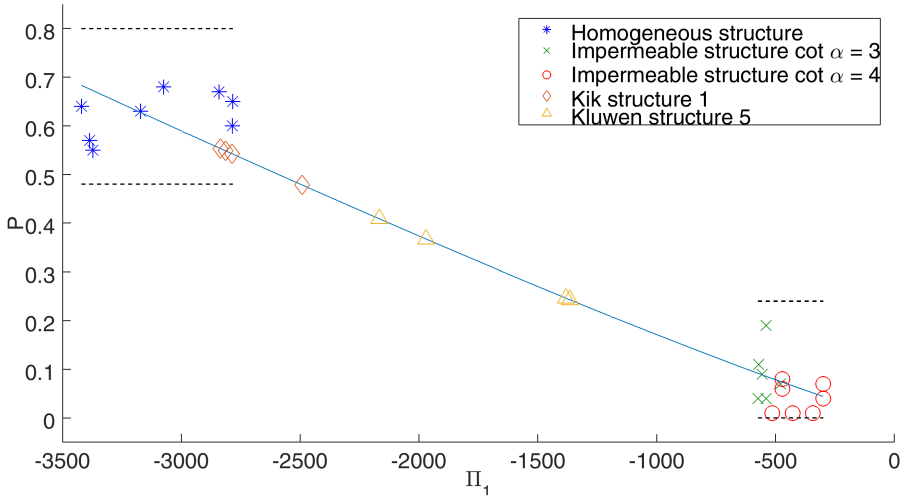

Figure 5.26: Application of $P = f(\Pi_4)$

The original P-values by Van der Meer were determined for three structures, based on a whole range of hydraulic parameters. Therefore, these P-values can be seen as an average of all hydraulic conditions. From which it follows that the calculation of P should be based on a range of Iribarren. Next, a safe P-value should be determined based on these results. The average P-value for Kik structure 1 is 0.53 with a standard deviation of 0.08, which is in good agreement with the expected value of 0.5-0.55. The average value for Kluwen structure 5 is 0.31 with a standard deviation of 0.08, which does not correspond with the expected value of 0.43-0.45. This can be explained by the fact that the functional relations are only based on the outer bounds and thus have an uncertain predicting performance for the intermediate P-values. Without further verification the functional relations are thus more a predictor for the outer bounds than for the whole possible range of P-values. Still, the above method does give a rough prediction of the notional permeability. As an example the average values for the four simulation was taken, but it should be noted that each test has its own unique P-value.

Application range In this work physical scale models are simulated. Therefore, as in reality, scale effects could play a role. This has to be kept in mind and scale effects should be investigated before application of the calculation method. Furthermore, the nominal stone diameter was kept constant at 0.036 and the

Table 5.6: Results of the application of the four functional relations

Kik structure 1					Kluwen structure 5				
test nr.	Π_1	Π_2	Π_3	Π_4	test nr.	Π_1	Π_2	Π_3	Π_4
1	0.36	0.61	0.69	0.55	56	0.23	0.21	0.27	0.25
3	0.40	0.56	0.62	0.54	60	0.21	0.39	0.27	0.24
4	0.47	0.49	0.58	0.55	64	0.34	0.23	0.38	0.37
6	0.45	0.61	0.49	0.48	68	0.31	0.43	0.47	0.41
μ	0.53				μ	0.31			
σ	0.08				σ	0.08			

porosity at 0.4.

6

CONCLUSIONS & RECOMMENDATIONS

The goal of this research is to give more physical background to the notional permeability and to find a correlation between P and pressure and flow patterns inside the a rubble mound structure. In this chapter the research questions are answered, conclusions are listed/drawn, and applicability of the functional relations is discussed. This chapter is concludes with recommendations for further research.

6.1. ANSWERS TO THE RESEARCH QUESTIONS

In this section the research questions are answered. Also reference is made to sections were more background information is given.

Research question 1 *Can the notional permeability be correlated to pressure and flow patterns inside a rubble mound structure under wave attack?*

To measure pressure and flow patterns inside a rubble mound breakwater, first, the numerical model was validated based on physical test measurements of pressure differences inside a breakwater. This was done by comparing the variance density spectra of the pressure oscillation time series of physical tests and numerical test. This showed that the model is able to simulate pressures accurately. *Section 4.5.*

Furthermore, the evaluation method showed that numerous correlations exist between the notional permeability and dimensionless numbers inside the armour layer and core of the rubble mound breakwaters based on the regular waves series tests. Similar conclusions could be drawn for the irregular wave series tests. *Sections 5.2-5.5.*

Research question 2 *Which physical processes, or combination of physical processes, inside a rubble mound structure can be used to describe the notional permeability?*

The physical processes were described with dimensionless numbers resulting from the Buckingham Π theorem, called Π terms. Each describing a ratio of two physical processes. *Section 3.4.*

Four of these Π terms at a height of 0.5 times the significant wave height below the initial water level, and in normal direction to the slope, were determined to provide the best predictors for the notional permeability. The four Π terms are shown in Equation 6.1. *Sections 5.6-5.7.*

$$
\begin{aligned}
\Pi_1 &= \frac{u_{\perp,\min}}{ngT_{u_\perp}} && \text{rate of acceleration} \\
\Pi_2 &= \frac{n^2}{\rho}\left(\frac{\Delta p}{u^2}\right)_{\perp,\min} && \frac{\text{pressure force}}{\text{inertial force}} \\
\Pi_3 &= \frac{u_{\perp,\min} T_{u_\perp}}{nD} && \frac{\text{drag force}}{\text{inertial force}} \\
\Pi_4 &= \frac{u_{\perp,\min} D}{\nu(1-n)} && \frac{\text{inertial force}}{\text{viscous force}}
\end{aligned} \tag{6.1}
$$

(See Figure 5.1 for the choice of the coordinate system.)

Although the Buckingham Π theorem states that P is a function of these four Π terms, it was chosen to use them as separate predictors for the notional permeability through four functional relations. Creating one functional relation would not provide any additional information since it is based solely on the outer bounds of notional permeability. Keeping the Π terms separate also allows one to better recognize the physical processes involved.

Through curve fitting the following functional relations were obtained:

$$
\begin{aligned}
P &= 3.1 \cdot 10^2 \left| \frac{u_{\perp,\min}}{ngT_{u_\perp}} \right|^{1.6} \pm 0.18 \\
P &= 4.1 \cdot 10^7 \left| \frac{n^2}{\rho}\left(\frac{\Delta p}{u^2}\right)_{\perp,\min} \right|^{11.2} \pm 0.18 \\
P &= 0.1 \left| \frac{u_{\perp,\min} T_{u_\perp}}{nD} \right|^{0.9} \pm 0.18 \\
P &= 7.2 \cdot 10^{-5} \left| \frac{u_{\perp,\min} D}{\nu(1-n)} \right|^{1.1} \pm 0.18
\end{aligned}
$$

6.2. CONCLUSIONS

In this section conclusions resulting from the various parts of this report are listed. Along with references to sections were more background information is given.

Literature Study

- Permeability has a large influence on the armour layer stability. *Section 2.4.*
- The permeability is incorporated in the stability formula of Van der Meer through the notional permeability. The definition of the word notional must always be kept in mind; 'existing as or based on a suggestion, estimate, or theory; not existing in reality'. *Section 2.5*
- The permeability is related to the flow of fluids through the pores of a porous media. *Section 2.5*
- The notional permeability is not only dependent on structural parameters, but on hydraulic parameters as well. Sections 2.6-2.7.
- The flow inside a rubble mound breakwater can be described by the extended Forchheimer equation. *Section 2.10*
- Based on the extended Forchheimer equation, a list of relevant variables with respect to the notional permeability can be made. *Section 2.11.*

Methodology

- The unknown influence of hydraulic parameters on the notional permeability is smallest for the outer bounds of P. *Section 3.1.*

- All parameters which can not be varied within the numerical model, e.g. stone grading, relative mass density, are kept constant. From this basic idea, 16 physical model tests for the impermeable structure are selected for numerical simulation and 8 for the homogeneous structure . *Section 3.2.*

- Applying the Buckingham Π theorem on the list of relevant variables results in four commonly used dimensionless numbers. *Section 3.4.*

- The uncertainty in the P-values can be determined by doing the analysis of Van der Meer (1988) over again. *Section 3.5.*

- Instead of using the definition of P as a parameter following from the curve fitting procedure, and is thus constant for a particular structure, P should be used as a variable for optimal damage prediction, and should therefore vary under different hydraulic conditions. Following this thought an 'optimum P-value' can be calculated for each physical test, assuming the stability formula as given. *Section 3.6.*

Evaluation of the numerical model

- The Matlab GUI, which generates the input files for the numerical model, provides an option 'reconstruct wave series'. This allows the user to give a water level elevation time series as input for the boundary condition. Sometimes, the tail of the corresponding variance density spectrum (the higher frequencies in the time series) is for some reason not present in the final boundary condition. Since the source code of the Matlab GUI is not available, the reason behind this could not be investigated. *Section 4.2.*

- Turbulence can not be included in the numerical model because of errors in the $k-\epsilon$ closure model. *Section 4.2.*

- For this research the turbulence outside of the breakwater is assumed to be irrelevant. Inside the breakwater the effect of turbulence on the pressure and flow velocities is assumed to be fully incorporated via the turbulent coefficient of the Forchheimer equation. *Section 4.2.*

- Dynamic updating of the turbulent Forchheimer coefficient via the KC number is not properly written in the source code. Rewriting a small part of the source code solved this problem. *Section 4.2.*

- Because of a small error in the description of the added mass coefficient in the manual, this parameter is overestimated in every simulation. The effect of this is, however, considered small due to the relatively small influence of the coefficient c in the Forchheimer equation. This was the only parameter which was not varied during the model evaluation. *Section 4.2.*

- The van der Meer PM spectra can be reproduced with a JONSWAP spectrum with a peak enhancement factor of 1.5. *Section 4.3.*

- Convergence tests showed that a grid size of $\Delta x = 0.24, \Delta y = 0.12$ and a simulation period of 400 seconds give optimal results with respect to a balance between computational time and accuracy of the results. *Section 4.4.*

- Absolute pressure values are difficult to compare between physical and numerical models and it is thus difficult to draw proper conclusions. Therefore the variance density spectra of the pressure signals are calculated, analogous to the variance density spectra of wave signals. Pressure should be expressed in meters head for convenience. *Section 4.5.*

- Based on the variance density spectra, pressures are very well simulated in the numerical model. *Section 4.5.*

- Turbulent flows inside the breakwater can be simulated with a 'fully turbulent' model. Which means the extended Forchheimer equation reduces to: $I = bu|u| + c\frac{\partial u}{\partial t}$. *Section 4.5.*

Results Correlations between the notional permeability and the dimensionless numbers are found for both regular and irregular waves. Their physical relevance is summarised below for both the x-direction and direction normal to the slope.

Results, normal to the slope

- Reflection occurs with higher frequencies than the incoming signal inside the impermeable structure, which can be concluded from the spectral plots of the flow velocity.
- The 'overall' acceleration parameter is lower for the impermeable structure.
- In normal direction to the slope, the flow in the impermeable structure is less turbulent compared to the homogeneous structure, but still 'fully turbulent' according to the classification by Troch (2000).
- The KC number in direction, does not dampen inside the core for the impermeable structure.
- In normal direction to the slope, inertial forces dominate over drag forces for the impermeable structure. For the homogeneous structure drag forces can not be neglected.
- The Acceleration parameter does not dampen inside the core for the impermeable structure.
- Lower Acceleration parameters outward of the structure are observed for the impermeable structure.
- In normal direction to the slope, the mean pressure over inertial forces ratio is lower for the impermeable structure.

Results, x-direction

- The Euler number associated with an outward directed pressure gradient, is smaller for the impermeable structure.
- The pressure over inertial forces ratio is lower for the impermeable structure for pressures directed inward of the structure.
- Reflection occurs with higher frequencies than the incoming signal for the impermeable structure, which can be concluded from the spectral plots of the flow velocity.
- Lower Acceleration parameters inward of the structure are observed for the impermeable structure.
- The pressure over inertial forces ratio is lower for the impermeable structure for pressures directed outward of the structure.

Results, functional relations

- Functional relations are best based on the irregular waves results. Particularly on the minimum values, inside the armour layer of the four Π terms (see the definition of the coordinate system in Figure 5.1). *Section 5.7*.
- The functional relations can best be presented as functions of the four separate Π terms, instead of one function of multiple variables. *Section 5.7*.
- The notional permeability as introduced by Van der Meer is an average value of P under a range of hydraulic conditions. Therefore the functional relations should be applied to a range of Iribarren numbers and based on these results a practical P-value should be chosen. *Section 5.8*.

Results, physical processes The functional relations represent the best correlations which were found between P and the Π-terms. Thus, they also describe the dominant physical processes behind P. These are:

All four Π terms show a positive correlation with P, namely:

- the rate of acceleration
- the pressure to inertial force ratio

- the drag to inertial force ratio
- the inertial to viscous force ratio.

Furthermore, at the lowest bound of P drag forces are small to negligible and the flow is classified as fully turbulent for all values of P.

6.3. RECOMMENDATIONS

The goal of this research was to find a physical correlation between the notional permeability and pressure and flow patterns inside a rubble mound breakwater. Some assumptions were made throughout the process of this research to achieve this goal. Based on the effect of these assumptions, the following recommendations are made:

- It was assumed that hydraulic parameters have a small influence on the notional permeability for the outer P-values, which is probably not entirely correct. Furthermore, as the target P-values of the physical tests the 'optimum P-values' (see Section 3.6) were calculated. Therefore, (numerical) tests should be carried out with constant hydraulic parameters for multiple structures. In this way the influence of the hydraulic parameters is at least kept constant for all tests and a more precise functional relation can be determined under those particular hydraulic conditions. If this is done for a number of different hydraulic conditions, the real influence on the notional permeability can be determined.
- The model validation was based on limited physical data from inside a rubble mound breakwater. While the model configurations showed almost perfect agreement with the physical data from Kik (2011), the absolute values of physical data from Kluwen (2012) could not be reproduced. In this case only the spectral shape gave good results. Therefore, the pressure and flow patterns inside a rubble mound breakwater resulting from the numerical model should ideally be further validated based on more physical data. In this regard more insight in the exact values of the turbulent Forchheimer and added mass coefficients is also preferred. At the moment the only way to determine these is through physical experiments with the porous media.
- The homogeneous structure was modelled with an 'armour layer' with a higher turbulent Forchheimer coefficient to account for the turbulence associated with wave impact on a rubble mound structure. This was done because the $k-\epsilon$ closure model does not work properly in the numerical model. The correctness of modelling a homogeneous structure with varying turbulent Forchheimer coefficient should be validated with physical data.

The goal should be to drop the word 'notional' from the notional permeability and determine the permeability of a rubble mound structure directly. If this is achieved a new stability formula can be derived, or P can be derived from the permeability. With the results from this research the latter is actually achieved for the outer bounds of permeability (fully impermeable and fully permeable), where the permeability is expressed in properties of the flow and directly transformed to the notional permeability values. To be able to calculate the real permeability with the same approach as in this research, the following recommendation is made:

- Design several fully impermeable structures, that is an impermeable core with an armour layer with varying structural properties (nominal stone diameter, porosity). The Forchheimer coefficients should ideally be known for all test cases. Stating that this type of structure is fully impermeable (and thus zero permeability), the flow inside the armour layer can be analysed for consistencies between the several tests cases. The same can be done for a fully permeable structure (100% permeability). In this way a first functional relation for the permeability can be derived.

The ultimate goal will be to predict the armour layer stability as accurate as possible. Hence this research, if P can be determined more accurately, then the armour layer stability can be determined more accurately as well. Calculating P is thus an intermediate step of calculating the armour layer stability. The armour layer stability is largely dependent on the notional permeability and can intuitively also be related to pressure and flow patterns inside the armour layer. Since the damage for each test of Van der Meer (1988) is known, the damage can be plotted as function of the dimensionless numbers which were calculated in this research. Several simple plots already show very promising results and thus show that this model is in principle able

to predict damage numbers based on pressure and/or flow patterns. An example is shown in Figure 6.1. It is therefore recommended to perform more numerical research to find a direct correlation between damage numbers and pressure and/or flow patterns.

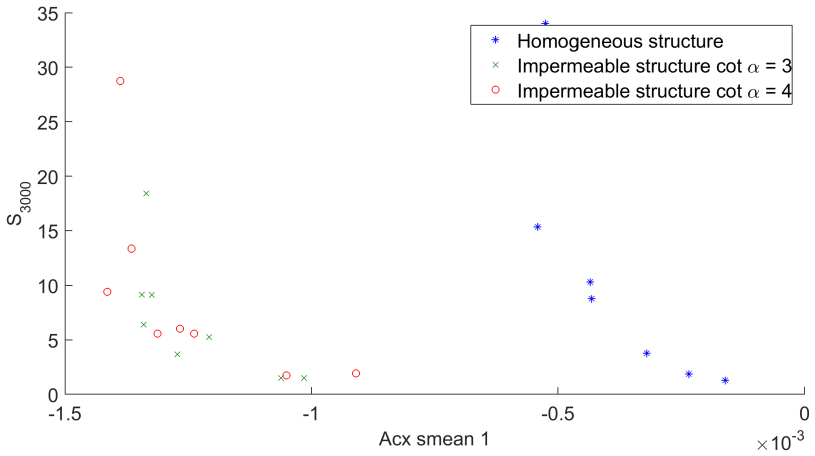

Figure 6.1: Damage as function of the mean Acceleration parameter (x-direction) inside the armour layer

Predicting damages could also be done directly with a numerical model by modelling stone movement. However, for this purpose individual stones have to be modelled which must also be able to 'move' within the numerical domain. Considering present-day computational resources this is not expected to be viable in the near future.

REFERENCES

J. Van der Meer, *Rock slopes and gravel beaches under wave attack,* (1988).

P. Troch, *Experimentele studie en numerieke modellering van golfinteractie met stortsteengolfbrekers,* (2000).

R. Kik, *Notional permeability of breakwaters,* (2011).

J. Kluwen, *Physical model tests of the notional permeability on breakwaters,* (2012).

H. Jumelet, *The influence of core permeability on armour layer stability,* (2010).

A. Vilaplana Domingo, *Evaluation of the volume-exchange model using van der meer laboratory tests results,* (2010).

P. Broekhoven, *The influence of armour layer and core permeability on the wave run-up,* (2011).

R. Iribarren Cavanilles, *Una fórmula para el cálculo de los diques de escollera,* (1938).

G. Schiereck and H. Verhagen, *Introduction to bed, bank and shore protection,* (2012).

T. Lykke Andersen, *Hydraulic response of rubble mound breakwaters,* (2006).

F. Barends, *Wave interaction with permeable coastal structures,* (1985).

P. Hölscher and F. Barends, *Transport in porous media,* (1986).

M. Van Gent, *Formulae to describe porous flow,* (1992).

M. Van Gent, *Geotechnical aspects of rubble mound breakwaters,* (1995).

I. Cantabria, *Ih-2vof course, october 4TH 2012 - october 5TH 2012,* (2012).

J. Zelt and J. Skjelbreia, *Estimating incident and reflected wave fields using an arbitrary number of wave gauges,* (1992).

J. Lara, I. Losada, M. Maza, and R. Guanche, *Breaking solitary wave evolution over a porous underwater step,* (2011).

Appendices

A

POST-PROCESSING OF THE NUMERICAL DATA

In this appendix a description is given of the post-processing procedure and tools used. First, two 'measuring' methods are described: by means of wave gauges and by storing every numerical result for each numerical cell in so-called 'drawfast folders'. Second, the numerical data handling and the calculation of the Π terms is described. This appendix shows and explains the most important post-processing methods and the relevant Matlab scripts. A full list of all post-processing tools is available at `http://datacentrum.3tu.nl/`. As well as all wave gauge data and numerical results for each cell inside the top layers (see Figure A.3) of the breakwaters.

A.1. WAVE GAUGES

Wave gauges are defined by their x-coordinates in the numerical model. The model consequently stores the free surface elevation at this point and the horizontal and vertical velocities over the entire vertical, all at a user-defined time interval. Only the free surface files are used. They are stored at a frequency of 30 Hz. To discern between incoming and reflected signals at least three wave gauges at a relative small distance from each other are needed. In total six wave gauges are defined, see the red arrows in Figure A.1, at x = 4.7, 5.0, 5.4, 14.7, 15.0 and 15.4 m. In this way the incoming and reflected signal can be measured at two locations in the numerical wave flume.

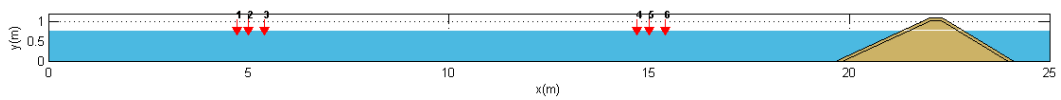

Figure A.1: Wave gauges

The free surface data for each wave gauge are stored in separate .txt files called 'heig1', 'heig2' till 'heig6'. Each file contains two columns, one for the time in seconds and the second for the free surface elevation in meters.

These files are used in the matlab script 'decomp', provided by the Laboratory of Fluid Mechanics of the TU Delft. The script uses a matrix decomposition (Lara *et al.*, 2011) and subsequently a fast fourier transform to calculate a variance density spectrum for both the incoming as reflected signals. These variance density spectra are used in Chapter 4 for the model evaluation.

Additionally a separated script is used to calculate the full variance density spectrum (that is without discerning between the incoming and reflected waves). This script also uses a fast fourier transform. This separate script was made because it is also used for analysis of other data from inside the breakwater. The main part of the script is shown below:

```
Fs = (length(t_t) - 1) / (t_t(end) - t_t(1));   %sampling frequency of waves series
L = length(t_t);    %length of wave series
N = 2^nextpow2(L);    %Nextpower of L, for optimised fft calculation
E = fft(series(iii,:),N);    %fast fourier transform
E = abs(E);    %get amplitudes (scaled)
E = E(1:N/2+1);    %discard half of frequencies (neccessary due to fft algorithm)
E(2:end-1) = 2*E(2:end-1);    %multiply by two for each frequency between 1 and end (neccessary due to fft
E = 1/Fs * 1/2 * E.^2;    %convert amplitude spectrum to variance density spectrum (scaled)
E = 1/L * E;   %scale results (neccessary due to fft algorithm)
f = Fs/2*linspace(0,1,N/2+1);   %corresponding frequency vector
```

Besides the variance density distribution over frequency, additional spectral parameters can be calculated. The main spectral parameters used in the report are the zero$^{\text{th}}$-order moment m_0, $T_{m-1,0}$ period, peak value E_p and the peak period T_p. The choice for $T_{m-1,0}$ period instead of the mean period is because it usually proves to be a better characteristic period of the total spectrum. m_0 and $T_{m-1,0}$ are defined as:

$$\begin{aligned} m_k &= \int_{-\inf}^{\inf} f^k E(f)\,df \\ m_0 &= \int_{-\inf}^{\inf} E(f)\,df \end{aligned} \tag{A.1}$$

$$\begin{aligned} T_{mk1,k2} &= \frac{m_{k1}}{m_{k2}} \\ T_{m-1,0} &= \frac{m_{-1}}{m_0} \end{aligned} \tag{A.2}$$

A.2. DRAWFAST FOLDERS

In the drawfast folders the horizontal and vertical velocities, pressure and VOF are stored for each time step. The GUI of the software does not provide an option to store only data for a part of the numerical domain. However, adding additional commands to the file 'input.txt' can achieve this. The following commands are added (see for a detailed description the manual of the software):

ibg = 793 ieg = 1043

This tells the software to only store data from the 793$^{\text{th}}$ cell in horizontal direction till the 1043$^{\text{th}}$ cell. Two more commands exist to limit data storage in vertical direction. In this way, a square is defined in the 2D domain in which data is stored. With these particular values and the spatial resolution used in this thesis, an area between x = 19 m (foot of the breakwater) and x = 25 (end of the numerical wave flume) is defined for data storage.

Each variable is stored in subfolders in .txt files. The structure of these files in visualised in Figure A.2. To limit the size of these files, the number of time steps that are stored before a new file is created can be adjusted with the 'number_lines' command in the input file. In this report the default of 1000 is reduced to 100 to ensure that the files can easily be load into RAM memory.

The .txt format in which the data is stored, is not ideal in terms of storage (amount of bytes) and data handling and analysis. Therefore, the .txt files are saved as matlab files, which is the main software package used in this report for analysis. The .mat files amount of bytes needed to store the .mat files is significantly less than the .txt files. Additionally, unlike Figure A.2 suggest, the number of columns in the text files is not equal to the number of vertical grid cells. In fact, the number of columns is always 5 (if 5 or more cells exist in the vertical). The matrices in the .txt file are distorted compared to the computational domain. Saving to a .mat file therefore has the additional advantage that the matrices can be stored in an obvious way, that is, the number of column is equal to the number of grid cells in the vertical and the number of rows equal to those in the horizontal.

Below, the script to transform the .txt to .mat files is shown. It is written in such a way that it works regardless of the choice of spatial resolution, simulation length, data storage frequency, number of time steps per .txt file and the computational area for which data is stored.

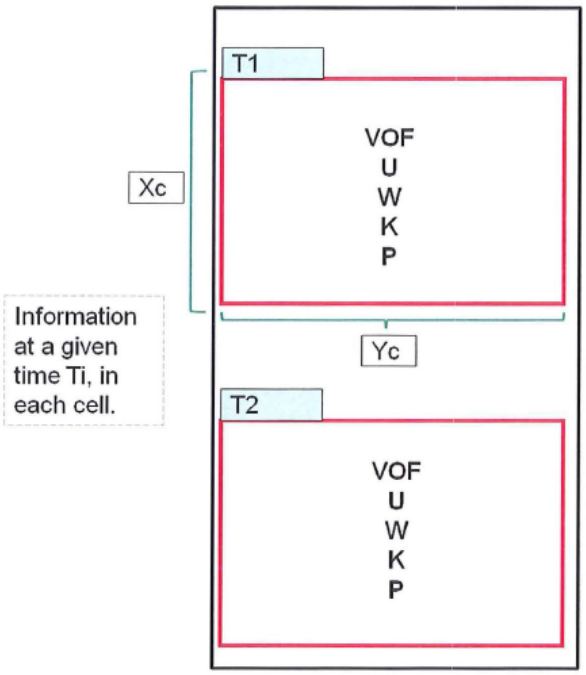

Figure A.2: Wave gauges

The result is a single matlab file for each variable (velocities, pressure and vof). The file contains two variables. The first is a 1xT cell variable, where T is the number of time steps. Each cell contains a XxY double matrix with the data for that particular time step. X and Y are the number of horizontal and vertical numerical cells respectively. The second variable is a 1xT double row vector, which contains the time in seconds for each time step.

Besides these matlab files, an additional file is made which contains two XxY double matrices which contains the x- and y-coordinates for each cell.

```
%postprocessing1_txttomat.m Save .txt files from the IH2VOF software as
%.mat files
%   This script saves .txt files from the IH2VOF software as
%   .mat files. It assumes that the horizontal velocity, vertical velocity,
%   pressure and vof were stored as output by the software. Thus, the
%   folders 'filesU', 'filesW', 'filesVOF' and 'filesPressure' need to be
%   present in the case folders. The .mat files are saved in a new
%   subfolder (in the case folder) called 'files' as the .txt. files. It
%   is written in such a way that it works regardless of the choice of
%   spatial resolution, simulation length, data storage frequency, number
%   of time steps per .txt file and the computational area for which data
%   is stored. Warning: the original .txt files are deleted to save
%   storage space.
%
%   INPUT: directories to the main folder and names of the case folders
%   (multiple possible)
%
%   OUTPUT:     u.mat (horizontal velocity), containing:
%                   u: 1xT cell (each cell contains: XxY double)
%                   u_t: 1xT double for the time in seconds
%
%               w.mat (vertical velocity), containing:
%                   w: 1xT cell (each cell contains: XxY double)
%                   w_t: 1xT double for the time in seconds
%
%               p.mat (pressure), containing:
%                   p: 1xT cell (each cell contains: XxY double)
%                   p_t: 1xT double for the time in seconds
```

```
%
%               t.mat (vof), containing:
%                   t: 1xT cell (each cell contains: XxY double)
%                   t_t: 1xT double for the time in seconds
%
%               cords.mat (coordinates), containing:
%                   x_cords: XxY double for the x-coordinates of each cell
%                   y_cords: XxY double for the y-coordinates of each cell
%
%               T = number of time steps
%               X = number of horizontal grid cells
%               Y = number of vertical grid cells

clc, clear all, close all

mainfolder = '..\IH2VOF\CASES\P01\'; %main folder
casefolders = { ...  %cases
    '36' ...
    };

%loop through each case folder
for i = 1:length(casefolders)
    clearvars -except i mainfolder casefolders

    %case folder
    folder = [mainfolder casefolders{i} '\'];

    %create results folder
    mkdir([folder 'files'])

    %import simulation length, output-frequency, 'number_lines' per file
    %and stored domain
    input = importinputfile([folder 'input']);
    idx = false(7,length(input));
    for j = 1:length(input)
        idx(:,j) = strcmp(input{j,1}, { ...
            'twfin' ...
            'freq_output' ...
            'number_lines' ...
            'ibg' ...
            'ieg' ...
            'jbg' ...
            'jeg' ...
            });
    end
    T = cell2mat(input(idx(1,:),2));
    fs = 1/cell2mat(input(idx(2,:),2));
    nr_lines = cell2mat(input(idx(3,:),2));
    ibg = cell2mat(input(idx(4,:),2));
    ieg = cell2mat(input(idx(5,:),2));
    jbg = cell2mat(input(idx(6,:),2));
    jeg = cell2mat(input(idx(7,:),2));

    %load x-coordinates
    x = load([folder 'xc_info.out']);
    if (1 < ibg) & (ibg < ieg)
        x = x(ibg:ieg);
    end

    %load y-coordinates
    y = load([folder 'yc_info.out']);
    if (1 < jbg) & (jbg < jeg)
        y = y(jbg:jeg);
    end

    %generate meshgrid and save
    [y_cords, x_cords] = meshgrid(y,x);
    save([folder 'files\cords.mat'],'y_cords','x_cords')

    %number of rows over which one 'y column' is distributed
    nr_rows = ceil(length(y)/5);
```

```
%initialise waitbar
h = waitbar(0,'');
set(h,'Name',casefolders{i});

%loop through folders filesPressure, filesU, filesVof and filesW
for j = 1:4
    %initialise variables
    B = cell(ceil(T/(nr_lines/fs)),nr_lines/fs);
    timesteps = NaN(ceil(T/(nr_lines/fs)),nr_lines/fs);

    %subfolder and variable names
    if j == 1
        subfolder = 'filesPressure\';
        varname1 = 'p';
        varname2 = 'p_t';
    elseif j == 2
        subfolder = 'filesU\';
        varname1 = 'u';
        varname2 = 'u_t';
    elseif j == 3
        subfolder = 'filesVof\';
        varname1 = 't';
        varname2 = 't_t';
    elseif j == 4
        subfolder = 'filesW\';
        varname1 = 'w';
        varname2 = 'w_t';
    end

    %loop through each text file
    for k = 1:ceil(T/(nr_lines/fs))
        waitbar(((j-1)*ceil(T/(nr_lines/fs))+k)/ ...
            (4*ceil(T/(nr_lines/fs))),h,'Reading text file')

        %determine 'time-length' of current file
        if k < ceil(T/(nr_lines/fs))
            endT = nr_lines/fs;
        elseif k == ceil(T/(nr_lines/fs))
            endT = T - (k-1)*(nr_lines/fs);
        end

        %filename
        filename = [folder subfolder varname1 sprintf('%03d',k) '.txt'];

        %import text file
        X = importfile(filename, 1, (1+nr_rows*length(x))*fs*endT);

        %loop through each time step in current text file
        for l = 1:fs*endT
            waitbar(l/(fs*endT),h,'Processing text file')

            %initialise cell in B for current timestep
            B{k,l} = NaN(length(x),5*nr_rows);

            %determine start and end row of current timestep in X
            startRow = l + (l-1)*length(x)*nr_rows;
            endRow = l + l*length(x)*nr_rows;

            %import into A
            A = X(startRow:endRow,:);

            %save timestep
            timesteps(k,l) = A(1,1);

            %reshape A and save in current cell of B
            B{k,l} = (reshape(A(2:end,:)',5*nr_rows,length(x)))';

            %delete NaN columns
            B{k,l}(:,all(isnan(B{k,l}))) = [];
        end
```

```
        end
        waitbar(1,h,'Saving to .mat file')

        %reshape B and timesteps into rowvector
        B = reshape(B',1,numel(B));
        timesteps = reshape(timesteps',1,numel(timesteps));
        B = B(~cellfun('isempty',B));
        timesteps = timesteps(~isnan(timesteps));
        timesteps(timesteps==0) = [];

        %rename B and timesteps
        waitbar(1,h,sprintf('Saving results...'))
        assignin('base',varname1,B)
        assignin('base',varname2,timesteps)

        %save to .mat
        save([folder 'files\' varname1 '.mat'],varname1,varname2,'-v7.3')
        clear(varname1,varname2);

        %delete folder
        rmdir([folder subfolder],'s')
    end

    close(h)
end
```

A.3. DATA ANALYSIS

The goal of this research is to find a physical correlation between the notional permeability and flow and pressure patterns inside the structures. Therefore, the second step is to only keep the data at points of interest to further shrink the amount of data and make processing easier and faster.

The area of interest is chosen as the entire armour layer and the part of the core directly behind the armour layer and of equal thickness as the armour layer. See Figure A.3 for an illustration. Note that the figured homogeneous structure actually does not have an armour layer, but that a fictitious 'armour layer' was defined during the model validation to account for the higher turbulent Forchheimer coefficient inside the top layer of the structure.

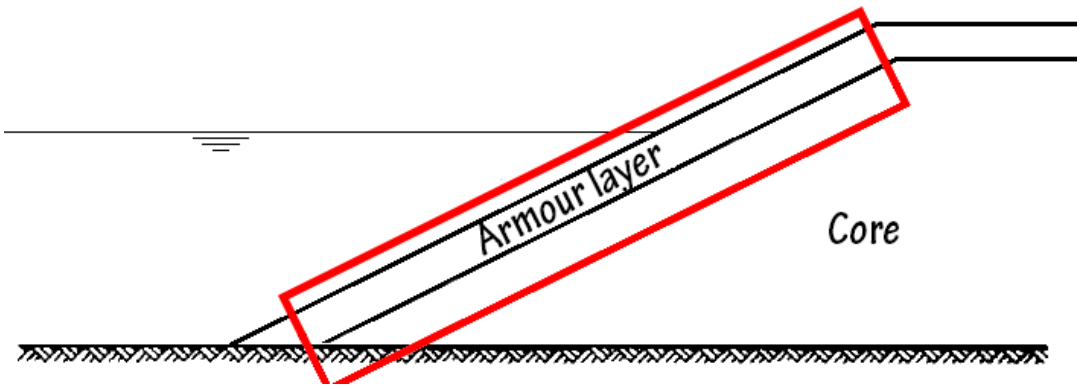

Figure A.3: Rough sketch of the area of interest for the homogeneous structure

The core of the impermeable structure is actually fully impermeable. The filter layer between the armour layer and the core is here designated as the 'core'. The thickness of this filter layer is smaller than the thickness of the armour layer. Thus, the entire filter layer is taken into account.

The matlab script to extract the area of interest is shown below.

```
%postprocessing2_extractlayer.m Extract the area of interest from the .mat
%files and save as .mat files

clc, clear all, close all

mainfolder = '..\IH2VOF\CASES\P01\'; %main folder
casefolders = { ...  %cases
    '36' ...
    };

porosity = 0.40;    %porosity
dy = 0.012; %dy

%Loop through each case folder
for i = 1:length(casefolders)
    %case folder
    folder = [mainfolder casefolders{i} '\'];

    %read structure info
    switch casefolders{i}
    case {'36','37','38','51','52','53','54','55'}
        layer1 = 0.08;  %thickness of first layer
        layer2 = 0.02; %thickness of second layer
        slope = 3;  %front slope angle in cot
        height = 1.15;  %height of structure
    case {'85','86','88','89','90','91','92','104'}
        layer1 = 0.08;  %thickness of first layer
        layer2 = 0.02; %thickness of second layer
        slope = 4;  %front slope angle in cot
        height = 1.15;  %height of structure
    case {'258','259','260','261','262','263','264','265','266','267','268','269','270','271','272','273'}
        layer1 = 0.08;  %thickness of first layer
        layer2 = 0; %thickness of second layer
        slope = 2;  %front slope angle in cot
        height = 1.1;  %height of structure
    end

    %load meshgrid
    load([folder 'files\cords.mat']);

    %load x-coordinates
    x = load([folder 'xc_info.out']);

    %load y-coordinates
    y = load([folder 'yc_info.out']);

    %load porousinfo
    porousinfo = load([folder 'porous_info.out']);

    %extract area of interest from porousinfo
    [~,ia,ib] = intersect(x,x_cords(:,1),'stable');
    [~,ja,jb] = intersect(y,y_cords(1,:),'stable');
    porousinfo = porousinfo(ja,ia);
    porousinfo = porousinfo';
    clear x y

    %treat everything above top of the core as no porous medium
    idx1 = y_cords(1,:)>(height-layer1-layer2);
    porousinfo(:,idx1) = 1;

    %treat (core - second layer) as no porous medium
    for ii = 1:length(porousinfo(1,:))
        porousinfo(x_cords(:,ii)>=(20+layer1/sin(atan(1/slope))+(ii-1)*dy*slope),ii) = 1;
    end

    %create logical matrix (true = porous cell)
    log = porousinfo==porosity;

    %shrink matrices
    [idx2, idx3] = find(log);
    log = log(min(idx2):max(idx2),1:max(idx3));
```

```
porousinfo = porousinfo(min(idx2):max(idx2),1:max(idx3));
x_cords = x_cords(min(idx2):max(idx2),1:max(idx3));
y_cords = y_cords(min(idx2):max(idx2),1:max(idx3));

%everything outside porous media = NaN
x_cords(~log) = NaN;
y_cords(~log) = NaN;

%save meshgrid
save([folder '\files\cords_porous.mat'],'x_cords','y_cords')

%determine thickness and length of layer (number of cells)
row = sum(log(:,1)==true);
col = length(porousinfo(1,1:end));

%extract layer cells from x_cords and y_cords
x_cords = x_cords(log);
y_cords = y_cords(log);

%reshape x_cords and y_cords matrix
x_cords = reshape(x_cords,row,col);
y_cords = reshape(y_cords,row,col);

%save meshgrid
save([folder '\files\cords_porous(reshaped).mat'],'x_cords','y_cords')

%initialise waitbar
h = waitbar(0,'');
set(h,'Name',casefolders{i});

%loop through p, u, t, w
for ii = 1:4
    waitbar(ii/4,h,'Loading .mat file')

    %variable names
    if ii == 1
        varname1 = 'p';
        varname2 = 'p_t';
    elseif ii == 2
        varname1 = 'u';
        varname2 = 'u_t';
    elseif ii == 3
        varname1 = 't';
        varname2 = 't_t';
    elseif ii == 4
        varname1 = 'w';
        varname2 = 'w_t';
    end

    %load results
    load([folder 'files\' varname1 '.mat'])

    %loop through each timestep
    for iii = 1:length(eval(varname1))
        %shrink matrices
        eval([varname1 '{iii} = ' varname1 '{iii}(min(idx2):max(idx2),1:max(idx3));'])

        %everything outside porous media = NaN
        eval([varname1 '{iii}(~log) = NaN;'])
    end

    %save to .mat
    save([folder '\files\' varname1 '_porous.mat'],varname1,varname2)

    %loop through each timestep
    for iii = 1:length(eval(varname1))
        %extract layer cells from varname1
        eval([varname1 '{iii} = ' varname1 '{iii}(log);'])

        %reshape layer matrix
        eval([varname1 '{iii} = reshape(' varname1 '{iii},row,col);'])
```

```
        end

        %save to .mat
        save([folder '\files\' varname1 '_porous(reshaped).mat'],varname1,varname2)

        clear(varname1,varname2);
    end
    close(h)
end

clc, clear, close all
```

The next step for the analysis in this report is to calculate the Π terms in each cell in the area of interest. Eventually it was decided to limit the area of interest further between 2.5 times the significant wave height below the initial water depth and the maximum water level on the slope. The Π terms are calculated with the script presented below.

The Π terms were initially calculated for the horizontal and vertical directions and the directions normal and parallel to the slope. Later it was decided to limit this to only the horizontal and normal to slope directions. Calculating the Ac parameter and KC and Reynolds numbers is straightforward since the flow velocities are stored in vectors in horizontal and vertical directions, and can easily be decomposed in the direction normal to the slope. However, the pressure difference, which is present in the Euler number, does not have a specific direction. The pressure difference in horizontal direction is straightforwardly calculated by subtracting the pressures from horizontally adjacent cells. However, in normal direction this is not easily done due to the orthogonal numerical grid. Besides this, different slope angles are used during the simulations.

Therefore, the numerical data is interpolated in horizontal direction using the 'spline' method in Matlab. The interpolation is done based on the slope angle, such that the difference in pressure between diagonal adjacent cells is automatically the pressure difference in the direction normal to the slope. See Figure A.4.

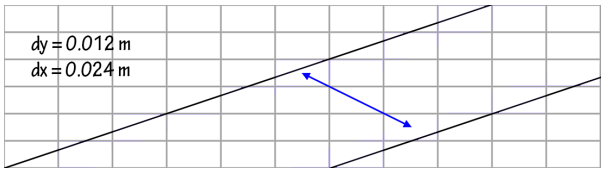

Numerical grid before interpolation. The blue arrow indicates the pressure difference between diagonal adjacent cells. The arrow is not in the direction normal to the slope.

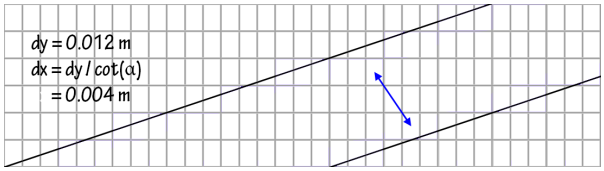

Numerical grid after interpolation. The blue arrow is now in the direction normal to the slope.

Figure A.4: Numerical grid/data interpolation

The matlab scripts to calculate the Π terms are shown below.

```
%postprocessing4_dimnrs.m Calculate and visualise the PI terms

clc, clear all, close all

mainfolder = '..\IH2VOF\CASES\P01\'; %main folder
casefolders = { ...  %cases
    '36' ...
    };

depth = 0.8; %inital water depth

%Loop through each case folder
for i = 1:length(casefolders)
    %case folder
```

```
    folder = [mainfolder casefolders{i} '\'];

    %read slope of structure
    switch casefolders{i}
    case {'36','37','38','51','52','53','54','55'}
        layer1 = 0.08;  %thickness of first layer
        layer2 = 0.02; %thickness of second layer
        slope = 3;  %front slope angle in cot
    case {'85','86','88','89','90','91','92','104'}
        layer1 = 0.08;  %thickness of first layer
        layer2 = 0.02; %thickness of second layer
        slope = 4;  %front slope angle in cot
    case {'258','259','260','261','262','263','264','265','266','267','268','269','270','271','272','273'}
        layer1 = 0.08;  %thickness of first layer
        layer2 = 0.08; %thickness of second layer
        slope = 2;  %front slope angle in cot

    %import Hs and Tm
    input = importgenerationreport([folder '\wave_series\' casefolders{i} '_reg\generation_report.txt']);
%     input = importgenerationreport([folder '\wave_series\Kik_6_reconstructed\generation_report.txt']);
    idx = false(2,length(input));
    for ii = 1:length(input)
        idx(:,ii) = strcmp(input{ii,1}, { ...
            'Hs' ...
            'Tmean' ...
            });
    end
    Hs = cell2mat(input(idx(1,:),2));
    Tmean = cell2mat(input(idx(2,:),2));

    %load variables & corresponding coordinates
    load([folder 'files\cords_porous(reshaped).mat']);
    load([folder 'files\t_porous(reshaped).mat']);

    %determine area to make calculations on
    vof = t{1};
    for ii = 2:length(t)
        vof = vof + t{ii};
    end
    vof = sum(vof);

    ie = length(find(vof))-1;
    [~, ib] = min(abs(y_cords(1,:)-(depth-2*Hs)));

        %load variables & corresponding coordinates
    load([folder 'files\cords_porous.mat']);
    load([folder 'files\p_porous.mat']);    %kPa
    load([folder 'files\u_porous.mat']);    %m/s
    load([folder 'files\w_porous.mat']);    %m/s

    %extract area of interest & round everything below abs(1e-2) to 2
    %decimals
    x_cords = x_cords(:,ib:ie);
    y_cords = y_cords(:,ib:ie);
    for ii = 1:length(p)
        p{ii} = p{ii}(:,ib:ie);
        p{ii}(abs(p{ii})<1e-2) = roundn(p{ii}(abs(p{ii})<1e-2),-2);
        u{ii} = u{ii}(:,ib:ie);
        u{ii}(abs(u{ii})<1e-2) = roundn(u{ii}(abs(u{ii})<1e-2),-2);
        w{ii} = w{ii}(:,ib:ie);
        w{ii}(abs(w{ii})<1e-2) = roundn(w{ii}(abs(w{ii})<1e-2),-2);
    end

    %preallocate
    dpx = cell(1,length(p));
    ux = cell(1,length(p));
    Eulerx = cell(1,length(p));

    %pressure calculations in x and y direction
    %interpolate coordinates
    x_x_cords = (x_cords(1:end-1,:) + x_cords(2:end,:)) / 2;
```

```
x_y_cords = (y_cords(1:end-1,:) + y_cords(2:end,:)) / 2;
y_x_cords = (x_cords(:,1:end-1) + x_cords(:,2:end)) / 2;
y_y_cords = (y_cords(:,1:end-1) + y_cords(:,2:end)) / 2;

dx = x_cords(1:end-1,:) - x_cords(2:end,:);
dx = abs(nanmean(nanmean(dx)));
dy = y_cords(:,1:end-1) - y_cords(:,2:end);
dy = abs(nanmean(nanmean(dy)));

%reshape
[idx1, row1, col1] = reshape_custom(x_x_cords);
[idx2, row2, col2] = reshape_custom(y_x_cords);
x_x_cords = reshape(x_x_cords(idx1),row1,col1);
x_y_cords = reshape(x_y_cords(idx1),row1,col1);
y_x_cords = reshape(y_x_cords(idx2),row2,col2);
y_y_cords = reshape(y_y_cords(idx2),row2,col2);

for ii = 1:length(p)
    %horizontal pressure gradient
    dpx{ii} = diff(p{ii},1,1);
    dpx{ii} = reshape(dpx{ii}(idx1),row1,col1);
    dpx{ii}(abs(dpx{ii})<1e-2) = roundn(dpx{ii}(abs(dpx{ii})<1e-2),-2);

    %flow velocity
    ux{ii} = (u{ii}(1:end-1,:) + u{ii}(2:end,:)) / 2;
    ux{ii} = reshape(ux{ii}(idx1),row1,col1);
    ux{ii}(abs(ux{ii})<1e-2) = roundn(ux{ii}(abs(ux{ii})<1e-2),-2);

    %Euler number
    Eulerx{ii} = 0.4^2 * dpx{ii} ./ (1000 * ux{ii}.^2);
    Eulerx{ii}(isnan(Eulerx{ii})) = 0;
    Eulerx{ii}(~isfinite(Eulerx{ii})) = 0;
end
clear dpx ux
plotdimnr(Eulerx, x_x_cords, x_y_cords, depth, Hs, layer1, layer2, t_t, 'Eulerx', casefolders{i})
clear Eulerx

%load reshaped variables & corresponding coordinates
load([folder 'files\cords_porous(reshaped).mat']);
load([folder 'files\p_porous(reshaped).mat']);  %kPa
load([folder 'files\u_porous(reshaped).mat']);  %m/s
load([folder 'files\w_porous(reshaped).mat']);  %m/s

%extract area of interest
x_cords = x_cords(:,ib:ie);
y_cords = y_cords(:,ib:ie);
for ii = 1:length(p)
    p{ii} = p{ii}(:,ib:ie);
    u{ii} = u{ii}(:,ib:ie);
    w{ii} = w{ii}(:,ib:ie);
end

%interpolate layer for pressures normal to layer
%coordinates for interpolation
x_old = x_cords(:,1);
x_new = x_old(1):1/slope*dy:x_old(end);

%interpolate
x_cords = interp1(x_old,x_cords,x_new,'spline');
y_cords = interp1(x_old,y_cords,x_new,'spline');
for ii = 1:length(p)
    p{ii} = interp1(x_old,p{ii},x_new,'spline');
    u{ii} = interp1(x_old,u{ii},x_new,'spline');
    w{ii} = interp1(x_old,w{ii},x_new,'spline');
end
clear x_old x_new

%preallocate
idx1 = (x_cords(end,end) - x_cords(1,1))*slope/dy + 1;
idx1 = round(idx1);
[~, idx2] = size(x_cords);
```

```
x_cords_temp = NaN(idx1,idx2);
y_cords_temp = NaN(idx1,idx2);
p_temp = cell(1,length(p));
u_temp = cell(1,length(p));
w_temp = cell(1,length(p));
for ii = 1:length(p)
    p_temp{ii} = NaN(idx1,idx2);
    u_temp{ii} = NaN(idx1,idx2);
    w_temp{ii} = NaN(idx1,idx2);
end

%return to normal matrix shape
[idx, ~] = size(x_cords);
idx1 = 1;
idx2 = idx;
x_cords_temp(idx1:idx2,1) = x_cords(1:end,1);
for ii = 1:length(x_cords(1,:))-1
    [idx3, ~] = find(round(x_cords(end,ii)*1e4)/1e4==round(x_cords(:,ii+1)*1e4)/1e4);
    idx1 = idx1 + (idx-idx3);
    idx2 = idx2 + (idx-idx3);

    x_cords_temp(idx1:idx2,ii+1) = x_cords(1:end,ii+1);
    y_cords_temp(idx1:idx2,ii+1) = y_cords(1:end,ii+1);

    for iii = 1:length(p)
        p_temp{iii}(idx1:idx2,ii+1) = p{iii}(1:end,ii+1);
        u_temp{iii}(idx1:idx2,ii+1) = u{iii}(1:end,ii+1);
        w_temp{iii}(idx1:idx2,ii+1) = w{iii}(1:end,ii+1);
    end
end

%delete temporary variables
x_cords = x_cords_temp; clear x_cords_temp
y_cords = y_cords_temp; clear y_cords_temp
p = p_temp; clear p_temp
u = u_temp; clear u_temp
w = w_temp; clear w_temp

%round everything below abs(1e-2) to 2 decimals
for ii = 1:length(p)
    p{ii}(abs(p{ii})<1e-2) = roundn(p{ii}(abs(p{ii})<1e-2),-2);
    u{ii}(abs(u{ii})<1e-2) = roundn(u{ii}(abs(u{ii})<1e-2),-2);
    w{ii}(abs(w{ii})<1e-2) = roundn(w{ii}(abs(w{ii})<1e-2),-2);
end

%preallocate
dpnor = cell(1,length(p));
unor = cell(1,length(p));
wnor = cell(1,length(p));
vnor = cell(1,length(p));
thetanor = cell(1,length(p));
Eulernor = cell(1,length(p));

%pressure calculations normal to slope
%interpolate coordinates
nor_x_cords = (x_cords(1:end-1,2:end) + x_cords(2:end,1:end-1)) / 2;
nor_y_cords = (y_cords(1:end-1,2:end) + y_cords(2:end,1:end-1)) / 2;

dnorx = x_cords(1:end-1,2:end) - x_cords(2:end,1:end-1);
dnorx = abs(nanmean(nanmean(dnorx)));
dnory = y_cords(1:end-1,2:end) - y_cords(2:end,1:end-1);
dnory = abs(nanmean(nanmean(dnory)));
dnor = sqrt(dnorx^2 + dnory^2);

%reshape
[idx1, row1, col1] = reshape_custom(nor_x_cords);
nor_x_cords = reshape(nor_x_cords(idx1),row1,col1);
nor_y_cords = reshape(nor_y_cords(idx1),row1,col1);

for ii = 1:length(p)
```

```
    %pressure gradient
    dpnor{ii} = (p{ii}(1:end-1,2:end) - p{ii}(2:end,1:end-1));
    dpnor{ii} = reshape(dpnor{ii}(idx1),row1,col1);
    dpnor{ii}(abs(dpnor{ii})<1e-2) = roundn(dpnor{ii}(abs(dpnor{ii})<1e-2),-2);

    %flow velocity
    unor{ii} = (u{ii}(1:end-1,2:end) + u{ii}(2:end,1:end-1)) / 2;
    wnor{ii} = (w{ii}(1:end-1,2:end) + w{ii}(2:end,1:end-1)) / 2;
    vnor{ii} = sqrt(unor{ii}.^2 + wnor{ii}.^2);
    thetanor{ii} = atan2(wnor{ii},unor{ii});
    vnor{ii} = cos(thetanor{ii}-(pi/2+atan(1/slope))) .* vnor{ii};
    vnor{ii} = reshape(vnor{ii}(idx1),row1,col1);
    vnor{ii}(abs(vnor{ii})<1e-2) = roundn(vnor{ii}(abs(vnor{ii})<1e-2),-2);

    %Euler number
    Eulernor{ii} = 0.4^2 * dpnor{ii} ./ (1000 * vnor{ii}.^2);
    Eulernor{ii}(isnan(Eulernor{ii})) = 0;
    Eulernor{ii}(~isfinite(Eulernor{ii})) = 0;
end
clear dpnor unor wnor vnor thetanor
plotdimnr(Eulernor, nor_x_cords, nor_y_cords, depth, Hs, layer1, layer2, t_t, 'Eulernor', casefolders{i})
clear Eulernor

%load variable & corresponding coordinates
load([folder 'files\cords_porous(reshaped).mat']);
load([folder 'files\p_porous(reshaped).mat']);  %kPa
load([folder 'files\u_porous(reshaped).mat']);  %m/s
load([folder 'files\w_porous(reshaped).mat']);  %m/s

%roundeverything to 2 decimals
x_cords = x_cords(:,ib:ie);
y_cords = y_cords(:,ib:ie);
for ii = 1:length(p)
    p{ii} = p{ii}(:,ib:ie);
    p{ii}(abs(p{ii})<1e-2) = roundn(p{ii}(abs(p{ii})<1e-2),-2);
    u{ii} = u{ii}(:,ib:ie);
    u{ii}(abs(u{ii})<1e-2) = roundn(u{ii}(abs(u{ii})<1e-2),-2);
    w{ii} = w{ii}(:,ib:ie);
    w{ii}(abs(w{ii})<1e-2) = roundn(w{ii}(abs(w{ii})<1e-2),-2);
end

%preallocate
vnor = cell(1,length(p));
thetanor = cell(1,length(p));

%other calculations without pressures
for ii = 1:length(p)
    %flow velocity normal to slope
    vnor{ii} = sqrt(u{ii}.^2 + w{ii}.^2);
    thetanor{ii} = atan2(w{ii},u{ii});
    vnor{ii} = cos(thetanor{ii}-(pi/2+atan(1/slope))) .* vnor{ii};
    vnor{ii}(abs(vnor{ii})<1e-2) = roundn(vnor{ii}(abs(vnor{ii})<1e-2),-2);
end

%calculate period matrix
Tu = calculateperiod(u,t_t);
Tvnor = calculateperiod(vnor,t_t);

%preallocate
KCx = cell(1,length(p));
KCnor = cell(1,length(p));

for ii = 1:length(p)
    %Keulegan-Carpenter number
    KCx{ii} = u{ii}.*Tu / (0.4*0.036);
    KCnor{ii} = vnor{ii}.*Tvnor / (0.4*0.036);
    KCx{ii}(isnan(KCx{ii})) = 0;
    KCx{ii}(~isfinite(KCx{ii})) = 0;
    KCnor{ii}(isnan(KCnor{ii})) = 0;
    KCnor{ii}(~isfinite(KCnor{ii})) = 0;
end
```

```
    plotdimnr(KCx, x_cords, y_cords, depth, Hs, layer1, layer2, t_t, 'KCx', casefolders{i})
    clear KCx
    plotdimnr(KCnor, x_cords, y_cords, depth, Hs, layer1, layer2, t_t, 'KCnor', casefolders{i})
    clear KCnor

    %preallocate
    Acx = cell(1,length(p));
    Acnor = cell(1,length(p));

    for ii = 1:length(p)
        %Acceleration parameter
        Acx{ii} = u{ii} ./ (0.4*9.81*Tu);
        Acnor{ii} = vnor{ii} ./ (0.4*9.81*Tvnor);
        Acx{ii}(isnan(Acx{ii})) = 0;
        Acx{ii}(~isfinite(Acx{ii})) = 0;
        Acnor{ii}(isnan(Acnor{ii})) = 0;
        Acnor{ii}(~isfinite(Acnor{ii})) = 0;
    end
    plotdimnr(Acx, x_cords, y_cords, depth, Hs, layer1, layer2, t_t, 'Acx', casefolders{i})
    clear Acx
    plotdimnr(Acnor, x_cords, y_cords, depth, Hs, layer1, layer2, t_t, 'Acnor', casefolders{i})
    clear Acnor

    %preallocate
    Rex = cell(1,length(p));
    Renor = cell(1,length(p));

    for ii = 1:length(p)
        %Reynolds number
        Rex{ii} = u{ii} * 0.036 / (10^(-6)*(1-0.4));
        Renor{ii} = vnor{ii} * 0.036 / (10^(-6)*(1-0.4));
        Rex{ii}(isnan(Rex{ii})) = 0;
        Rex{ii}(~isfinite(Rex{ii})) = 0;
        Renor{ii}(isnan(Renor{ii})) = 0;
        Renor{ii}(~isfinite(Renor{ii})) = 0;
    end
    plotdimnr(Rex, x_cords, y_cords, depth, Hs, layer1, layer2, t_t, 'Rex', casefolders{i})
    clear Rex
    plotdimnr(Renor, x_cords, y_cords, depth, Hs, layer1, layer2, t_t, 'Renor', casefolders{i})
    clear Renor

    clearvars -except mainfolder casefolders depth i
    close all
end
```

B

DATA POINTS FOR CURVE FITTING OF THE STABILITY FORMULA

In this appendix the data points for the curve fitting of the Van der Meer stability formula are presented, which was redone in this report to find the spread in the notional permeability values. Only the relevant data points (surging region) are provided.

Table B.1: P value for each physical test (surging region)

Test nr.	$\cot\alpha$	D_{85}/D_{15}	Description	Δ	T_m	D_{n50}	S	ξ_m,1000	$\frac{H_s}{\Delta D}$,1000	ξ_m,1000	$\frac{H_s}{\Delta D}$,1000
1	2	2.25	Imperm.	1.00	1.16	0.016	2	3.15	1.41	3.49	1.15
2	2	2.25	Imperm.	1.00	1.16	0.016	3	3.01	1.55	3.32	1.27
3	2	2.25	Imperm.	1.00	1.16	0.016	5	0.00	0.00	3.08	1.48
11	2	2.25	Imperm.	1.70	1.16	0.016	2	3.85	1.27	4.05	1.15
12	2	2.25	Imperm.	1.70	1.16	0.016	3	3.63	1.43	3.92	1.23
13	2	2.25	Imperm.	1.70	1.16	0.016	5	3.37	1.66	3.70	1.38
14	2	2.25	Imperm.	1.70	1.16	0.016	8	3.25	1.78	3.50	1.54
15	2	2.25	Imperm.	1.70	1.16	0.025	2	3.00	1.40	3.58	0.98
16	2	2.25	Imperm.	1.70	1.16	0.025	3	0.00	0.00	3.31	1.15
21	2	2.25	Imperm.	1.70	1.31	0.016	2	4.27	1.32	4.37	1.26
22	2	2.25	Imperm.	1.70	1.31	0.016	3	4.09	1.44	4.22	1.35
23	2	2.25	Imperm.	1.70	1.31	0.016	5	3.95	1.54	4.09	1.44
24	2	2.25	Imperm.	1.70	1.31	0.016	8	0.00	0.00	4.00	1.50
25	2	2.25	Imperm.	1.70	1.31	0.026	2	3.47	1.33	3.65	1.20
26	2	2.25	Imperm.	1.70	1.31	0.026	3	3.34	1.44	3.47	1.33
27	2	2.25	Imperm.	1.70	1.31	0.025	5	3.21	1.56	3.34	1.44
28	2	2.25	Imperm.	1.70	1.31	0.025	8	0.00	0.00	3.25	1.52
29	2	2.25	Imperm.	1.70	1.31	0.033	2	0.00	0.00	3.02	1.32
33	2	2.25	Imperm.	1.63	1.85	0.036	2	4.20	1.29	4.41	1.17
34	2	2.25	Imperm.	1.63	1.85	0.036	3	4.85	1.39	4.25	1.26
35	2	2.25	Imperm.	1.63	1.85	0.036	5	3.94	1.47	4.08	1.37
37	2	2.25	Imperm.	1.63	2.19	0.036	2	5.01	1.27	5.25	1.16
38	2	2.25	Imperm.	1.63	2.19	0.036	3	4.90	1.33	5.03	1.26
39	2	2.25	Imperm.	1.63	2.19	0.036	5	4.76	1.41	4.85	1.36
40	2	2.25	Imperm.	1.63	2.19	0.036	8	0.00	0.00	4.76	1.41
41	2	2.25	Imperm.	1.63	2.69	0.036	2	5.95	1.36	6.06	1.31
42	2	2.25	Imperm.	1.63	2.69	0.036	3	5.82	1.42	5.91	1.38
43	2	2.25	Imperm.	1.63	2.69	0.036	5	5.74	1.46	5.82	1.42
44	2	2.25	Imperm.	1.63	2.69	0.036	8	5.74	1.46	5.80	1.43

Continued on next page

Table B.1 – *Continued from previous page*

Test nr.	$\cot\alpha$	D_{85}/D_{15}	Description	Δ	T_m	D_{n50}	S	ξ_m,1000	$\frac{H_s}{\Delta D}$,1000	ξ_m,1000	$\frac{H_s}{\Delta D}$,1000
45	2	2.25	Imperm.	1.63	3.11	0.036	2	6.88	1.36	6.96	1.33
46	2	2.25	Imperm.	1.63	3.11	0.036	3	6.78	1.40	6.88	1.36
47	2	2.25	Imperm.	1.63	3.11	0.036	5	6.62	1.47	6.69	1.44
48	2	2.25	Imperm.	1.63	3.11	0.036	8	6.49	1.53	6.55	1.50
257	2	1.25	Perm.	1.62	1.70	0.036	2	3.45	1.63	3.59	1.51
258	2	1.25	Perm.	1.62	1.70	0.036	3	0.00	0.00	3.45	1.63
262	2	1.25	Perm.	1.62	2.16	0.036	2	4.27	1.72	4.44	1.59
263	2	1.25	Perm.	1.62	2.16	0.036	3	4.12	1.85	4.28	1.71
264	2	1.25	Perm.	1.62	2.16	0.036	5	3.93	2.03	4.09	1.87
265	2	1.25	Perm.	1.62	2.16	0.036	8	3.77	2.21	3.92	2.04
266	2	1.25	Perm.	1.62	2.16	0.036	12	3.67	2.33	3.83	2.14
267	2	1.25	Perm.	1.62	2.89	0.036	2	5.12	2.14	5.43	1.90
268	2	1.25	Perm.	1.62	2.89	0.036	3	5.01	2.24	5.26	2.03
269	2	1.25	Perm.	1.62	2.89	0.036	5	4.78	2.46	4.99	2.25
270	2	1.25	Perm.	1.62	2.89	0.036	8	4.60	2.65	4.79	2.45
271	2	1.25	Perm.	1.62	2.89	0.036	12	4.48	2.79	4.64	2.61
294	2	1.25	Hom.	1.62	1.74	0.036	2	3.41	1.75	3.49	1.67
295	2	1.25	Hom.	1.62	1.74	0.036	3	3.23	1.95	3.34	1.82
296	2	1.25	Hom.	1.62	1.74	0.036	5	0.00	0.00	3.14	2.06
299	2	1.25	Hom.	1.62	2.18	0.036	2	4.09	1.91	4.21	1.80
300	2	1.25	Hom.	1.62	2.18	0.036	3	3.94	2.06	4.09	1.91
301	2	1.25	Hom.	1.62	2.18	0.036	5	3.70	2.33	3.88	2.12
302	2	1.25	Hom.	1.62	2.18	0.036	8	3.53	2.56	3.73	2.30
303	2	1.25	Hom.	1.62	2.18	0.036	12	3.38	2.79	3.55	2.54
304	2	1.25	Hom.	1.62	2.86	0.036	2	4.85	2.34	5.17	2.06
305	2	1.25	Hom.	1.62	2.86	0.036	3	4.77	2.42	4.85	2.34
306	2	1.25	Hom.	1.62	2.86	0.036	5	4.54	2.67	4.74	2.45
307	2	1.25	Hom.	1.62	2.86	0.036	8	4.35	2.91	4.48	2.74
308	2	1.25	Hom.	1.62	2.86	0.036	12	4.22	3.08	4.32	2.95
329	2	1.25	Perm.	0.92	1.25	0.035	2	3.12	1.97	3.28	1.79
330	2	1.25	Perm.	0.92	1.25	0.035	3	0.00	0.00	3.11	1.99
334	2	1.25	Perm.	0.92	1.57	0.035	2	3.90	1.99	4.14	1.77
335	2	1.25	Perm.	0.92	1.57	0.035	3	3.74	2.17	3.95	1.94
336	2	1.25	Perm.	0.92	1.57	0.035	5	3.52	2.44	3.73	2.18
337	2	1.25	Perm.	0.92	1.57	0.035	8	3.36	2.67	3.56	2.40
338	2	1.25	Perm.	0.92	1.57	0.035	12	3.35	2.70	3.40	2.61
339	2	1.25	Perm.	2.05	1.97	0.036	5	3.28	1.81	3.43	1.65
340	2	1.25	Perm.	2.05	1.97	0.036	8	3.14	1.97	3.28	1.81
341	2	1.25	Perm.	2.05	1.97	0.036	12	0.00	0.00	3.09	2.04
344	2	1.25	Perm.	2.05	2.36	0.036	2	3.98	1.87	4.12	1.75
345	2	1.25	Perm.	2.05	2.36	0.036	3	3.87	1.98	3.96	1.89
346	2	1.25	Perm.	2.05	2.36	0.036	5	3.71	2.15	3.78	2.08
347	2	1.25	Perm.	2.05	2.36	0.036	8	3.61	2.28	3.65	2.22
348	2	1.25	Perm.	2.05	2.36	0.036	12	0.00	0.00	3.62	2.26

C

BOUNDARY CONDITIONS

In this appendix all boundary conditions are listed for the numerical tests carried out in this research. They are presented as variance density spectra, corresponding spectral values and water level elevation time series.

C.1. MODEL EVALUATION

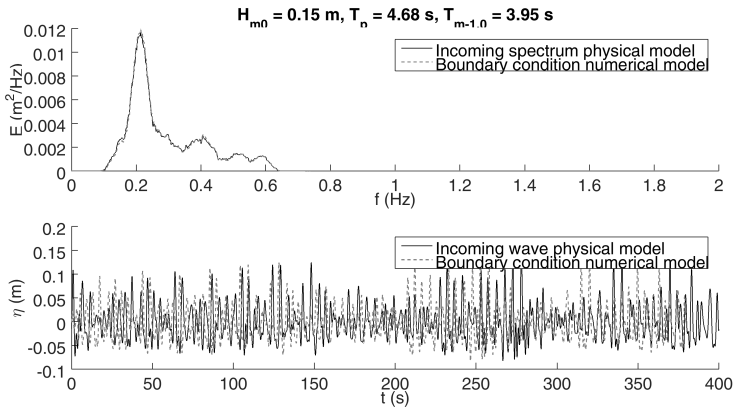

Figure C.1: Test 1 of Kik

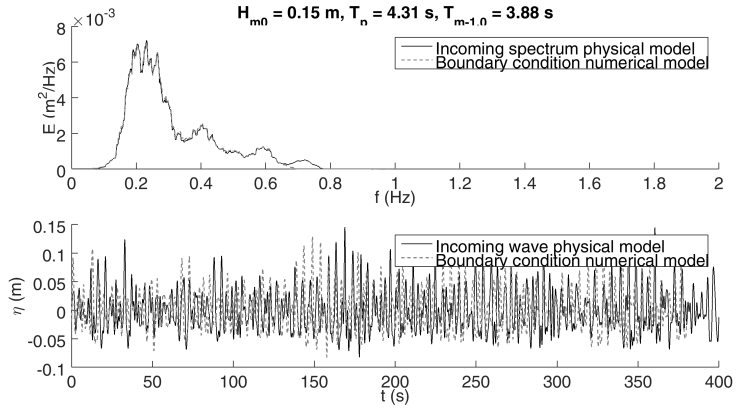

Figure C.2: Test 3 of Kik

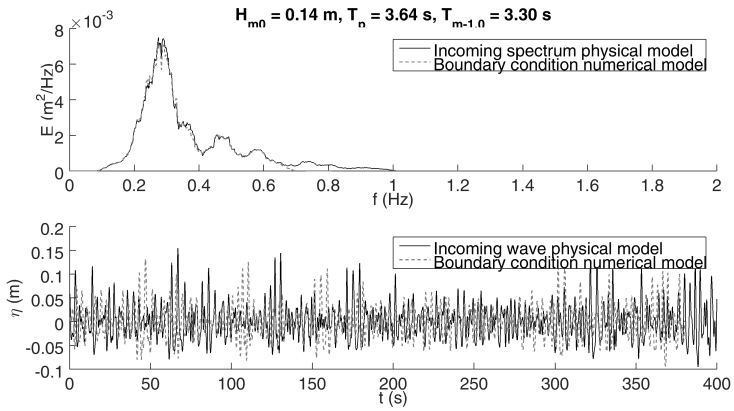

Figure C.3: Test 4 of Kik

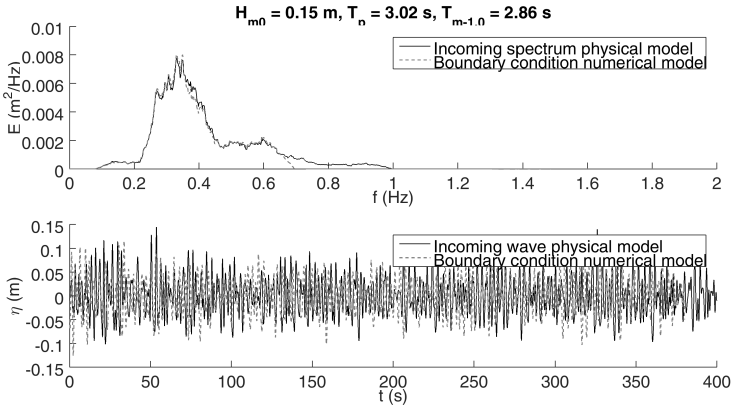

Figure C.4: Test 6 of Kik

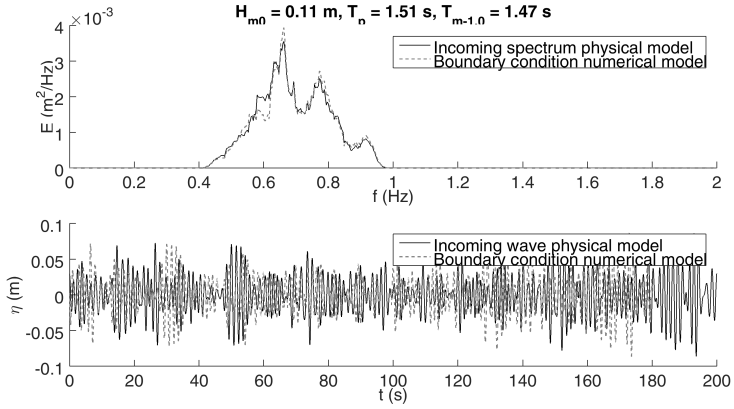

Figure C.5: Test 56 of Kluwen

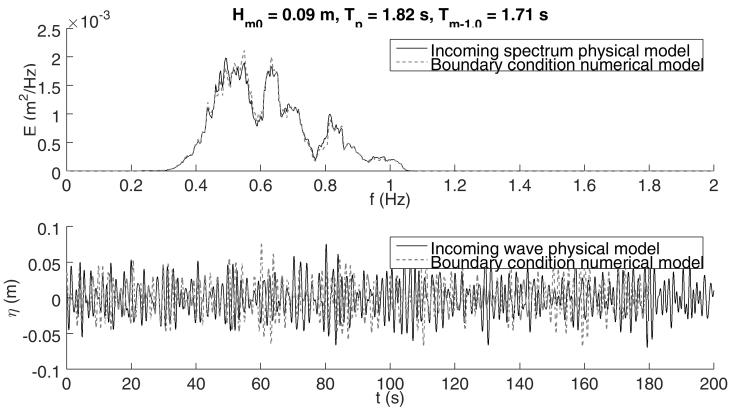

Figure C.6: Test 60 of Kluwen

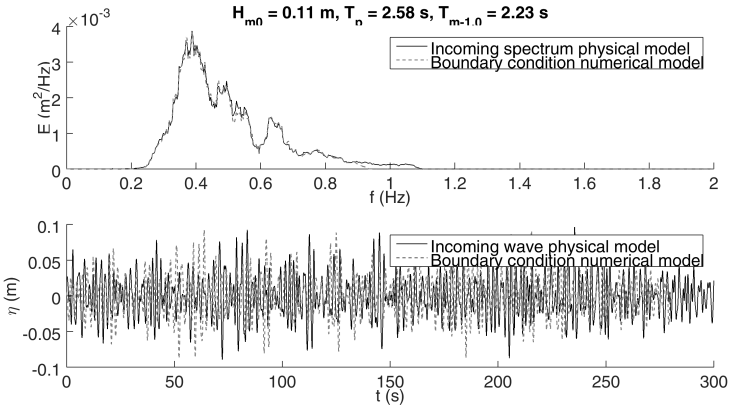

Figure C.7: Test 64 of Kluwen

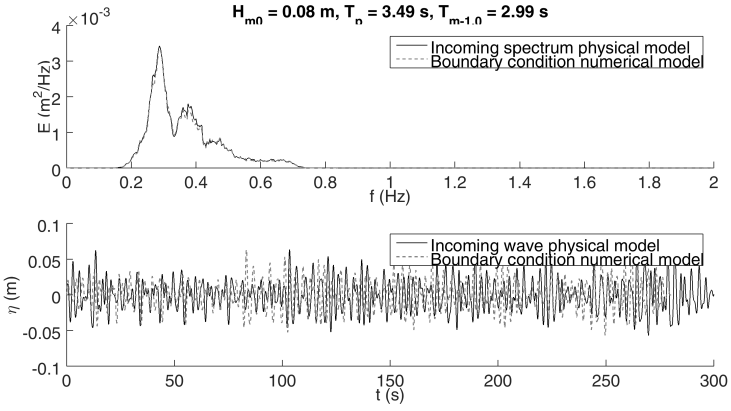

Figure C.8: Test 68 of Kluwen

C.2. FINAL NUMERICAL TESTS, IMPERMEABLE STRUCTURE

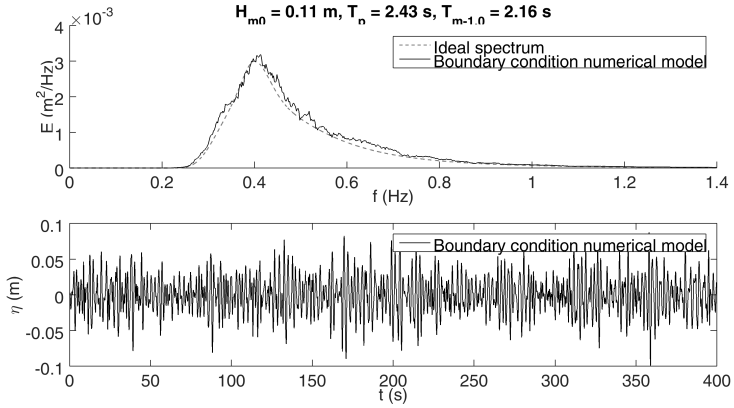

Figure C.9: Test 36

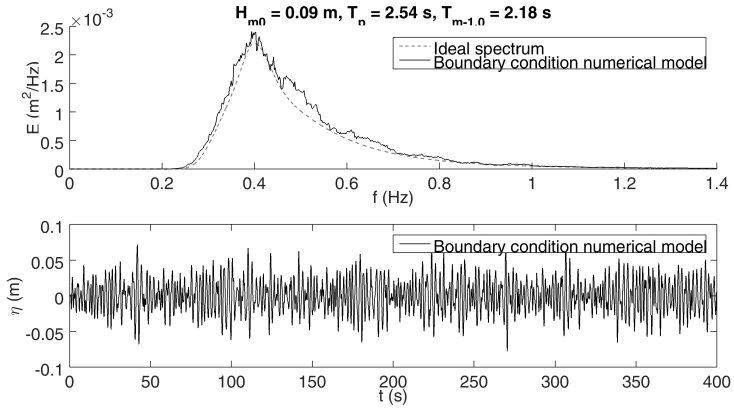

Figure C.10: Test 37

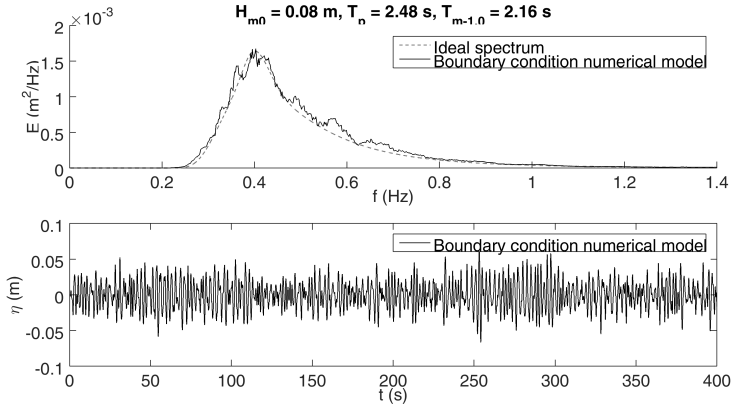

Figure C.11: Test 38

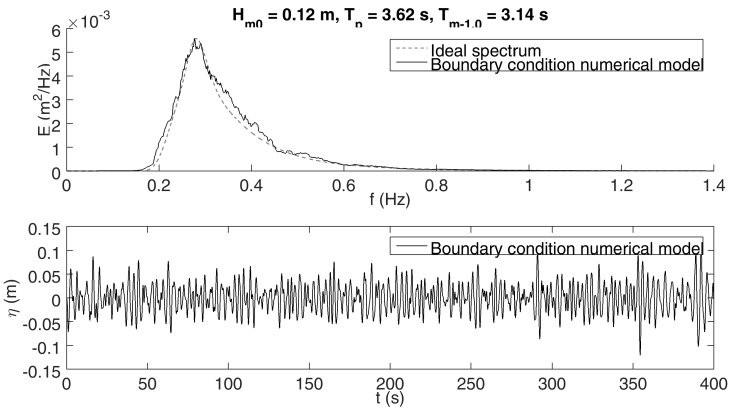

Figure C.12: Test 51

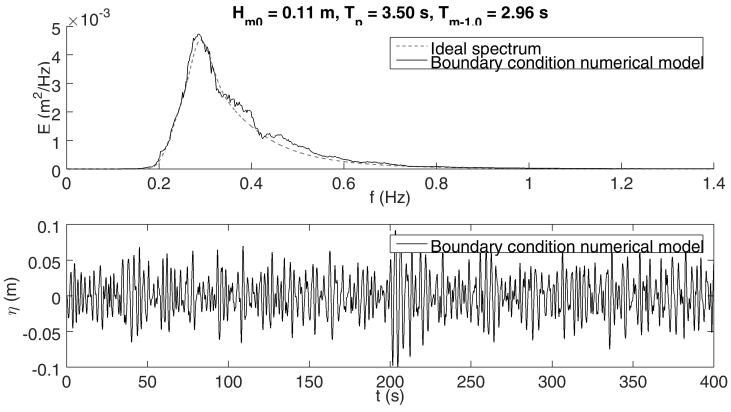

Figure C.13: Test 52

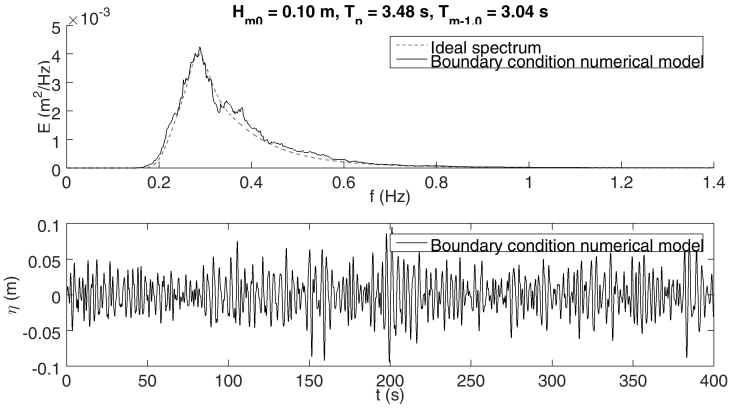

Figure C.14: Test 53

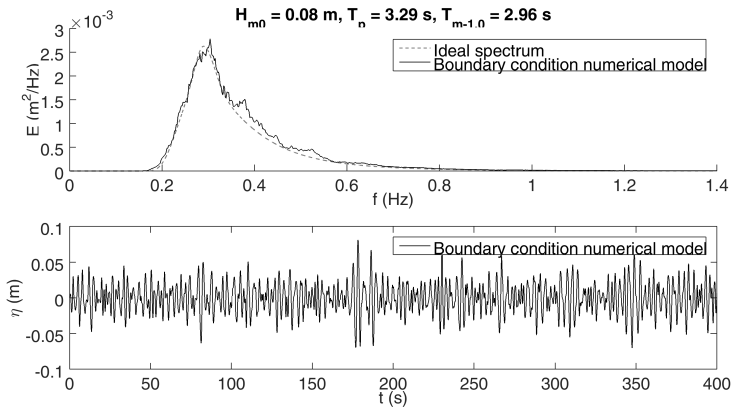

Figure C.15: Test 54

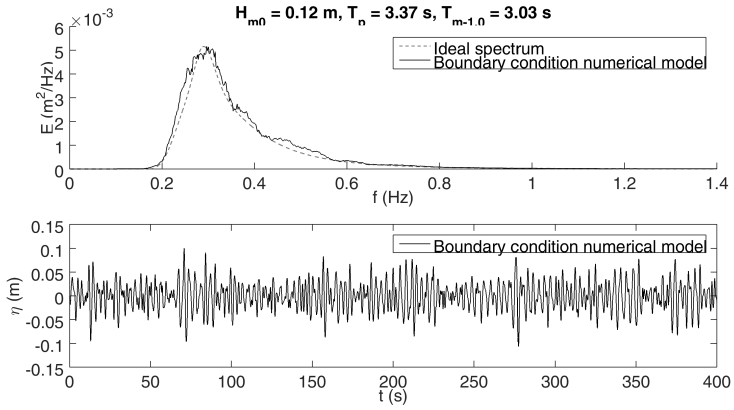

Figure C.16: Test 55

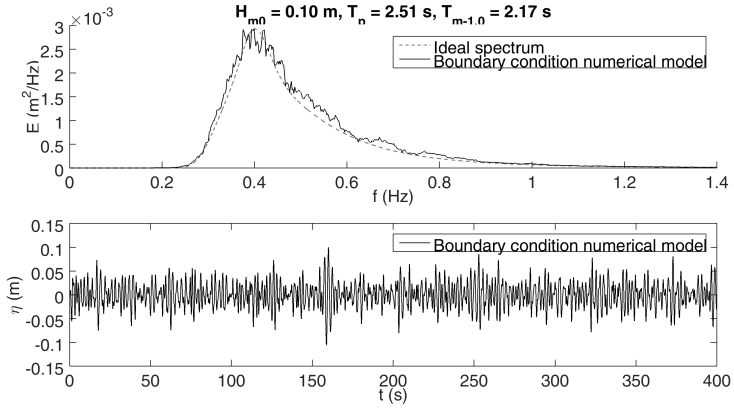

Figure C.17: Test 85

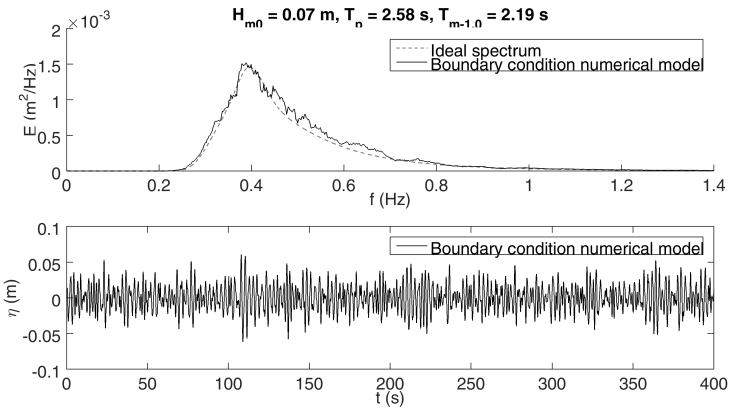

Figure C.18: Test 86

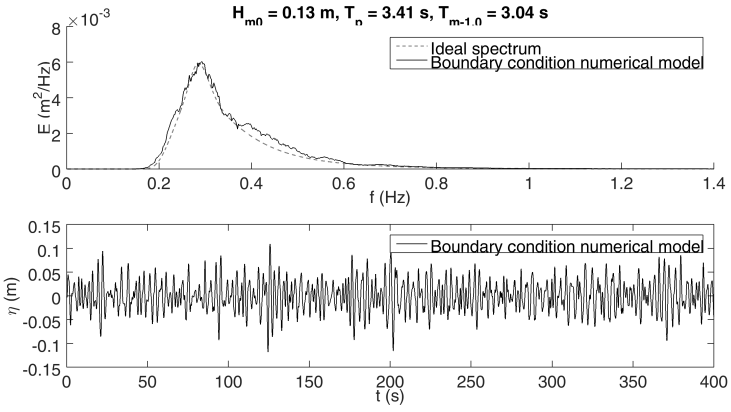

Figure C.19: Test 88

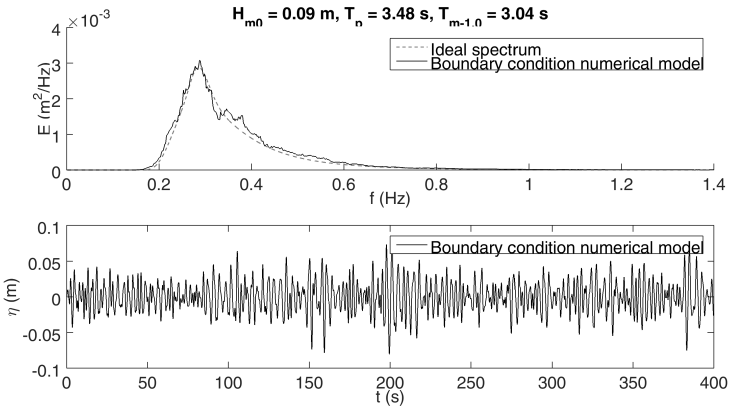

Figure C.20: Test 89

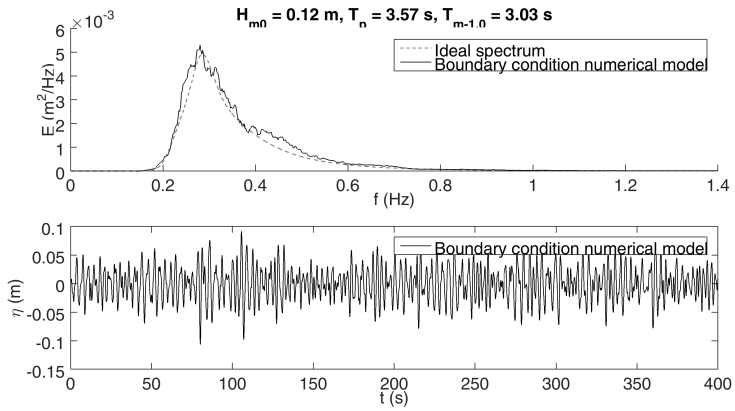

Figure C.21: Test 90

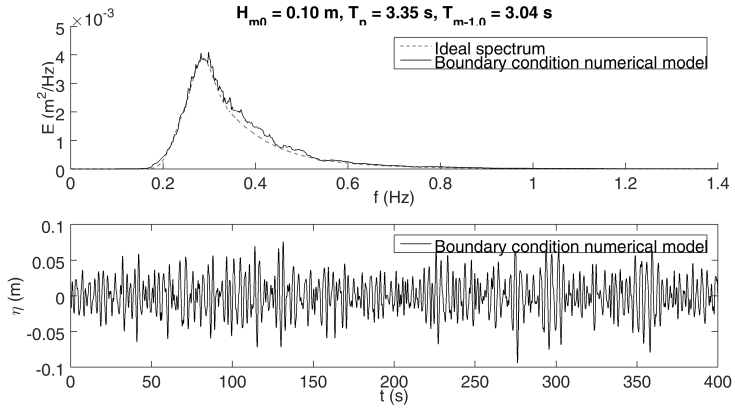

Figure C.22: Test 91

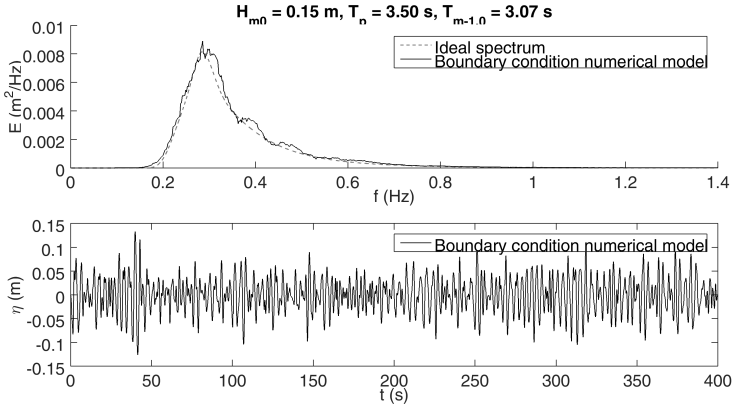

Figure C.23: Test 92

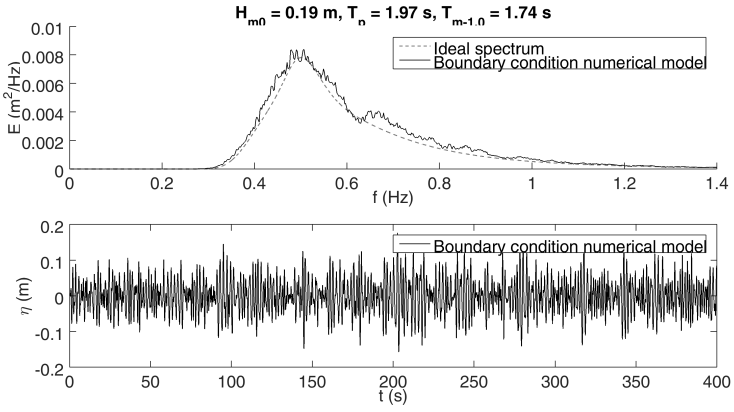

Figure C.24: Test 104

C.3. FINAL NUMERICAL TESTS, HOMOGENEOUS STRUCTURE

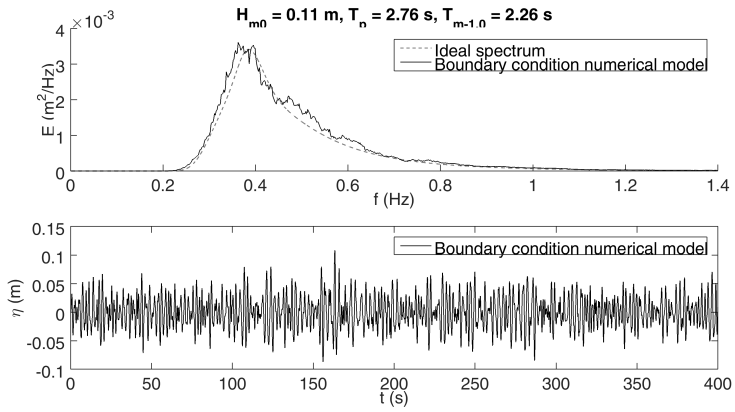

Figure C.25: Test 258

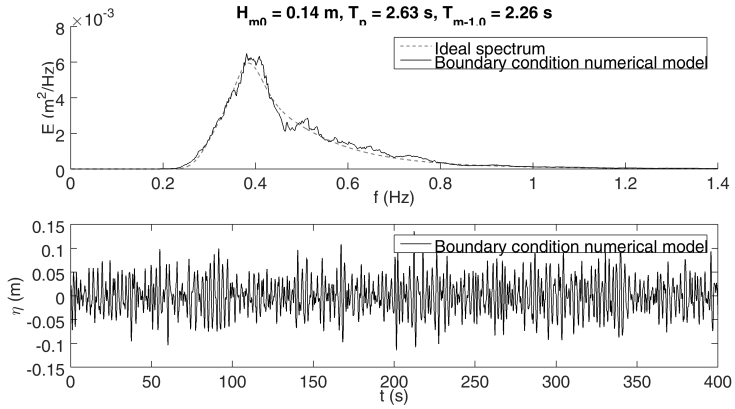

Figure C.26: Test 259

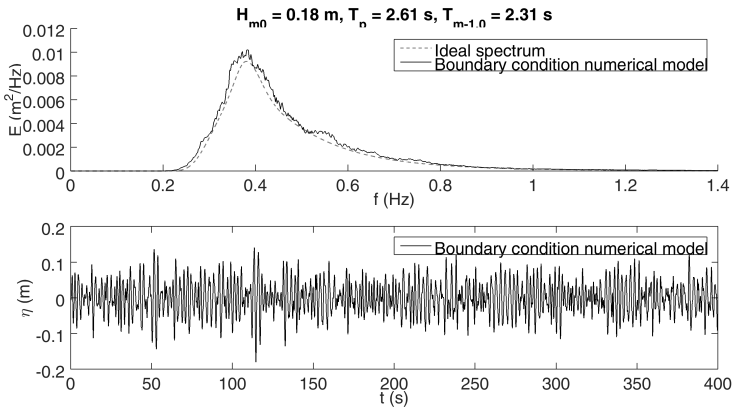

Figure C.27: Test 260

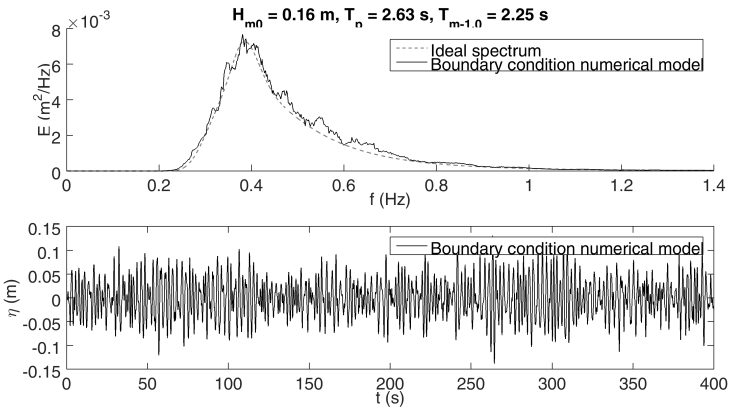

Figure C.28: Test 261

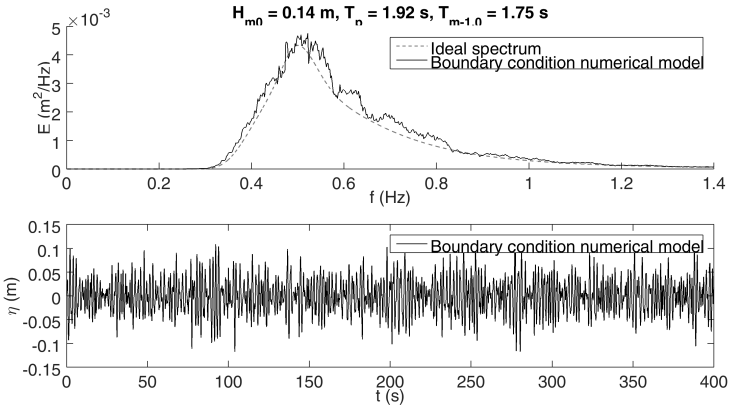

Figure C.29: Test 262

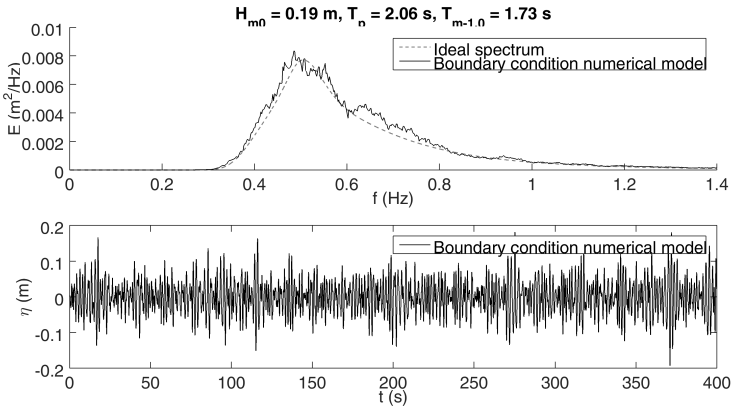

Figure C.30: Test 263

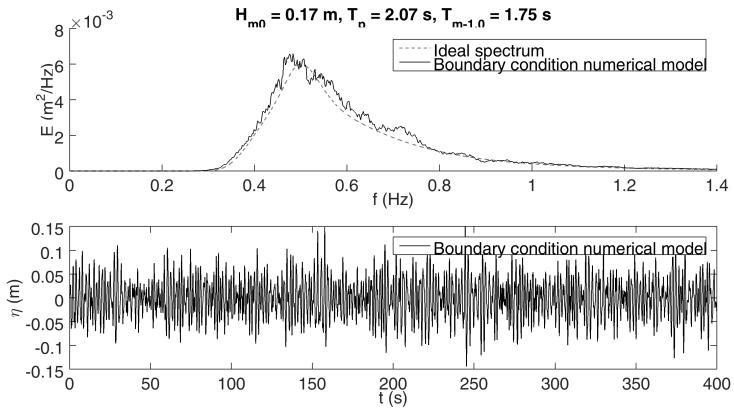

Figure C.31: Test 264

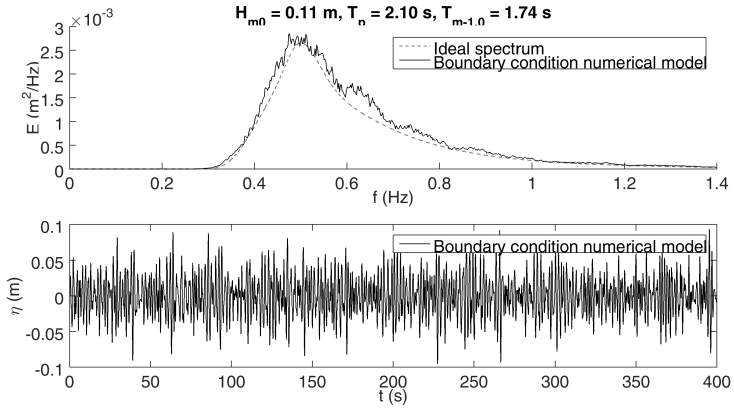

Figure C.32: Test 265

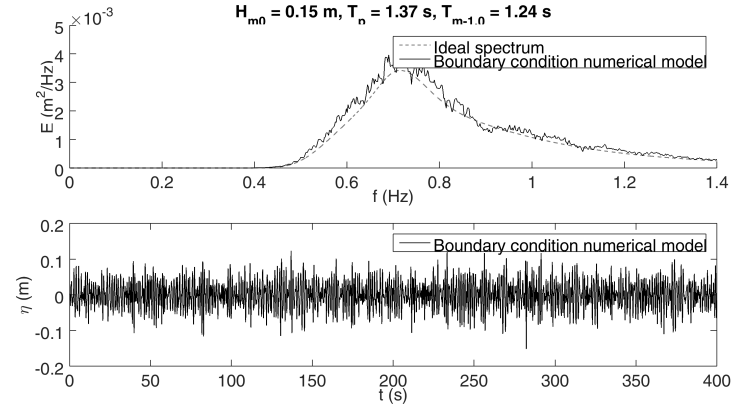

Figure C.33: Test 266

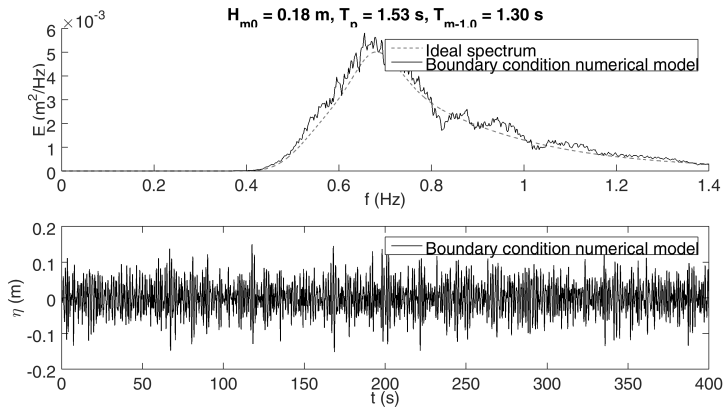

Figure C.34: Test 267

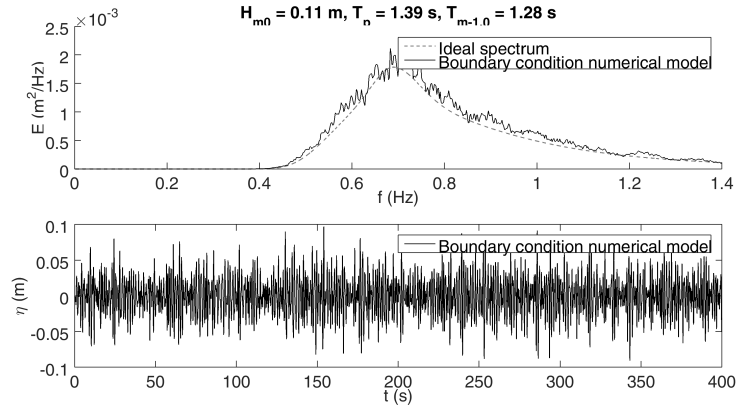

Figure C.35: Test 268

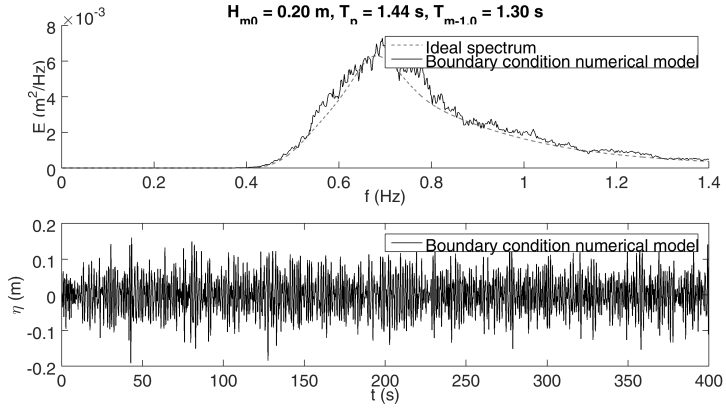

Figure C.36: Test 269

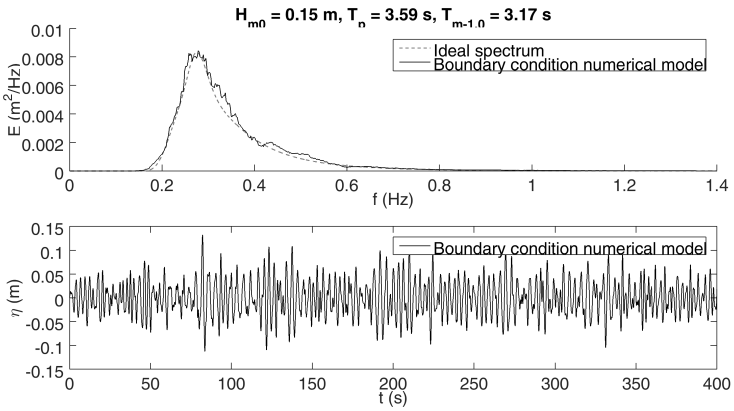

Figure C.37: Test 270

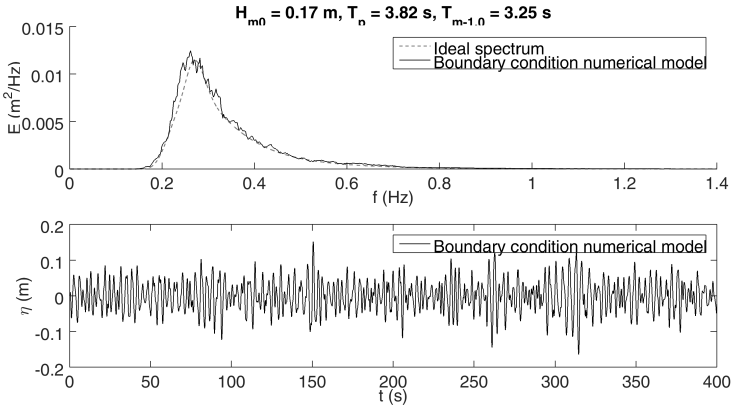

Figure C.38: Test 271

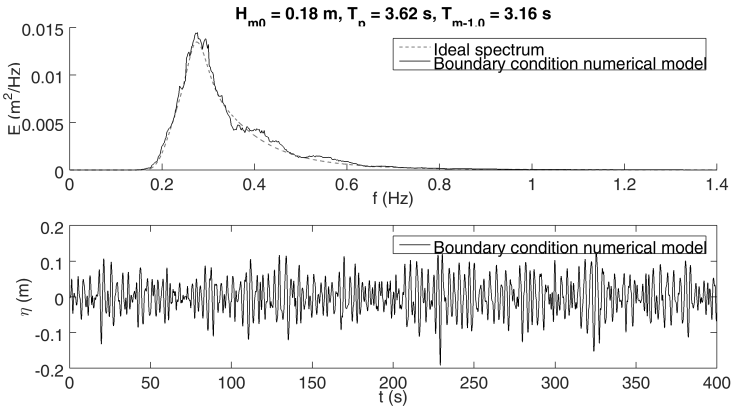

Figure C.39: Test 272

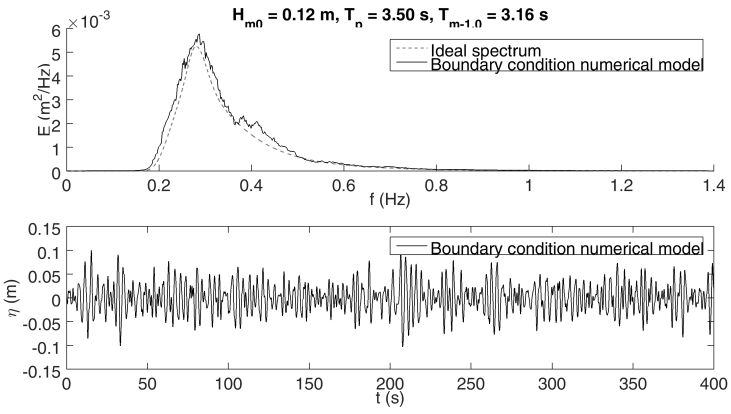

Figure C.40: Test 273

D

VALIDATION RESULTS FOR KIK TEST 4

In this appendix the visual results of the validation tests for test 4 by Kik (2011) are shown. First of all an overview of the tested structure and the test matrix is given.

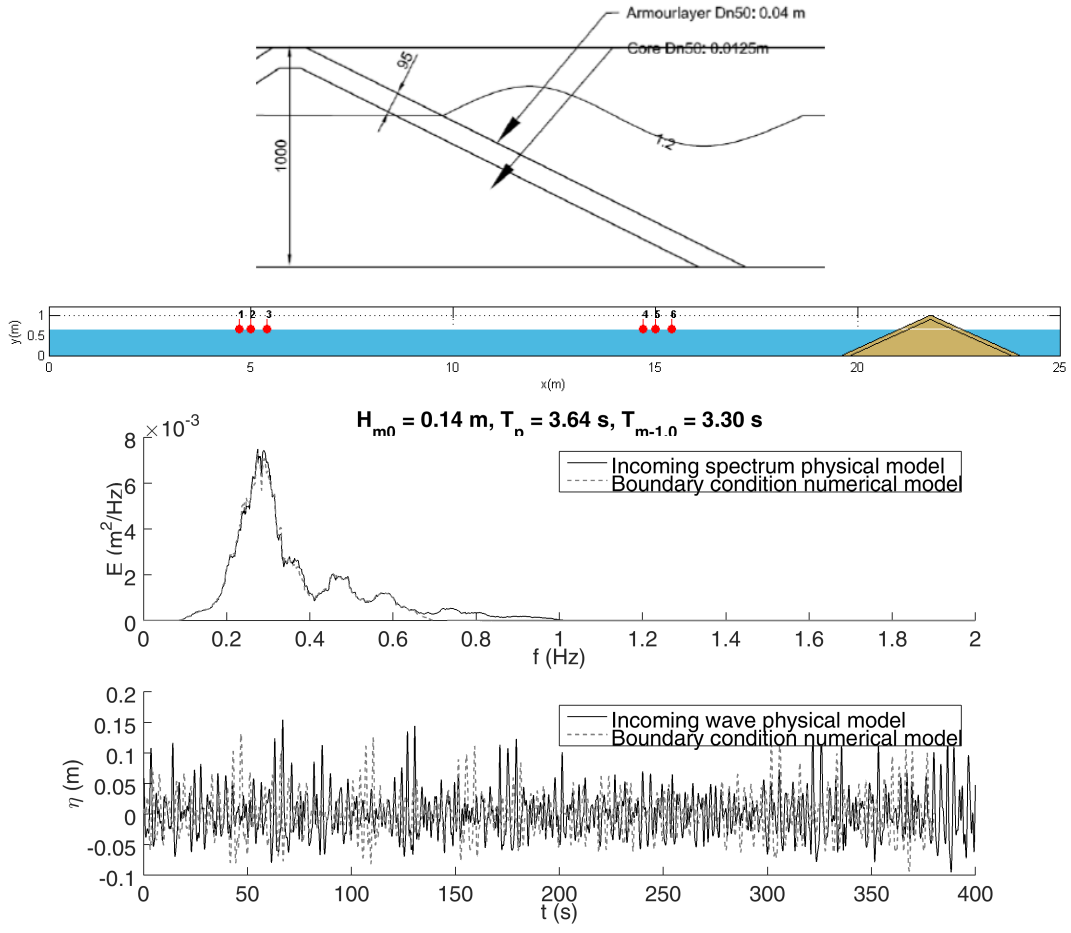

Figure D.1: Schematisation of physical structure (above), computational domain (middle) and spectra and wave series (below)

Table D.1: Test matrix

	Armour layer				Core				
Test nr.	α	β	c	n	α	β	c	n	T
1	1100	2.4	0.51	0.4	700	2.7	0.51	0.4	T_m
2	1100	2.4	0.51	0.4	700	2.7	0.51	0.4	$0.5T_m$
3	11000	2.4	0.51	0.4	700	2.7	0.51	0.4	T_m
4	1100	5.0	0.51	0.4	700	2.7	0.51	0.4	T_m
5	1100	2.4	0.51	0.6	700	2.7	0.51	0.4	T_m
6	1100	2.4	0.51	0.4	7000	2.7	0.51	0.4	T_m
7	1100	2.4	0.51	0.4	700	5.0	0.51	0.4	T_m
8	1100	2.4	0.51	0.4	700	2.7	0.51	0.6	T_m
9	11000	2.4	0.51	0.4	7000	2.7	0.51	0.4	T_m
10	1100	5.0	0.51	0.4	700	5.0	0.51	0.4	T_m
11	1100	2.4	0.51	0.6	700	2.7	0.51	0.6	T_m
12	1100	2.4	0.51	0.4	700	2.7	0.51	0.4	$2T_m$
13	0	2.4	0.51	0.4	1100	2.7	0.51	0.4	T_m
14	700	2.4	0.51	0.4	0	2.7	0.51	0.4	T_m
15	0	2.4	0.51	0.4	0	2.7	0.51	0.4	T_m
16	11000	5.0	0.51	0.4	700	2.7	0.51	0.4	T_m
17	11000	5.0	0.51	0.4	700	5.0	0.51	0.4	T_m
18	11000	5.0	0.51	0.4	700	1.1	0.51	0.4	T_m
19	1100	5.0	0.51	0.4	700	1.1	0.51	0.4	T_m
20	0	5.0	0.51	0.4	700	2.7	0.51	0.4	T_m
21	0	5.0	0.51	0.4	700	5.0	0.51	0.4	T_m
22	0	5.0	0.51	0.4	700	1.1	0.51	0.4	T_m
23	0	5.0	0.51	0.4	0	2.7	0.51	0.4	T_m
24	0	5.0	0.51	0.4	0	5.0	0.51	0.4	T_m
25	0	5.0	0.51	0.4	0	1.1	0.51	0.4	T_m

Figures description

Above Maximum and minimum horizontal pressure distribution inside the structure (0.46 m from the bottom). The circles indicate the measurement points during the physical model tests.

Middle Maximum pressure gradient inside the structure (0.46 m from the bottom). The blue circles indicate the measurement points during the physical model tests.

Below Energy spectra of pressure time signals at three different locations. Left: Armour layer surface, middle: interface between armour layer and core, right: inside the core.

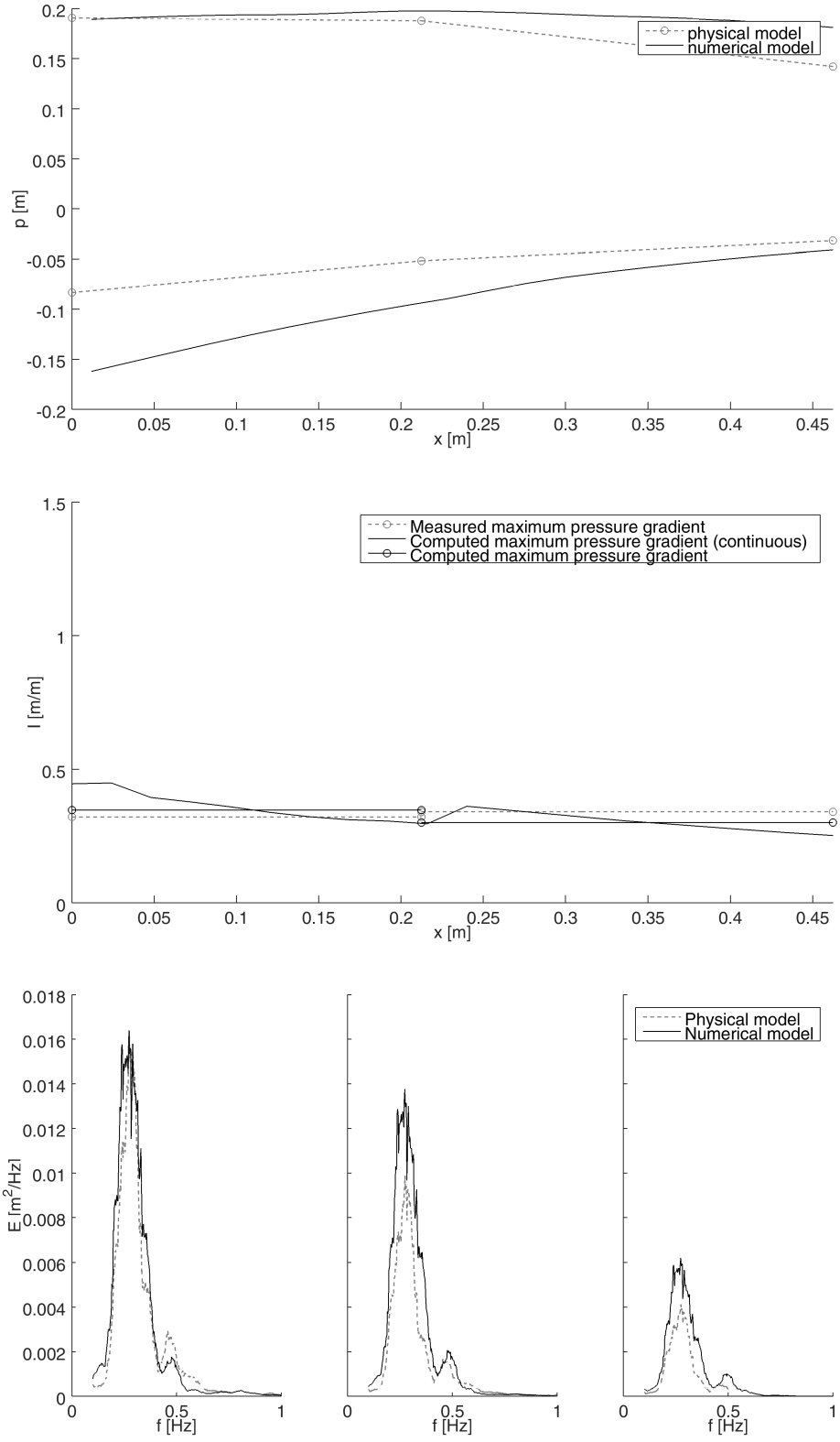

Figure D.2: Model validation test 1

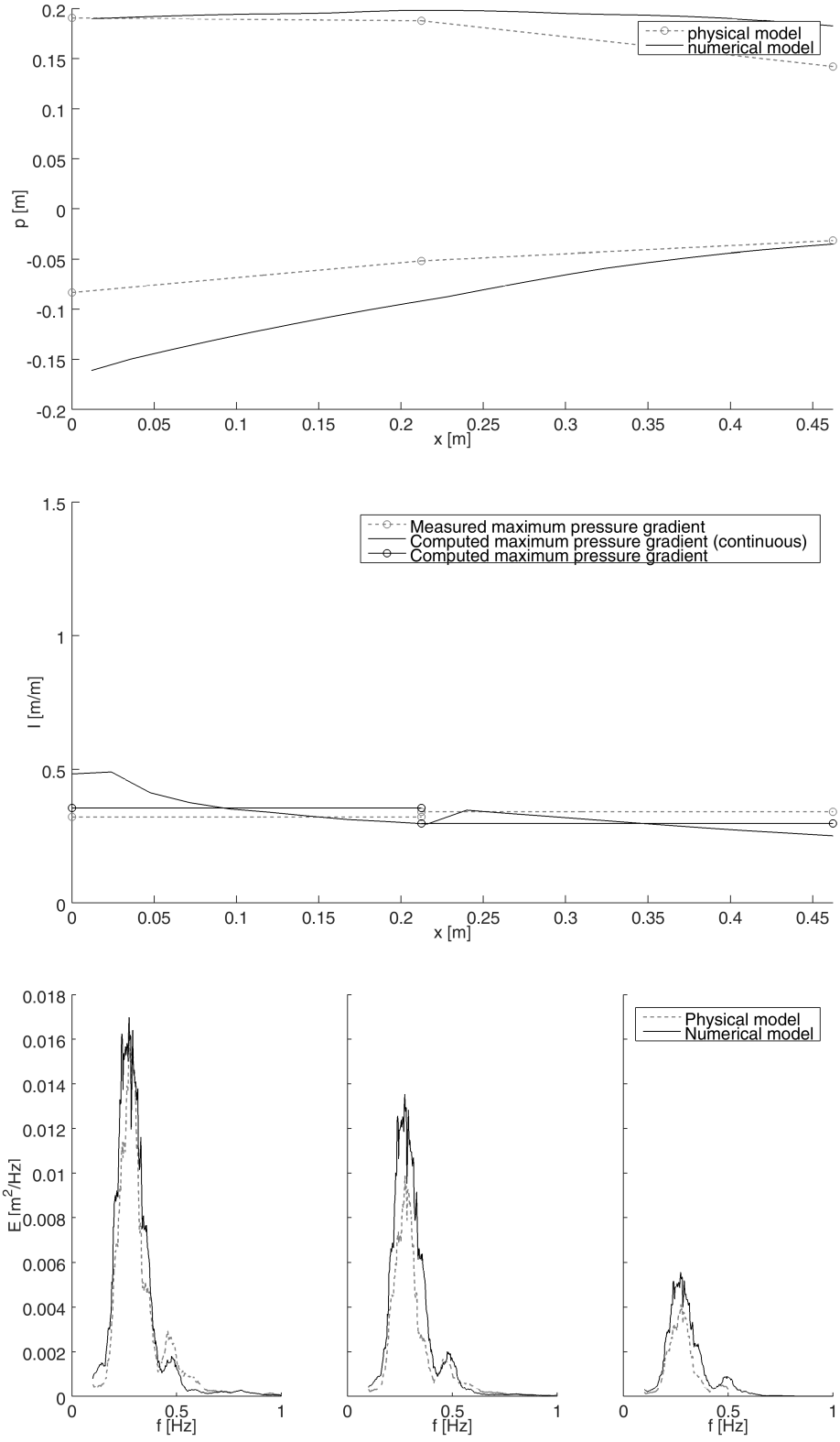

Figure D.3: Model validation test 2

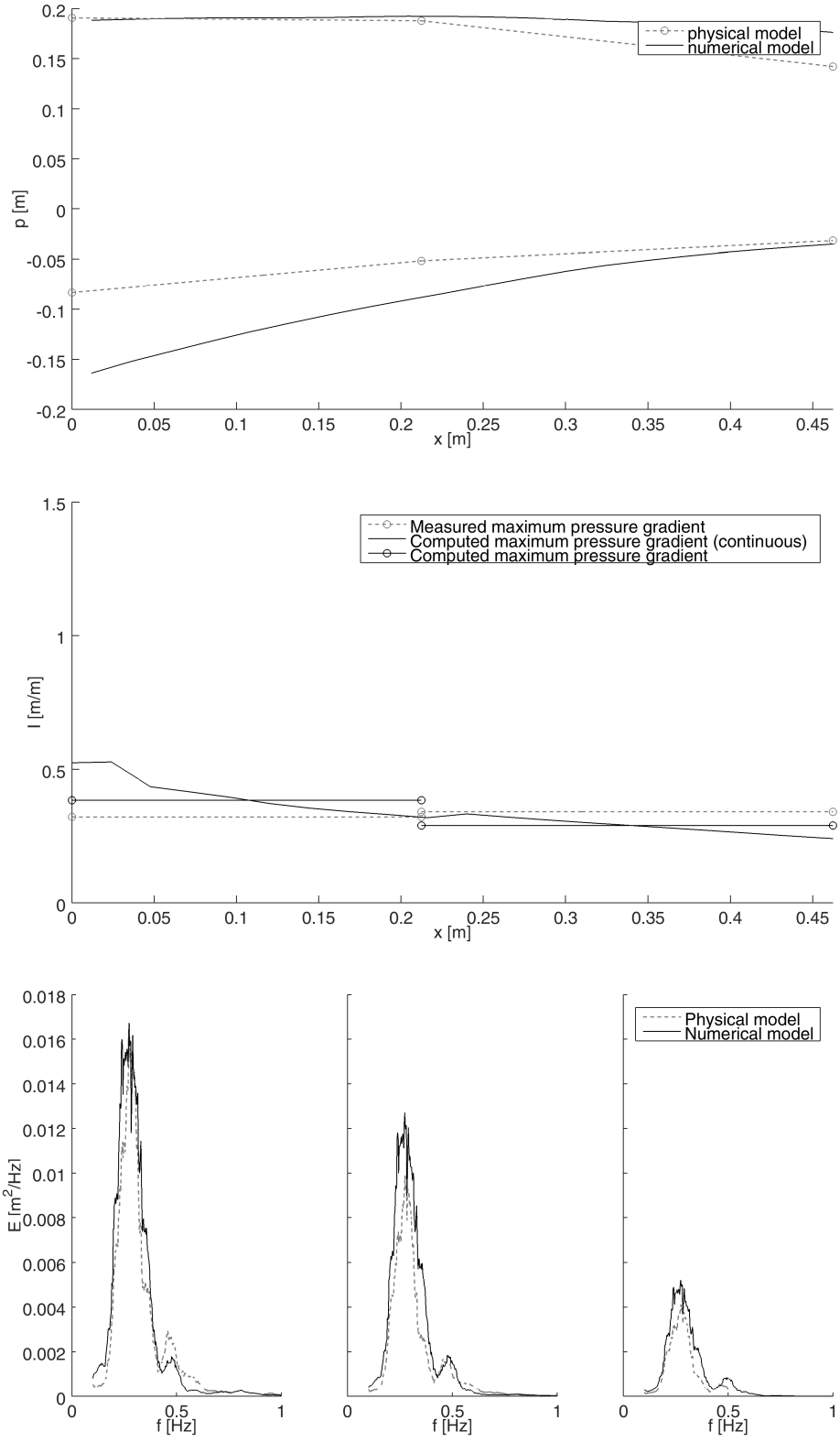

Figure D.4: Model validation test 3

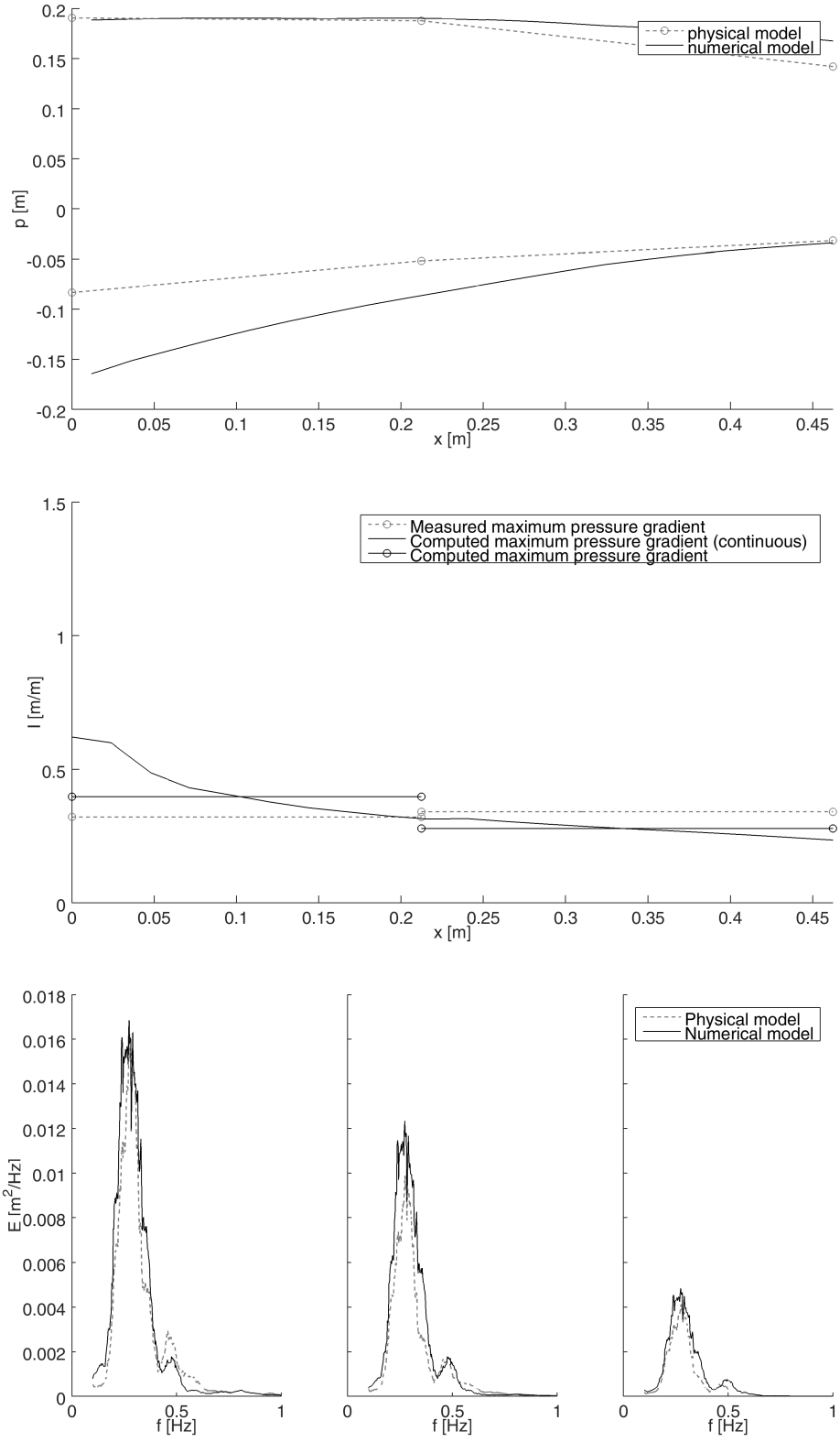

Figure D.5: Model validation test 4

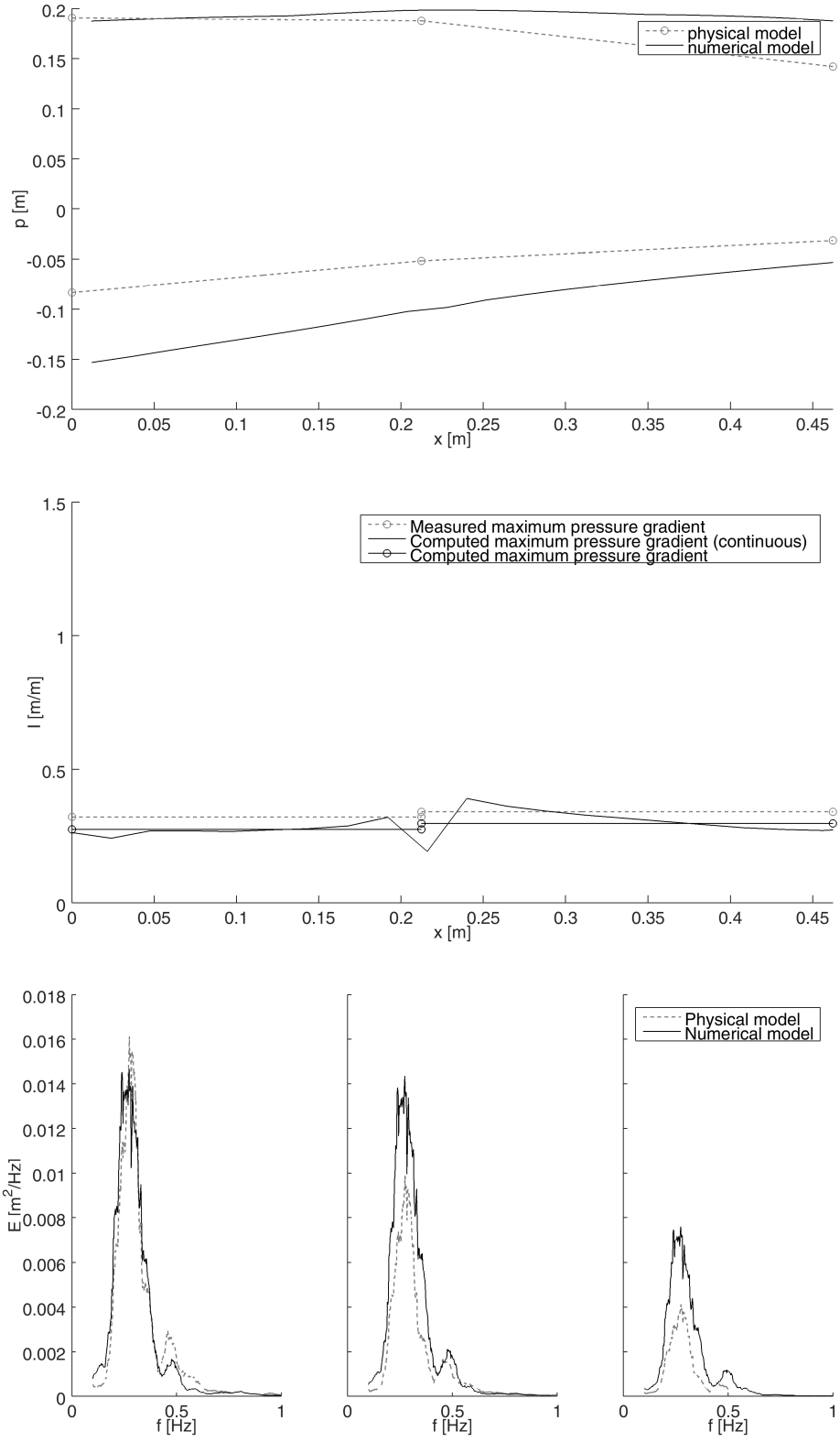

Figure D.6: Model validation test 5

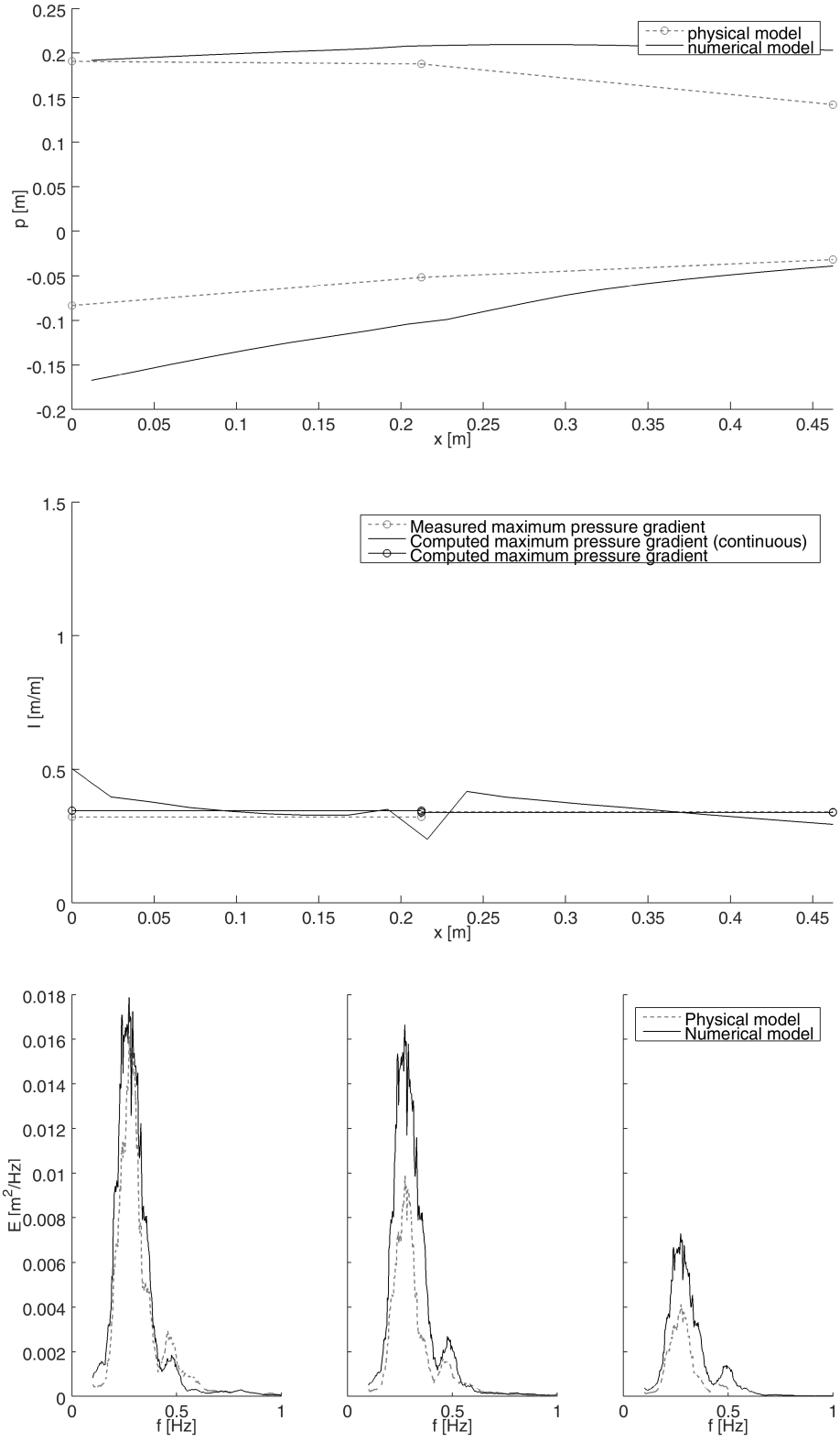

Figure D.7: Model validation test 6

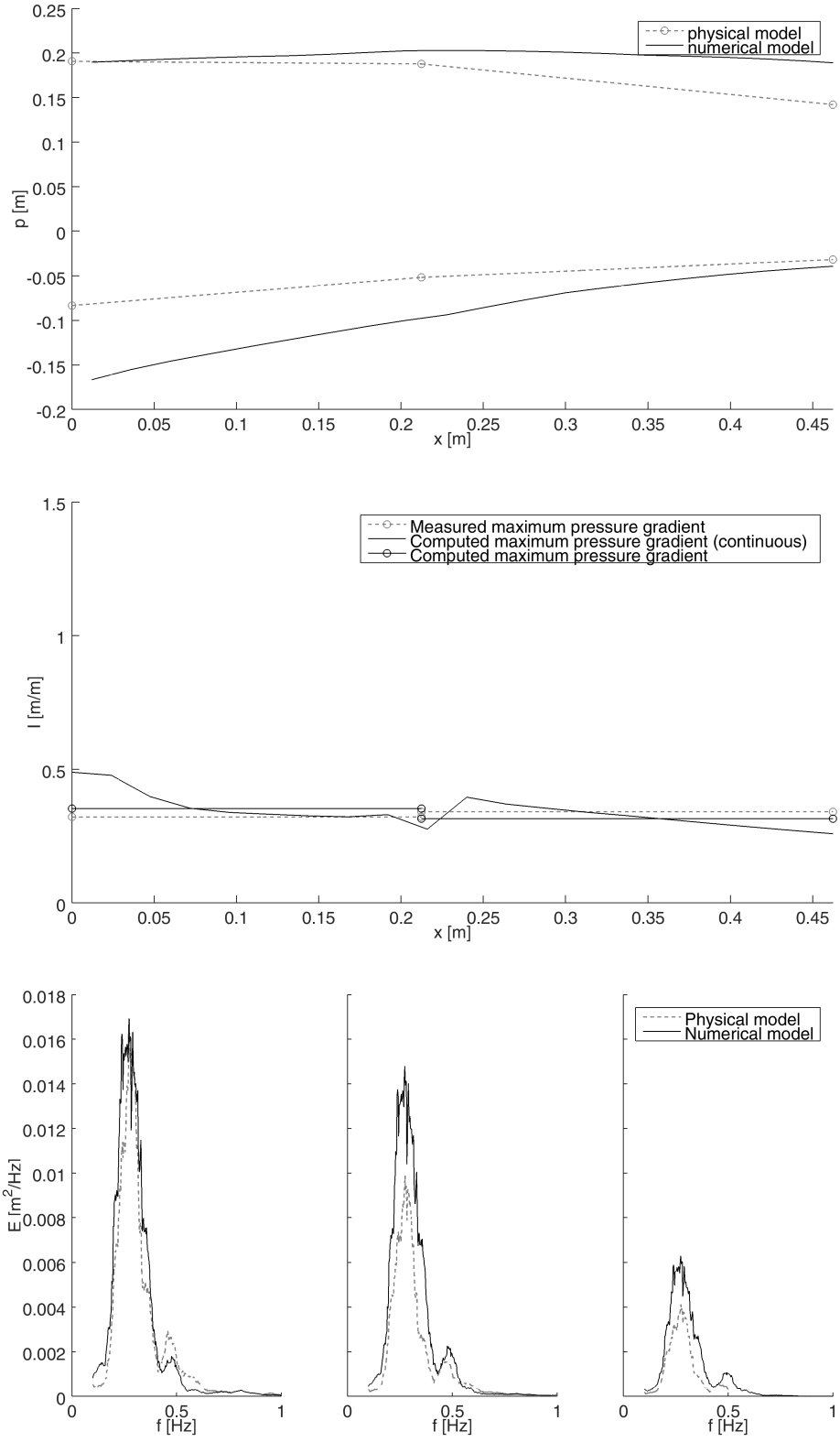

Figure D.8: Model validation test 7

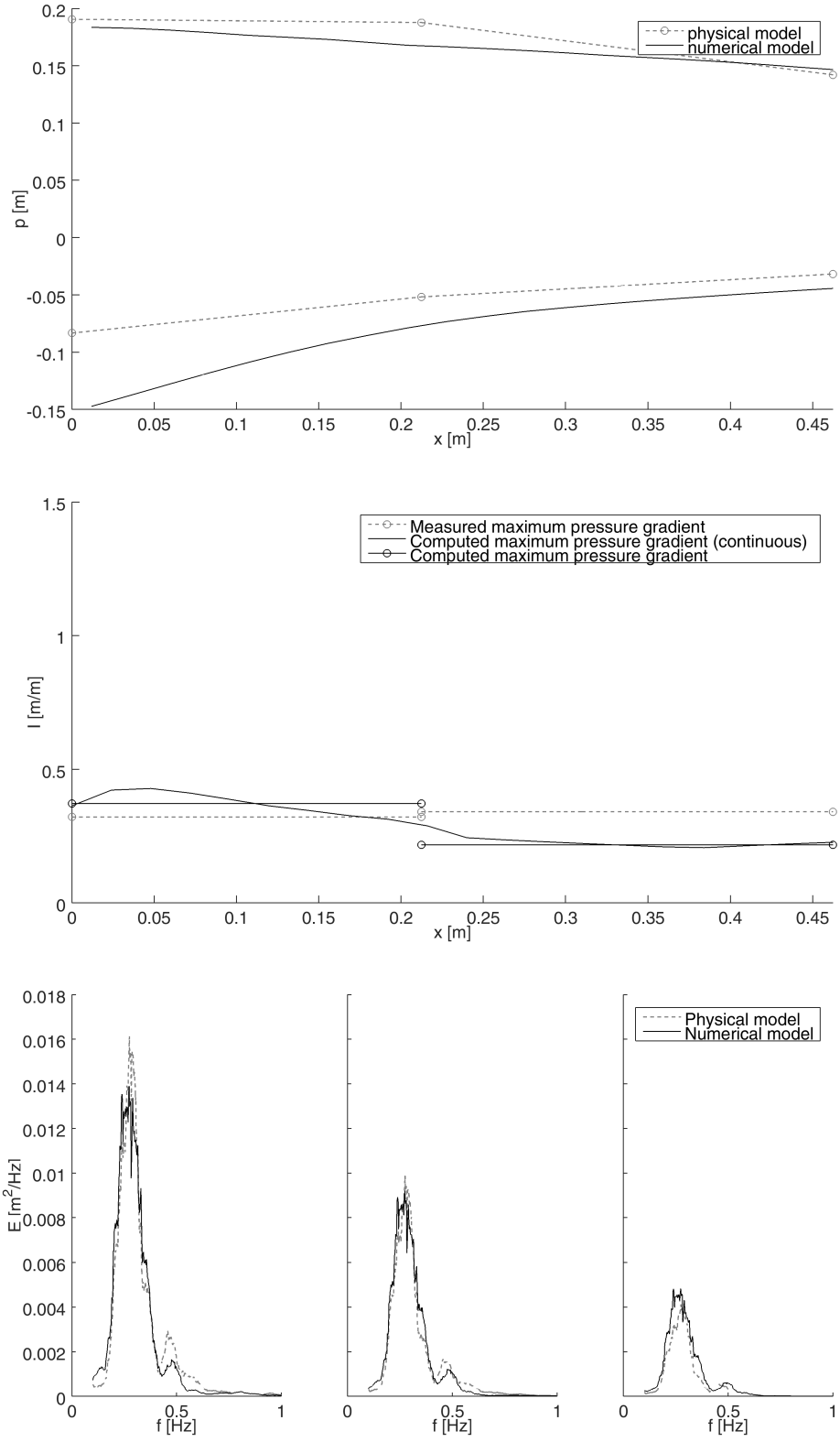

Figure D.9: Model validation test 8

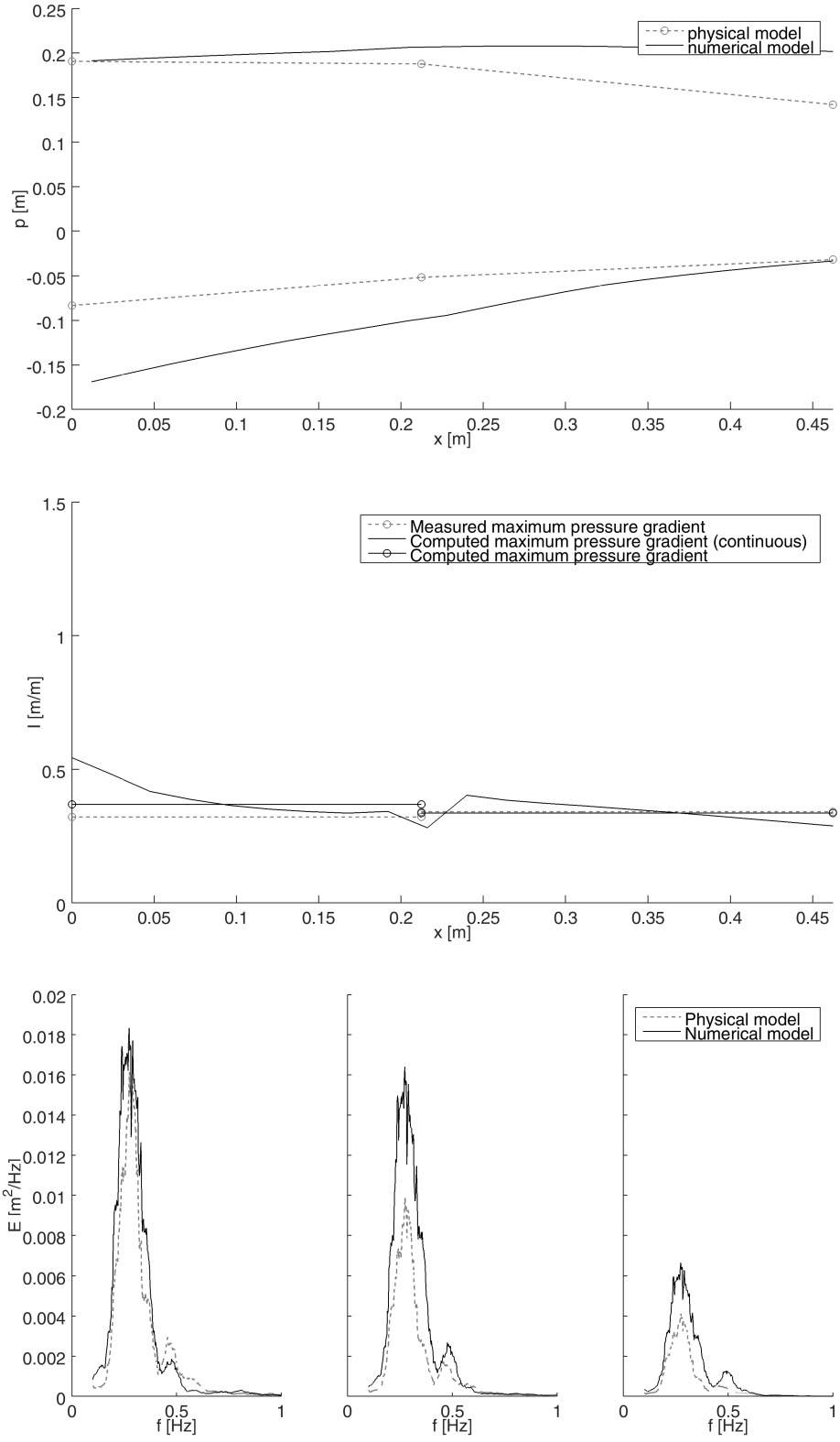

Figure D.10: Model validation test 9

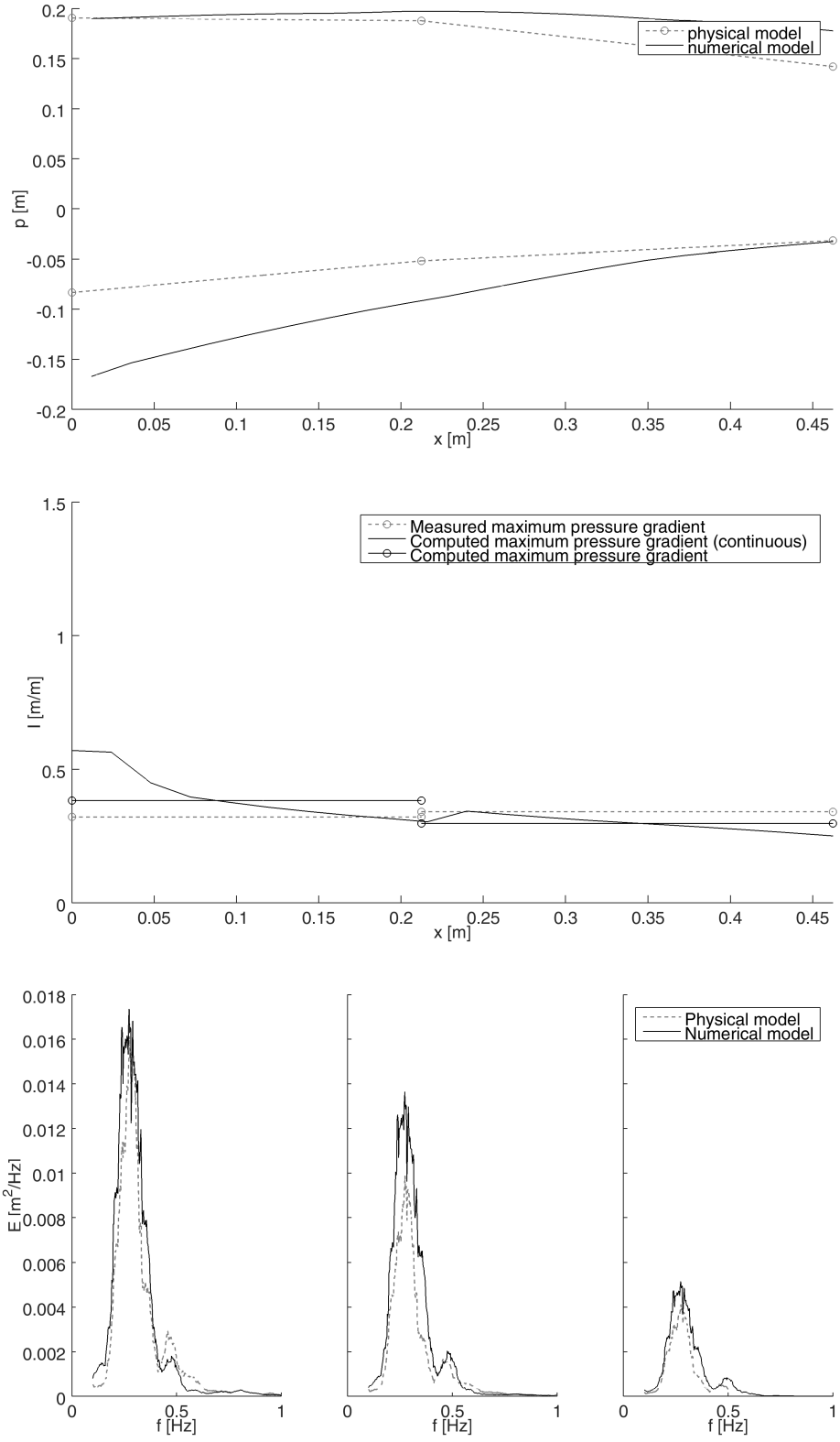

Figure D.11: Model validation test 10

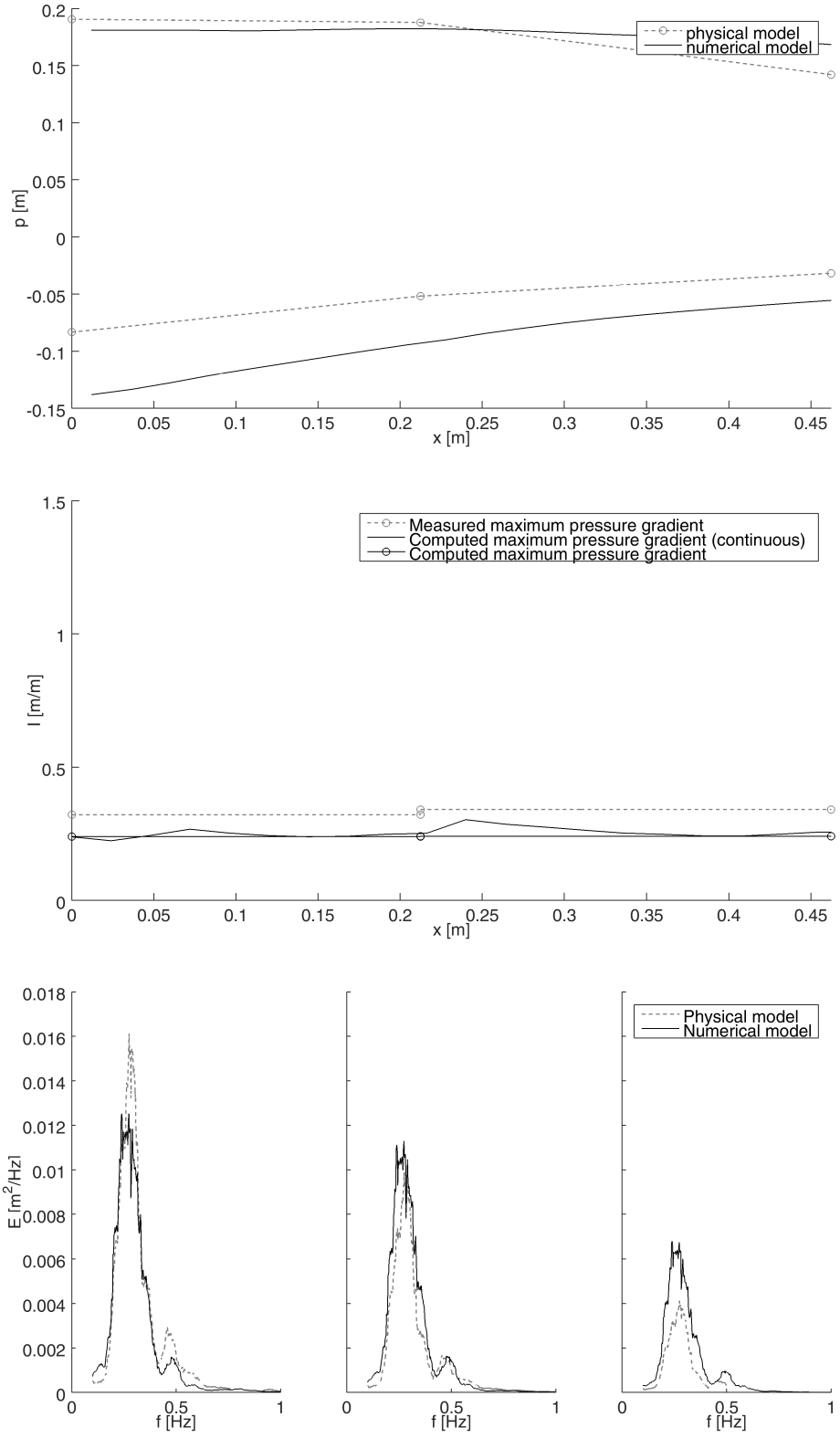

Figure D.12: Model validation test 11

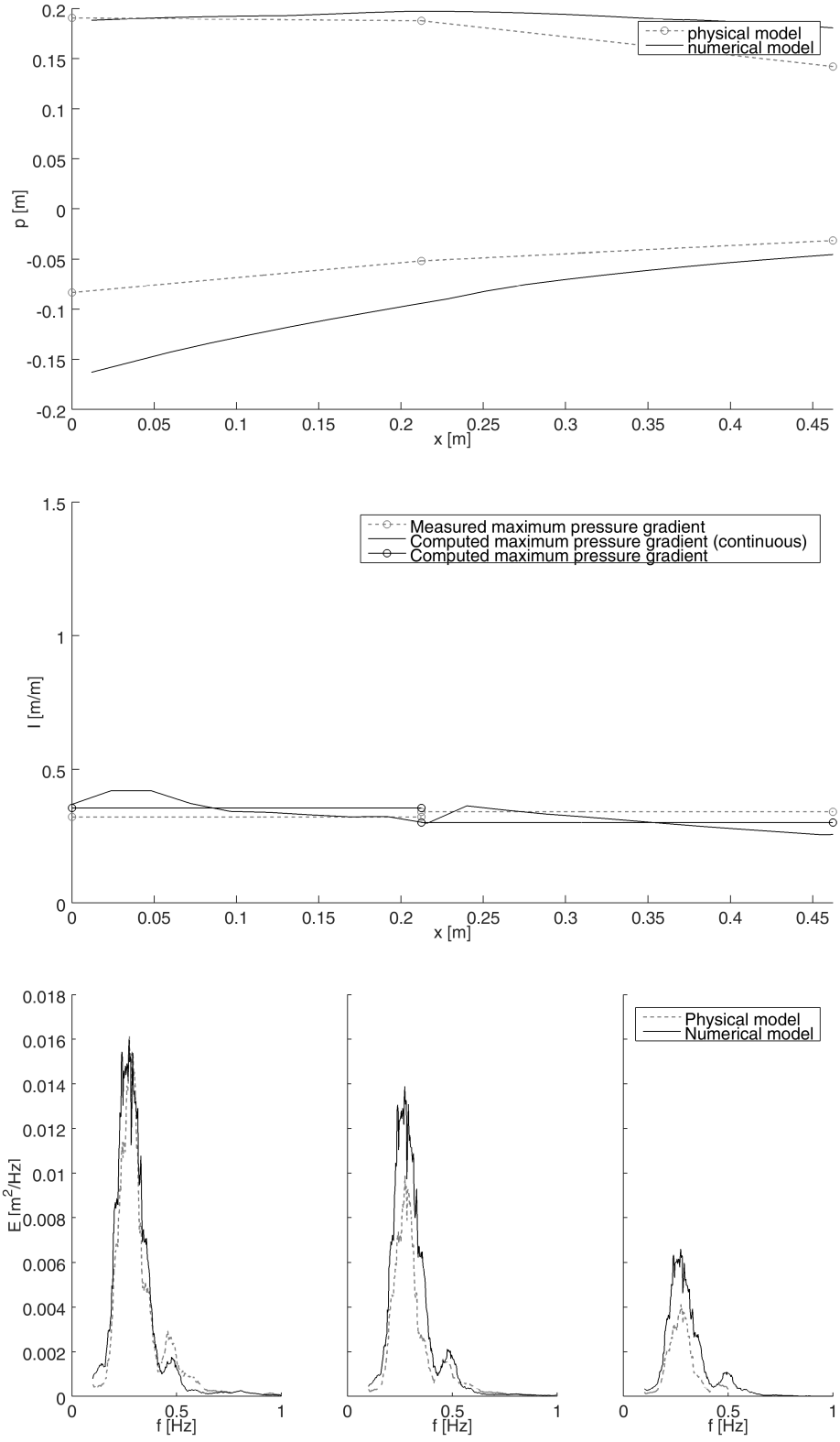

Figure D.13: Model validation test 12

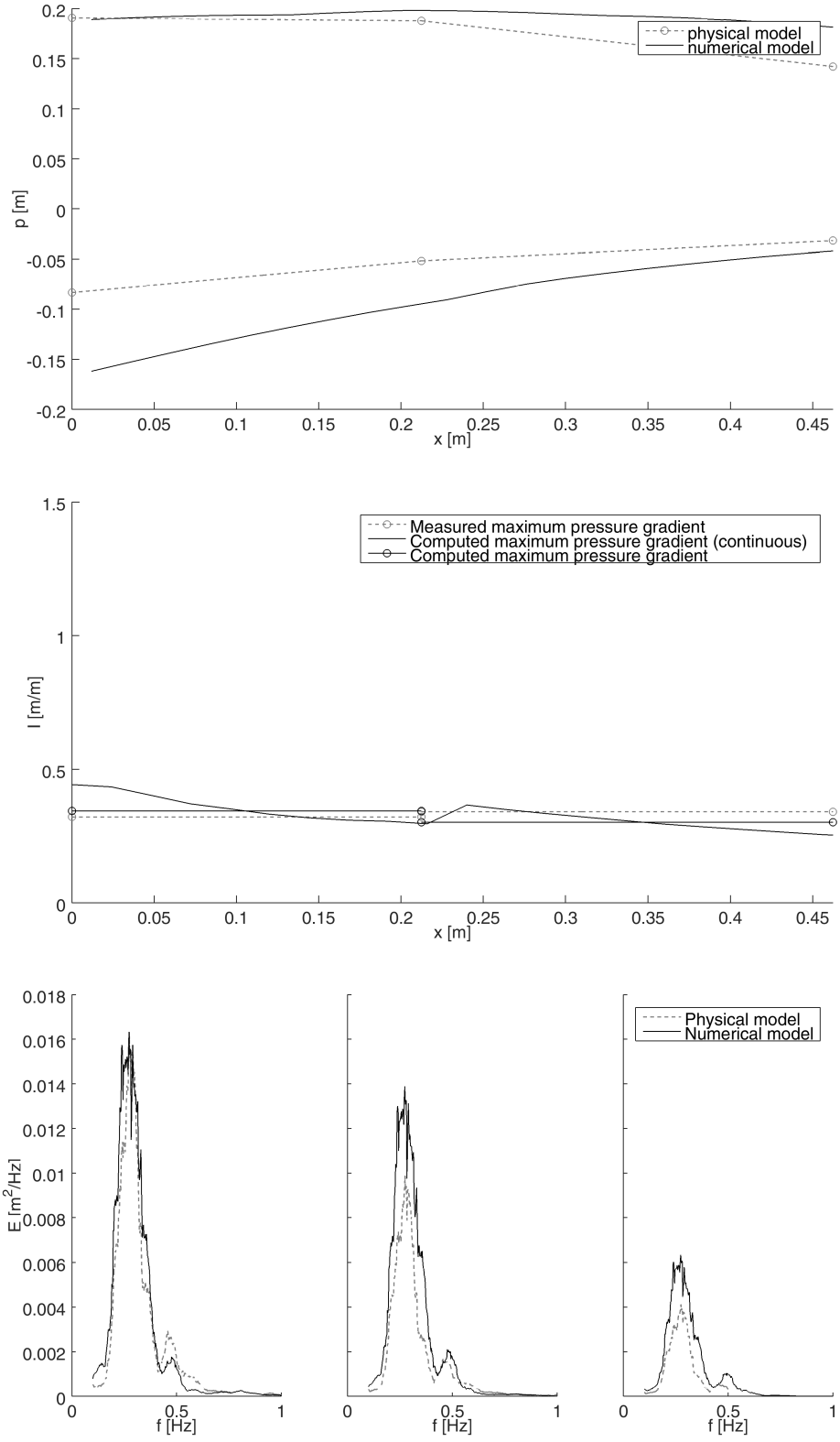

Figure D.14: Model validation test 13

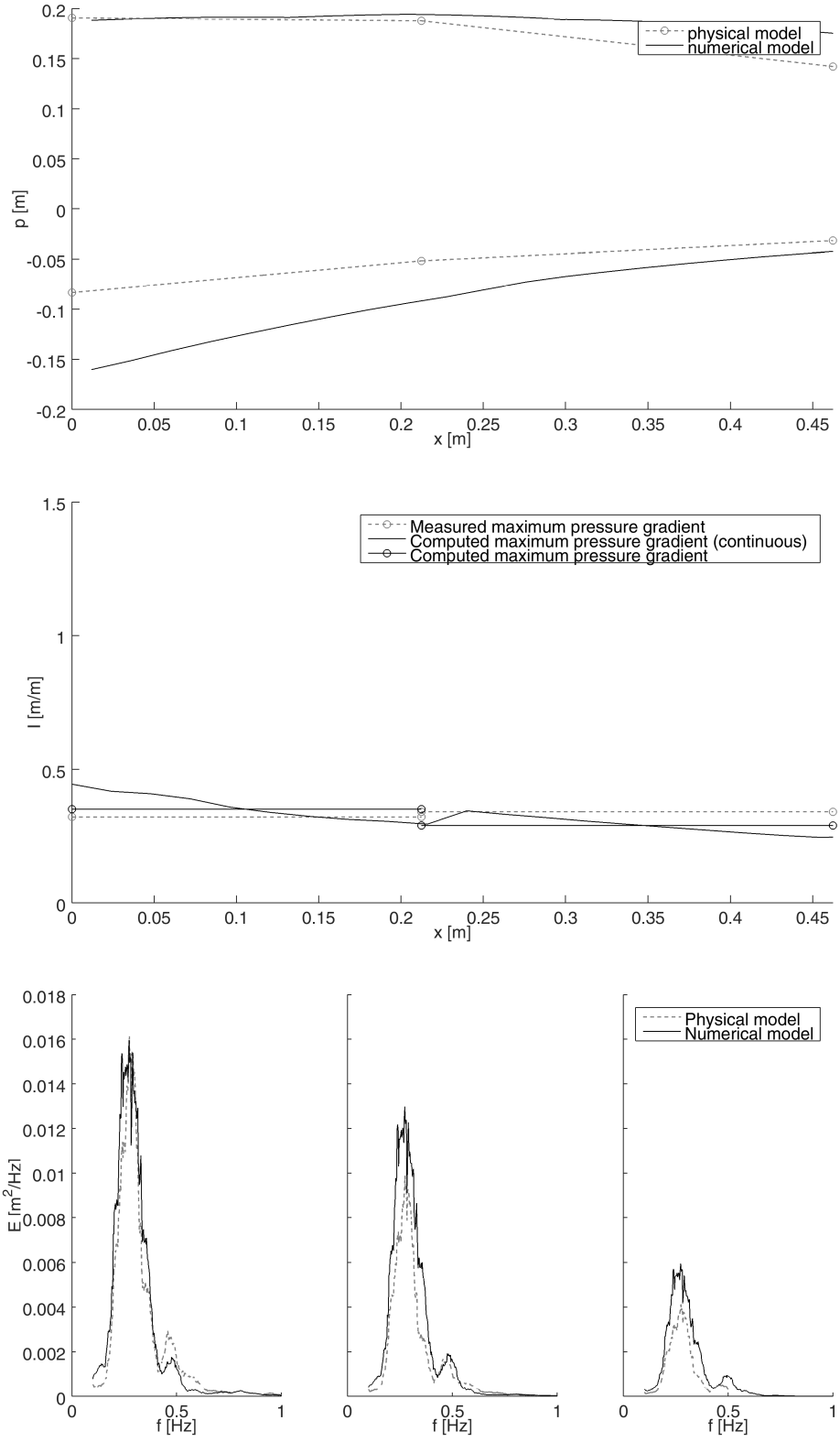

Figure D.15: Model validation test 14

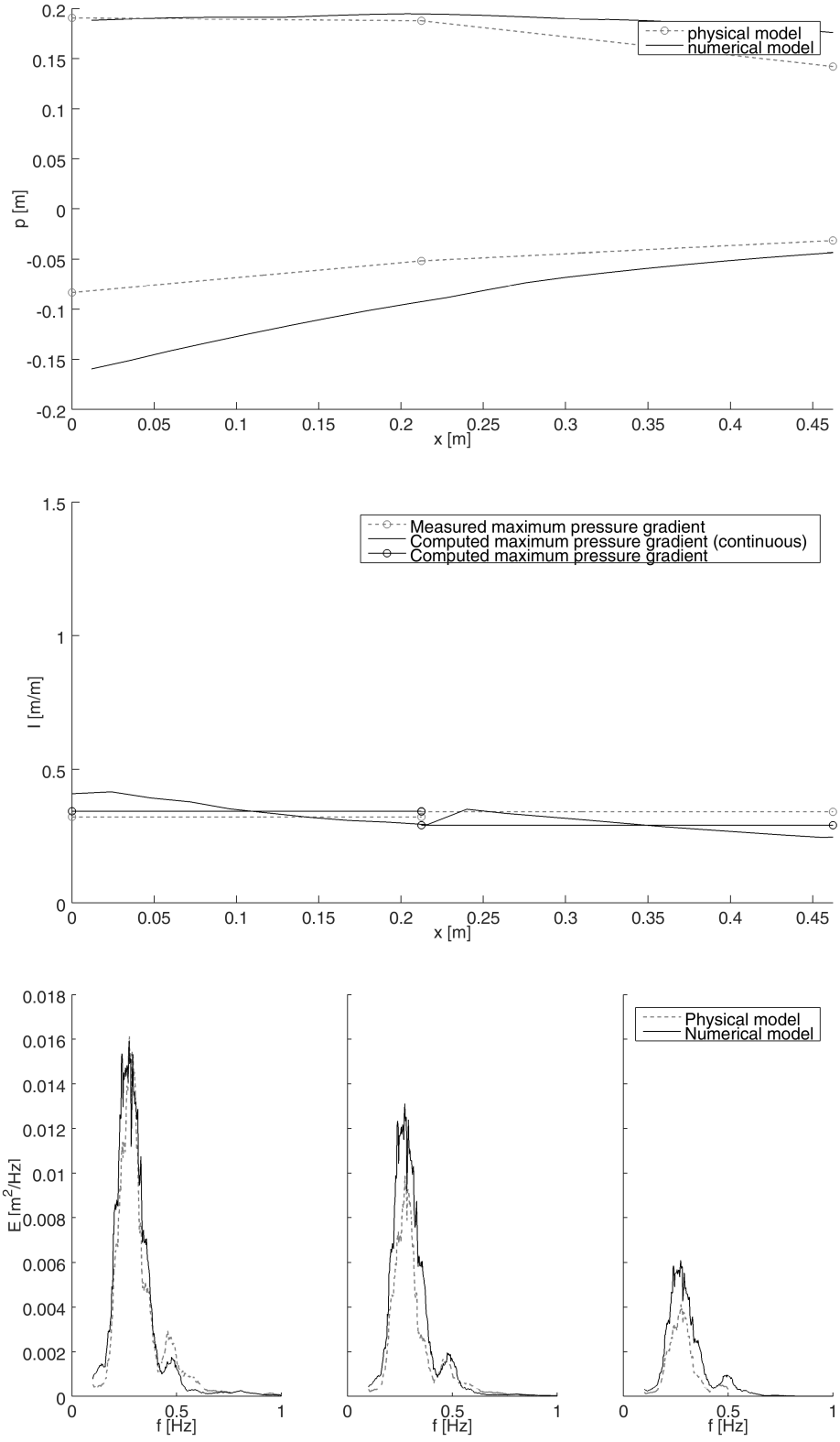

Figure D.16: Model validation test 15

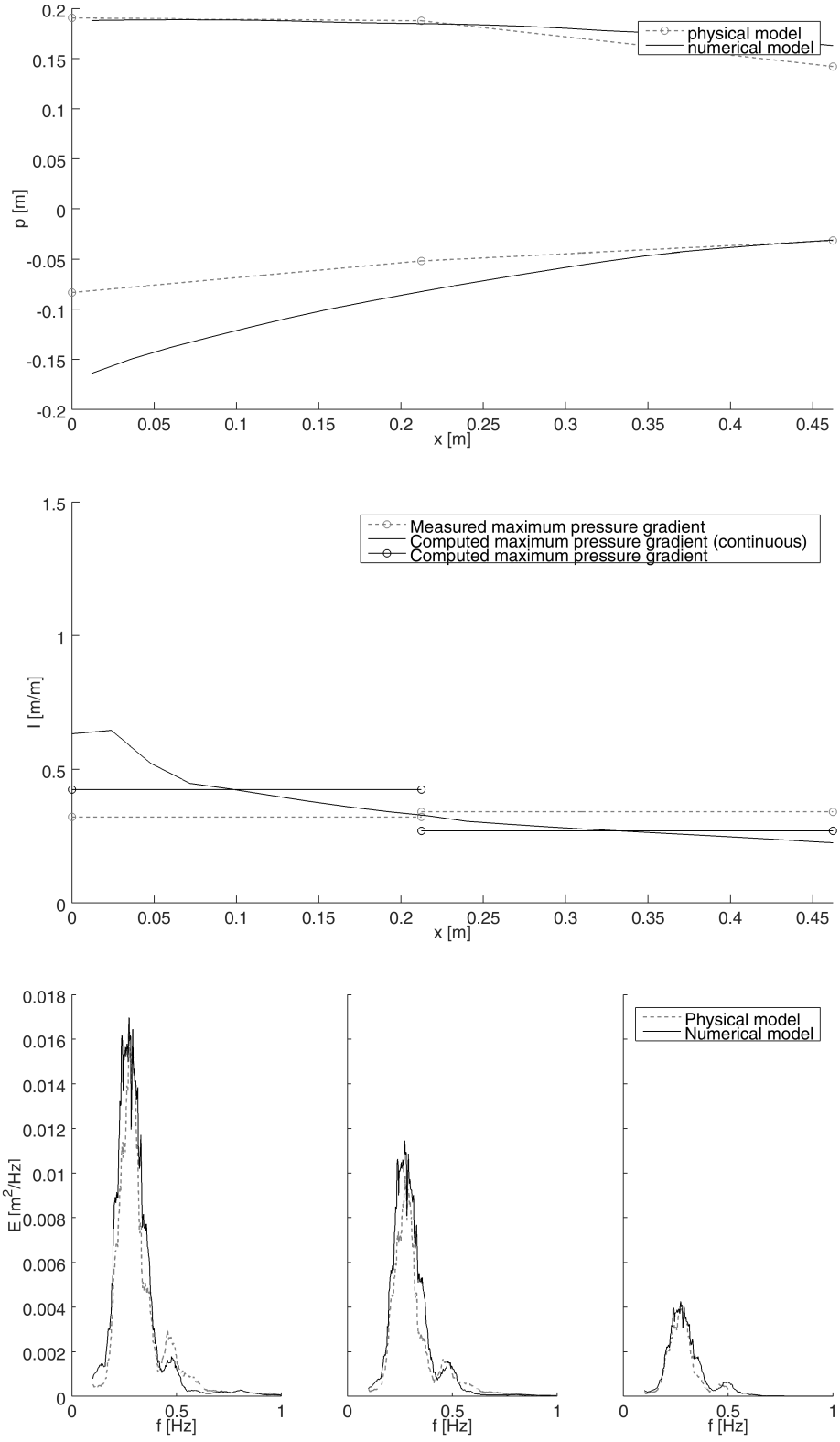

Figure D.17: Model validation test 16

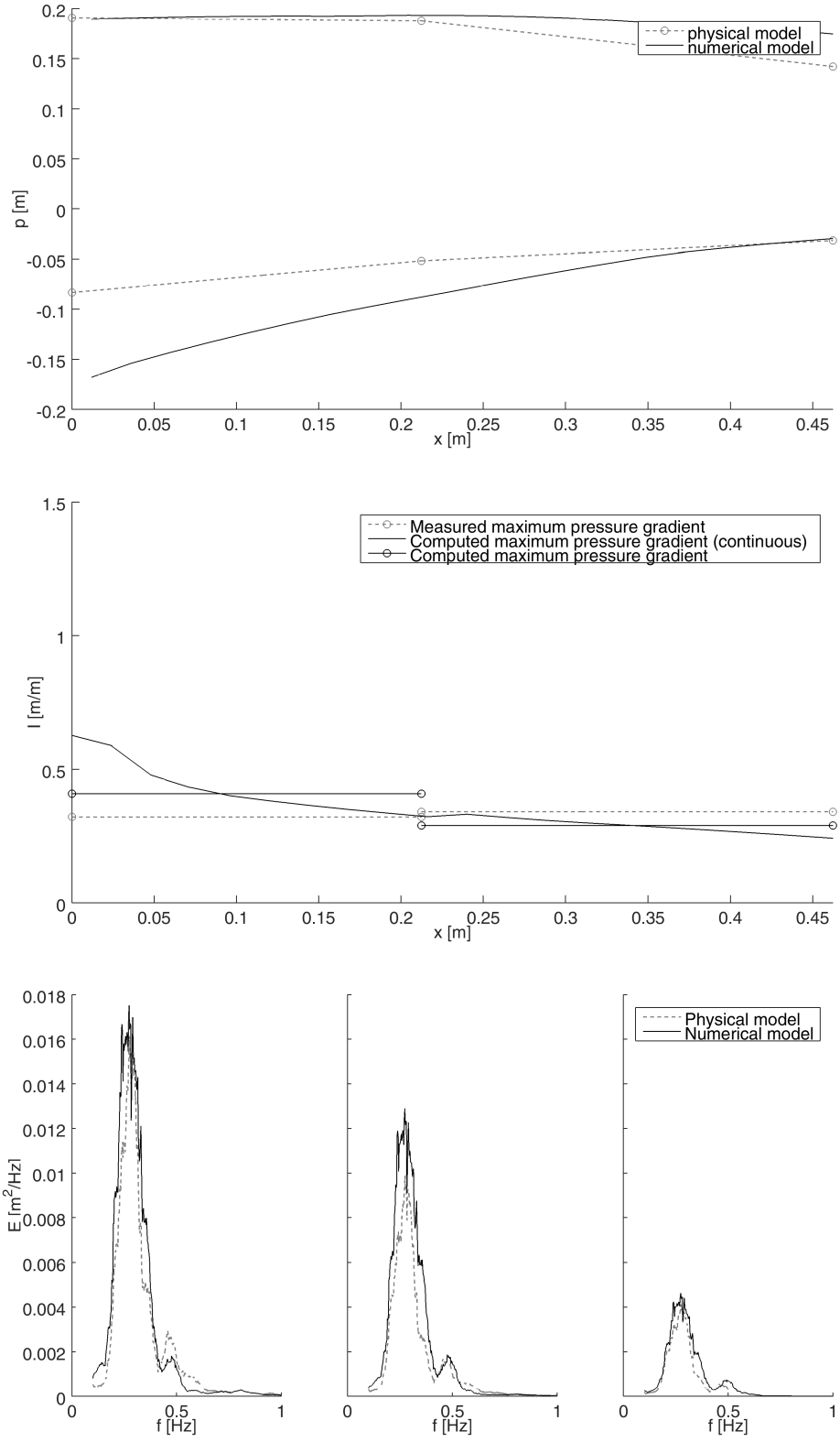

Figure D.18: Model validation test 17

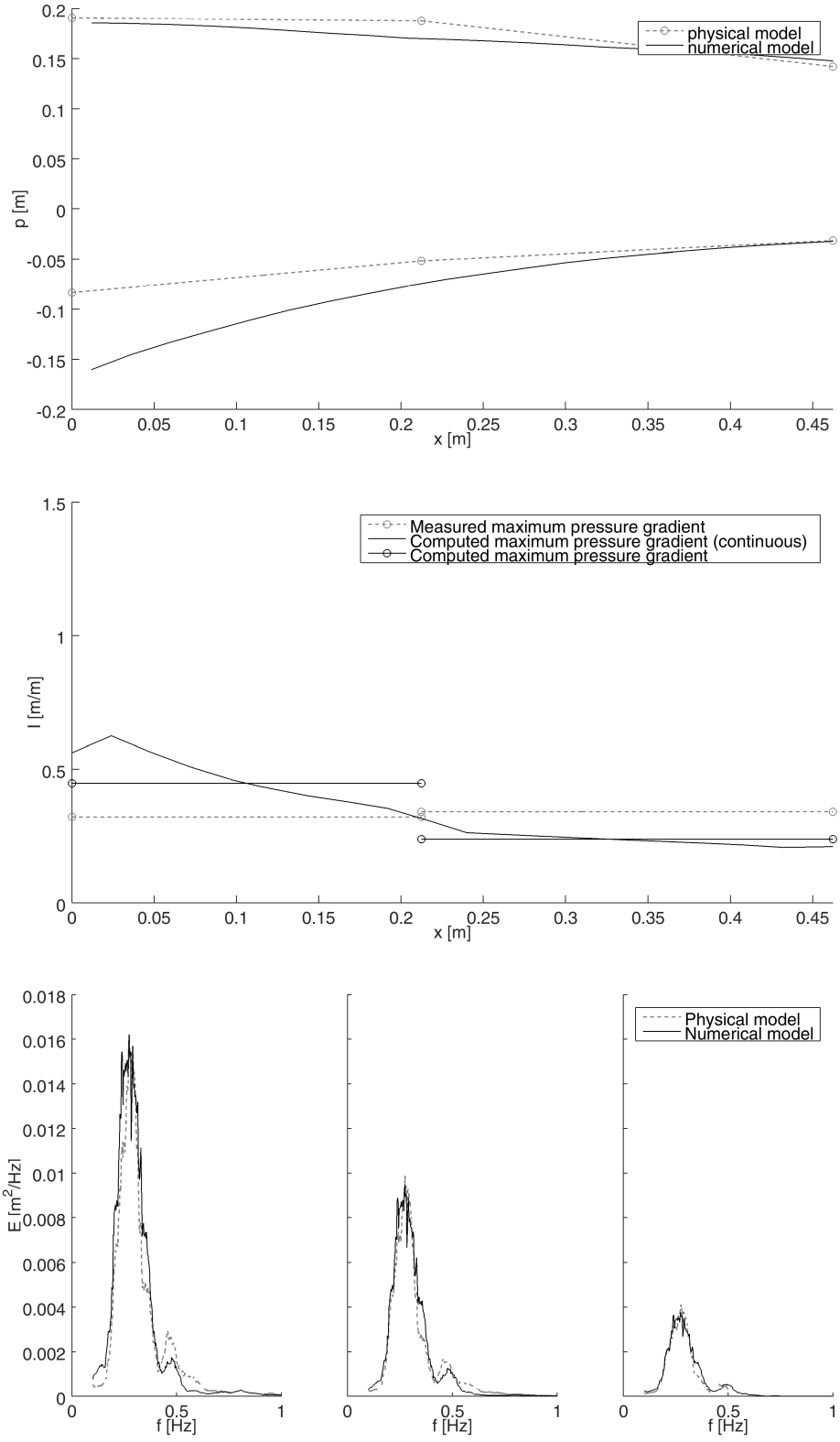

Figure D.19: Model validation test 18

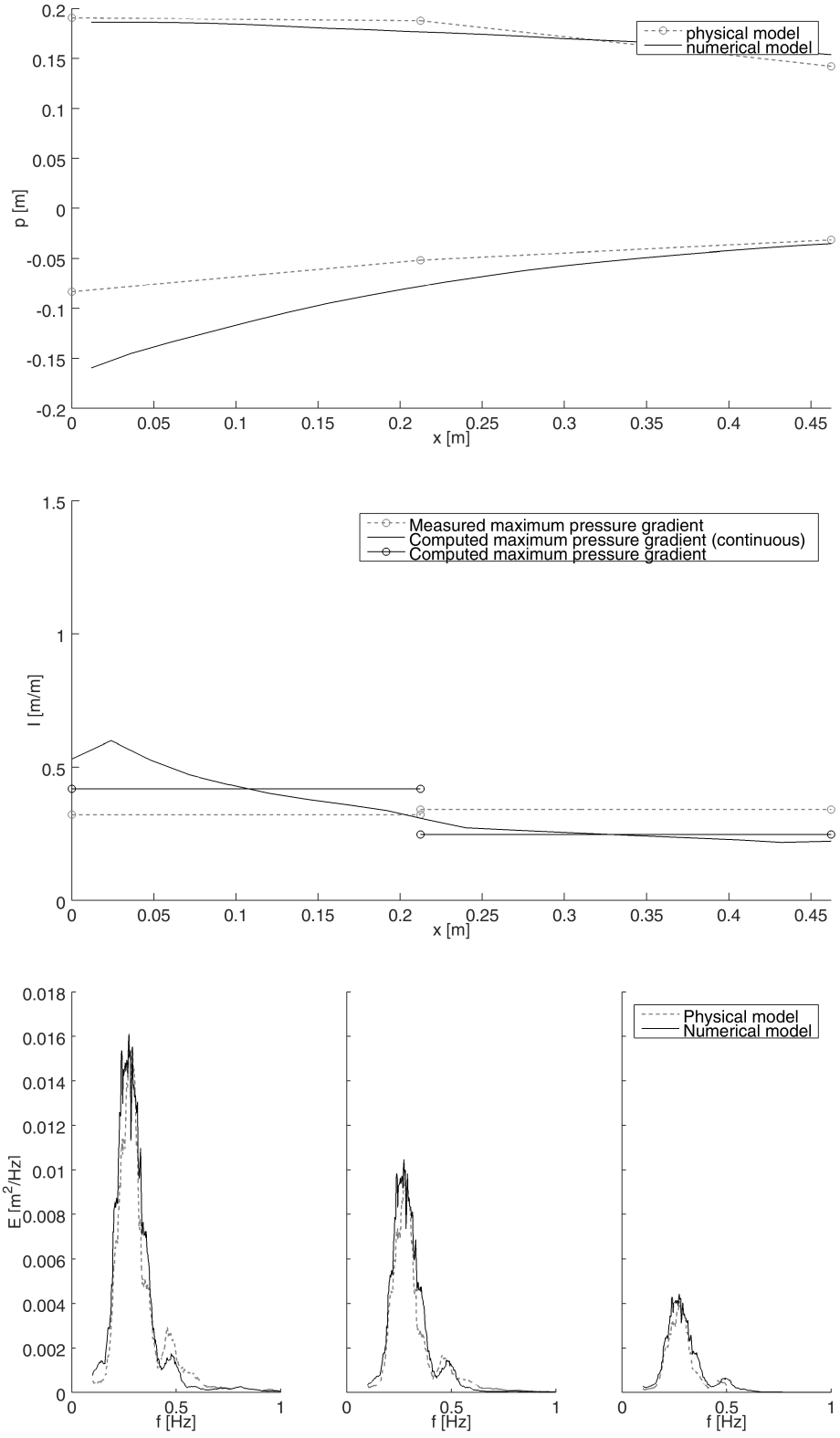

Figure D.20: Model validation test 19

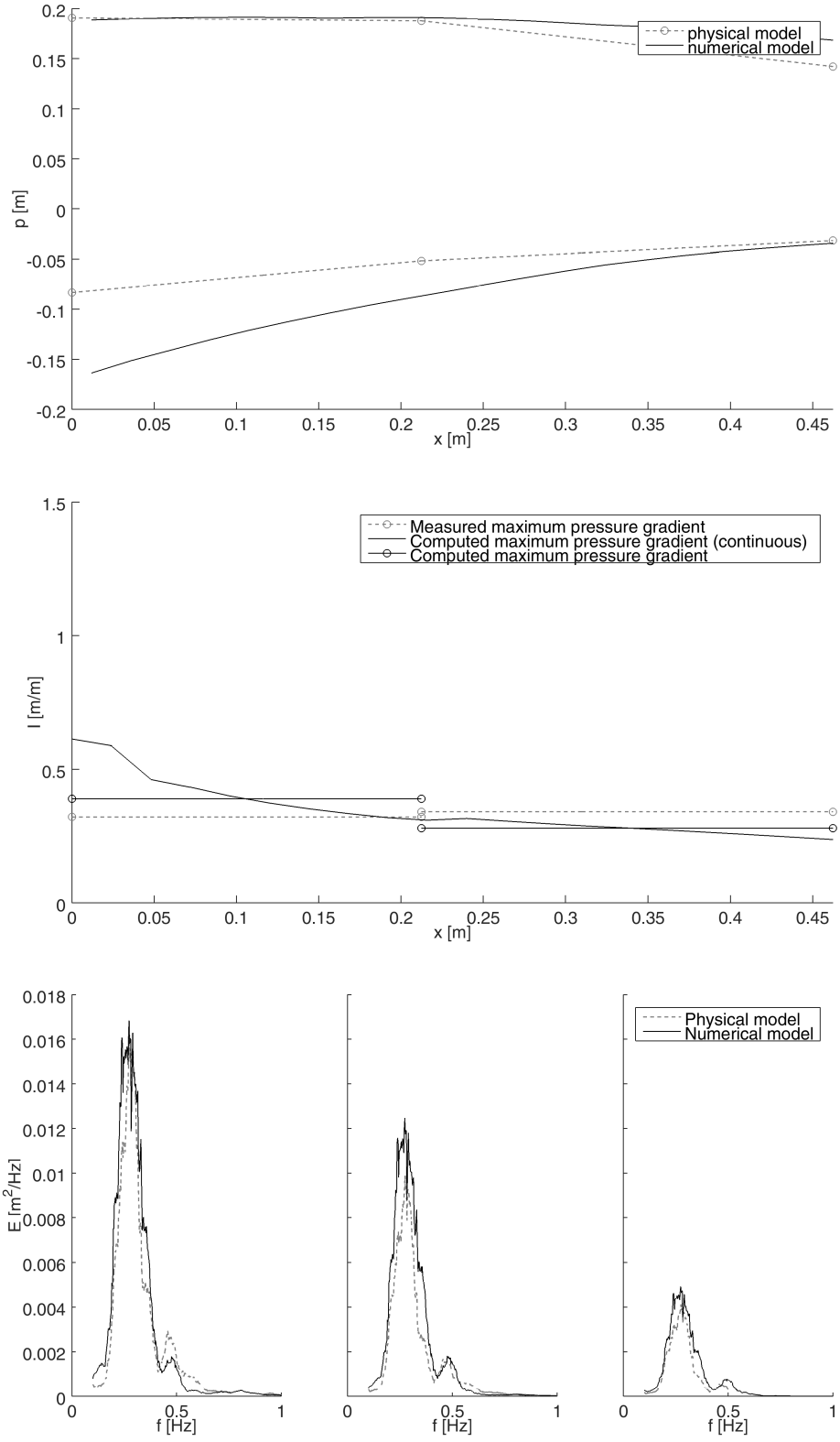

Figure D.21: Model validation test 20

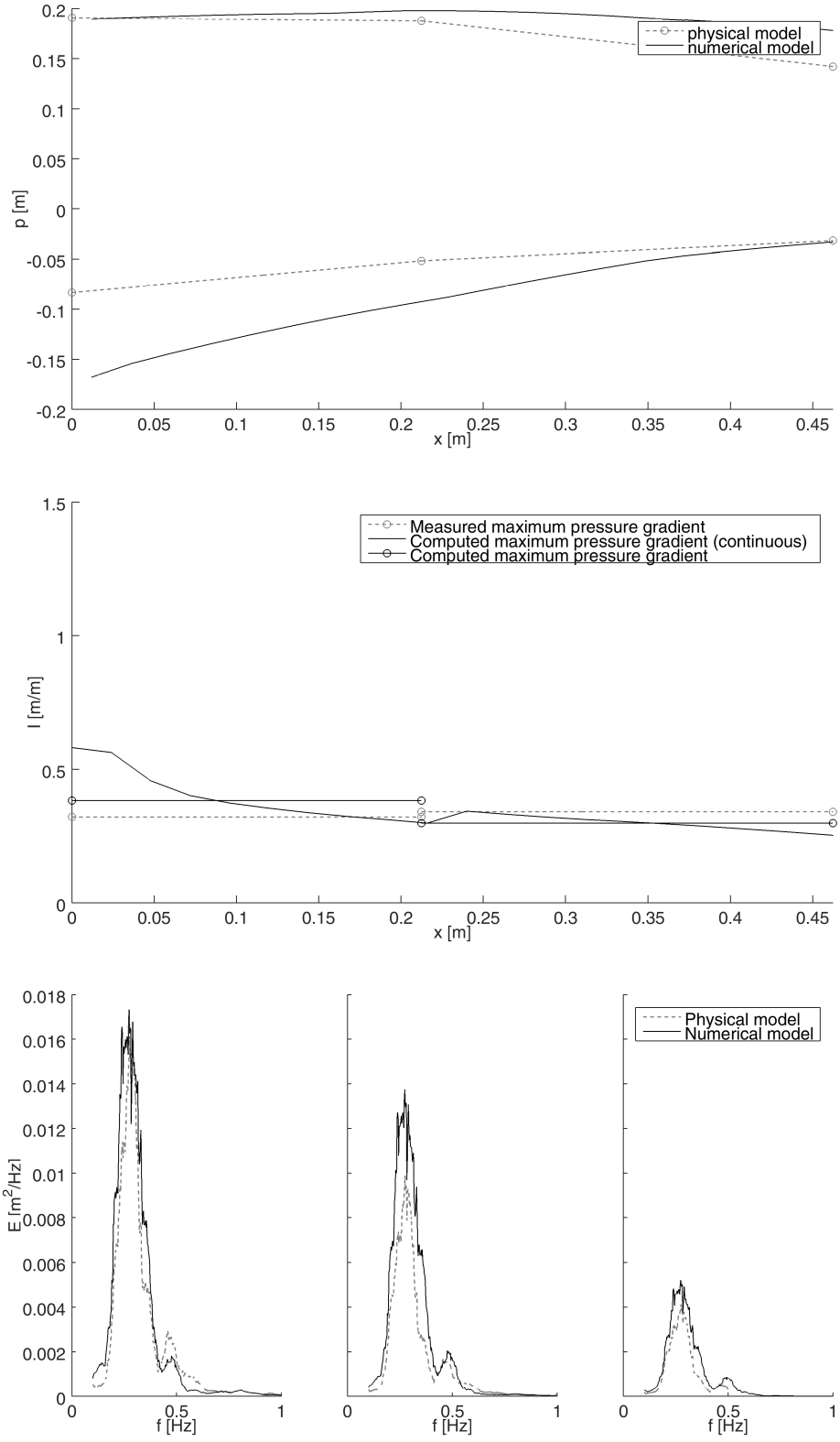

Figure D.22: Model validation test 21

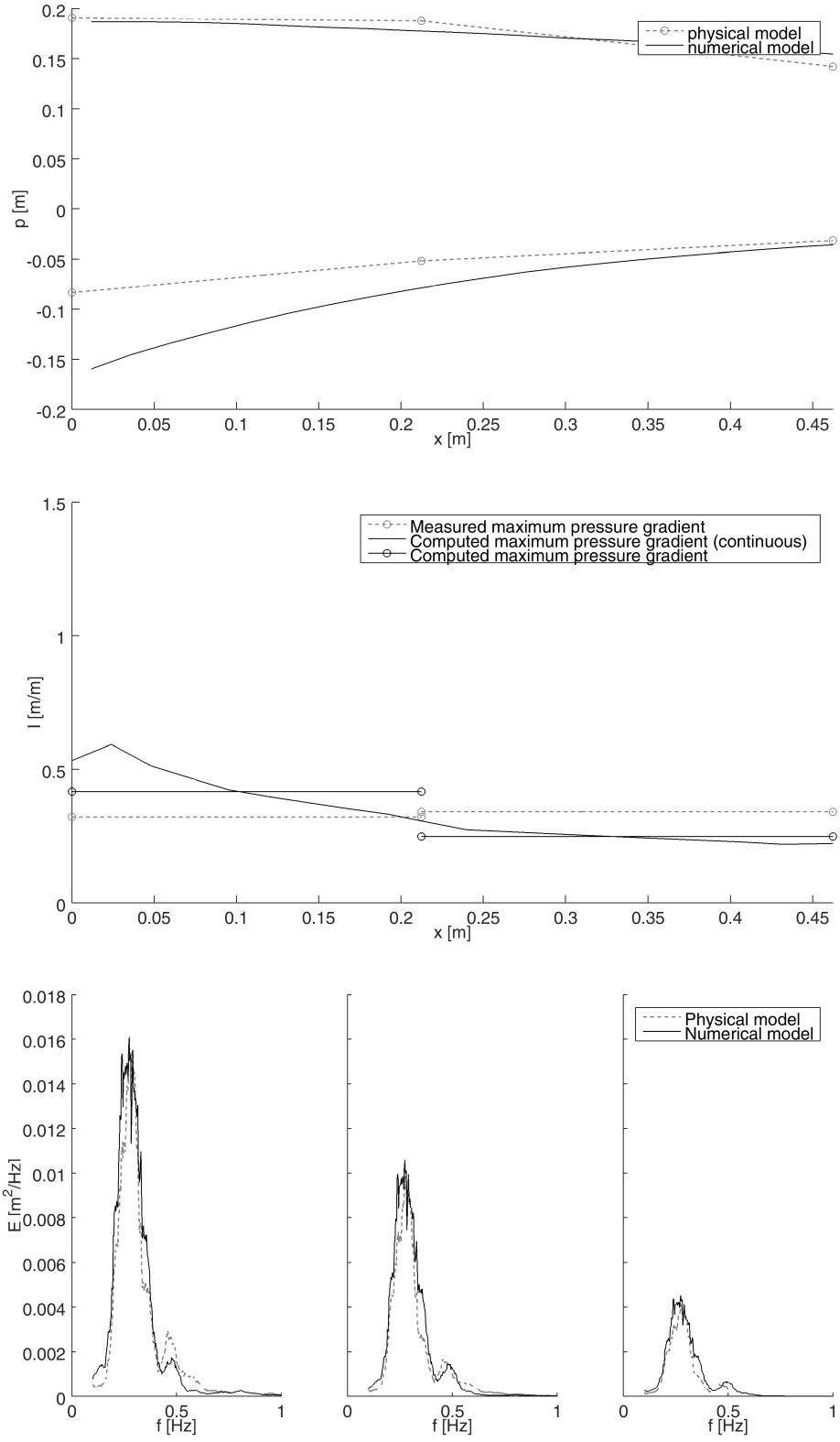

Figure D.23: Model validation test 22

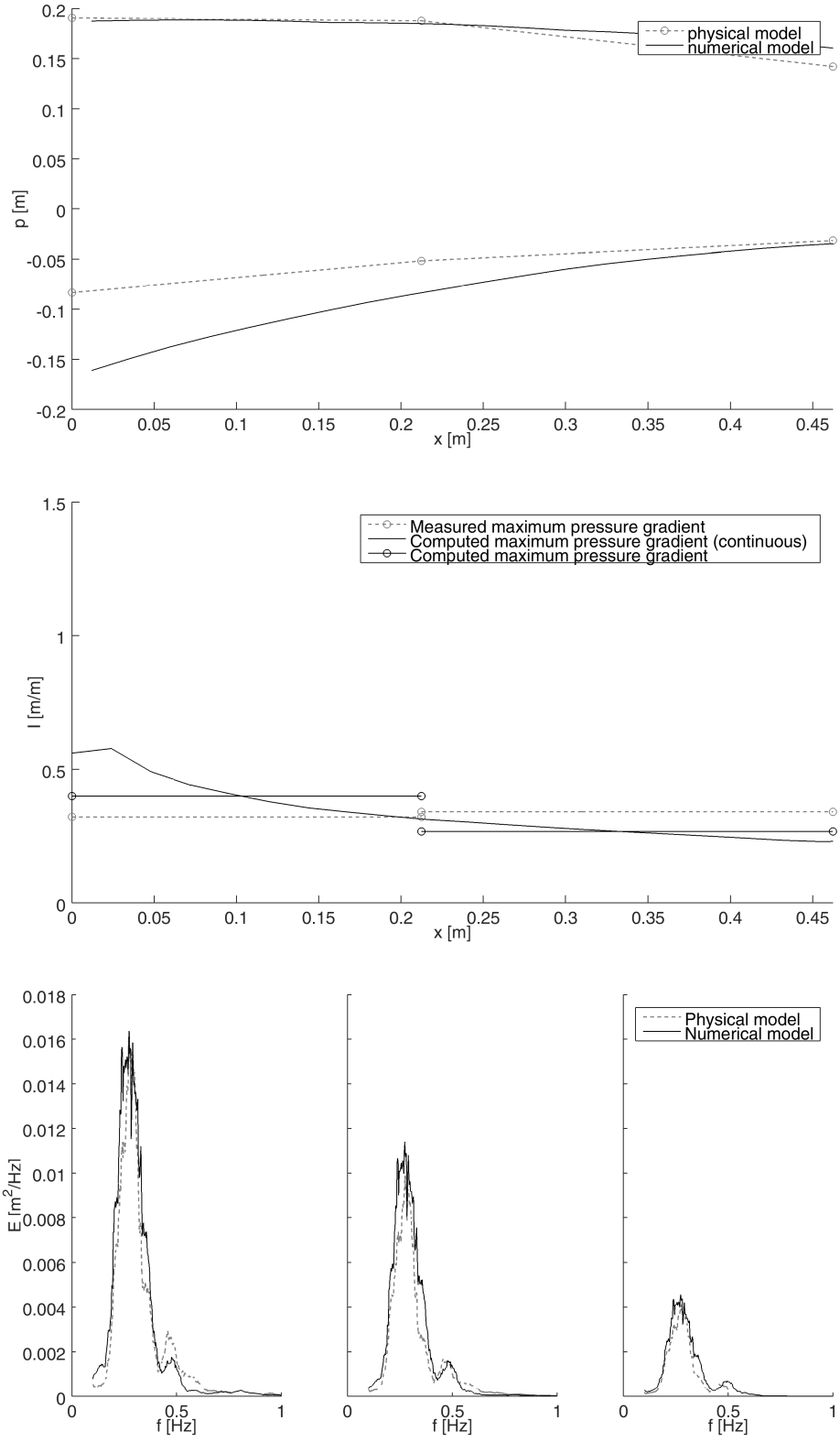

Figure D.24: Model validation test 23

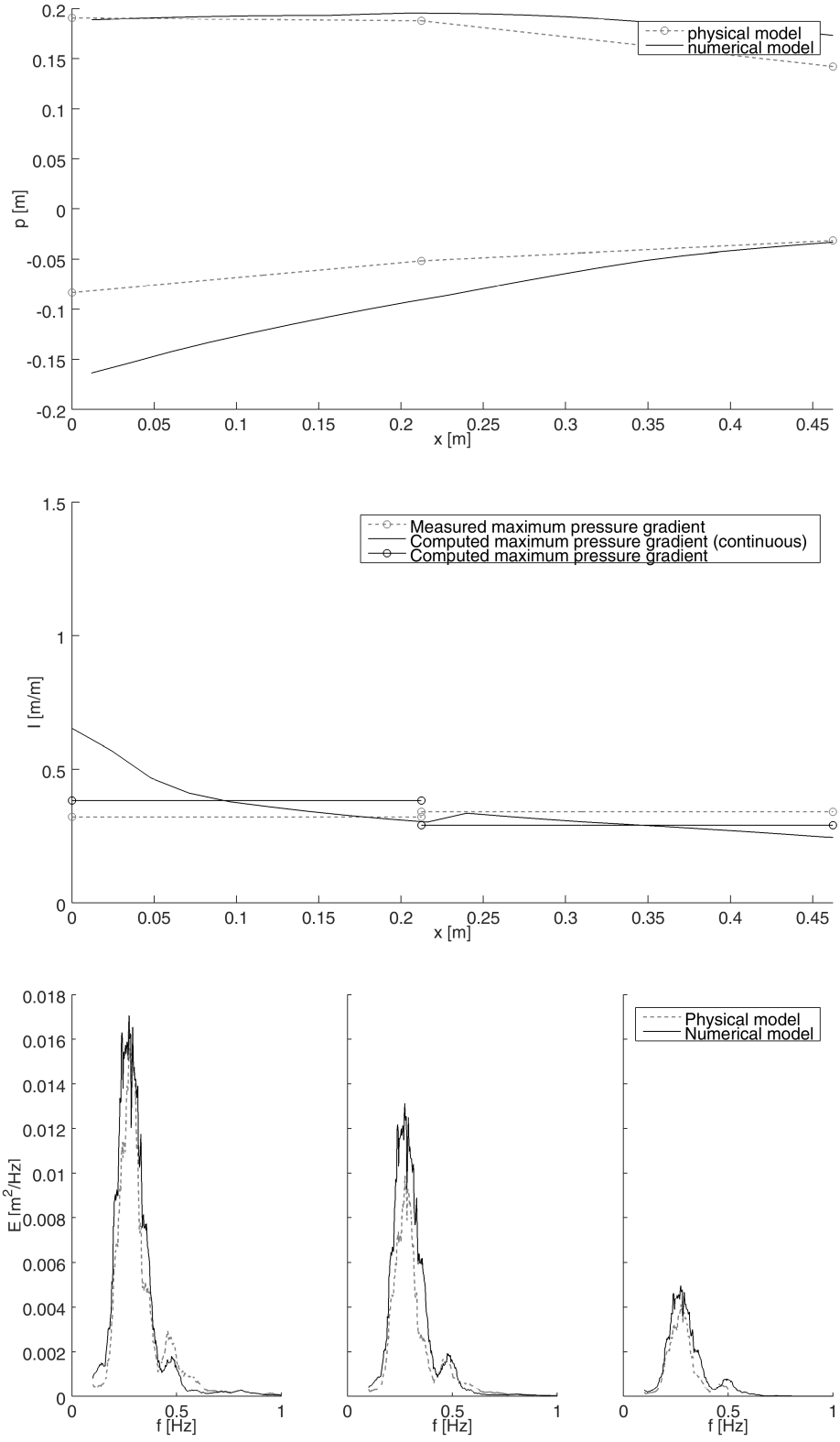

Figure D.25: Model validation test 24

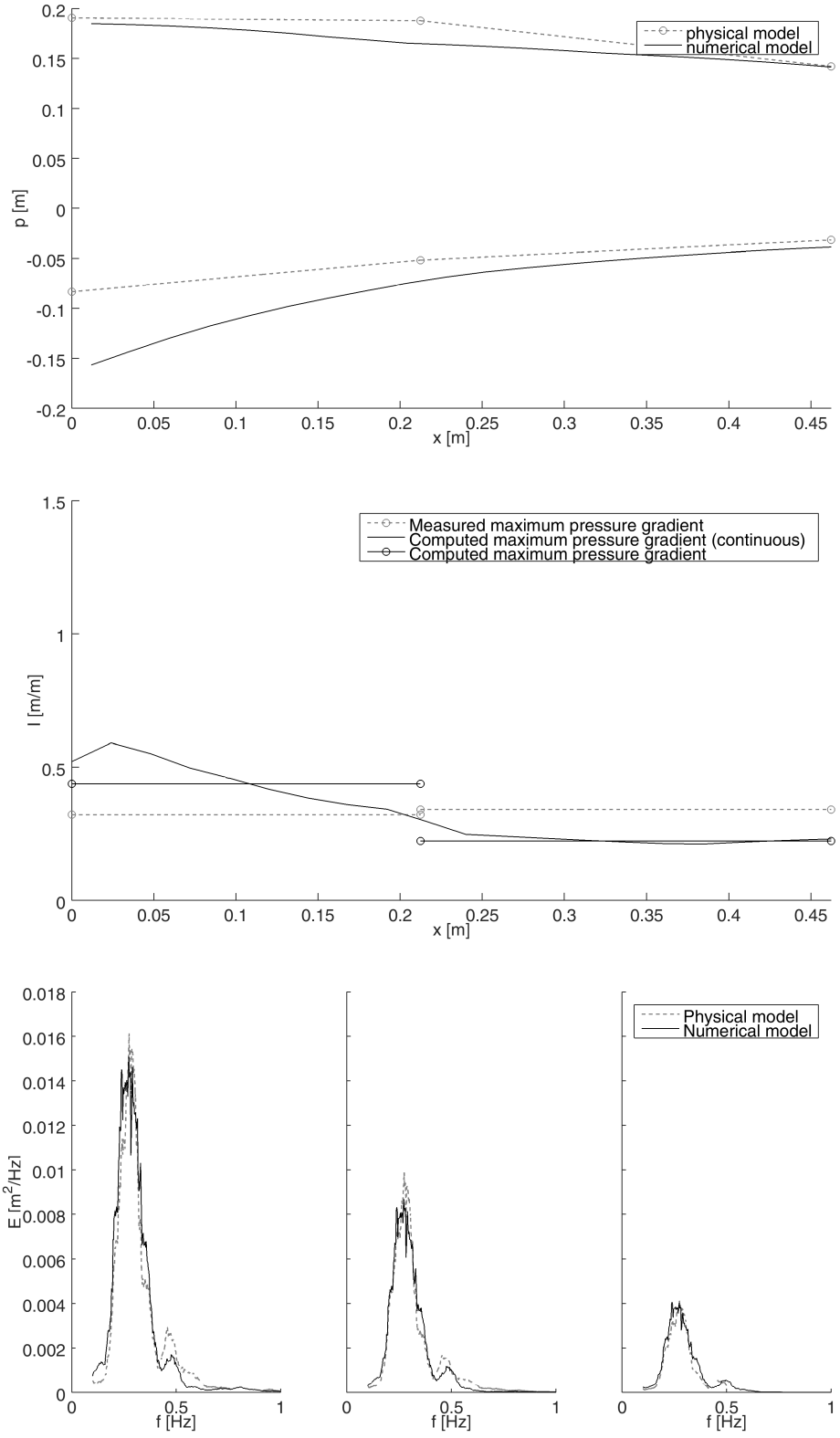

Figure D.26: Model validation test 25

E

VALIDATION RESULTS FOR OTHER PHYSICAL MODEL TESTS

In this appendix the visual results of the validation tests for the other physical model tests are shown, namely Kik test 1, 3 and 6 and Kluwen test 56, 60, 64 and 68. First of all an overview of the tested structure and the test matrix is given.

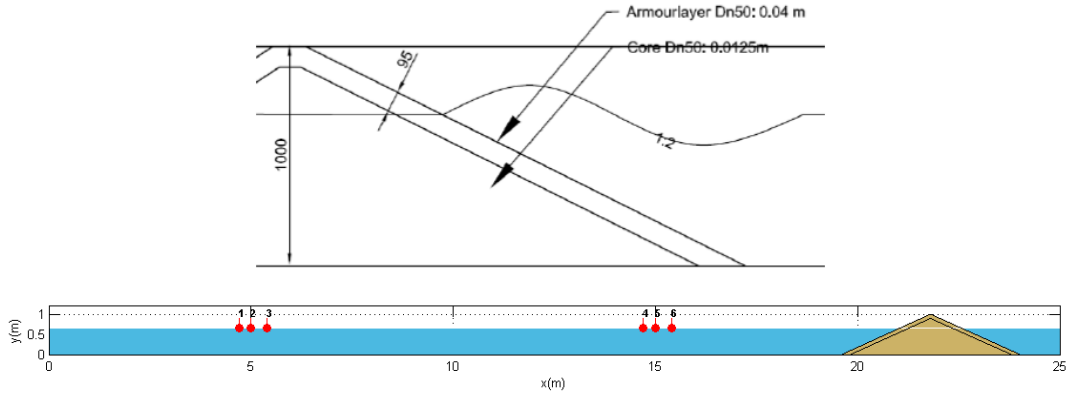

Figure E.1: Kik structure: schematisation of physical structure (above) and computational domain (below)

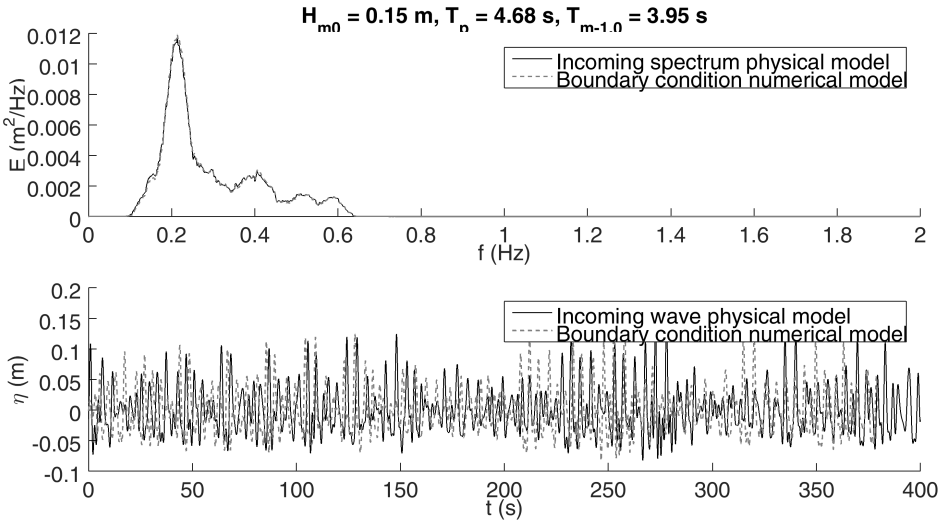

Figure E.2: Kik test 1: spectra and wave series

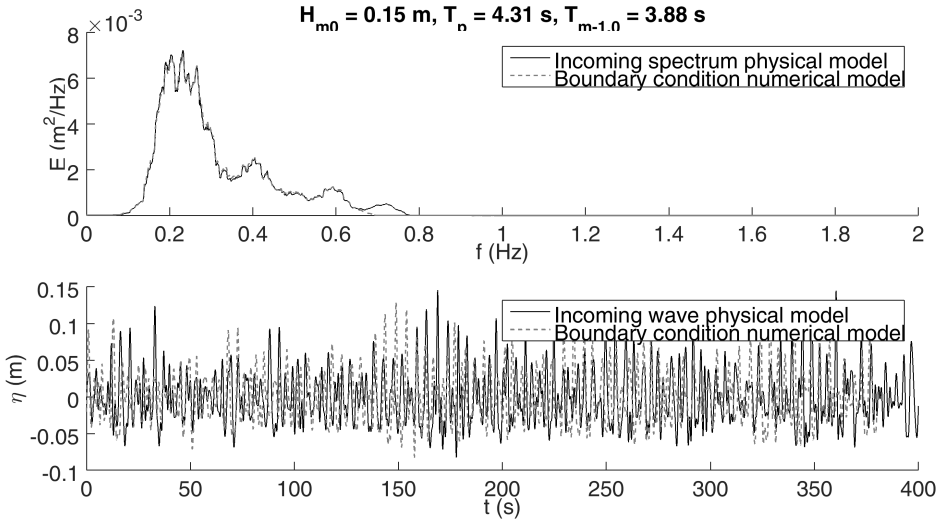

Figure E.3: Kik test 3: spectra and wave series

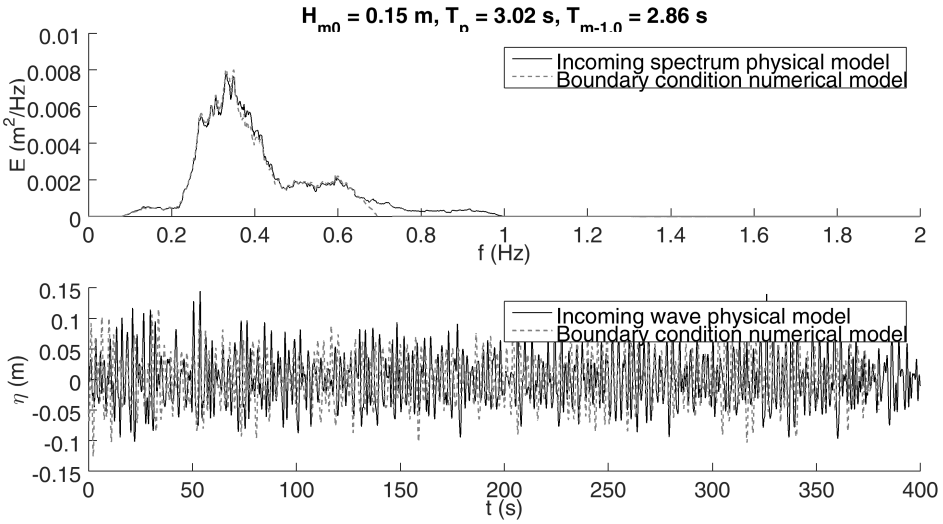

Figure E.4: Kik test 6: spectra and wave series

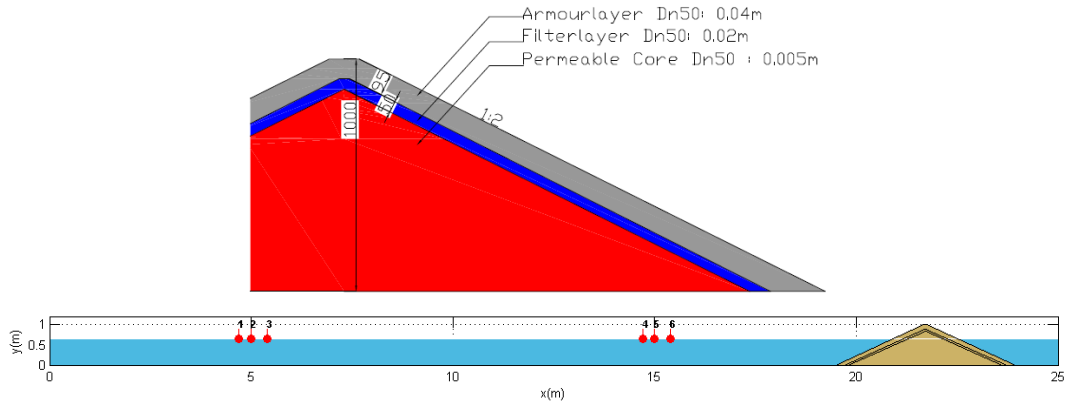

Figure E.5: Kluwen structure: schematisation of physical structure (above) and computational domain (below)

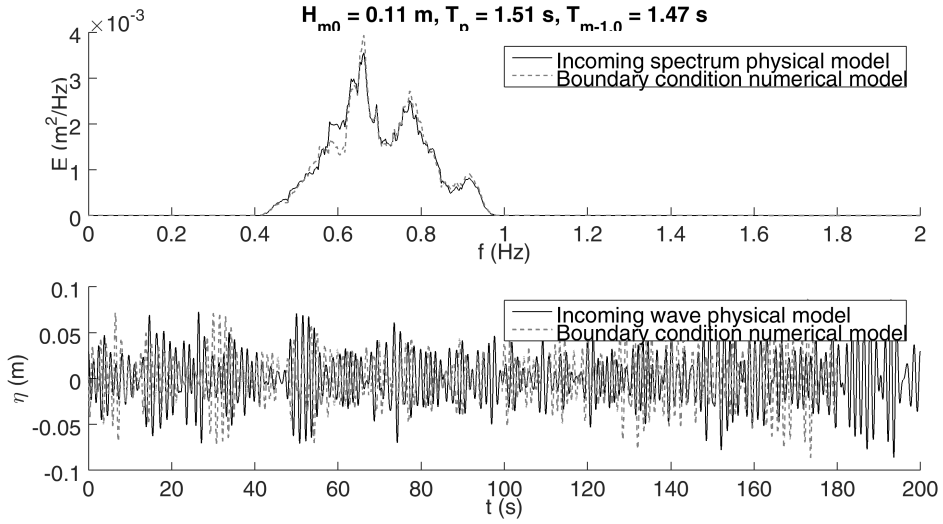

Figure E.6: Kluwen test 56: spectra and wave series

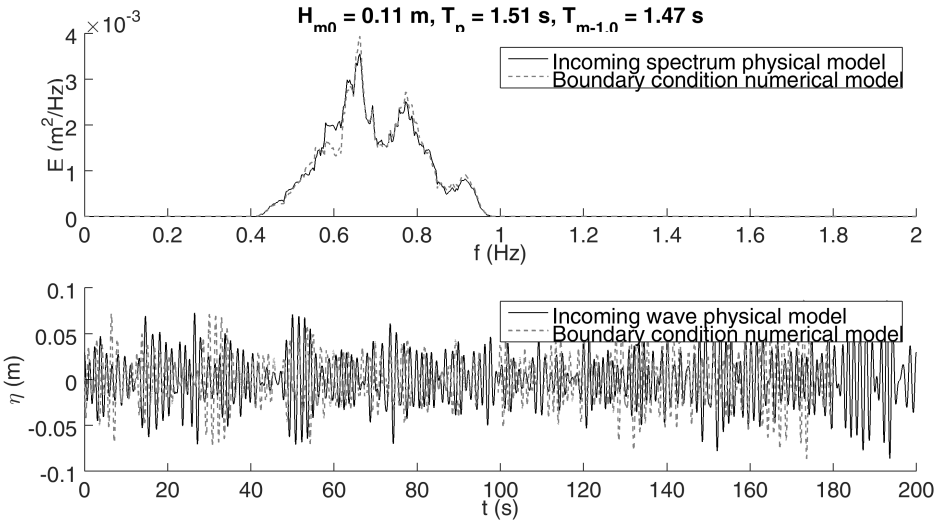

Figure E.7: Kluwen test 60: spectra and wave series

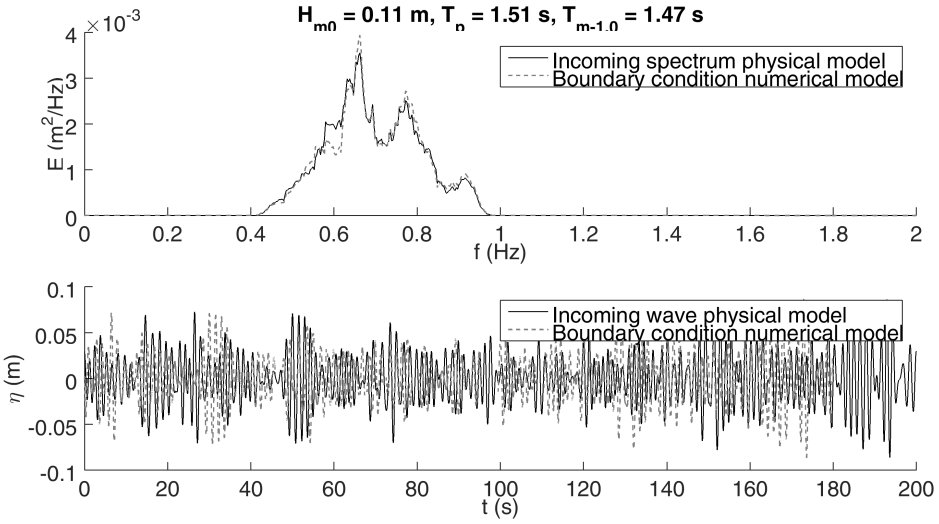

Figure E.8: Kluwen test 64: spectra and wave series

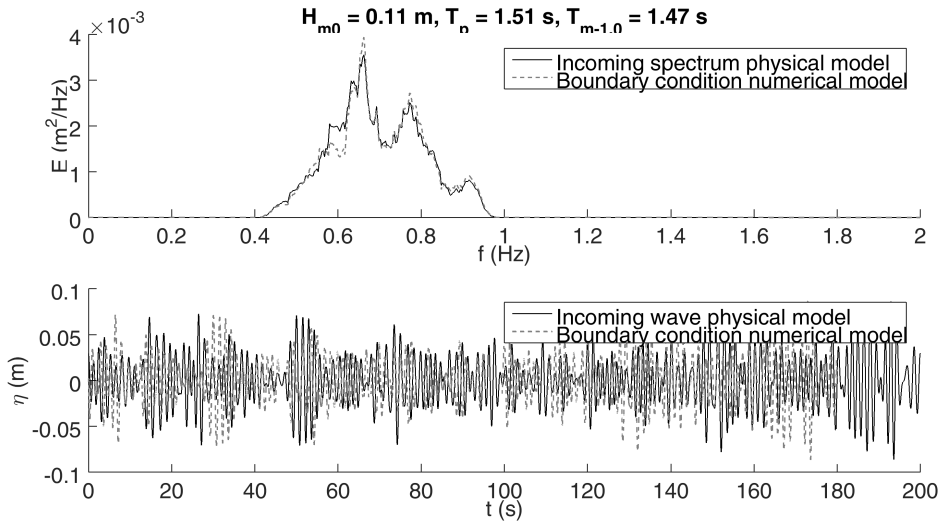

Figure E.9: Kluwen test 68: spectra and wave series

Figures description

Above Maximum and minimum horizontal pressure distribution inside the structure (0.46 m from the bottom). The circles indicate the measurement points during the physical model tests.

Middle Maximum pressure gradient inside the structure (0.46 m from the bottom). The blue circles indicate the measurement points during the physical model tests.

Below Energy spectra of pressure time signals at three different locations. Left: Armour layer surface, middle: interface between armour layer and core, right: inside the core.

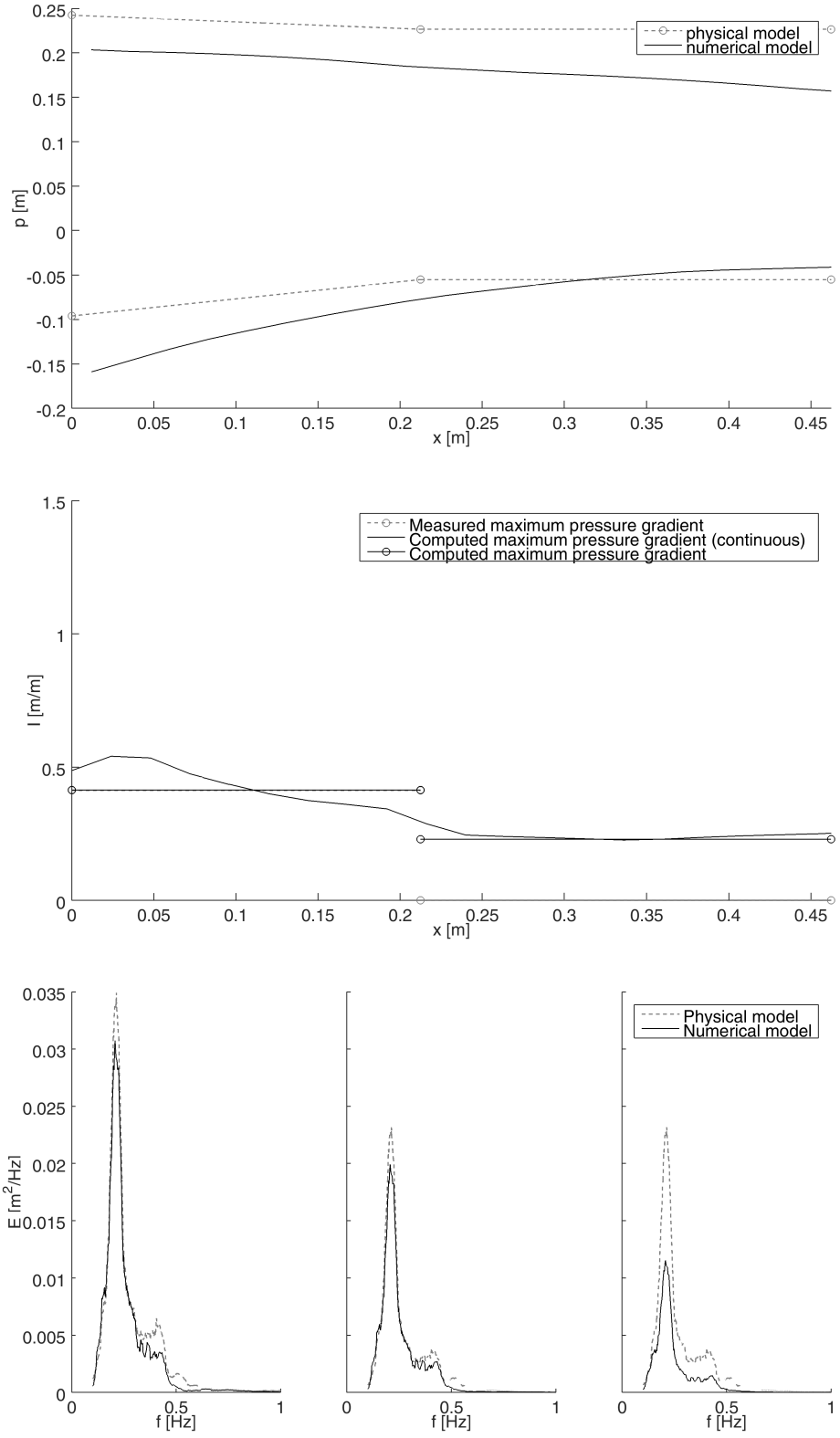

Figure E.10: Kik test 1

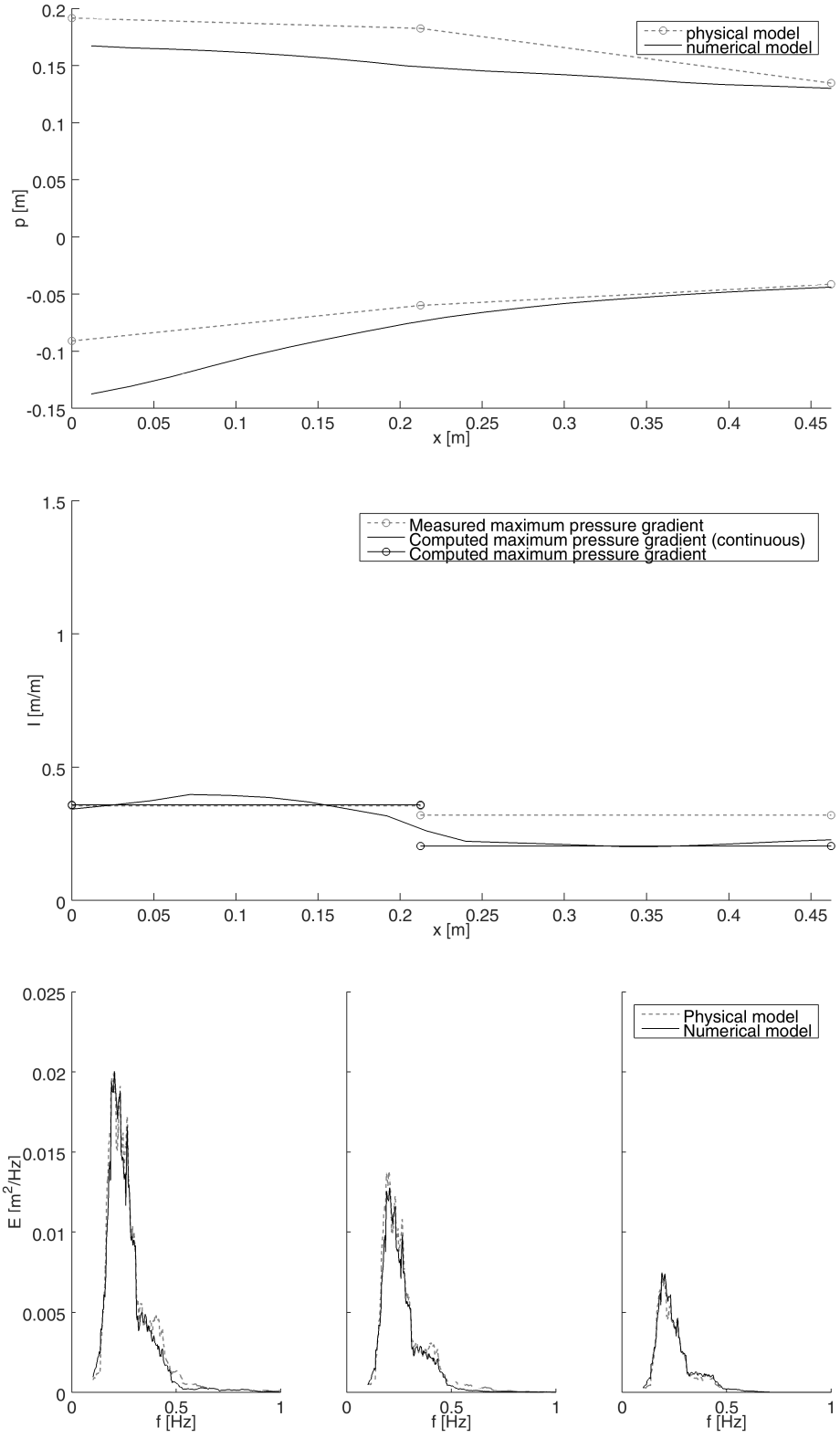

Figure E.11: Kik test 3

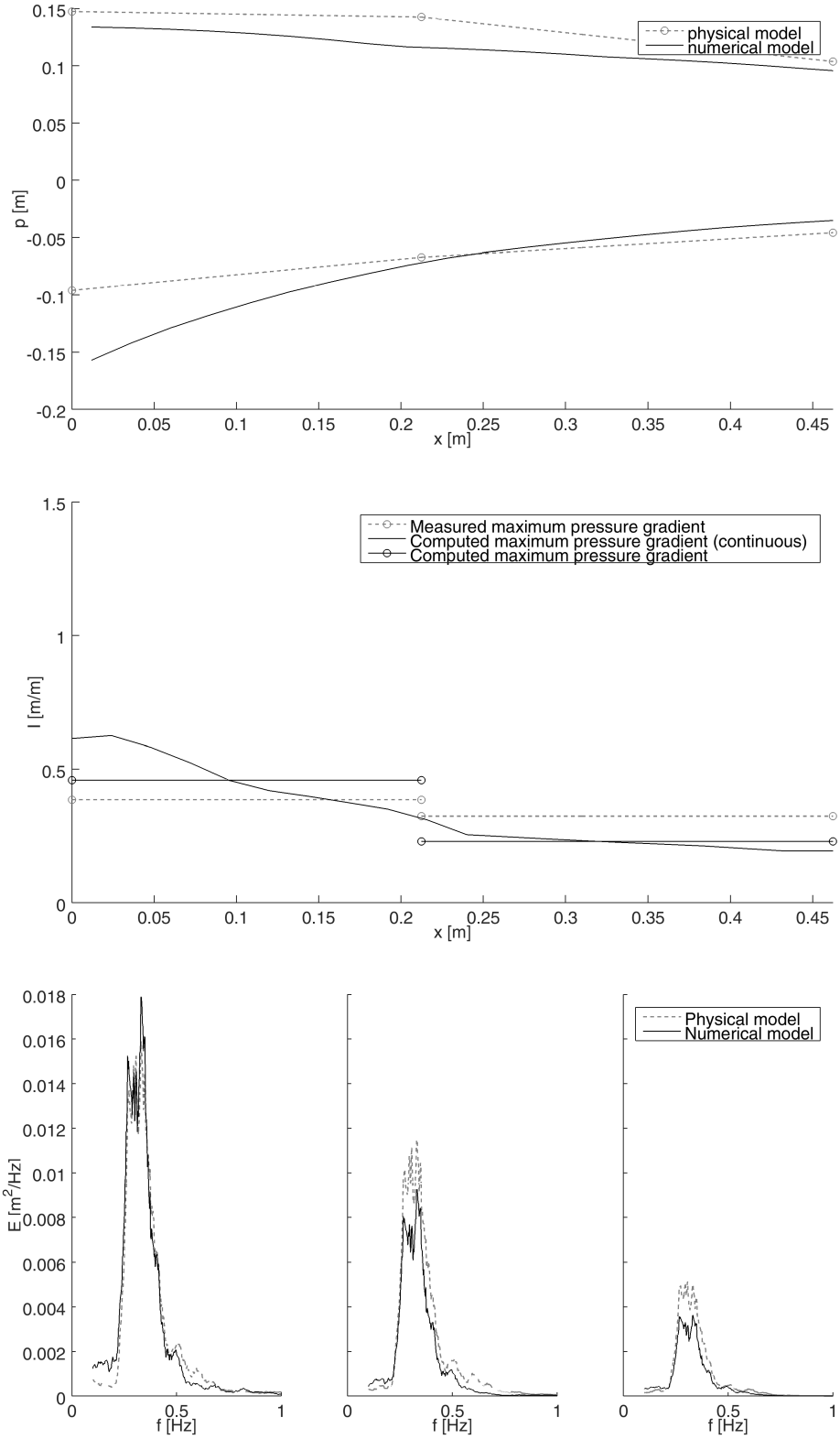

Figure E.12: Kik test 6

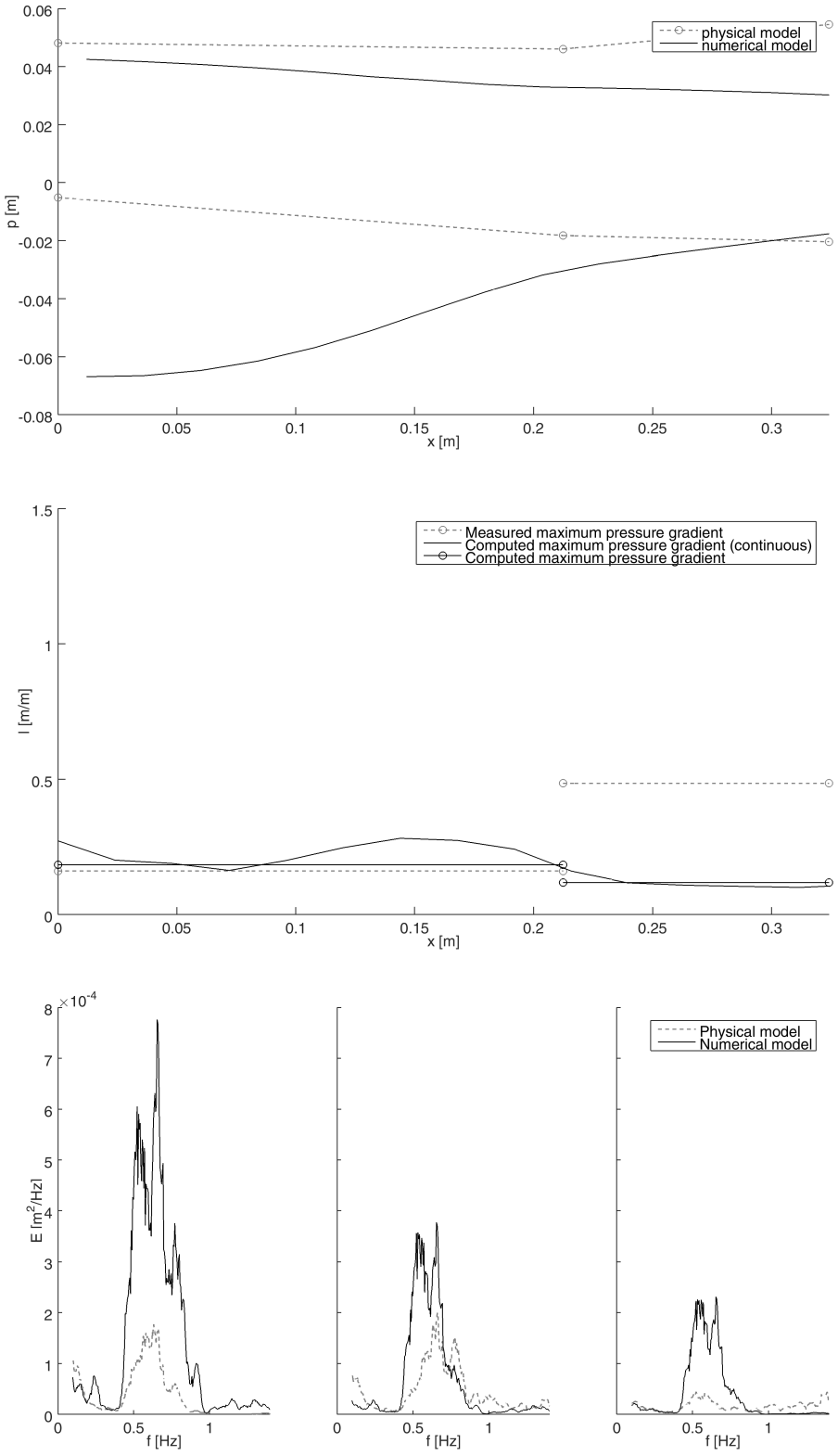

Figure E.13: Kluwen test 56

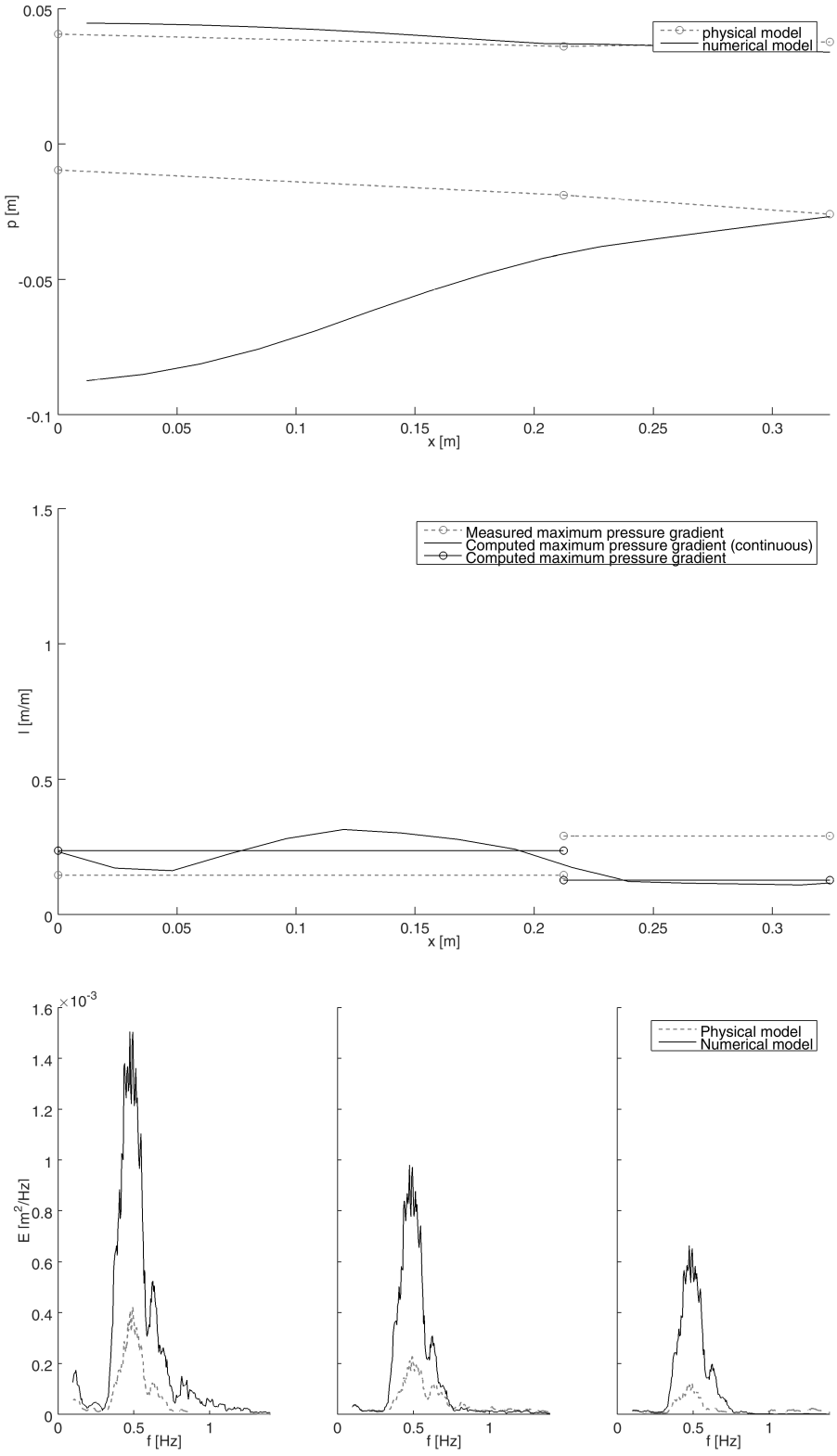

Figure E.14: Kluwen test 60

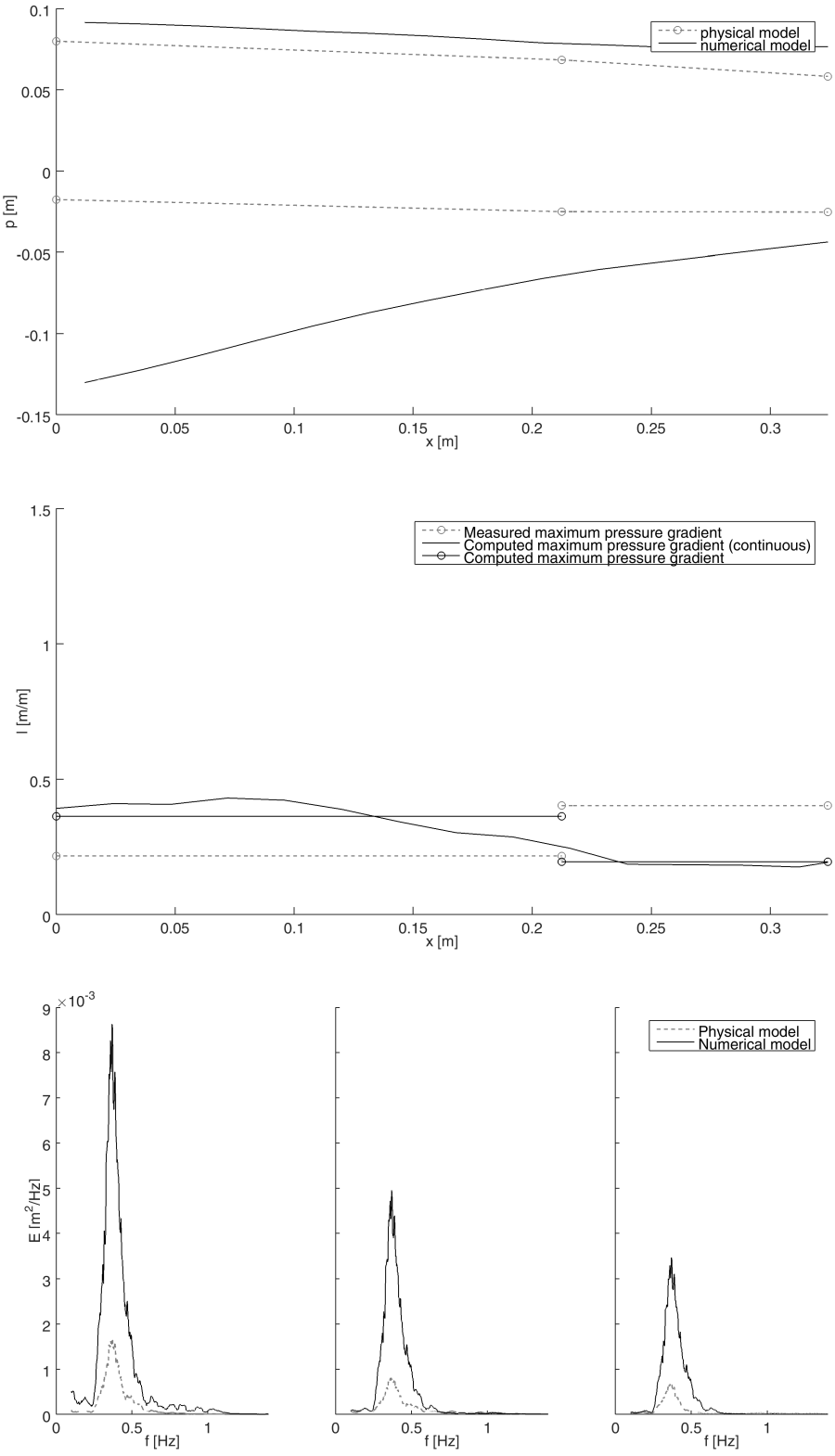

Figure E.15: Kluwen test 64

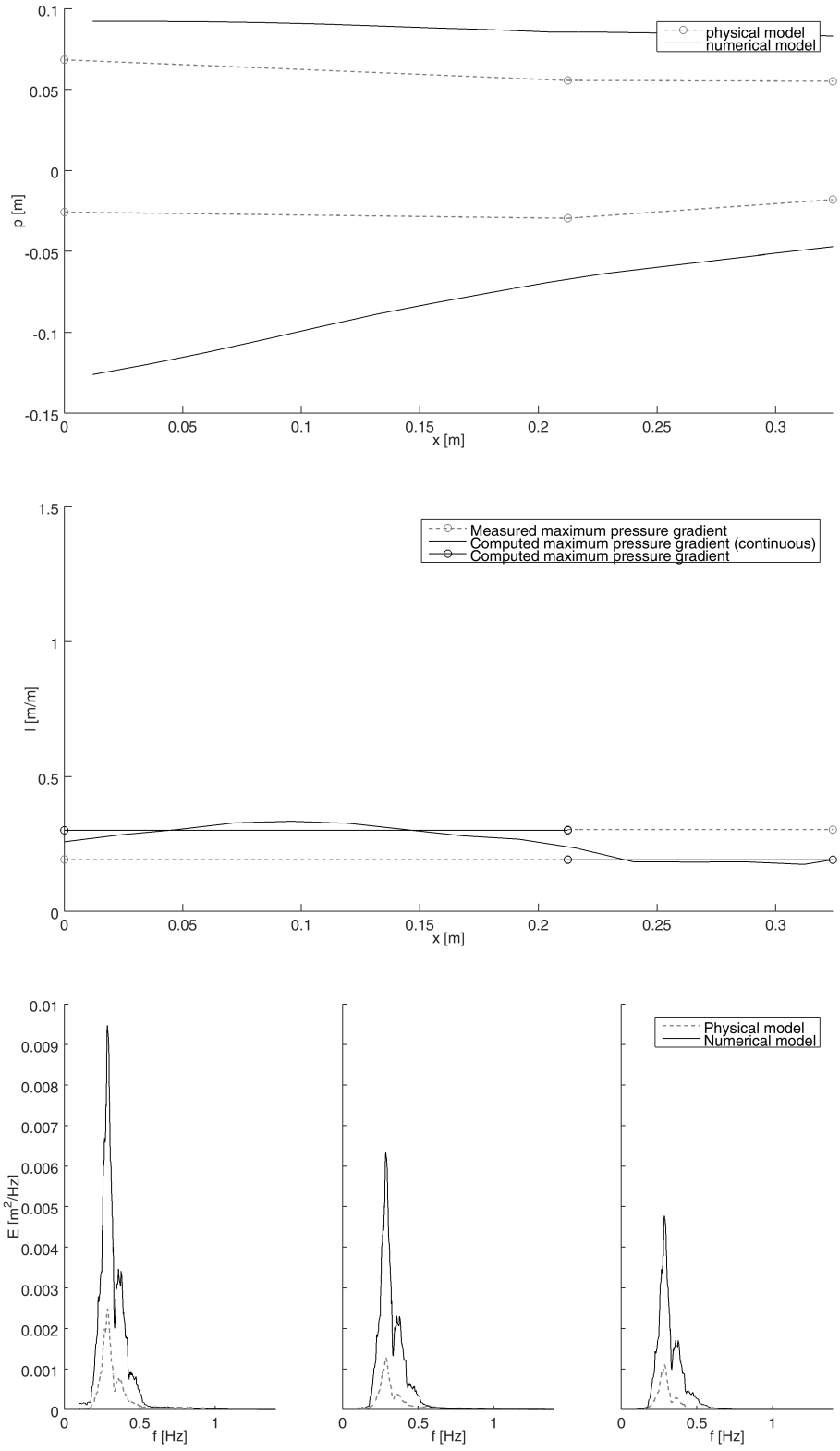

Figure E.16: Kluwen test 68

F

P-PI PLOTS

In this appendix the $P - \Pi$ plots are presented. The results from Chapter 5 are based on these plots. The analyses were also partially based on other relevant plots of time series and spectra. It is however not practical to present all these figures in this report due to the number of figures. Instead the numerical data from which the figures are made can be found at the 3TU Datacentre: `http://datacentrum.3tu.nl/`. Or contact the author directly.

Legend for all figures:

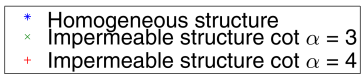

F.1. 2.5 H_s BELOW INITIAL WATER LEVEL

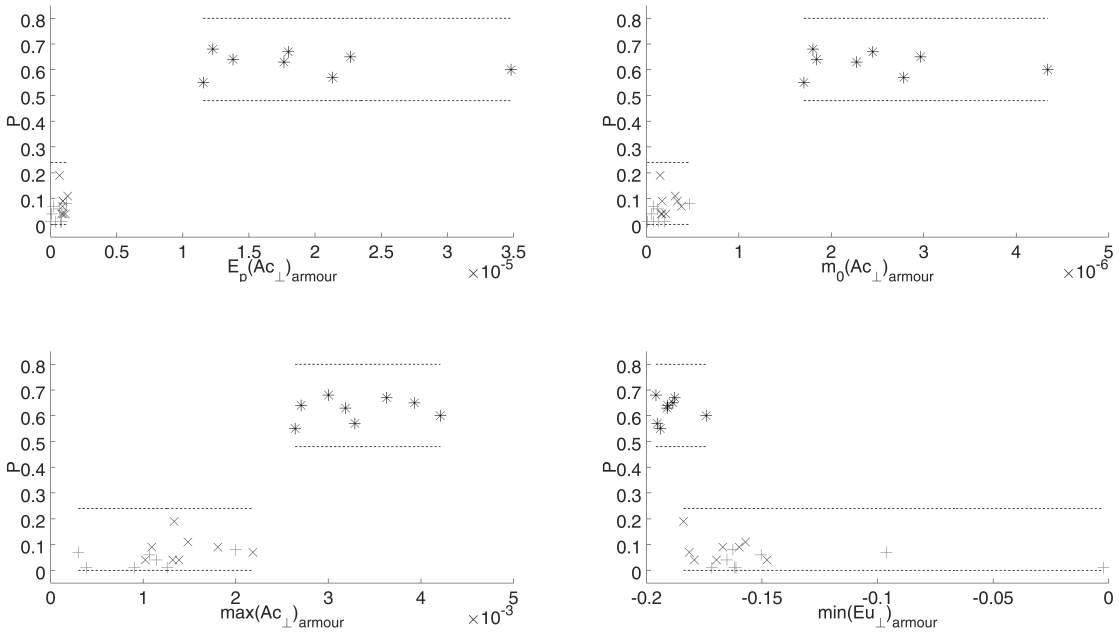

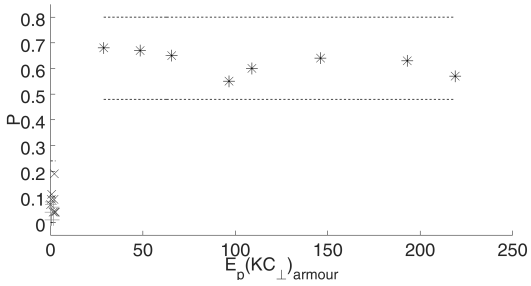
P
$E_p(KC_\perp)_{armour}$

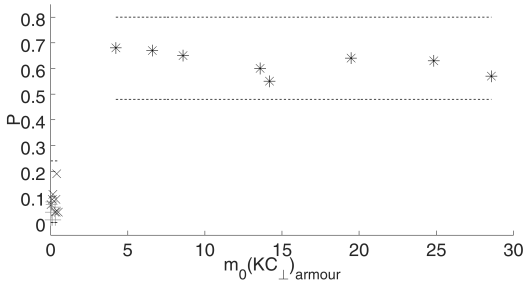
P
$m_0(KC_\perp)_{armour}$

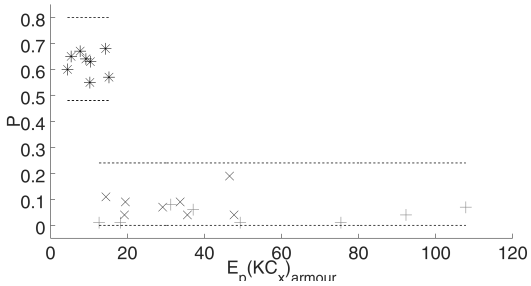
P
$E_p(KC_x)_{armour}$

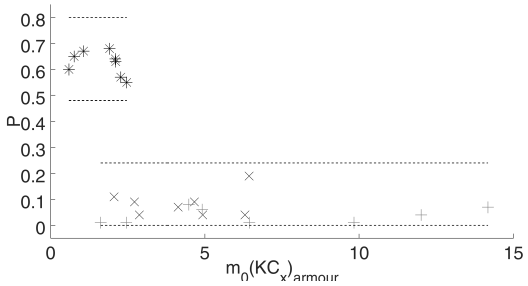
P
$m_0(KC_x)_{armour}$

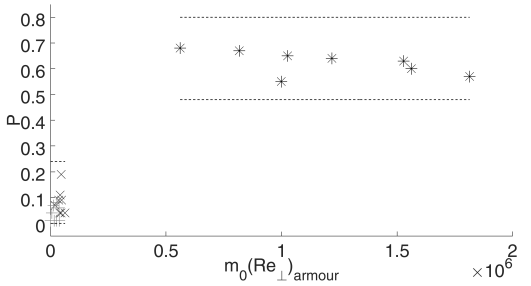
P
$m_0(Re_\perp)_{armour}$
$\times 10^6$

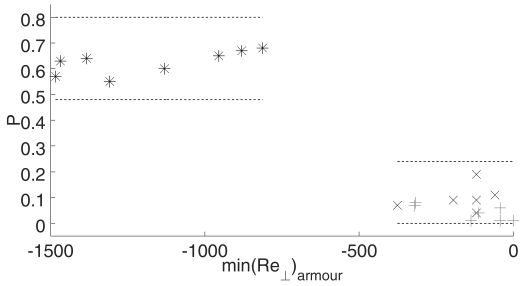
P
$min(Re_\perp)_{armour}$

F.2. 1.5 H_s BELOW INITIAL WATER LEVEL

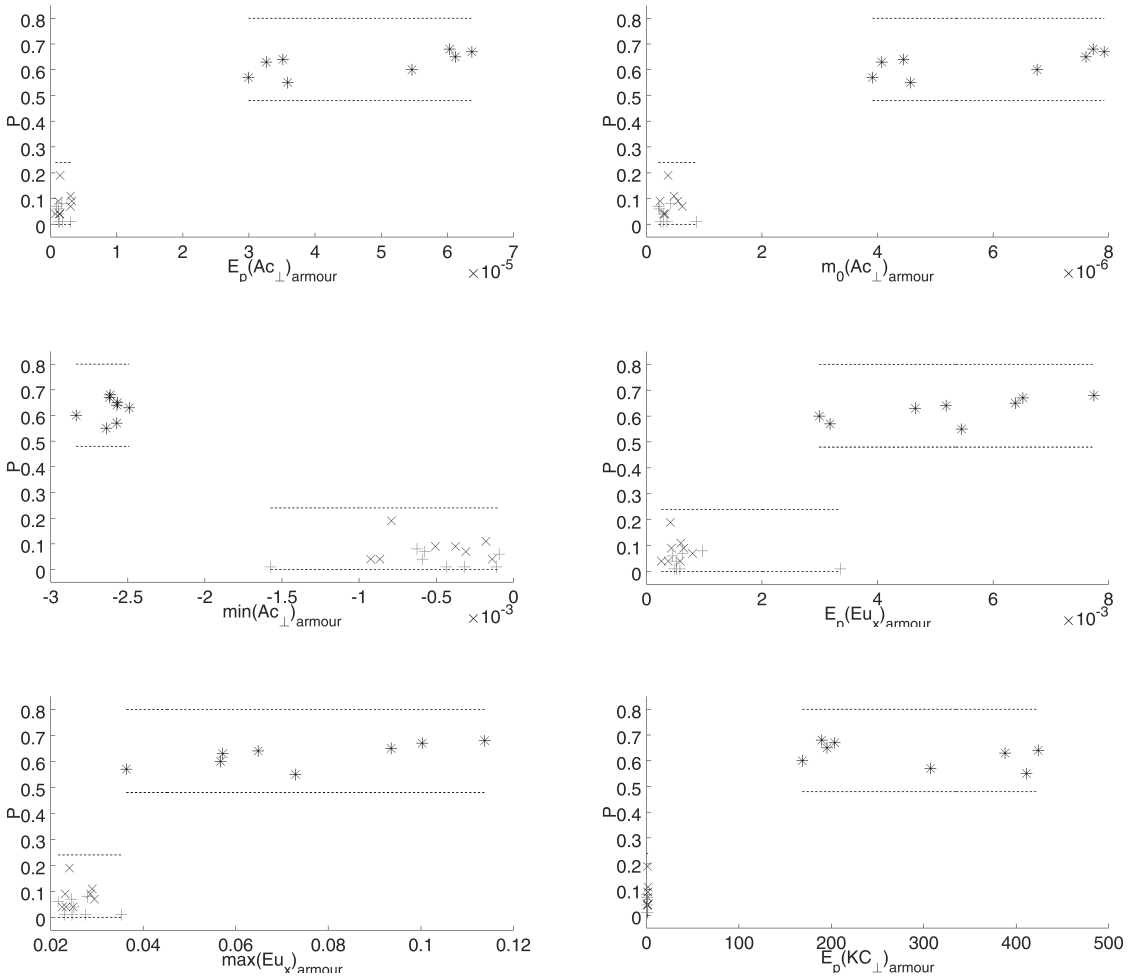

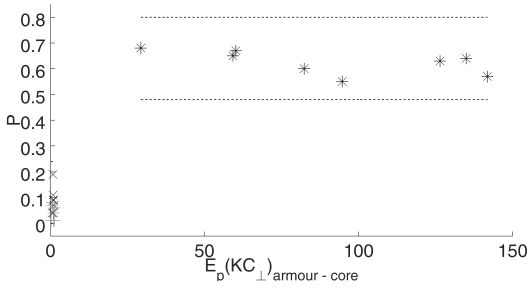
P
$E_p(KC_\perp)_{armour\ -\ core}$

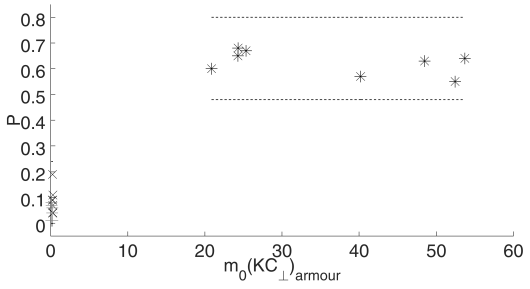
P
$m_0(KC_\perp)_{armour}$

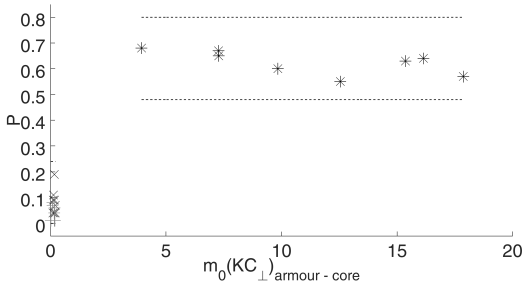
P
$m_0(KC_\perp)_{armour\ -\ core}$

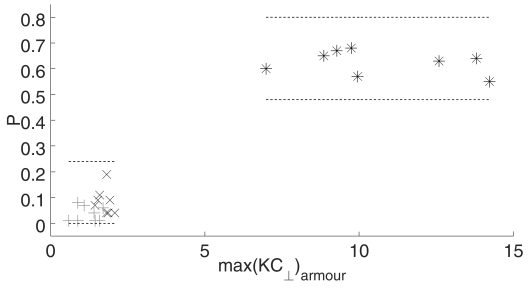
P
$max(KC_\perp)_{armour}$

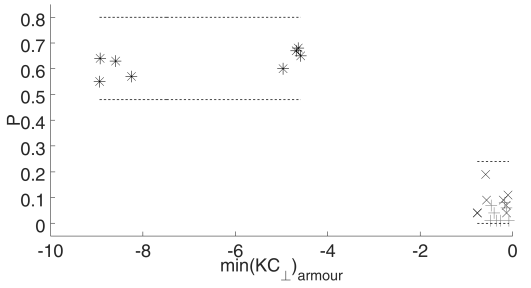
P
$min(KC_\perp)_{armour}$

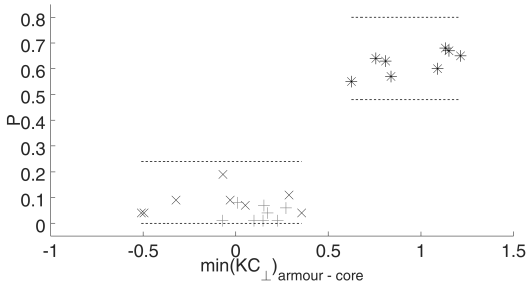
P
$min(KC_\perp)_{armour\ -\ core}$

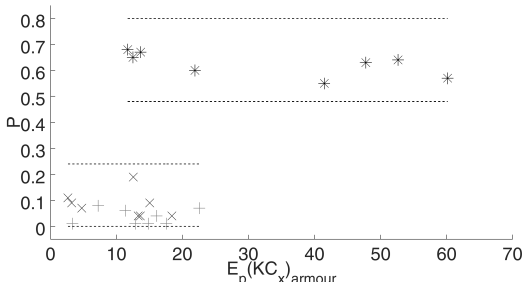
P
$E_p(KC_x)_{armour}$

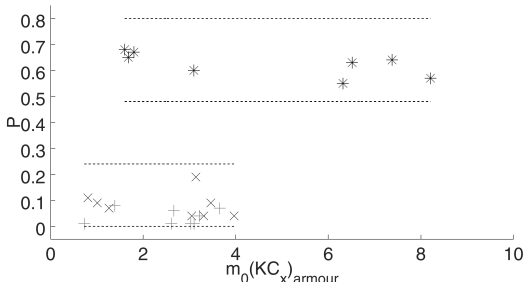
P
$m_0(KC_x)_{armour}$

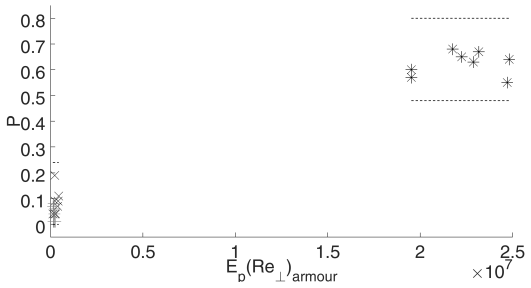
P
$E_p(Re_\perp)_{armour}$
$\times 10^7$

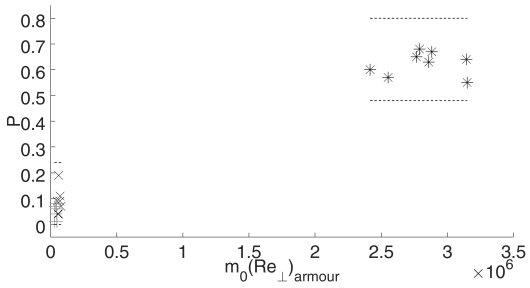
P
$m_0(Re_\perp)_{armour}$
$\times 10^6$

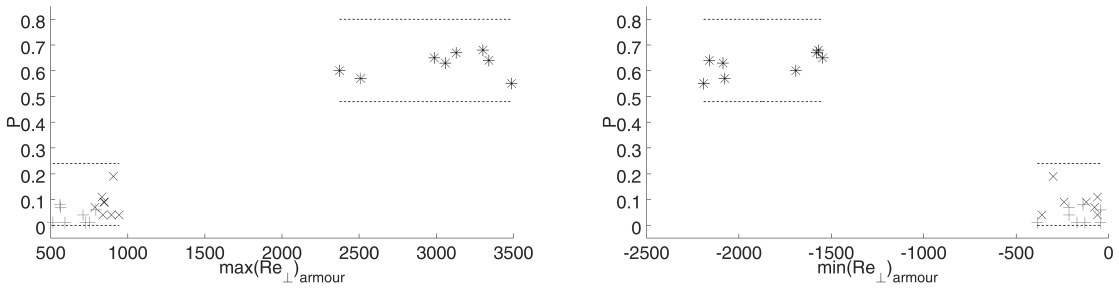
0.8
0.7
0.6
0.5
0.4
0.3
0.2
0.1
0
P
500
1000
1500
2000
2500
3000
3500
max(Re⊥)armour
-2500
-2000
-1500
-1000
-500
0
min(Re⊥)armour

F.3. 0.5 H_s BELOW INITIAL WATER LEVEL

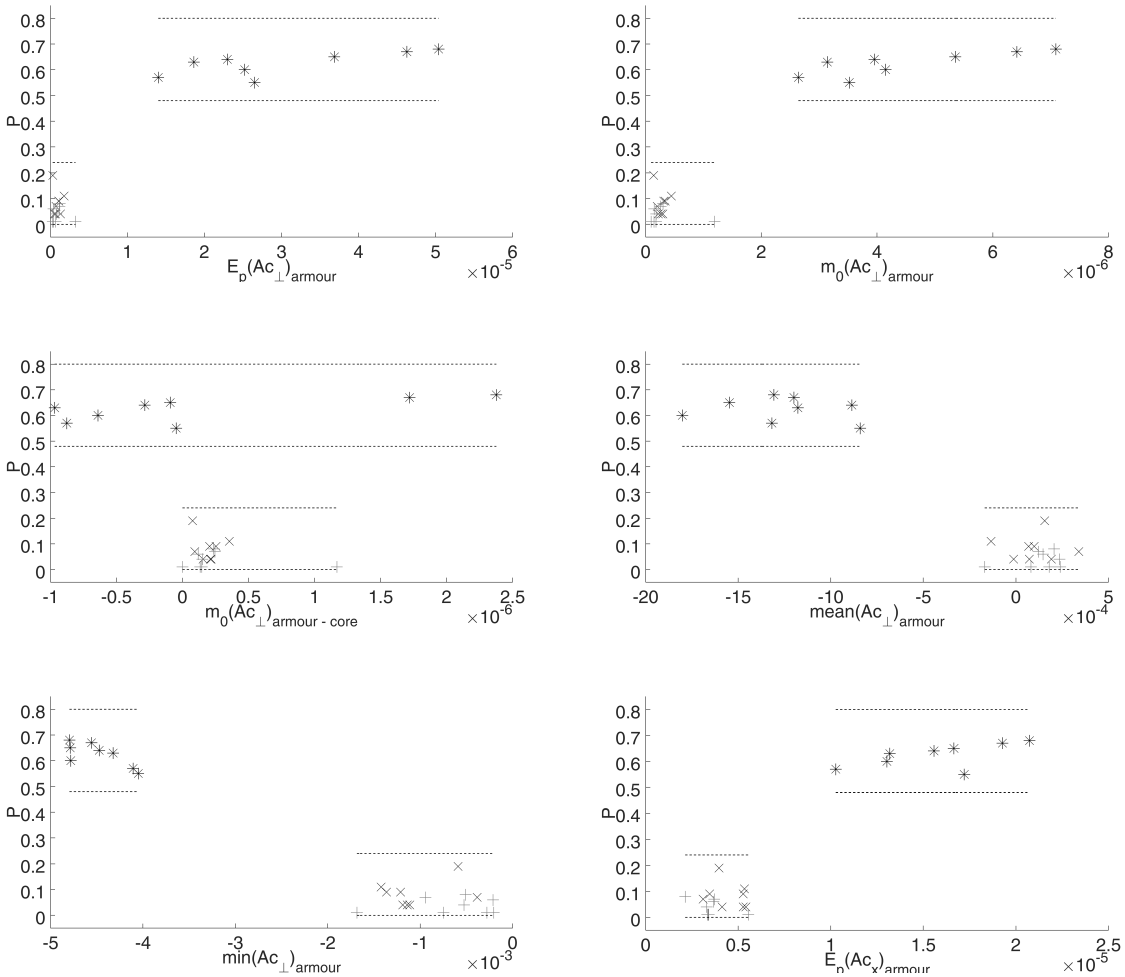

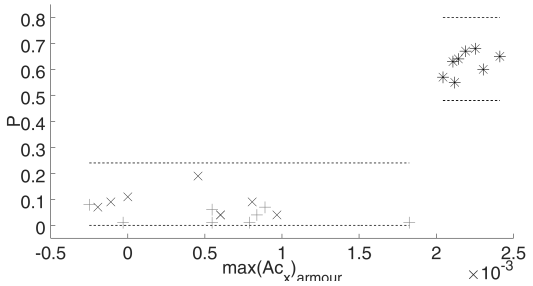
P
max(Ac_x)_armour
×10^-3

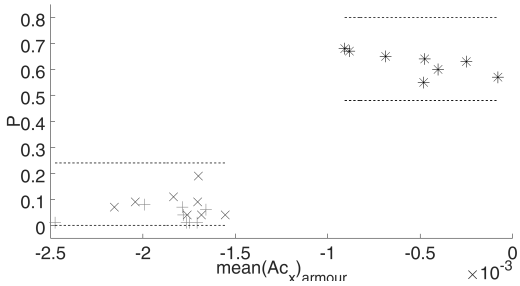
P
mean(Ac_x)_armour
×10^-3

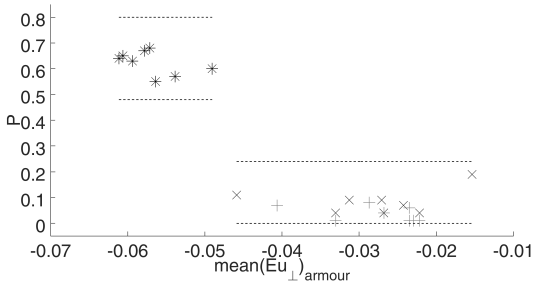
P
mean(Eu⊥)armour

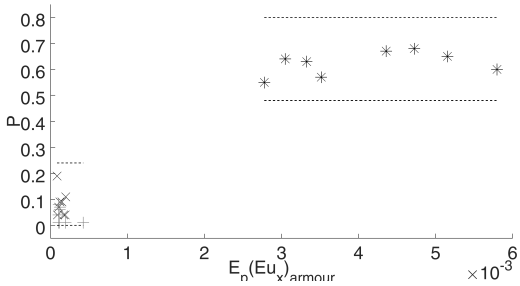
P
Ep(Eux)armour
×10^-3

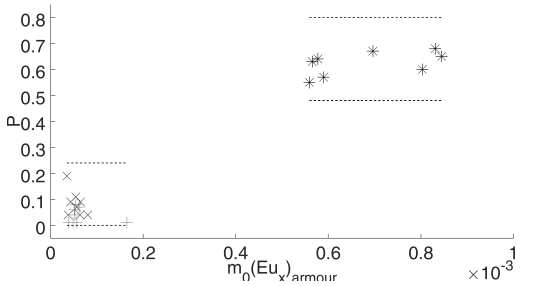
P
m0(Eux)armour
×10^-3

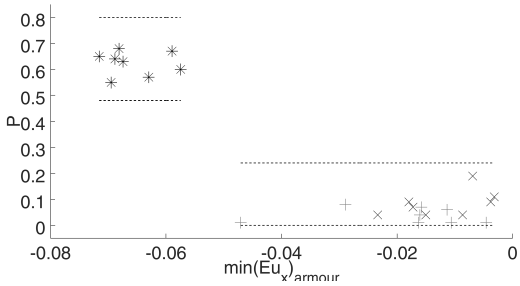
P
min(Eux)armour

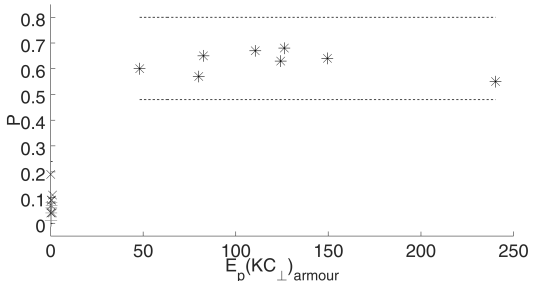
P
Ep(KC⊥)armour

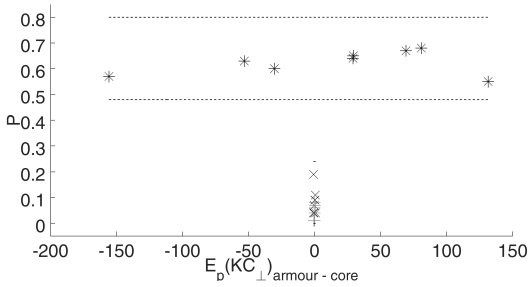
P
Ep(KC⊥)armour - core

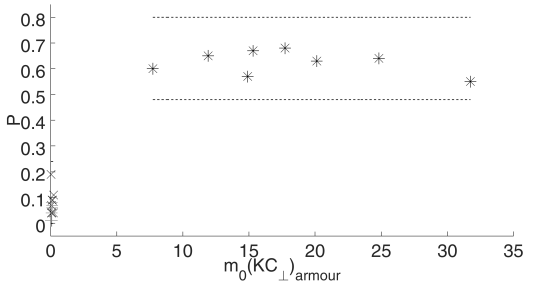
P
m0(KC⊥)armour

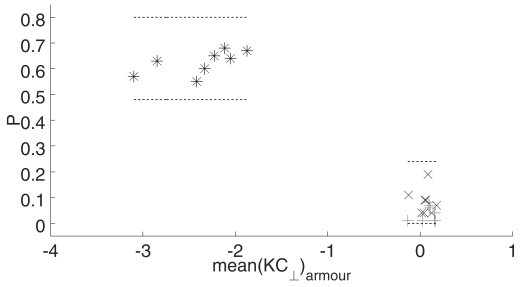
P
mean(KC⊥)armour

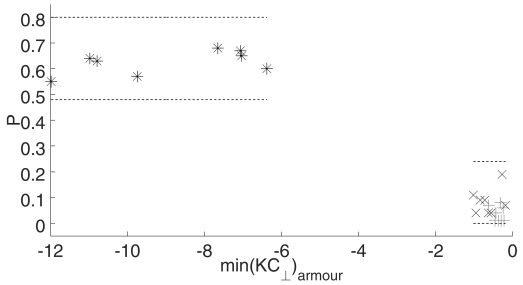
P
min(KC⊥)armour

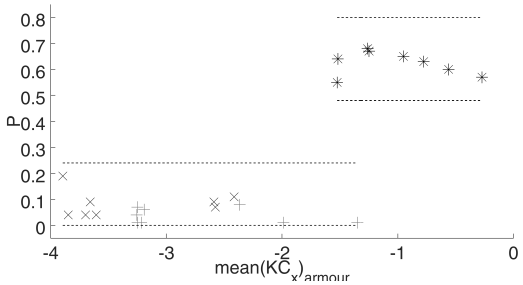
P
mean(KCx)armour

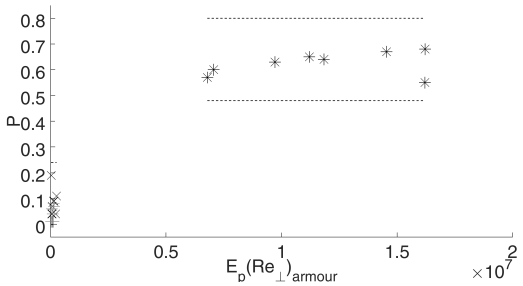
P
Ep(Re⊥)armour
×10^7

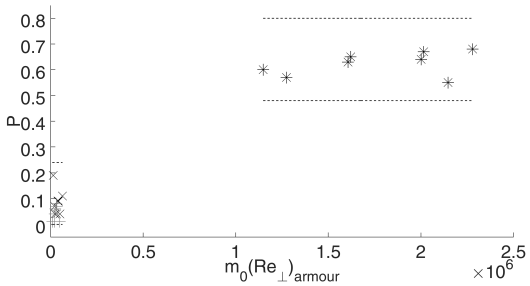
P
m0(Re⊥)armour
×10^6

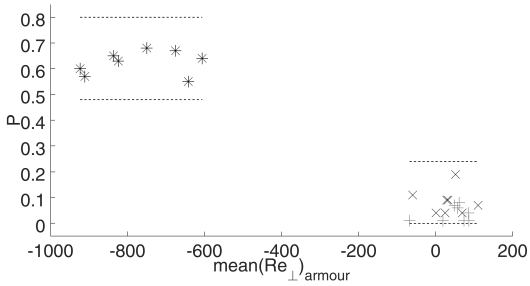
P
mean(Re⊥)armour

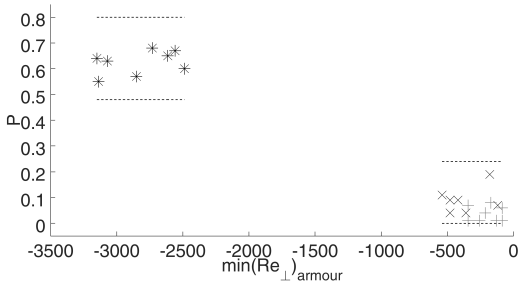
P
min(Re⊥)armour

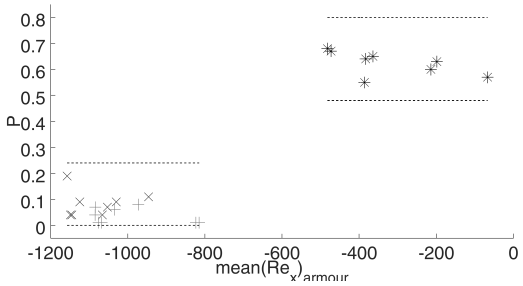
P
mean(Rex)armour